UNIVERSITA' DEGLI STUDI DI PADOVA

Sede Amministrativa: Università degli Studi di Padova

Dipartimento di Innovazione Meccanica e Gestionale

SCUOLA DI DOTTORATO DI RICERCA IN : Ingegneria Industriale
INDIRIZZO : Ingegneria della Produzione Industriale
CICLO XX

NUMERICAL AND EXPERIMENTAL INVESTIGATION OF THE POLYMER INJECTION FORMING PROCESS

Direttore della Scuola : Ch.mo Prof. Paolo F. Bariani
Supervisore : Ch.mo Prof. Paolo F. Bariani
Correlatore : Ing. Giovanni Lucchetta

Dottorando : Ruggero Baesso

UNIVERSITA' DEGLI STUDI DI PADOVA

Sede Amministrativa: Università degli Studi di Padova

Dipartimento di Innovazione Meccanica e Gestionale

SCUOLA DI DOTTORATO DI RICERCA IN : Ingegneria Industriale
INDIRIZZO : Ingegneria della Produzione Industriale
CICLO XX

NUMERICAL AND EXPERIMENTAL INVESTIGATION OF THE POLYMER INJECTION FORMING PROCESS

Direttore della Scuola : Ch.mo Prof. Paolo F. Bariani
Supervisore : Ch.mo Prof. Paolo F. Bariani
Correlatore : Ing. Giovanni Lucchetta

Dottorando : Ruggero Baesso

DATA CONSEGNA TESI
31 gennaio 2008

A Chiara

TABLE OF CONTENTS

PREFACE

This thesis is based on a research work carried out at the DIMEG Labs, University of Padova, Italy, from January 2005 until December 2007, under the supervision of ing. Giovanni Lucchetta, to whom I wish to express my sincere gratitude. Moreover I would like to thank Prof. P. F. Bariani for all the scientific and educational opportunities he gave me through these years.

I would like to thank also all my younger and older colleagues at DIMEG, for the pleasant working atmosphere and for the useful and stimulating discussions (not always scientific). In particular, I gratefully acknowledge Marco S., Roberto, Matteo, Silvia, Marco C., Alberto T., Silvio, Francesca, Alessandro C., Manuel, Alessandro V., Alberto G. and Francesco.

Finally, I wish to express my greatest thanks to Chiara and my family. Without their unique support and love this thesis would never had become a reality.

ABSTRACT

It has been recognized that certain performance functions are best handled by one kind of material such as metals, and that other functions are best handled by another kind of material such as polymers. This suggests that a union of two or several kinds of different materials will give synergistic results. End products that perform better than would have been possible if only one material were used, are the expected results.

Generally speaking, there are two kinds of composites: one with a matrix reinforced by particulate, fibres, etc. such as metal-matrix and polymer-matrix composites; and another one termed here as macro-composites, manufactured with materials having different properties. As for the latter, metal/polymer combined macro-composite components are representative of a unique combination of two kinds of different material used to achieve improved quality of the products, which have been used in a wide variety of applications in electronics, automotive and aerospace industries, etc. This work refers to macro-composite components consisting of one sheet-metal outer panel with a polymeric core material behind it.

However, the techniques for manufacturing such kinds of components are few and are usually time-consuming and labour intensive, resulting in a very expensive production. In most cases, the metal part and the polymer part are first fabricated separately by sheet metal forming processes and injection moulding respectively, and then they are joined together mainly by adhesion bonding. In this approach, good dimensional tolerance of both sheet metal and plastic parts is required for matching of the outer surface of the plastic part to the inner surface of the sheet metal part. It is not easy to achieve this when the bonding surface is complex and it is difficult to obtain a stable adhesion bonding interface.

In this Ph.D. dissertation, a new technique to manufacture the above mentioned metal/polymer macro-composite components is presented. In this process, the injected polymer melt from the injection machine forces the sheet metal blank to deform according to the contour of the mould and the space between the formed sheet blank acts as the moulding cavity of the polymer melt. As the melt cools down, it adheres to the surface of the formed sheet blank. The process, known in the academic and industrial world as "Polymer Injection Forming (PIF) process" is covered by a world patent by the English company Corus, which is an international company, providing steel and aluminium products and services to customers worldwide.

The aim of this Ph.D. dissertation consists on increasing the scientific knowledge about the Polymer Injection Forming process by means of both a numerical and an experimental approach. Several aspects of this new manufacturing process have been studied:

(i) the influence of the main injection moulding process parameters on the sheet metal formability has been experimentally investigated according to the Design of Experiments

(DOE) method. This task required the design and set-up of a special injection mould in order to carry out experimental tests of the Polymer Injection Forming process. The experimental process was designed so that industrial operating conditions were approximated as closely as possible.

(ii) A combination of the finite element method (FEM) and Finite Volume Method (FVM) has been used to simulate the simultaneous forming process of both the plastic part and the sheet metal blank. The adopted multi-physics numerical approach allowed to investigate both state variables of the polymeric melt within the mould cavity and the deformation features, thickness distribution and evolution of plastic strains of the sheet metal.

(iii) The mechanism of adhesion bonding between the polymer and the surface of the formed sheet blank and the influence of the main injection moulding process parameters on the adhesion quality has been experimentally investigated according to the Design of Experiments method. The adhesion strength between the plastic and the metal part was measured by means of a custom shear test. This task required the design and set-up of special tools for clamping and testing the macro-composite part, which was used as specimen.

(iv) A software for the monitoring and control, in particular of the switch-over point, of the Polymer Injection Forming process has been developed in order to optimize the process and maximize its repeatability. Several experimental tests were carried out in order to study the influence of different switchover methods on both part quality and process variability. The efficiency of the proposed control algorithm was tested comparing the results obtained by the traditional control strategies with the ones obtained by the developed control method.

The work presented in this thesis was carried out at the DIMEG Labs, University of Padua, Italy, from January 2005 to December 2007, under the supervision of ing. Giovanni Lucchetta.

SOMMARIO

È noto che alcune tipologie di materiali, come ad esempio i metalli, presentano determinate caratteristiche funzionali mentre altre tipologie, come ad esempio i materiali polimerici, ne presentano di diverse. Da questo si evince che attraverso l'unione di due o più diversi materiali è possibile raggiungere un effetto sinergico per cui il materiale composito risultante presenta delle caratteristiche superiori rispetto a quelle ottenibili da ciascun singolo materiale componente.

Generalmente i materiali compositi si distinguono in due categorie. La prima include i materiali costituiti da una matrice rinforzata con altri materiali presenti allo stato particellare o fibroso, come ad esempio i materiali compositi a matrice metallica o polimerica. La seconda include i cosiddetti materiali macro-compositi costituiti da differenti materiali macroscopicamente distinguibili tra loro. Tra questi emergono i materiali macro-compositi costituiti dall'unione di una parte in metallo e da una in plastica, già utilizzati in diversi settori tecnologici, quali l'elettronico, l'aerospaziale e l'automobilistico proprio per le loro caratteristiche superiori a quelle dei singoli materiali costituenti. In questo lavoro di tesi ci si riferirà ai componenti macrocompositi costituiti da una parte esterna in lamiera metallica unita ad una parte in materiale polimerico.

Tale tipologia di componenti soffre di alcuni svantaggi in fase di produzione. Infatti, le tecnologie di fabbricazione sono poche e generalmente richiedono tempi lunghi e molto lavoro, causando alti costi di produzione. In genere, la parte metallica e quella in materiale plastico vengono prima prodotte separatamente, rispettivamente per mezzo dei tradizionali processi di formatura della lamiera e di stampaggio ad iniezione, e successivamente unite insieme mediante un'operazione di incollaggio. Questo tipo di lavorazione richiede delle buone tolleranze dimensionali sia per la parte in metallo che per quella in plastica al fine di garantire un buon accoppiamento tra la superficie esterna del componente in plastica e la superficie interna del componente in metallo. Questo obiettivo, tuttavia, non è facilmente perseguibile quando la superficie di adesione è complessa, e risulta così difficile anche ottenere un' interfaccia stabile del giunto incollato.

In questo lavoro di tesi di dottorato verrà presentata una nuova metodologia per la produzione dei componenti macro-compositi metallo/polimero. Questo nuovo processo di fabbricazione prevede che il polimero fuso iniettato dalla pressa ad iniezione forzi la lamiera, posizionata all'interno dello stampo, a deformarsi in accordo con la geometria dello stesso. Durante la solidificazione del polimero fuso avviene anche l'adesione tra la parte in plastica e la parte in metallo. Il processo, noto nel mondo accademico e in quello industriale con il nome di "Polymer Injection Forming (PIF)" è coperto da un brevetto mondiale da parte della multinazionale inglese Corus, la quale vende in tutto il mondo prodotti in acciaio e alluminio.

Lo scopo della presente tesi di dottorato consiste nell'approfondire la conoscenza scientifica del processo di Polymer Injection Forming attraverso un approccio sia sperimentale che numerico. Sono stati studiati diversi aspetti di questo innovativo processo produttivo:

(i) mediante la metodologia del Design of Experiments (DOE) è stata analizzata l'influenza dei principali parametri del processo di stampaggio ad iniezione sulla formabilità della lamiera metallica. La realizzazione di tale obiettivo ha richiesto la progettazione e la realizzazione di uno speciale stampo ad iniezione al fine di condurre i test sperimentali del processo di Polymer Injection Forming. Il processo sperimentale è stato progettato in modo tale da riprodurre quanto più fedelmente possibile le reali condizioni operative dell'ambiente industriale.

(ii) Attraverso l'utilizzo combinato del metodo ad elementi finiti (FEM) e del metodo ai volumi finiti (FVM) è stato numericamente simulato il processo della formatura contemporanea della parte in plastica e di quella in metallo. L'approccio numerico multifisico che è stato adottato ha permesso di investigare sia le variabili di stato relative al polimero fuso all'interno dello stampo, sia l'evoluzione della formatura e la distribuzione e l'evoluzione delle deformazioni plastiche della lamiera metallica.

(iii) Attraverso la metodologia del Design of Experiments si è sperimentalmente indagata l'influenza dei principali parametri del processo di stampaggio ad iniezione sulla qualità dell'adesione tra plastica e metallo. La forza di adesione tra metallo e polimero è stata misurata per mezzo di un particolare test a taglio. La realizzazione di tale obiettivo ha richiesto la progettazione e la realizzazione di una speciale attrezzatura al fine di garantire il corretto afferraggio del componente macro-composito utilizzato come provino del test.

(iv) È stato sviluppato un programma per il monitoraggio ed il controllo, in particolare del punto di commutazione tra controllo di velocità e controllo di pressione, del processo di Polymer Injection Forming al fine di ottimizzare il processo stesso e massimizzare la sua ripetibilità. Sono stati condotti dei test sperimentali al fine di studiare l'influenza di differenti strategie di commutazione sia sulla qualità del pezzo sia sulla variabilità di processo. I risultati così ottenuti sono stati confrontati con quelli ottenuti utilizzando l'algoritmo di controllo sopra menzionato. Da tale confronto è stato possibile testare l'efficienza della strategia di controllo proposta.

Il lavoro presentato in questa tesi è stato svolto presso i laboratori del DIMEG, dell'Università di Padova, in Italia, nel periodo compreso tra i mesi di gennaio 2005 e dicembre 2007, sotto la supervisione dell'ing. Giovanni Lucchetta.

CHAPTER 1
INTRODUCTION

Composite parts made of a sheet metal blank bonded to a plastic substrate are increasingly used in manufacturing aesthetic and functional parts for many industrial sectors such as automobiles, aircrafts, electronics and electrical appliances. The manufacturing of this kind of components is usually time-consuming and labour intensive resulting in a very expensive production. In most cases, the polymer and the metal parts are first manufactured separately by injection moulding and sheet metal forming processes respectively. Then they are joined together mainly by the adhesion bonding method.

Polymer Injection Forming (PIF) is a new technology to manufacture metal/polymer macro-composite components. The process consists in forming a sheet metal blank on a injection moulding machine, by means of the injected polymer and according to the contour of the mould cavity. In the same step, the polymer is permanently bonded to the metal sheet resulting in a fully finished part in only one production step.

In spite of its industrial relevance, the scientific knowledge of the above process is still very poor. Experimental investigations, both in the laboratory and in the field, continue to be more common than numerical ones. Models and simulations suffer from many heavy assumptions, mainly those related to the description of the polymer-metal interactions [1], and prove to be inadequate to evaluate the effects of process parameters on process performance and product quality. The causes of these are both the complexity of the phenomena to model as well as the recentness of this technology.

In this Ph.D. thesis, a in-depth investigation on the Polymer Injection Forming process has been carried out by means of both numerical simulations and experimental tests.

1.1 The industrial problem

Recent consumer research has shown that natural materials, such as glass, wood and steel are a challenging issue. A steady increasing number of polymer products are fitted with a metal look, especially in automotive applications. Although highly appreciated by consumers, these products may look like steel or aluminium but they lack the durability and properties of metals. The majority of coatings applied to polymer products are expensive, and tend to show wear due to frequent use. Production of metal products can be costly and will require multiple production steps, not to mention the laborious assembly method.

The solution to these problems is the manufacturing of end products made by a union of a plastic part and a metal one. Such kind of components, termed as macro-composites, performs better, in terms of functionality, than would have been possible if only one material were used.

The work presented in this Ph.D. thesis gets its main relevance in automotive applications, especially in manufacturing aluminium/polymer macro-composite components for frames and trims in car dashboard (see Figure 1.1).

(a) *(b)* *(c)*

Figure 1.1: Frames and trims in car dashboards are typical sheet metal-polymer macro-composites in automotive applications.

Such components not only have to satisfy aesthetic and functional requirements but also they have to be characterized by good mechanical properties and impact resistance with sound-insulating, vibration-insulating and thermal-insulating properties. An example of a metal/polymer macro-composite component for an automotive application is reported in Figure 1.2. It is the cover frame of the gearbox lever of BMW 1 series car.

Figure 1.2: Cover frame of the gearbox lever of BMW 1 series car.

Until few years ago, only luxury cars were equipped with metal or metal-like components in the inside. Due to low sales volume of such expensive cars, cost efficiency in manufacturing those components was not an issue. In the last few years, however, also second-class cars are provided with such kind of equipments. It is common, nowadays, to find out applications of

metal/polymer macro-composites in second-class cars as door handles or as covers for dashboard air mouths, threshold, central tunnel, steering wheel and so on.

The traditional manufacturing technology of such macro-composite components is usually time-consuming and labour intensive, resulting in a very expensive production. In most cases, the polymer and the metal parts are first manufactured separately by injection moulding and sheet metal forming processes respectively. Then they are joined together mainly by the adhesion bonding method. In this approach, good dimensional tolerance of both sheet metal and plastic parts is required for matching of the outer surface of the plastic part to the inner surface of the sheet metal part. It is not easy to achieve this when the bonding surface is complex.

Due to these drawbacks, companies in the automotive field, and not only, are looking for other innovative manufacturing processes in order to increase productivity and, at the same time, minimize production costs and improve the quality of the final metal/polymer macro-composite products.

1.2 The aim of the work

The present work comes from a scientific collaboration between the Department of Innovation in Mechanics and Management (DIMEG), at University of Padova, and the company Plastal, which is a leading supplier of engineered plastics to the automotive industry. The final objective of this scientific project, called PLASTOMET, consists in innovating the traditional manufacturing processes of metal/polymer macro-composite components in order to increase productivity and part quality and, at the same time, minimize production costs.

Polymer Injection Forming is an innovative one-step production process that creates a composite material between a metal sheet and a polymer using standard injection moulding machinery (Figure 1.3).

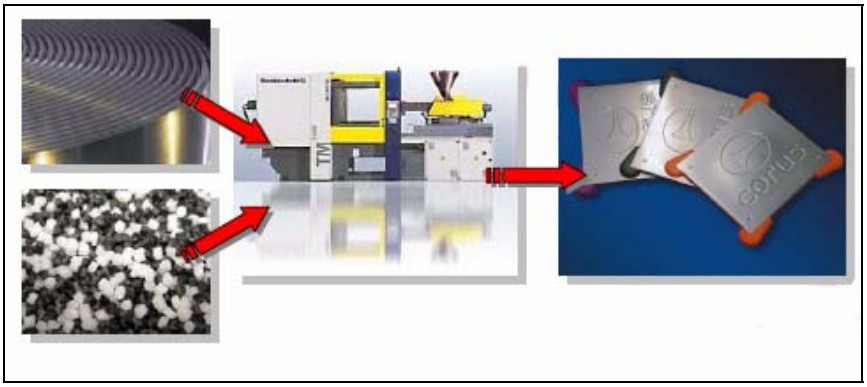

Figure 1.3: The Polymer Injection Forming process: raw materials, the injection moulding machine and the finished metal/polymer macro-composite part.

During this process, several production steps are carried out inside the mould that normally would require separate production and assembly steps using conventional production methods. This single step process means integrating the cutting and shaping of the metal in the same injection mould in which the adhesion between metal sheet and polymer is created, and making use of the freedom of polymer forming to (optionally) bond two different

blanks of metal sheet by a living hinge, for example, to create clamps and snaps to facilitate easy assembly. Cycle times for the manufacture of a single PIF part are comparable to that of injection moulding, and by diminishing bottlenecks in the production process the cycle time can be reduced.

The aim of the present work consists on developing a set of integrated tools - both numerical and experimental - that are able to provide designers of metal/polymer macro-composite components with a more in-depth scientific knowledge about the Polymer Injection Forming process.

To fulfil this task the following goals have been outlined:

- Design and set-up of a special injection mould for the Polymer Injection Forming process. The geometry of the mould cavity was designed considering both experimental and numerical requirements of the investigation carried out in the present work.
- Set-up of an experimental test of the Polymer Injection Forming process approximating industrial operating conditions as closely as possible.
- Evaluation of the influence of the main injection moulding process parameters on the sheet metal formability.
- Evaluation of the influence of the main injection moulding process parameters on the adhesion quality between the aluminium sheet and the polymer part.
- Design and set-up of a numerical environment in order to simulate the PIF process.
- Development of a software for the monitoring and control, in particular the switch-over point, of the PIF process.

1.3 The organization of the work

The work is organized in eight chapters. The first chapter is a general introduction to efficiency limits of traditional manufacturing processes of metal/polymer macro-composite components. A new industrial process, termed as Polymer Injection Forming (PIF), for a more efficient production of such kinds of components is then presented, as well as its scientific relevance.

In the second chapter a literature review is reported regarding the most recent technologies for sheet metal forming processes, in particular the Viscous Pressure Forming (VPF) process. VPF is a recently developed sheet metal forming process on the basis of conventional flexible sheet forming technology, such as hydro-forming, using an elastic body as the pressure-carrying medium. Due to its similarity with the Polymer Injection Forming process, several useful considerations can be inferred from its investigation. The second part of this chapter reports a in-depth description of working of the PIF process, as well as the approach used by other authors for its numerical modelling.

The third chapter describes the equipment designed in order to experimentally investigate the Polymer Injection Forming. Obtained results regarding the influence of the main injection moulding process parameters on the sheet metal formability are then reported.

The fourth chapter introduces the adhesion mechanisms between metal and polymer and the main destructive tests for measuring the adhesion quality. Then, experimental tests carried out in order to investigate the influence of the main injection moulding process parameters on adhesion strength between metal and polymer, as well as obtained results, are described.

The fifth chapter describes the material characterization of both sheet metal and polymer. Obtained data were used as input parameters in the numerical simulation described in the following chapter.

The sixth chapter presents the implementation of a numerical environment suitable for analyzing the Polymer Injection Forming process.

The seventh chapter reports a state of the art of methods and techniques developed in order to control the switch-over point in the traditional injection moulding process. Then the algorithm developed for controlling the switch-over point in the Polymer Injection Forming process as well as obtained results are presented.

The last chapter, the eighth one, reports conclusions of this work, as well as future works.

CHAPTER 2
LITERATURE REVIEW

Due to the recentness of the Polymer Injection Forming technology, the scientific knowledge of this process is still very poor. However some useful considerations could be inferred analyzing the most recent technologies for injection moulding and sheet metal forming processes.

This chapter addresses the Viscous Pressure Forming (VPF) technology for sheet metal forming process and the Polymer Injection Forming (PIF) process for manufacturing metal/polymer macro-composite components. First, the state of the art of VPF in formability analysis of sheet metals, pressure control, numerical simulation, applications and forming devices will be presented. Then a description of the PIF process will be illustrated.

2.1 The Viscous Pressure Forming process

Viscous Pressure Forming (VPF) is a recently developed sheet metal forming process on the basis of conventional flexible sheet forming technology, such as hydro-forming, using an elastic body (a rubber or polyurethane pad) as the pressure-carrying medium.

VPF was invented in 1992, and it is different from conventional flexible sheet technology, in that it uses a kind of semi-solid, flowable and viscous materials as the pressure-carrying medium [2]. In VPF, the viscous medium is used as a soft punch when it is applied on one side of the sheet metal and used as a soft punch and back-pressure when it is applied on both sides of the sheet metal. Trough the injection of viscous medium, the pressure distribution is applied in the die-container and the sheet is formed under the pressure of the viscous medium.

In the simplest implementation of the VPF process, the forming medium is pumped under pressure into the cavity on one side of the sheet to be formed and controllably released trough a single or multiple ports from the other side (Figure 2.1). A more sophisticated variation of the process provides a real-time "adaptive die" that can be used to controllably alter the shape and forming experience of the material in order to flexibly refine the precision of the formed component [3, 4].

A schematic diagram of VPF is shown in Figure 2.1.

a) First, the sheet metal blank is positioned over the die opening. The chamber is then clamped shut and the blank binder is engaged.
b) The viscous medium is then introduced to both sides of the sheet, filling the die and diffuser cavities and raising the isostatic pressure to the predetermined level. The medium is then withdrawn from the die cavity by the outflow control devices while additional medium is introduced above the sheet. This is controlled in such a manner that the predetermined differential pressure distribution across the deforming sheet is maintained.
c) The process is continued in coordination with the blank holder force until the sheet material is forced against the die surface with sufficient pressure to acquire acceptable die form detail.
d) The chamber is then depressurized, opened and the formed part ejected.

Compared to conventional sheet metal forming processes, the viscous medium can fill a complex-shaped surface very well. The parts formed by VPF have a good surface quality and high dimensional accuracy.

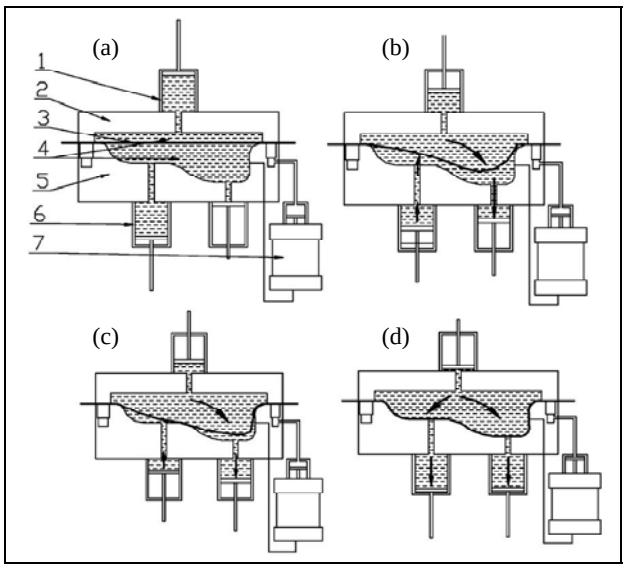

Figure 2.1: A schematic diagram of VPF [2]: (1) medium injection cylinder; (2) upper die; (3) blank sheet; (4) viscous medium; (5) die; (6) medium outlet cylinder; (7) blank holder cylinder.

2.1.1 Property of viscous medium

The pressure-carrying-medium which best exploits the potential of the VPF process is a multi-phase, polymeric material which has rather complicated material properties. Its thermodynamic state is between the liquid and the solid and it shows strong strain-rate sensitivity to load conditions. The most diffuse types are commercially named "C-11", "C-21" and "W-45". The property of viscous medium has a key effect on the sheet metal in VPF. When the viscosity of the viscous medium is low, VPF is similar to hydroforming, whilst, when a viscous medium with higher viscosity is used as the working medium, VPF is similar to rigid punch forming.

Extrusion experiments were carried out in order to obtain the relationship curves between the flow stress and the strain of the viscous medium by Liu et al. [5, 6]. However, the

deformation of the viscous medium in VPF is a compression deformation. Thus, it is very important to research the relationship between stress and strain of the viscous medium under compression conditions. In order to determine such kind of relationship, Xinyun carried out compression experiments which provided an experimental basis for analyzing the mechanical properties of the viscous medium [7].

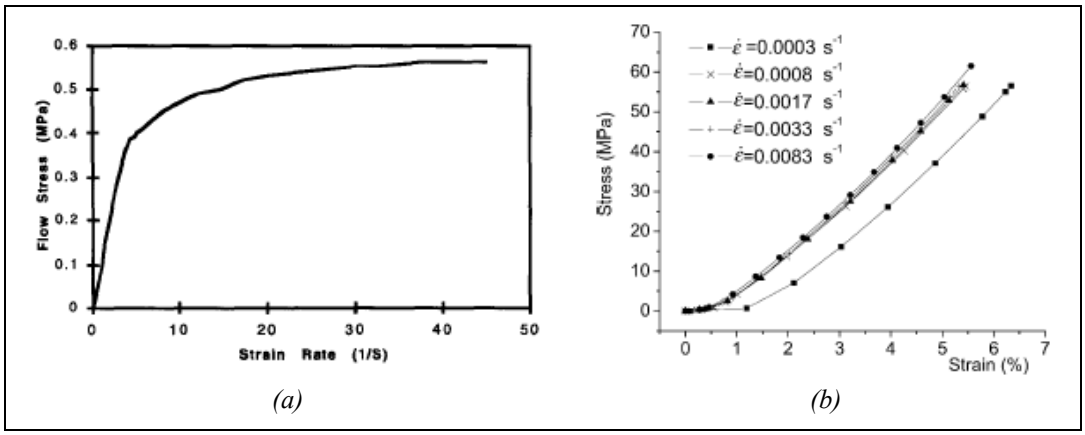

Figure 2.2: (a) Flow stress vs. strain rate curve of C-11 viscous media [5]; (b) Relationship curves between the stress and strain of the viscous medium W-45 [7].

2.1.2 Force state of the sheet metal blank

During the VPF process, the sheet metal is affected not only by the normal pressure of the viscous medium but also by the tangential adhesive stress of the viscous medium. This is one of main characteristics of VPF that is different from those of other sheet metal forming processes.

Considering, for example, the four different bulging methods describes in (Figure 2.3). The force states of the sheet during bulging are shown in Figure 2.4. The friction role can be ignored during oil or water bulging, so the sheet only bears the normal pressure (Figure 2.4 (a)). When the steel or polyurethane medium is adopted, only a local area of sheet bears the normal pressure and friction force due to its rigidity (Figure 2.4 (b)). Of course, the normal pressure and the friction force will be distributed over the whole sheet surface gradually, when bulging with polyurethane. As for VPF, the friction role cannot be ignored because of the high viscosity of the viscous medium. Thus, besides the normal pressure, there is a tangential friction force (Figure 2.4 (c) and (d)) [8].

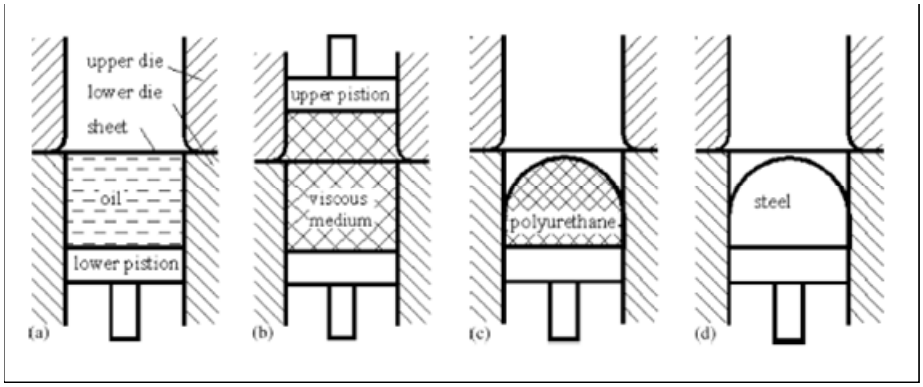

Figure 2.3: Different bulging methods [8]: (a) hydro-bulging; (b) viscous medium bulging; (c) polyurethane bulging; (d) steel bulging.

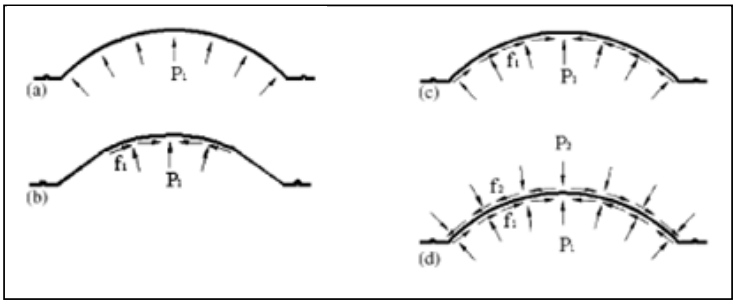

Figure 2.4: Force states of the sheet [8]: (a) hydro-bulging; (b) steel or polyurethane bulging; (c) viscous medium bulging; (d) back-pressure viscous medium bulging.

The action of the viscous medium on sheet metal can postpone local necking in the sheet metal, improve the sheet metal formability and make the thickness distribution more uniform. The value of tangential viscous adhesive stress is affected by the viscous medium pressure, viscosity and forming time.

2.1.3 Experimental results of VPF applications

Wang et al. [8] carried out bulging experiments using a sheet metal blank of stainless steel (*i*Cr18Ni9Ti). The pressure-carrying media were viscous medium, polyurethane and steel. The bulged parts are shown in Figure 2.5. Those parts having the same dome height were selected as the analysis objects. Their thickness distribution curves are shown in Figure 2.6 (b). From Figure 2.6 (b), it is seen that, compared to the other two parts, the part bulged with the steel punch has the greatest thickness in the central area but the smallest thickness at the area where the relative radius is about 0.2. As for polyurethane bulging, the interface area still increases during the forming process until the sheet contacts the whole sheet surface, thus its thickness distribution curve is more smooth and regular than that of the part bulged with steel punch. The smoothest curve was obtained with VPF, i.e. the part formed with VPF has a more uniform thickness distribution. The reason is the non-uniform stress field and strain rate sensitivity of the viscous medium during the VPF process.

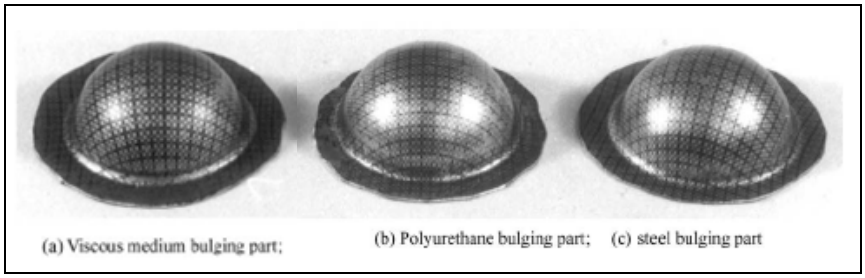

Figure 2.5: Parts obtained in the bulging experiment: (a) viscous medium bulging part; (b) polyurethane bulging part; (c) steel bulging part.

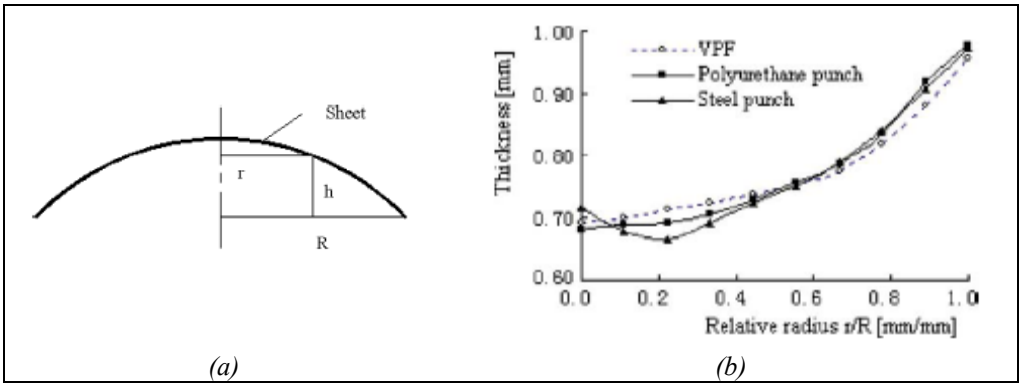

Figure 2.6: (a) Coordinate system used in the analysis; (b) thickness distribution curves of the bulged parts.

2.1.3.1 Viscous medium bulging with backward pressure

During VPF, the sheet deforms under a three-direction stress state when the backward pressure is applied, and the reduction of wall thickness can be constrained well. Thus the distribution of the wall thickness is more uniform, and the formability of sheet can be improved.

A bulging experiment with back-pressure was performed by Wang et al. [8] to study the effect of back-pressure on the formability of an aluminium alloy (5A02Y2) sheet metal blank. The back-pressure value was set to 0 (namely no back-pressure), 3, 6, 10, 15, 20 and 24 MPa. The bulged parts are shown in Figure 2.7 (a).

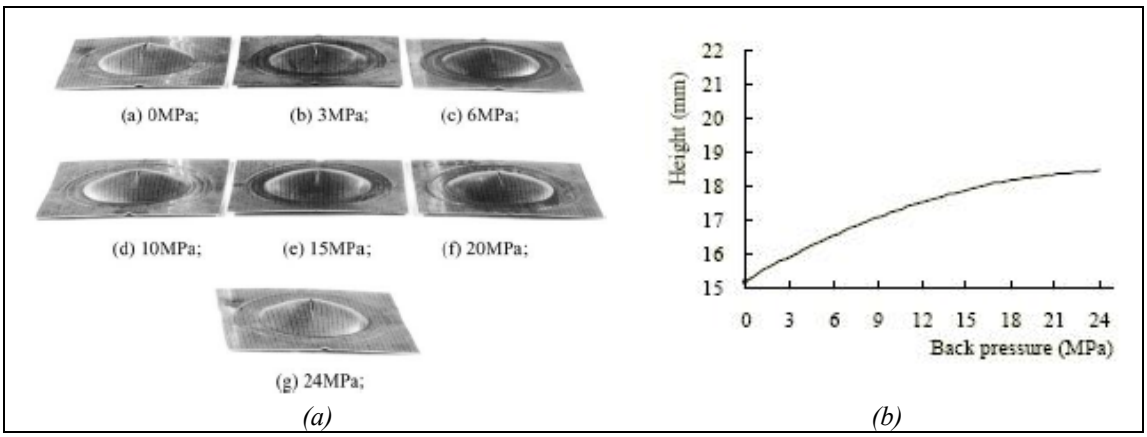

Figure 2.7: (a) Parts bulged under different back-pressure; (b) height distribution of the specimens.

The distribution of the height of specimens is presented in Figure 2.7 (b) and it shows that the higher the back-pressure, the greater the benefit to the improvement of sheet metal formability. Because a higher back-pressure results in a higher compression stress, the role of restricting fracture occurs and the welding of a micro-crack is more effective. Thus, the sheet is able to sustain greater deformation, resulting in a grater dome height.

In order to highlight the beneficial effect of back-pressure on formability of the metal blank, Wang et al. in [8] selected two bulged parts that have the same dome height. One was bulged without back-pressure (or back-pressure 0 MPa), and the other was under a back-pressure of 6MPa. The sheet material was an aluminium alloy (2A12M). The curves of distribution of thickness strain are presented in Figure 2.8, and show that the thickness strain curve obtained under 6MPa back-pressure lies above that for forming without back-pressure. The reason is that the stress state is improved due to the back-pressure. At the same time, the stress state is beneficial in welding the micro cracks occurring in the forming process. Thus, the bulging does not concentrate on a certain area, but is a diffused process, i.e. there is a thickness-uniformity phenomena during the back-pressure bulging process, which results in the thinning of a part that is bulged with back-pressure.

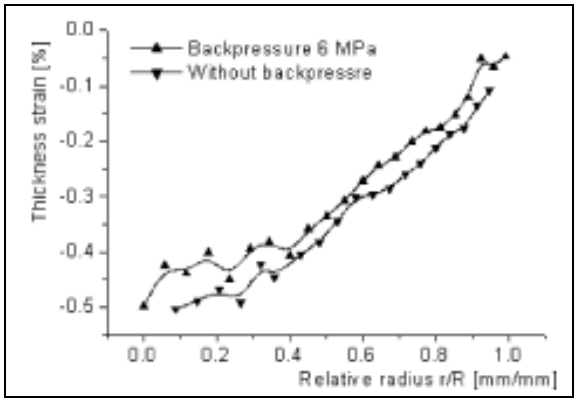

Figure 2.8: Distribution of thickness strain.

The same results were obtained by Wang et al. in [1] and show that the limiting bulging height with back viscous medium improves significantly and that thickness of the specimens is more uniform than that of specimens formed without back viscous pressure in the VPF bulging process. The thickness strain distributions of specimens obtained by VPF bulging with back viscous pressure and without are shown in Figure 2.9.

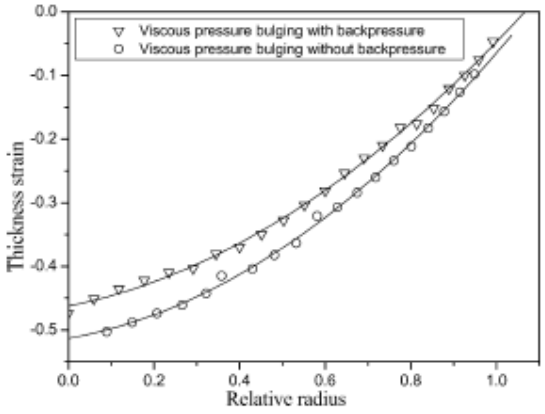

Figure 2.9: Thickness strain distribution curves of specimens obtained by VPF bulging with and without back viscous pressure.

2.1.3.2 Effect of BHF load relationship on forming process

In [9], Wang et al. investigated the effect of load relationships between viscous medium pressure and blank holder force (BHF) on dimensional accuracy of a small radius corrugated and non-uniform depth thin-walled nickel-based superalloy sheet part (Figure 2.10 (a)). The shape and the main dimensions of the corrugated sheet part with small radius are shown in Figure 2.10 (b), where the width is 81 mm, the wall-thickness is 0.3 mm and the radius of all ripples with non-uniform depth is 2.3 mm.

With rigid punch forming, the wall-thickness of parts would thin severely and even fracture at corrugated surfaces during forming, because the wall-thickness is much smaller that the match tolerance between the rigid punch and the female die and the friction between rigid punch/female die and sheet blank would be harmful to sheet blank deformation unless with rigid punch/female dies within a close tolerance. With rubber or polyurethane flexible punch forming, corrugated surfaces could not be formed with the requirements of dimensional accuracy due to resistance limits of rubber or polyurethane. With VPF, the dimensions of small radius corrugated surface can meet the requirements of dimensional accuracy.

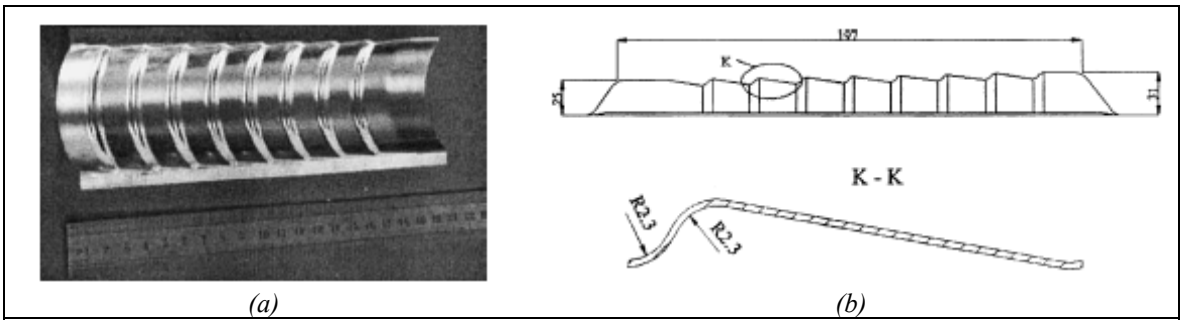

Figure 2.10: (a) Corrugated thin-walled sheet part with small radius; (b) main dimensions of the experimental VPF corrugated thin-walled sheet part with small radius.

Obtained results show that the load relationship between viscous medium pressure and BHF affects the rate of sheet blank drawn into a die. On the condition of the same forming pressure, if BHF is too low, the flange of the sheet blank wrinkles easily when the sheet blank

is drawn into the die, then the viscous medium will leak, if BHF is too high, deformation of the flange of sheet blank is restricted. Under ideal BHF, sheet blank can be drawn into the die easily and the flange of the sheet blank does not wrinkle, wall-thickness reduction of sheet blank will be a minimum. The two type of viscous medium pressures versus BHF curves obtained by experiment are shown in Figure 2.11. The specimens obtained with the two types of load curves mentioned above are shown in Figure 2.12. The dimensional accuracy of specimens obtained with load curve 1 meet the requirements. The effects of load relationship between viscous medium pressure and BHF on dimensional accuracy of specimens indicate the same tendency to both superalloy and stainless steel.

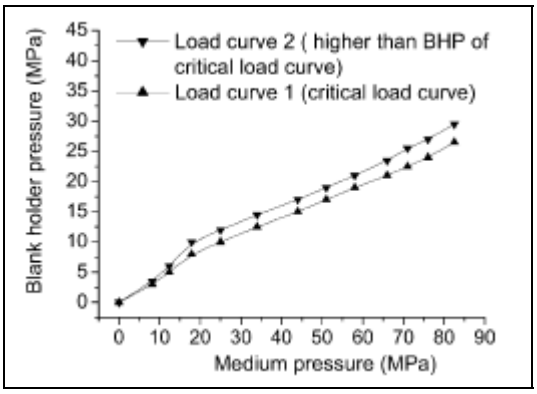

Figure 2.11: Relationship curves between the viscous medium pressure and BHF.

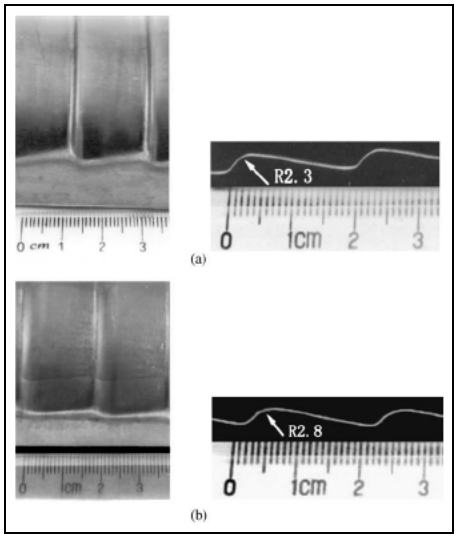

Figure 2.12: Corrugated surface shape of superalloy specimens with the two load curves of Figure 2.11: (a) with load curve 1; (b) with load curve 2.

In conclusion, the load relationship between viscous medium pressure and blank holder force (BHF) affects the dimensional accuracy and quality of parts. There is an optimal (or ideal) load relationship for a certain sheet material, which is the smallest in load relationships at any given time during the forming process and does not brings to defects such as wrinkling, fracturing, larger wall-thickness reduction and inaccuracy of dimensions etc. Non-optimal load relationship curves could result in the flange wrinkling of sheet blank and viscous medium

leaking, fracturing and inaccuracy of dimensions. The optimal load relationship curves for different strength materials such as superalloy and stainless steel have the same varying tendency.

2.1.4 FEM simulations of the VPF process

A successful simulation of VPF should include the modelling of bulk forming of the viscous medium, forming of the sheet and the interface between them.

Liu et al. [5] chosen the finite element code DEFORM in order to carry out a preliminary numerical simulation of the viscous pressure forming process. In their work, a round part geometry similar to Limiting Dome Height (LDH) test was used with the following process parameters:

- Friction: μ_m= 0.2 at medium/sheet interface,
  μ_s = 0.09 at sheet/die interface.
- Sheet blank (AA2008-T4): R 66.3 x 1 mm.

2.1.4.1 Effect of viscosity of the medium

In [5] the effect of viscosity of the medium on the VPF forming process was investigated by numerical simulations using the geometry shown in Figure 2.13 and considering the viscous medium acting on top of the sheet only. There was no outlet in the die. The stretching of the sheet metal parts was simulated by using two different viscous media, i.e. C-21 (η = 5000 Pa·s) and C-11 (η = 10000 Pa·s). Figure 2.14, which graphs obtained results, shows that with a lower viscosity medium (C-21), the stretching is more uniform and no local necking is observed, which is similar to the hydroforming (Figure 2.3 (a)). When higher viscosity medium (C-11) is used, there is a larger traction on the interface between the sheet and the medium (Figure 2.14 (b)). In this case, the local necking of the sheet metal occurs at the early deformation stage, which is similar to the matched tooling stamping.

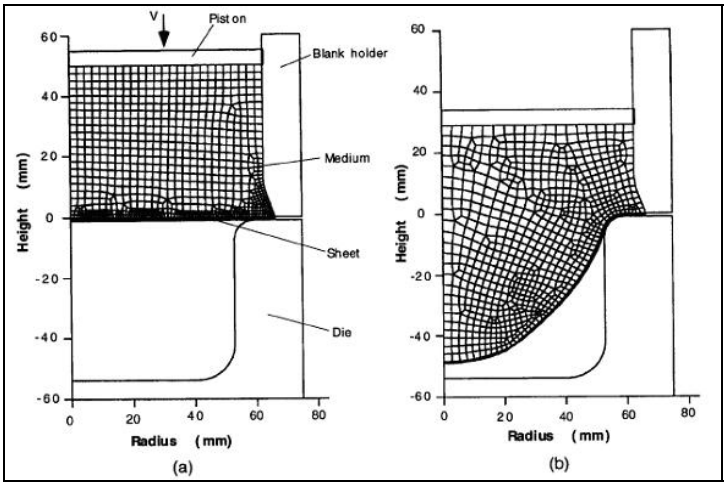

Figure 2.13: Deformation of the sheet and the medium in VPF stretching (medium on top of the sheet only).

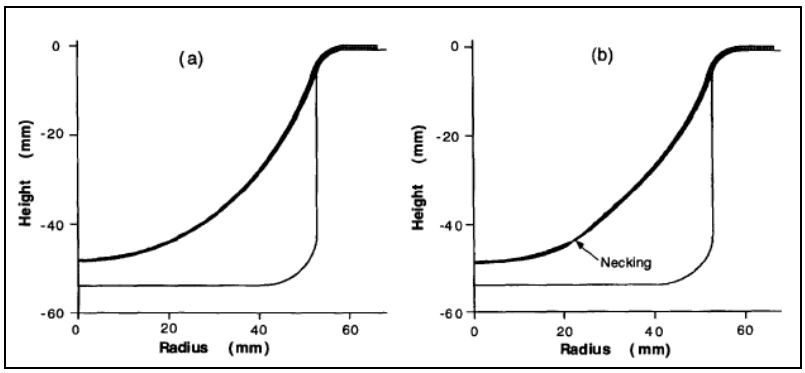

Figure 2.14: Effect of the viscosity on the sheet deformation in VPF stretching where viscous medium is on top of the sheet only: (a) lower viscosity (C-21, η = 5000 Pa·s) and (b) higher viscosity (C-11, η = 10000 Pa·s).

2.1.4.2 Effect of location of the outlet port

In VPF, compared with the conventional sheet forming process, the sheet metal can be formed in a definite sequence through controlling the pressure distribution of the viscous medium. The pressure distribution of the viscous medium is non-uniform: different pressure distribution models can be set by controlling the position of the inlet ports and outlet ports of the viscous medium. The non-uniform pressure is favourable to the forming of complex-shaped parts.

In order to investigate the effect of location of the outlet port in the VPF process, Liu et al. [5] carried out numerical simulations on two parts stretched by C-11 medium with two different locations of the outlet (Figure 2.15). The geometry of FE models and process parameters are described in §2.1.4. The viscous medium was placed both on top and bottom of the sheet.

When the outlet is located at the centre of the die, the viscous medium is trapped around the die corner. When the outlet is located at the corner of the die, the viscous medium is trapped at the narrow space between the sheet and the die flat bottom surface. Therefore, the sheet can not completely contact the die surface. The trapped medium between the bottom side of the sheet and the die flat bottom surface is like a lubricant which allows the sheet to stretch easily.

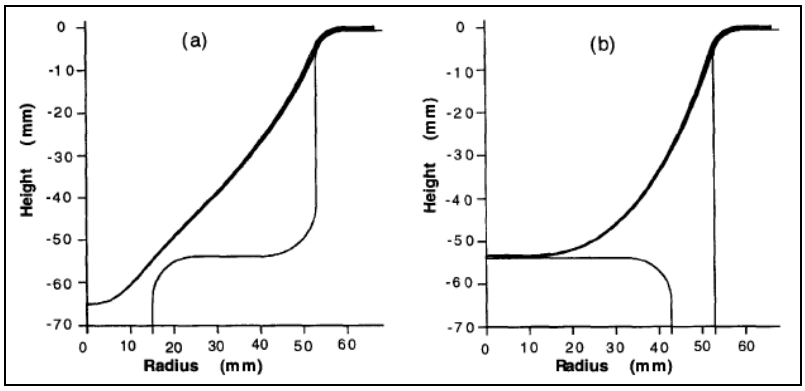

Figure 2.15: Part geometry stretched by C-11 medium: (a) central outlet, and (b) comer outlet (Medium C-11 on both sides of the sheet).

In conclusion, numerical simulation results show that the position of the outlet ports of the viscous medium has an important effect on viscous medium drawing. Different-shaped parts can be obtained when the outlet is located at the centre or corner of the die. The formability of the sheet metal can be improved by reasonable locating the outlet port of the viscous medium.

2.1.4.3 Effect of the medium on one side only or both sides of the sheet

In [5] Liu et al. found out that when the viscous medium is introduced not only on the top (Figure 2.16 (a)) but also on the bottom of the sheet (Figure 2.16 (b)), the sheet has a larger uniform deformation as compared to the case where the medium is only on the top of sheet (Figure 2.17).

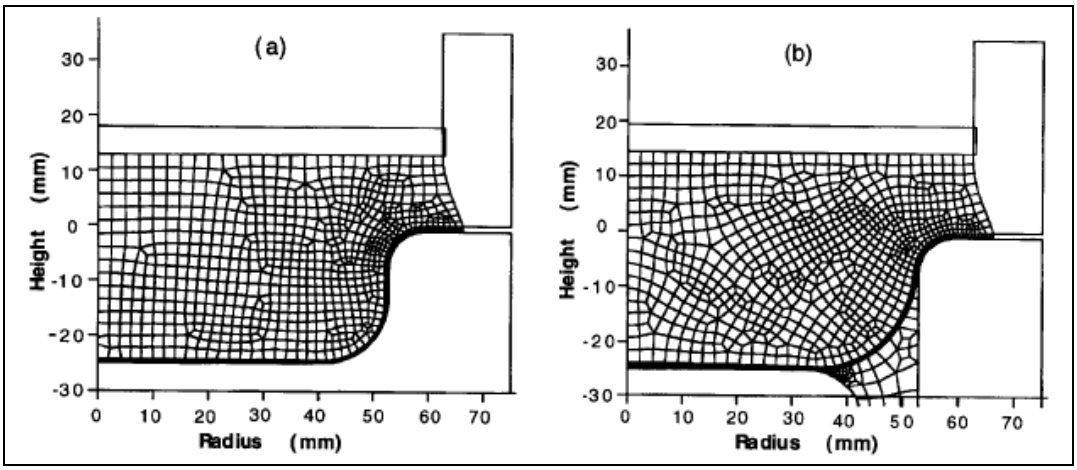

Figure 2.16: Deformation of the sheet and the media in VPF stretching with a shallow die: (a) C-11 medium on top of the sheet only, and (b) C-11 medium on both sides of the sheet.

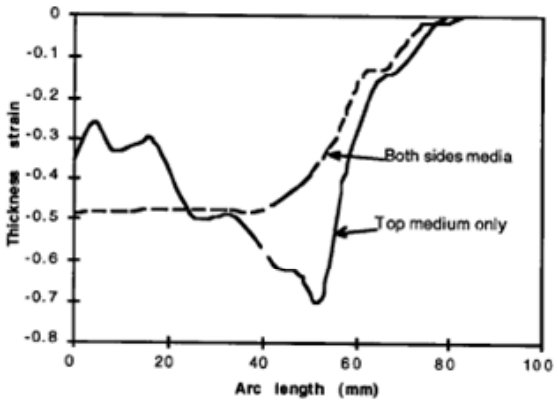

Figure 2.17: Thickness strain distributions in the sheet stretched by (a) medium on top only, and (b) medium on both sides of the sheet (Arc length is the length along the deformed sheet).

2.1.4.4 Effect of the friction at medium/sheet interface

In order to study the effect of the friction (different friction coefficients and friction models) at the interface between the sheet and the viscous medium on the sheet deformation, three different cases were simulated by Liu et al. in [5], i.e.:

- (a) Coulomb friction coefficient, $\mu = 0.2$, with $\tau = \mu \cdot \sigma_n$, where τ is shear stress and σ_n is normal stress at the interface,
- (b) Coulomb friction coefficient, $\mu = 0.02$, and
- (c) Shear friction factor, $m = 0.4$, with $\tau = m\,\sigma_f / \sqrt{3}$, where σ_f is flow stress.

In all cases, the Coulomb friction coefficient at the interface between the sheet and the die was assumed to be $\mu_s = 0.09$. The medium was on both sides of the sheet (Figure 2.16 (b)).

The thickness strain distributions in the sheet under three different friction conditions are shown in Figure 2.18. It was found that the thickness strain decreases with increasing friction values. The traction at the medium/sheet interface was larger if the friction was larger. However, the differences were small.

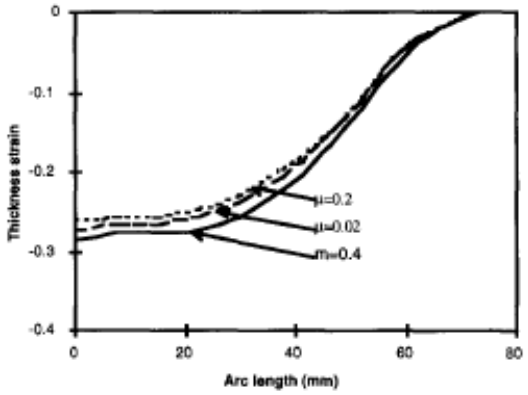

Figure 2.18: Sheet thickness strain distributions for different friction at medium/sheet interface in VPF stretching ($\mu_s = 0.09$ at sheet/die interface).

In conclusion, increasing the tangential adhesive stress, the thickness distribution of the sheet specimens tends to become uniform. However, Jianguang et al. in [10] found out that when the tangential adhesive stress exceeds some critical value, the thickness distribution of the sheet specimens become more non-uniform (Figure 2.19).

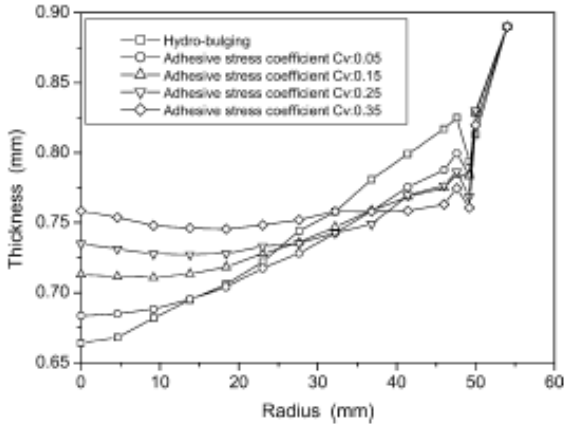

Figure 2.19: Thickness distribution curves of sheet specimens obtained by the numerical simulation of VPF bulging.

2.1.4.5 FEM simulation of VPF of corrugated thin-walled sheet part with small radius

In [11] Wang et al. used the code DEFORM in order to simulate the forming process by VPF of the thin-walled corrugated part described in §2.1.3.2.

In every corrugation segment, the maximum strain occurs at the centreline of the transverse section. One corrugation segment was selected to simulate the deformation process. The velocity of the rigid punch or piston (in VPF) was 0.1 mm/s. The value of friction coefficient μ and friction factor m was 0.4 and 0.01, respectively. The models used in the numerical simulation are shown in Figure 2.20.

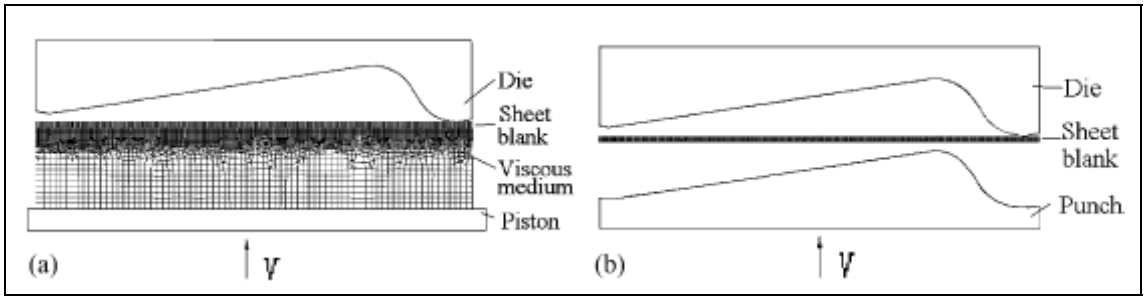

Figure 2.20: Finite-element simulation models of a superalloy thin-walled corrugated part: (a) VPF; (b) metal punch forming.

The comparison of the deformation process of the superalloy thin-walled corrugated part with VPF and with metal punch forming is shown in Figure 2.21.

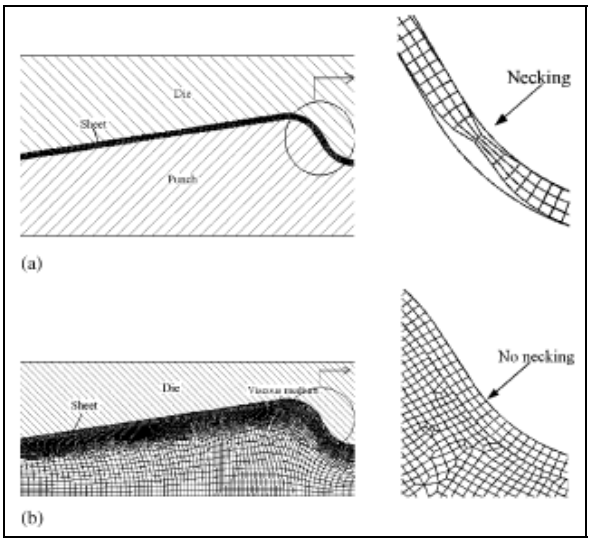

Figure 2.21: Comparison of the deformation process of a superalloy thin-walled corrugated part: (a) with rigid punch forming; (b) with VPF.

Under all friction conditions with rigid punch forming, severe wall thickness reduction and necking occur between two surfaces of r = 2.3 mm, but this defect is avoided with VPF. Under the condition of VPF, the wall thickness reduction becomes small with the increment of friction factor. It can be seen that VPF is more suitable for the manufacturing of high strength and hard-to-form materials such as superalloy than rigid punch forming.

2.1.4.6 FEM simulation of viscous pressure forming dome test

In [12] Liu et al. simulated by the finite element-based code DEFORM the process of sheet stretching with VPF (similar to hydrostatic bulge test) and compared the numerical results with the experimental measurements.

A set of VPF tooling was installed into an hydraulic press (Figure 2.22).The viscous medium is filled in the chambers of the lower and/or upper die. The sheet metal is clamped by the upper and lower dies through the cushion force provided by cushion pins. Thus, the sheet material is only allowed to stretch but not draw-in. When the ram moves down, the piston pushes the medium into the lower die chamber upwards and pressure is generated within the medium. This pressure acts on the lower side of sheet surface, and then the sheet is stretched. The medium in the upper die is compressed and a counter pressure is generated on the upper side of the sheet surface as the ram moves down. This counter pressure can be controlled by changing the restrictive setting of the outlet nozzle. After forming, the ram moves up and the sheet metal part is removed from the upper die.

In order to compare the VPF dome tests with the hemispherical punch dome tests, the viscous medium is filled only into the chamber of the lower die in the VPF experiments and simulations. The upper die is empty. The process parameters used in the simulations are listed in Table 2.1. The viscous medium C-11 was employed in the simulation and experiments. The flow stress of the medium was determined using extrusion tests in conjunction with FEM simulations [5], (Figure 2.23 and Figure 2.2 (a)).

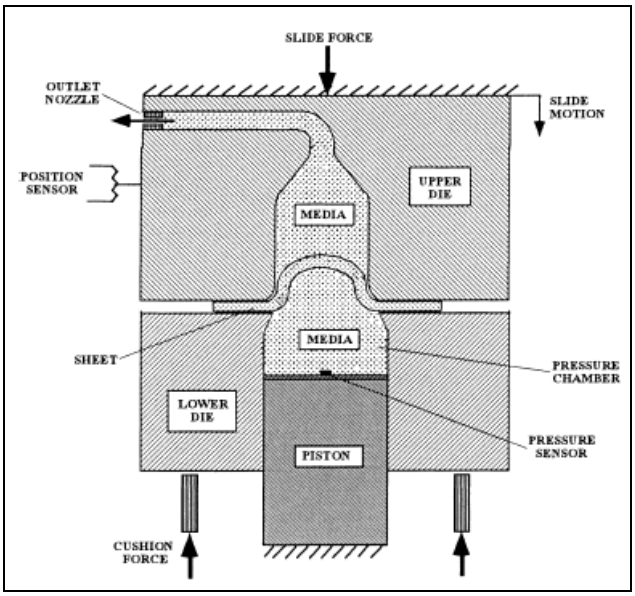

Figure 2.22: Sketch of the VPF dome test tooling.

Table 2.1:Process parameters used in the simulation of VPF dome test.

Piston velocity	V=20 mm/s
Friction at sheet/media interface	Shear friction factor, m=0.2, with $\tau = m\bar{\sigma}/\sqrt{3}$, where $\bar{\sigma}$ is the flow stress
Friction at sheet/die interface	Coulomb friction coefficient, μ=0.09, with $\tau=\mu\sigma_n$, where τ is the shear stress, and σ_n is the normal stress at the interface
Sheet blank (Al 6111-T4)	Flow stress: $\bar{\sigma} = 533\bar{\epsilon}^{0.238}$ (MPa), diameter: 132.6 mm, thickness: 1 mm
Boundary condition	Locked
Working media	C-11

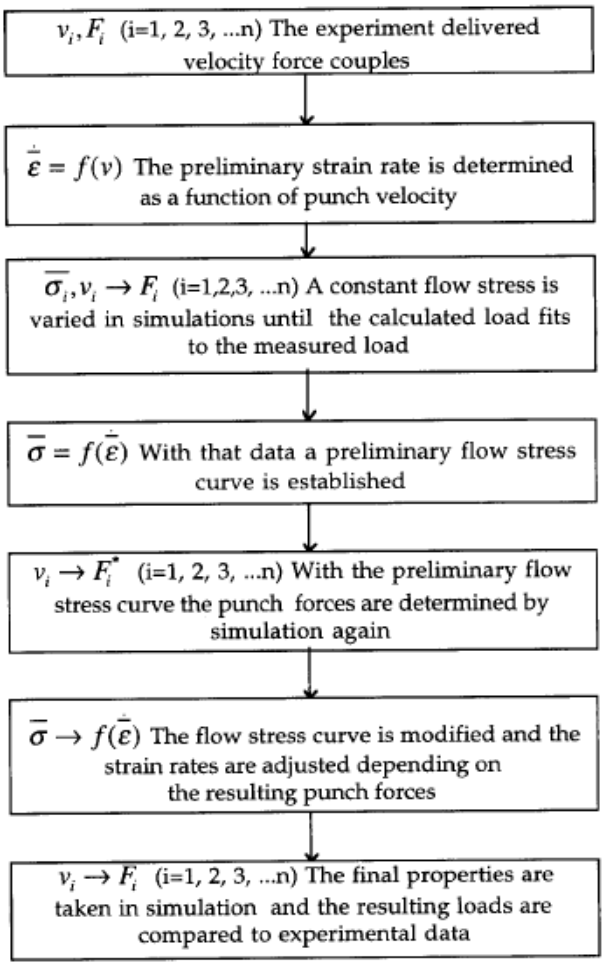

Figure 2.23: Procedure to determine the flow stress of viscous medium by using a combination of extrusion test and FEM simulation.

In the DEFORM simulations, the viscous medium was only introduced into one side of the sheet surface, i.e. piston side (in the simulations piston side was placed on the top position), and it was meshed with about 1000 quadrilateral elements. In its thickness direction,

the sheet was divided into two layers of elements and it was meshed with about 250 quadrilateral elements. The FEM model used in the simulation is shown in Figure 2.24 (a).

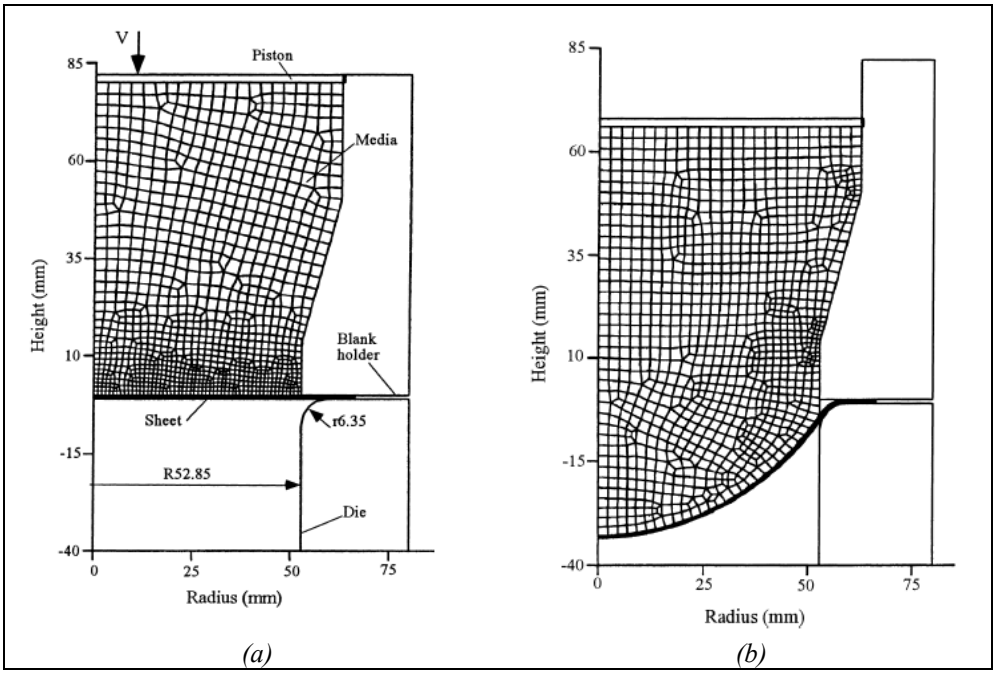

Figure 2.24: (a) FEM model used in DEFORM simulation; (b) Viscous medium and sheet deformation at dome height of 33 mm.

The deformation of the viscous medium and the sheet in the VPF dome test is shown in Figure 2.24 (b). Both, predicted and measured thickness distributions, were obtained at a dome height of 33 mm. The thickness strain distribution in the dome part is shown in Figure 2.25. It is seen that the FEM predictions are in good agreement with the experimental measurements. Due to low friction that exists at the viscous medium/sheet interface, the sheet thickness decreases uniformly from die corner to the centre of the dome. The maximum thinning occurs at the centre of the dome. These results are very similar to those observed in hydraulic stretch forming test. The sheet thickness decreases locally at the die profile radius due to bending of the sheet.

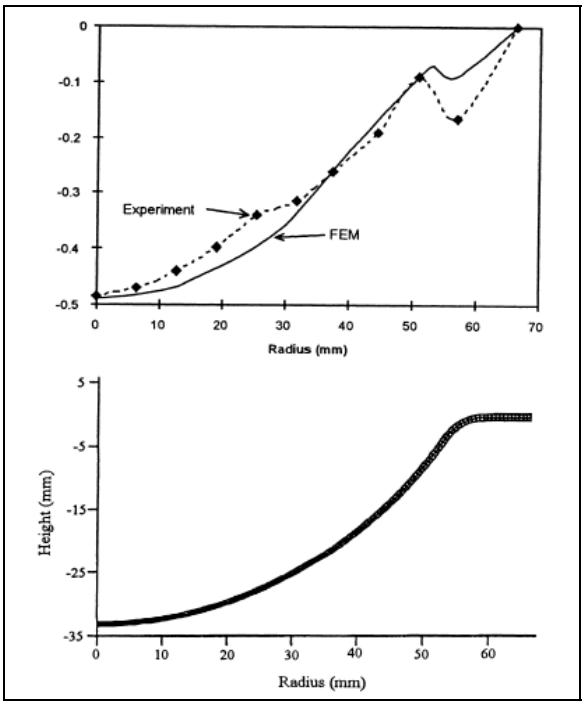

Figure 2.25: Thickness strain distribution on the sheet at dome height of 33 mm in VPF stretching.

The forming pressure vs. piston stroke curves obtained from the DEFORM simulations and experimental measurements in VPF stretching are shown in Figure 2.26. It is seen that the simulation result is overall in good agreement with the experimental data.

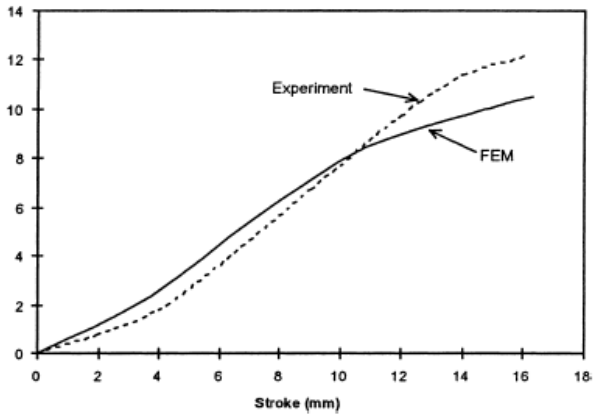

Figure 2.26: Forming pressure vs. piston stroke in VPF stretching.

2.1.4.7 FEM simulation of VPF applied to the forming of a non-symmetric part

In [13] Ahmetoglu et al. carried out a comparison between numerical predictions and experimental results of the application of VPF to the forming of the non-symmetric part shown in Figure 2.27 (a). The experimental apparatus was the same described in §2.1.4.6.

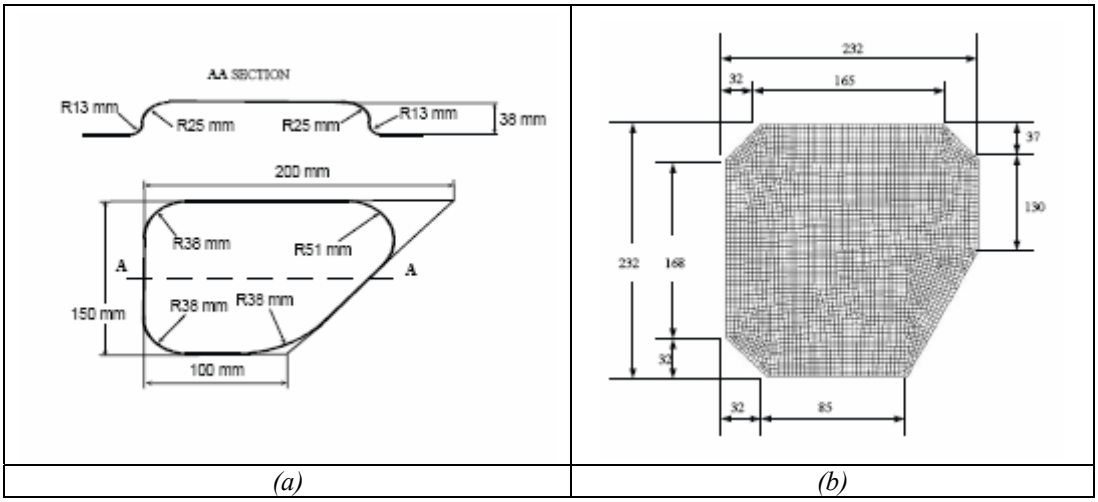

Figure 2.27: Part and blank geometries used in both simulations and experiments: (a) part geometry; (b) blank geometry (dimensions are in "mm").

The material of the sheet metal blank was a AKDQ steel, which mechanical properties are summarized in Table 2.2.

Table 2.2: Mechanical properties of the AKDQ steel.

AKDQ steel:	
Initial thickness, t_0	0.76 mm (0.03 in.)
Young's modulus, E	200 GPa (29×10^6 psi)
Poisson's ratio, γ	0.3
Tensile strength, $\sigma_u(R_m)$	345 MPa (50,000 psi)
Yield strength, $\sigma_y(R_{p\,0.2})$	171 MPa (24,800 psi)
Flow stress, $\bar{\sigma} = K\bar{\varepsilon}^n$	$K = 536$ MPa (77,720 psi), $n = 0.227$
Anisotropy	$r_0 = 1.8$, $r_{45} = 1.29$, $r_{90} = 2.1$

The viscous medium used in this study is marketed under the commercial name C-11. The VPF medium was modelled as a "Newtonian" fluid, i.e. a strain-rate no-sensitive material, due to its rather complicated and poorly understood material properties. The flow stress of a Newtonian fluid can be expressed as:

$$\sigma = k \cdot \dot{\varepsilon} \quad \text{(MPa)}$$

where $k = 3\eta \times 10^{-6}$, η is the viscosity of the medium (Pa·s). The viscosity of the C-11 medium used in the present study was 10,000 PaS [14].

The numerical simulations were conducted using the FEM code PAM-STAMP. The FEM model used in these simulations is shown in Figure 2.28. Sheet metal was modelled using shell elements and the VPF process was modelled as sheet hydroforming, i.e. the viscous material was considered to be incompressible and to flow like water. This approximation was necessary because the software PAM-STAMP, used for simulating metal flow in sheet forming, could not account for the compressibility and viscosity of the VPF medium used in this study. The Coulomb's friction coefficient at the sheet/binder interface was set to be 0.06.

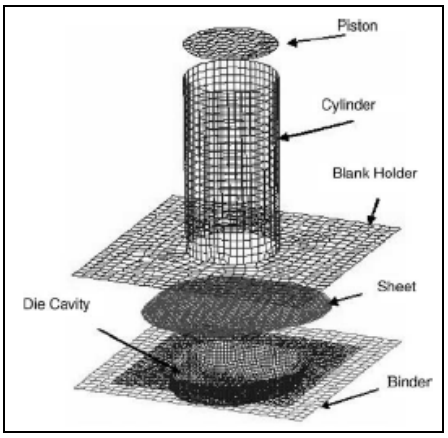

Figure 2.28: FEM model for the VPF simulations.

The final part geometry predicted by FE simulations is shown in Figure 2.29. The pressure profile measured during the experiments was compared with the pressure profile obtained from simulations as shown in Figure 2.30. There is a sharp drop in the experimentally measured pressure value at the end of the stroke. This may be due to the viscous nature of the medium, which may undergo elastic recovery as soon as the press is stopped.

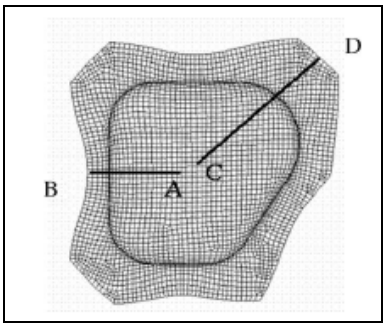

Figure 2.29: AKDQ steel part geometry as predicted by PAM-STAMP.

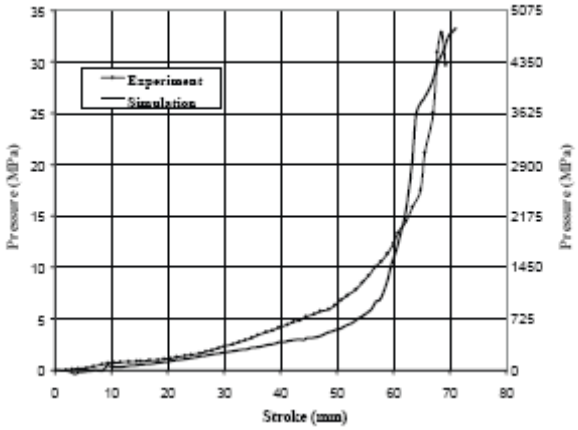

Figure 2.30: Variation of viscous medium pressure with press stroke in VPF of AKDQ steel.

Thickness measurements and predictions along AB and CD directions (Figure 2.29) are shown in Figure 2.31 (a) and Figure 2.31 (b), respectively.

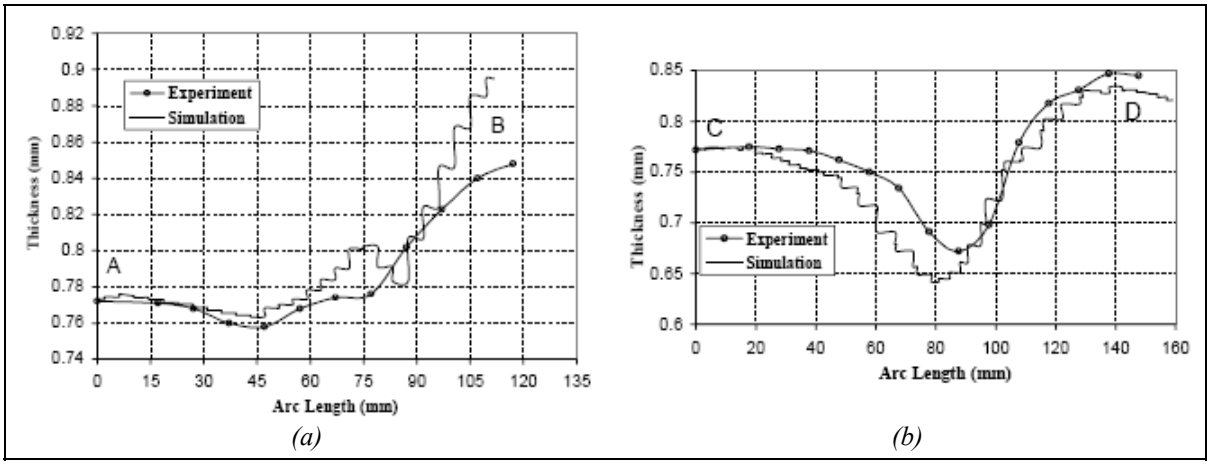

Figure 2.31: Thickness distribution of AKDQ steel along: (a) AB direction (see Figure 2.29); (b) CD direction (see Figure 2.29).

The same FEM model used for the AKDQ steel part was used to perform a numerical simulation of a part made by Inco 718 SPF alloy. Mechanical properties of this material are reported in Table 2.3.

Table 2.3: Mechanical properties of the Inco 718 SPF alloy.

Inco 718 SPF:	
Initial thickness, t_0	0.76 mm (0.03 in.)
Young's modulus, E	200 GPa (29×10^6 psi)
Poisson's ratio, γ	0.294
Tensile strength, $\sigma_u(R_m)$	1350 MPa (195,800 psi)
Yield strength, $\sigma_y(R_{p\,0.2})$	730 MPa (105,850 psi)

The anisotropy coefficient for this material was not available. Flow stress data for Inco 718 SPF is as follows:

Strain	Stress (GPa/ksi)
0.075	0.80/116
0.1	0.86/125
0.2	0.97/141
0.3	1.025/149
0.4	1.035/150

VPF of the non-symmetric part from Inco 718 SPF was compared to solid punch forming in computer simulations. The same die that was used in VPF simulations was also used in solid punch forming simulation. However, in this case, instead of the viscous medium, a solid punch was generated from the part geometry taking the sheet thickness into consideration and used to form the sheet metal. The punch travel was limited by the part height and the final part geometry was the same as that formed in VPF. In the solid punch forming simulations, the friction coefficient at both sheet/die and sheet/punch interfaces were set to 0.06 and 0.12 in. two different simulations. The thickness predictions from these simulations were compared to the thickness predictions obtained from the VPF simulation as shown in Figure 2.32: Predicted thickness distribution along C–D direction (see Figure 2.29) for the non-symmetric part in VPF and solid punch forming simulations..

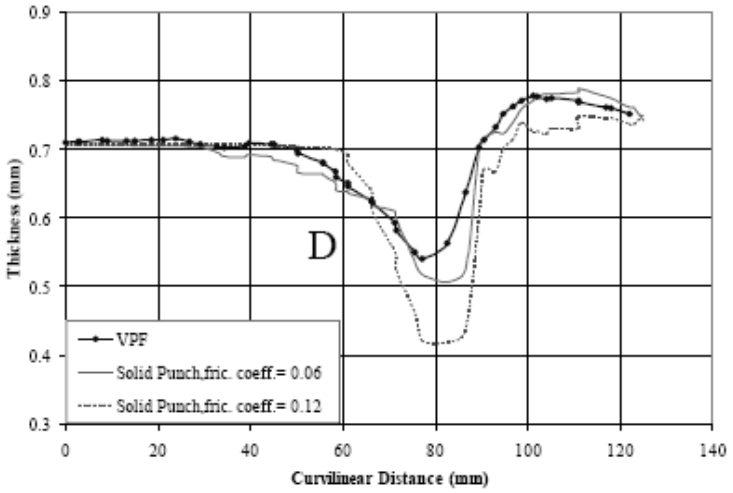

Figure 2.32: Predicted thickness distribution along C–D direction (see Figure 2.29) for the non-symmetric part in VPF and solid punch forming simulations.

The thickness distribution obtained in the solid punch forming simulation with a friction coefficient of 0.06 is close to the VPF results. However, due to additional friction surface at

the sheet/punch interface (which did not exist in VPF) the thickness distribution is not uniform and the maximum thinning is larger. In conventional deep drawing with a regular drawing lubricant, the friction coefficient will be closer to 0.12. In this case, due to higher friction coefficient at the sheet/punch interface, the sheet metal over the flat punch is not stretched as much, and therefore, the maximum thinning in the part is increased.

The stress state of the sheet metal with VPF and steel punch forming are shown in Figure 2.33: Stress state of the sheet blank by: (a) VPF; (b) rigid punch forming.. The stress state of sheet metal with VPF can avoid inner wrinkling that is brought about with steel punch forming [15].

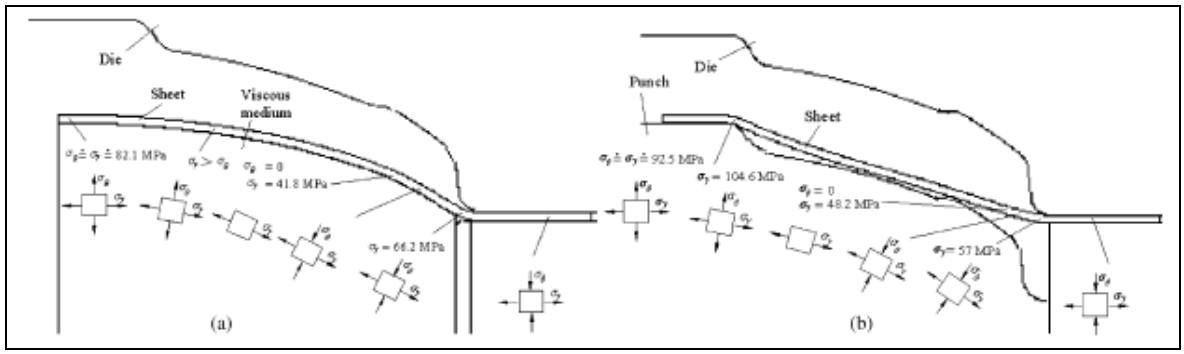

Figure 2.33: Stress state of the sheet blank by: (a) VPF; (b) rigid punch forming.

2.2 The Polymer Injection Forming process

Polymer Injection Forming (PIF) is a new technology to manufacture sheet metal/polymer macro-composite components in one-operation production process. During this process, a metal blank is shaped inside an injection mould by using the injection pressure of the molten polymer.

The sheet metal blank is held in position along its edge by means of the clamping unit of the injection moulding machine. Then plasticized polymer melt is injected from the nozzle of the injection machine and flows along the sprue gate of the mould. It forces the sheet metal blanks to deform according to the contour of the mould cavity. The higher the pressure of the polymer melt, the more deformation the sheet metal blank suffers, and the greater the contact areas between the sheet metal blank and the mould cavity. The greater the contact area, the higher the pressure of the polymer melt that can be built up in the deformed sheet blank. It is an interrelated process. Thus, the PIF technology is a combination of the injection moulding and sheet metal forming processes.

After the injection stage, the polymer melt cools down and transforms into the solid state gradually, during which it adheres directly to the surface of the deformed sheet metal blank. Thus a macro-composite component, with a sheet metal part and a plastic part is fabricated. The final shape of the sheet metal part is determined by the mould cavity. The space between the deformed sheet metal part acts as the moulding cavity of the polymer melt.

By means of this technology, a fully finished metal/polymer macro-composite part is manufactured in only one production step.

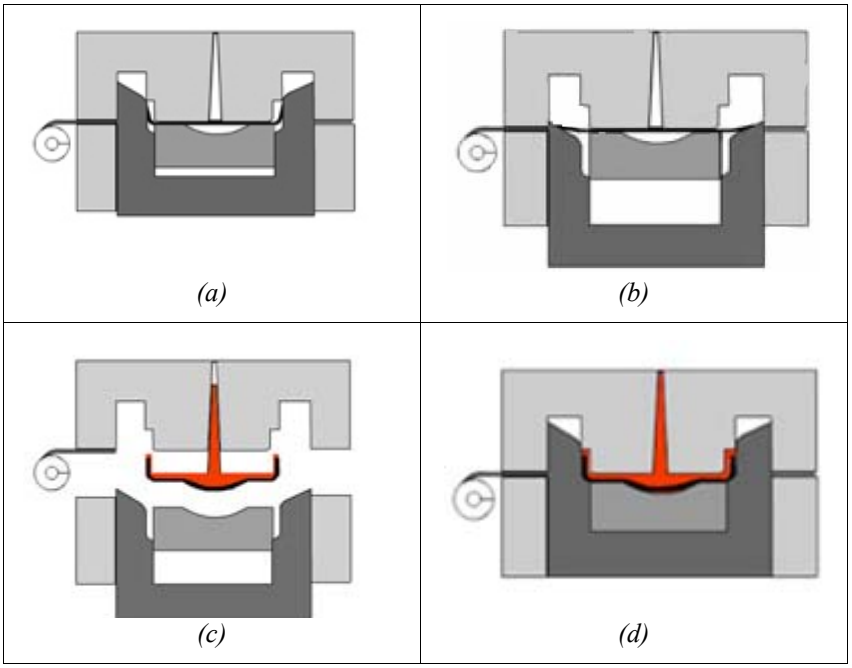

Figure 2.34: Polymer Injection Forming process sequence[16].

The process sequence is described in Figure 2.34:

a) A metal sheet is inserted between the open halves of a mould.
b) When the mould closes, the metal sheet is cut to the desired blank size. During the same operation the blank can be shaped by deep drawing or by bending the sheet metal into the basic product shape.
c) When the mould is completely closed, the polymer is injected into the remaining cavity and a second, hydrostatic, deformation step is applied to shape the metal sheet into its definite form. In this phase of the PIF process, the physical adhesion between the metal sheet and the injected polymer is obtained.
d) Finalising the production cycle, the product is ready and is removed from the mould.

PIF not only reduces the number of needed production steps, but also facilitates easy assembly because the technique offers great opportunities in embedding several product functionality features into one product. Since sheet metal-polymer macro composites combine the beneficial properties of both metal and polymer, products manufactured by means of the PIF process:

- Have the stunning look and feel of metal products.
- Possesses the flexibility and freedom of form of injection moulded products.
- Can be embossed with a tactile texture, pattern or logo using the injection pressure of the molten polymer. This makes Polymer Injection Forming ideal for mass customisation of products.
- Can be easily printed on, making use of natural gloss of the metal sheet to enhance the aesthetics appearance of the product.

- Ensure full product safety, because the polymer not only adds a corrosion resistant layer to the metal sheet, but also covers the edge of the metal sheet.
- Possess the material properties, such as magnetic and thermal conductivity as well as the shielding of electro magnetic currents produced by mobile phones [17].

2.2.1 Numerical simulations of the PIF process

In [18] Chen et al. presented a new manufacturing approach, and the correlated numerical simulation, for a macro-composite component with two sheet metal parts with a sandwiched plastic part between them. Figure 2.35 shows a schematic diagram of the manufacturing approach and the macro-composite component formed by this approach.

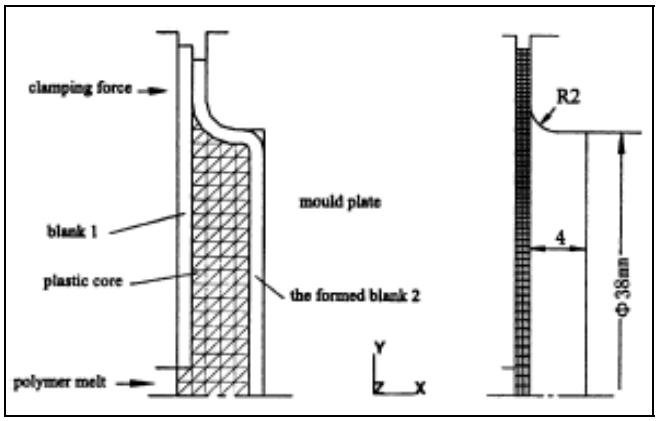

Figure 2.35: Schematic diagram of metal/polymer macro-composite component, the manufacturing approach and the finite element meshes.

The two sheet metal blanks are held together along their edges through the clamping operation of the mould on an injection machine. Then the melted polymer injected from the nozzle of the injection machine forces the sheet metal blanks to deform according to the contour of the mould cavity.

Experiments were carried out using commercial, half-hard, pure aluminium circular sheet with 50 mm diameter and 1 mm thickness, and polyethylene on an injection machine.

Simulation of the forming process of blank 2 in Figure 2.35 was carried out using the MARC finite element code. The metal blank was treated as an axisymmetric problem. 4×65 elements were used to mesh the sheet blank with 65 elements along the radial direction and four elements through the thickness for good description of the bending effects. The element used was the two-dimensional, four-nodes, isoparametric, quadrilateral axisymmetric solid element (MARC element type 10) with four Gaussian integration points.

The mould plates were assumed to be rigid. Because of axisymmetry, the nodes at the central axis were not allowed to move in the Y-direction. The clamping depth of the sheet blank along its thickness by the clamping operation of the mould was 0.05 mm. The friction conditions at the interfaces of the sheet blank and the mould were described with a Coulomb model. The friction coefficients at the interfaces were set to be 0.05.

The sheet material was treated as elastic–plastic with isotropic hardening. Temperature effects of the polymer melt on the sheet blank were neglected because of the very short contact time between them before the pressure reaches its maximum value. The characteristic

parameters of the sheet metal material are Young's modulus of 70,000 MPa, Poisson's ratio of 0.33 and initial yield stress of 70 MPa. The yield condition according to Von Mises and the associated flow rule were used.

Since the duration of the filling and packing stages is around 1 s, and since the thermal conductivity of the molten polymer is extremely low, the stages may reasonably be assumed to be isothermal and the temperature change within the polymer melt can be neglected. In injection moulding, the polymer melt will lose its pressure to some extent, determined by variables such as the temperature of the mould and melt, injection rate, size of the flowing channels and properties of the polymer, etc., so the pressure of the polymer melt in the mould cavity is not constant for all positions of the cavity. The mould cavity is filled by polymer melt gradually.

According to Chen, this is not the case for manufacturing of the macro-composite components mentioned above. It is the polymer melt that forces the sheet blanks to deform, so there is no unfilled space left from the beginning. Hence a uniform pressure distribution within the deformed sheet blanks is assumed.

The pressure build-up in the polymer melt is shown in Figure 2.36. The time elapsed until the maximum pressure is reached is 1.3 s.

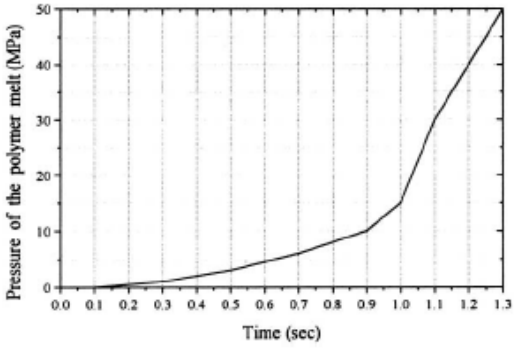

Figure 2.36: Pressure of the polymer melt in the deformed sheet blank.

Figure 2.37 shows the progress of deformation of the meshes of the sheet blank. The sheet blank begins to deform as the polymer melt is injected to contact with it. When the pressure of the polymer melt reaches almost 2 MPa, the sheet blank is deformed to touch the bottom of the mould. As the polymer melt is injected continually, it forces forming of the sheet blank to proceed. This results in an increase of the contact area between the sheet blank and the mould cavity. The greater the contact areas, the higher the pressure of the polymer melt needed for deformation of the sheet blank to proceed, and the higher the pressure that can be built up in the deformed sheet blank.

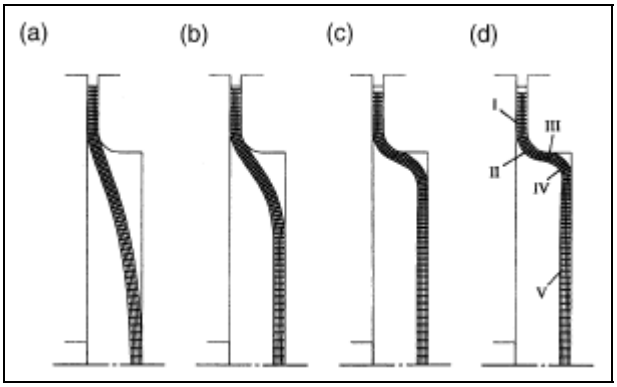

Figure 2.37: The deformed meshes of the sheet blank under different pressures: (a) 2 MPa, (b) 6 MPa, (c) 30 MPa and (d) 50 MPa.

Figure 2.38 shows the thickness distribution of the formed sheet blank by FEM simulation and experimental measurement. The two smallest thicknesses of the sheet blank after forming by FEM simulation are 0.725 mm and 0.738 mm. The two smallest thicknesses of the formed sheet blank by experiment are 0.643 mm and 0.702 mm, respectively, located at the same sites as in the FEM simulation. It was concluded that the simulated results agree with the experimental results.

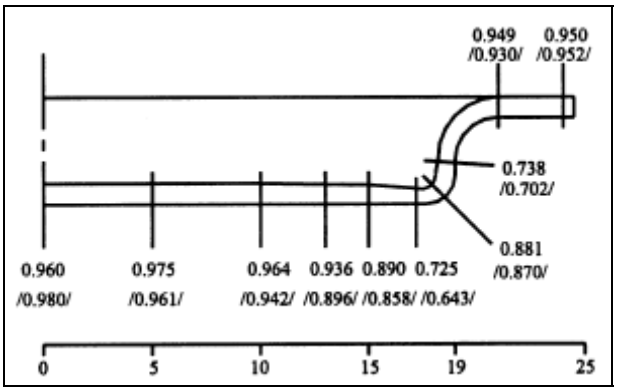

Figure 2.38: Thickness distribution of the formed sheet blank by FEM simulation and experiment (mm). Values within // are the experimental values.

CHAPTER 3

EXPERIMENTAL INVESTIGATION ON PIF PROCESS

As mentioned in the introduction, the main topic of the present work is both an experimental and numerical investigation on the new technology termed Polymer Injection Forming.

The experimental investigation of the deformation process of the sheet metal blank during the PIF process is the main topic of this chapter. In order to perform these tasks and determine the capabilities of the PIF process, a series of experiments was conducted at the *Net Shape Forming* Laboratory of DIMEG.

In this chapter a description of the apparatus used for accomplishment of the PIF process will be presented. The geometry of the mould cavity was well designed to achieve both efficacy and simplicity. Relative to efficacy, the mould geometry was designed in order to manufacture components which well summarized the main features of the metal-polymer macro-composite components which nowadays are produced by means of the traditional manufacturing technologies. Relative to simplicity, the mould geometry was designed in order to be easily modelled in the numerical simulation environment of the PIF process described in chapter 6.

Finally, the experimental tests carried out in order to investigate the influence of the main process parameters on the sheet metal formability will be illustrated. The metal blank formability was mainly evaluated measuring the thickness distribution curves of the deformed sheet metal parts. In this chapter it will be described also the measuring activities performed at the *Metrology* Laboratory of DIMEG by means of a CMM Prismo machine.

3.1 Experimental equipment

The experimental investigation of the PIF process was carried out at the *Net Shape Forming* Laboratory of DIMEG. A set of PIF tooling was built and installed into the ENGEL™ injection machine located at that laboratory. The experimental equipment consists as follows.

3.1.1 Injection Machine

The injection machine is an all-electric 1000 kN ENGEL™ injection moulding machine with a screw diameter of 40 mm (Figure 3.1).

Figure 3.1:The injection moulding machine at DIMEG Lab.

Connected to the machine are the drying unit of the row plastic material and two chillers which force water (up to a pressure of 5 bar and a temperature of 140 °C) into the cooling channels of the mould.

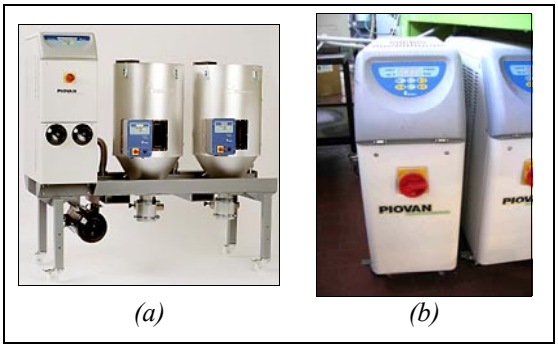

(a) *(b)*

Figure 3.2: (a) Drying unit; (b) cooling system of the mould.

3.1.2 Set of PIF moulds

The geometry of the mould cavity was designed considering both experimental and numerical requirements of the investigation carried out in the present work. The experimental approach requires that the component produced by the PIF process well summarized the main features of the metal-polymer macro-composites which are nowadays employed especially in automotive applications. In this manner it is possible to test the real capabilities of the process for industrial applications and productions.

On the other hand, considering the complexity of the process to be simulated, the numerical investigation described in chapter 6 requires the most simple FEM model. The simplicity of the geometry is preferred in order to efficiently set up an effective numerical environment for the simulation of the PIF process.

Due to the previous considerations, the designed test composite part is a rectangular cover plate with dimensions of 156 x 91 x 5 mm, which is made of a metal blank joint to a polymeric substrate (Figure 3.3 and Figure 3.4).

Figure 3.3: Test part (it can be seen the plastic and the metal parts, which are joined together to form the metal-polymer macro-composite, and the freeze sprue of the injection system of the mould).

Figure 3.4: Detail of the deformed sheet metal part of the test macro-composite.

The designed set of PIF moulds consists on three main parts which are assembled into a typical mould base for the traditional injection moulding process.

The three main parts are:

a) The injection system.

b) The fixed insert.

c) The mobile insert.

3.1.2.1 The injection system

The feed system enables the molten plastics to flow from the nozzle of the injection moulding machine to the mould cavity.

Shape and dimensions of the designed feed channel are shown in Figure 3.5.

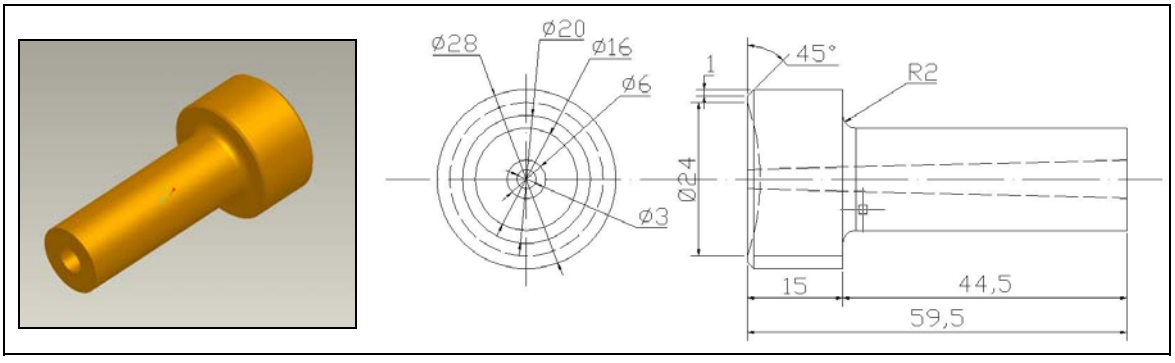

Figure 3.5: 3D model and dimensions of the feed channel.

3.1.2.2 The fixed insert

The space between the sheet metal part and the fixed insert acts as the moulding cavity of the polymer melt. At the beginning of each PIF cycle, the sheet metal blank is undeformed, so the moulding cavity of the melted polymer consists only on the cavity milled on this insert.

The fixed insert is screwed on the mould base and trough its centre hole the feed channel is well placed (Figure 3.6 (a) and (b)).

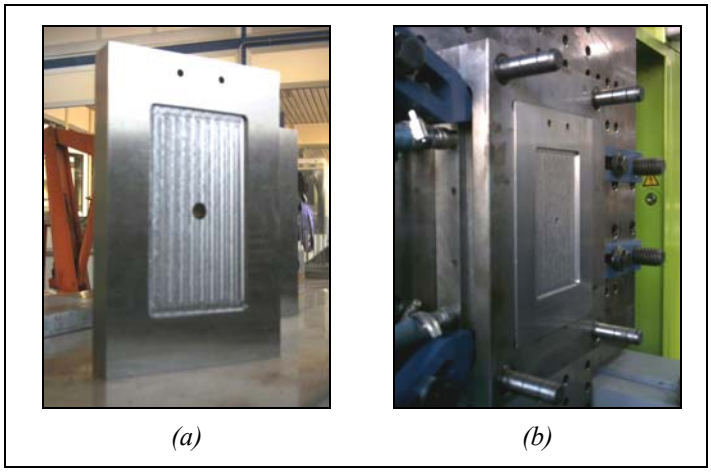

Figure 3.6: (a) Fixed insert; (b) fixed insert assembled into the fixed half of the mould base.

The holes of the cooling system of the mould can be seen in the working drawing of the fixed insert (Figure 3.7 (b)). In the same picture, the inside draft of 3° can be noticed. It is necessary in order to let an easy manual demolding of the component after each cycle.

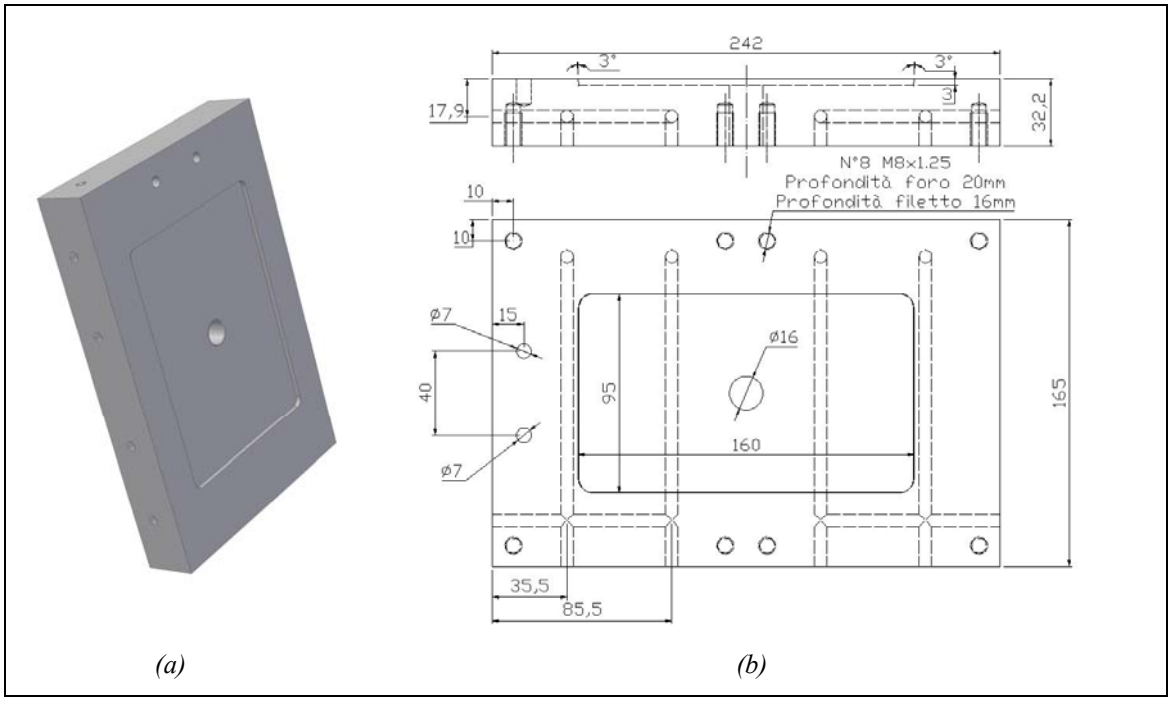

Figure 3.7: The fixed insert: (a) 3D model; (b) working drawing.

On the front side of the fixed insert (see Figure 3.7 (a)) two blind holes are visible. They are part of the positioning system of the sheet metal into the mould, as discussed in the following section.

3.1.2.3 The mobile insert

This insert is screwed on the mobile half of the mould base (Figure 3.8 (b)). During the PIF process, the sheet metal blank is forced to deform according to the geometry of the cavity of the mobile insert.

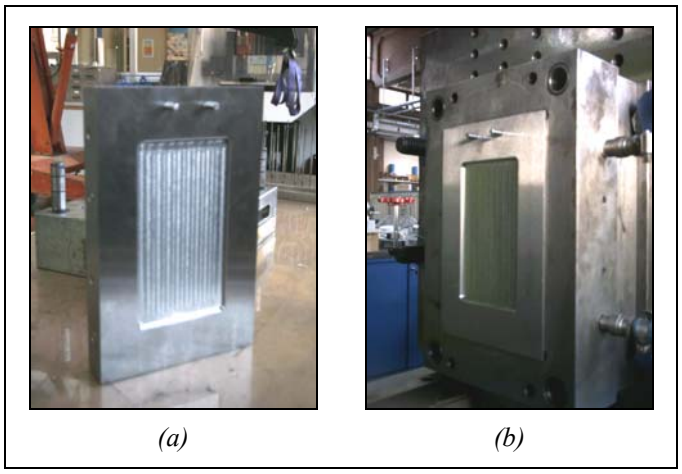

Figure 3.8: (a) Mobile insert; (b) mobile insert assembled into the mobile half of the mould base.

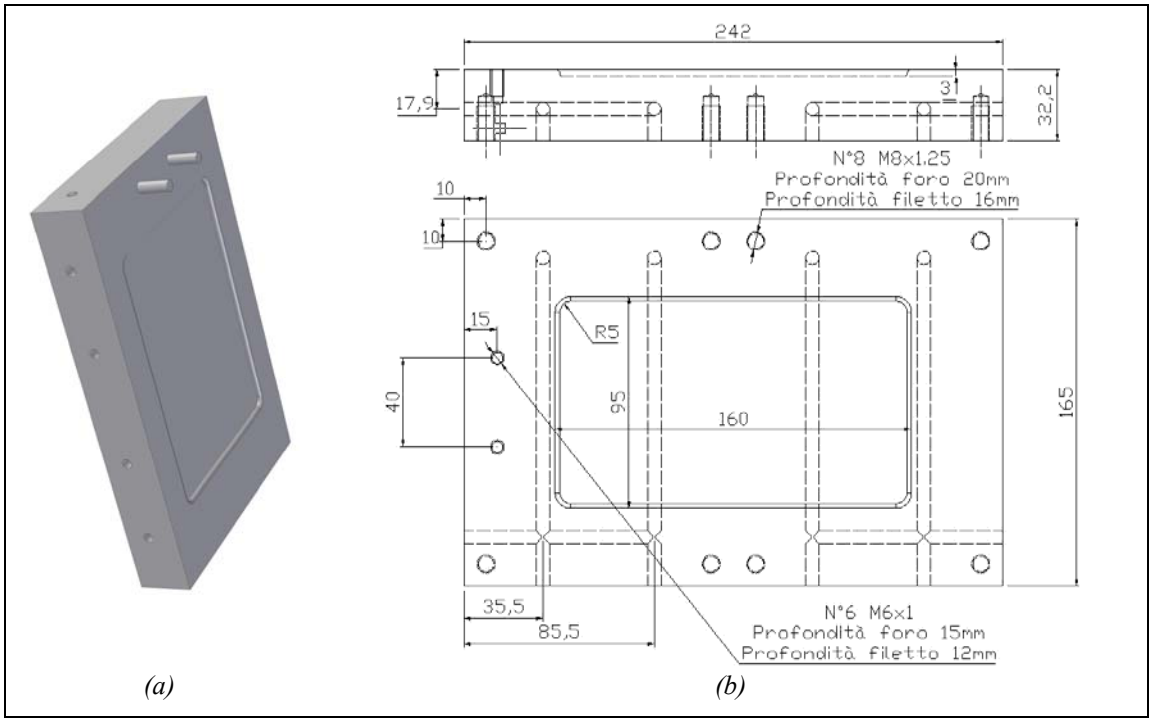

Figure 3.9: The mobile insert: (a) 3D model; (b) working drawing.

The cooling channels of this insert are placed symmetrically with respect to the fixed insert, in order to achieve a uniform cooling of the plastic part (see Figure 3.9 (b)).

In Figure 3.8 two pins are visible. They are screwed on the mobile insert and they are used in order to easy place and fix the sheet metal blank during the mould closing. When the mould is clamped, the pins enter into the two special holes on the fixed insert (Figure 3.7).

Figure 3.10 (a) is a cross sectional view of the fixed and mobile inserts, when they are clamped together without the sheet metal blank. Figure 3.10 (b) is the same view when the sheet metal blank is clamped between the two inserts.

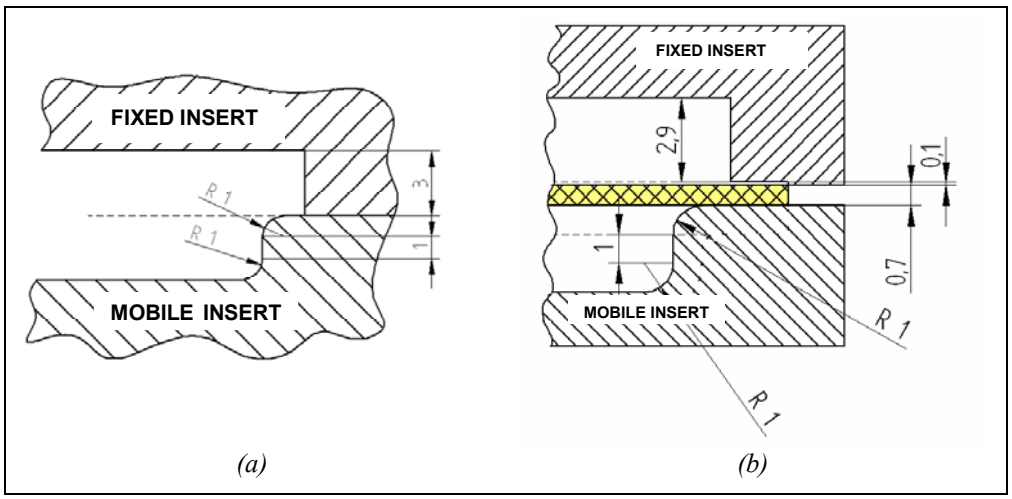

Figure 3.10: Fixed and mobile inserts clamped together: (a) without sheet metal blank; (b) with the sheet metal blank between them.

3.2 Experimental tests

This section is focused on the deformation process of the sheet metal blank during the PIF process. In particular, the influence of the main injection moulding process parameters on the sheet metal formability has been experimentally investigated according to the Design Of Experiments (DOE) method.

Two series of experimental tests were conducted and the results are presented in the following paragraphs. The first one was a screening DOE and it was aimed at decreasing the number of factors to investigate. The critical variables in the process were so found out. A second DOE was then carried out to get more detailed information and more in-depth insights in the Polymer Injection Forming process. In order to perform this task, a full 2^2 factorial design was employed and the effects of the critical variables were evaluated.

The employed metal blanks were rectangular sheets of 0.7 mm of thickness made by an AA1050-O aluminium alloy. The AA1050-O is an annealed aluminium alloy. It is particularly suitable to sustain high strains which are typical in deep stretching and drawing operations. Nowadays, this material is often employed in production of components for automotive applications. The approximate dimensions of the sheet blanks were 220 x 130 mm.

3.2.1 The first set of experiments

The objective of the first set of experiments was to define the most critical forming parameters in PIF. A screening DOE was utilized for the experimental plan. A five factor 2 level fractional factorial design (2^{5-1} DOE) in 16 runs and 3 replications was used. The experimental parameters varied were: polymer viscosity, injection speed, melt temperature, mould temperature and clamping force.

Polymer viscosity was varied by using two polypropylenes with different rheological characteristics, namely a HC115MO and a HJ320MO by Borealis, which have a MFR (230°C/2.16 kg) respectively of 4 and 55 g/10 min.

The design of experiment plan was based on standard statistical practice [19]. The two levels in the experiments were designated as high (+) and low (-). Each setting of high or low was based on work previously carried out in PIF at DIMEG. The specific settings are listed in Table 3.1.

Table 3.1: Factors levels for the screening experimental plan.

Factor	Unit	-	+
Viscosity	MFR (g/10 min)	4	55
Injection speed	mm/s	30	90
Melt temperature	°C	200	300
Mould temperature	°C	20	80
Clamping force	kN	10	100

The response to the experiment was a judgment of the mean quality of the formed sheet metal blank. The response was numerically evaluated from number 1 (bad or failed part) to number 4 (good part). An example of a failed and a good part is respectively shown in Figure 3.11 (a) and (b).

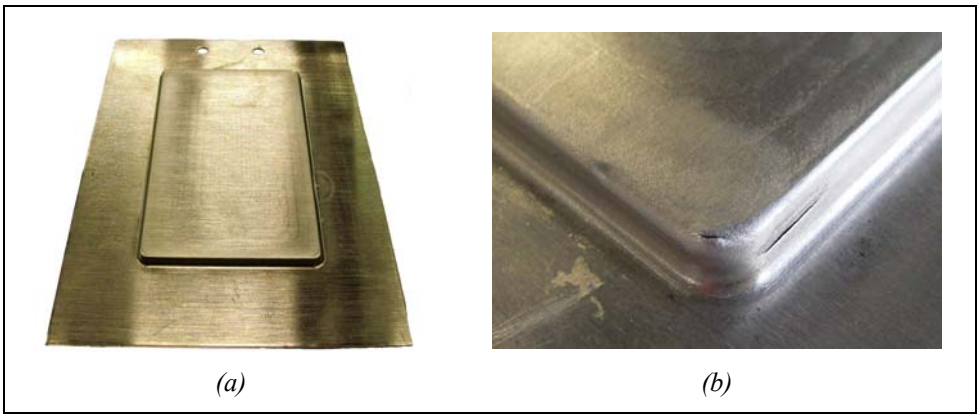

(a) *(b)*

Figure 3.11: Example of: (a) good deformed sheet metal part; (b) failed deformed sheet metal part.

The employed factorial designed and the obtained results are listed in Table 3.2. The response variable is the mean of the quality judgments for each of the three used replications.

Table 3.2: 2^{5-1} factorial design and obtained results.

Visc	In. Speed	T melt	T mould	Force	RUN 1	RUN 2	RUN 3	Mean of Quality
-1	1	-1	1	1	2	2	2	2
-1	-1	-1	1	-1	2	2	2	2
1	1	1	1	1	4	3	3	3,3
1	-1	-1	-1	-1	3	2	3	2,7
-1	-1	1	-1	-1	3	3	3	3
-1	1	-1	-1	-1	3	3	3	3
1	1	1	-1	-1	2	2	2	2
1	-1	1	-1	1	3	2	3	2,7
1	1	-1	1	-1	3	3	3	3
1	-1	1	1	-1	3	3	3	3
-1	1	1	-1	1	1	2	1	1,3
-1	-1	1	1	1	1	1	1	1
-1	1	1	1	-1	3	3	3	3
1	-1	-1	1	1	2	2	2	2
-1	-1	-1	-1	1	1	1	1	1
1	1	-1	-1	1	2	2	2	2

The results of the screening experiment are shown in a standard factor plot in Figure 3.12. The factor plot shows that viscosity and clamping force have the major effect upon formability. Injection speed, mould temperature and melt temperature result to have little influence on the response variable.

Figure 3.12: Standard factor plot of main effects.

However, in order to compare the relative magnitude of the effects and evaluate their statistical significance, two other graphs it is better to employ.

The first one is the normal probability plot of the effects (Figure 3.13). In this plot, points that do not fall near the line usually signal important effects. Important effects are larger and further from the fitted line than unimportant effects. Unimportant effects tend to be smaller and centred around zero. In order to identify important effects, a p-value equal to 0.05 was used.

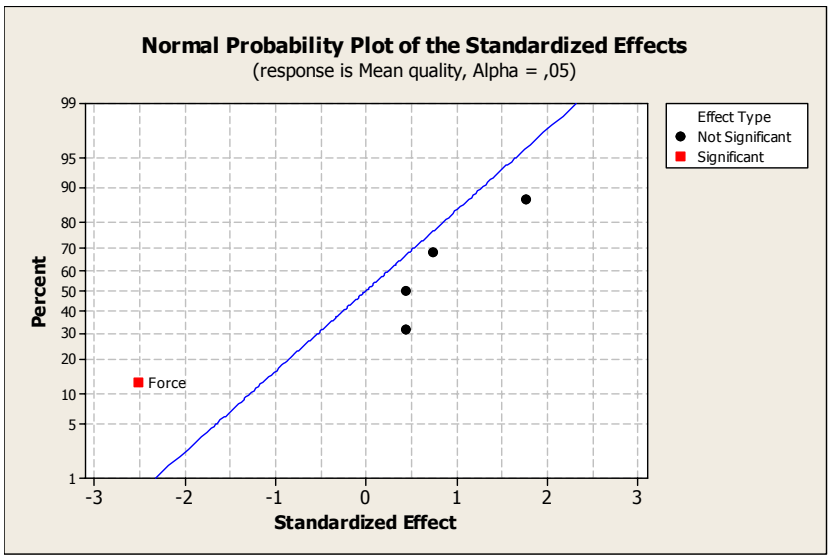

Figure 3.13: Normal probability plot of the effects.

The second one (Figure 3.14) is the Pareto chart which allows to look at both the magnitude and the importance of an effect. This chart displays the absolute value of the effects, and draws a reference line on the chart. Any effect that extends past this reference line is potentially important. The reference line was determined considering a p-value equal to 0.05.

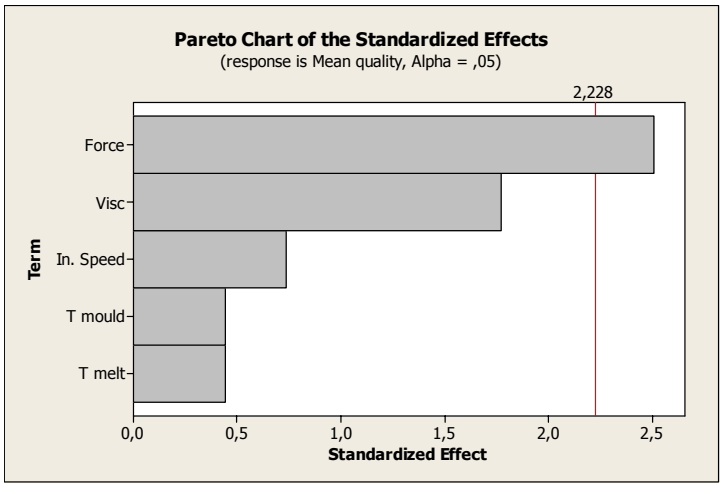

Figure 3.14: Pareto chart.

Both the normal probability plot and the Pareto chart show that only clamp force is statistically significant at the 0.05 α-level. The ability to deform the sheet is more likely if low values of clamping force are used. When the mould is closed with high value of clamping force the injected polymer deforms the blank by pure stretching whereas a combination of drawing and stretching occurs with a low clamping force.

Although increasing its temperature, the AA1050-O enhance its formability, since the higher the temperature the larger its ductility and the lower its flow stress [20], melt and mould temperature result to be not statistically significant on sheet formability. This is probably due to the fact that the duration of the filling phase, which coincides with the main deformation process of the sheet metal blank, is around 0.7 s. This amount of time is too short for melt temperature to heat sufficiently the sheet metal. Considering: (a) the short time gap between the placement of the sheet metal on the injection mould and the starting time of the PIF cycle (typically 5 s), (b) the short duration of the filling phase, (c) the air gap between the metal blank and the mould during most of the filling time, the deformation process of the metal blank may reasonably be assumed to be adiabatic and the heat exchanged with the mould can be neglected [21].

3.2.2 The second set of experiments

During the first set of experiments, the polymer viscosity was varied in order to analyze the influence of the tangential adhesive stress of the polymer on the sheet metal formability. Since no clear conclusion could be drawn from the screening DOE results, additional experiments were carried out by using two polymers with viscosity that ranges from very low to very high values. The polymer with the lowest viscosity was a polypropylene from Sabic, (Stamylan P 48 M10). The high viscosity polymer was a PC+ABS+20%GF from Bayer (Bayblend T88-4N). The rheological behaviour of the two materials is plotted in Figure 3.15 (a) and (b) respectively ® [22].

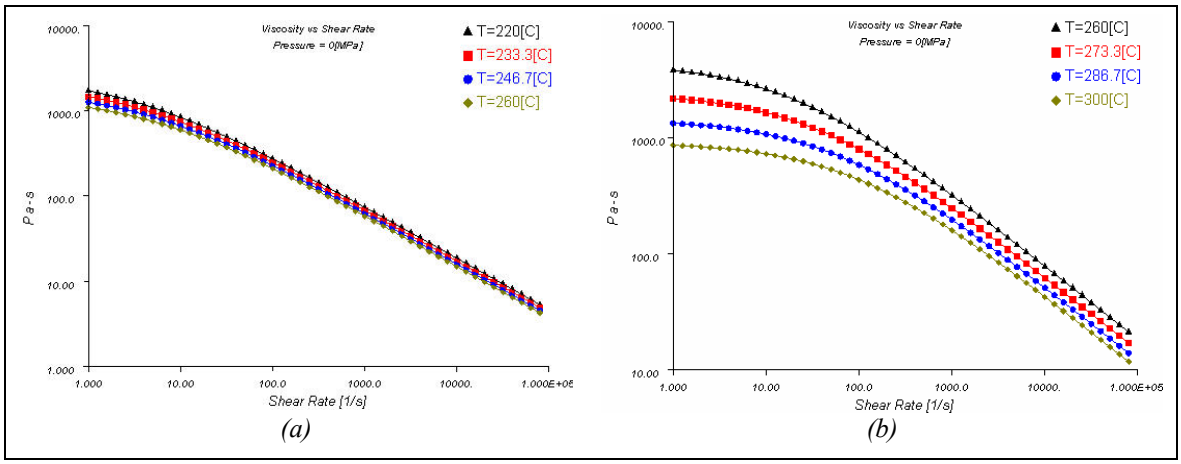

Figure 3.15: Viscosity vs. shear rate at different temperatures of: (a) Stamylan P 48 M10; (b) Bayblend T88-4N.

A full 2^2 factorial design in 4 runs and 3 replications was used. The experimental parameters varied were: polymer viscosity, as described previous and clamp force, since it was the unique statistically significance parameter of the first set of experiments. The two levels in

the experiments were designated, as usual, as high (+) and low (-). The specific settings are listed in Table 3.3.

Table 3.3: Factors levels for the screening experimental plan.

Factor	Unit	-	+
Viscosity	/	Stamylan P 48 M10	Bayblend T88-4N
Clamping force	kN	10	100

In order to investigate the influence of the main injection moulding process parameters on the sheet metal formability, in this second set of experiments the uniformity of thickness distribution was defined as the response. This one was calculated as the y distance (Δy) between the lowest sheet thickness and corresponding value of ideal uniform thickness (Figure 3.16).

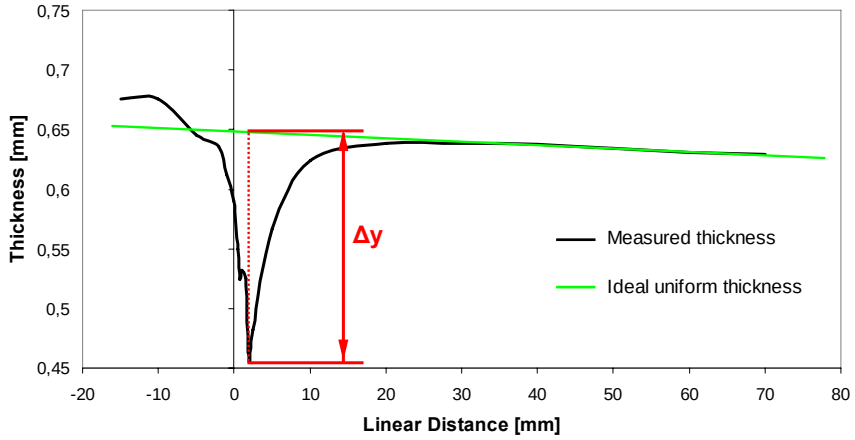

Figure 3.16: Evaluation procedure of thickness uniformity of sheet metal.

The employed factorial designed and the obtained results are listed in Table 3.4. The response variable is the mean of Δy distance for each of the three used replications.

Table 3.4: 2^2 full factorial design and obtained results.

Visc	Force	RUN 1	RUN 2	RUN 3	Δy
1	1	0,186	0,191	0,178	0,18
1	-1	0,091	0,078	0,081	0,08
-1	1	0,193	0,186	0,203	0,19
-1	-1	0,096	0,100	0,091	0,09

The results of the full factorial design are shown in Figure 3.17, which plots the main effects of factors. This graph shows that clamp force has a great effect on thickness uniformity of the sheet metal.

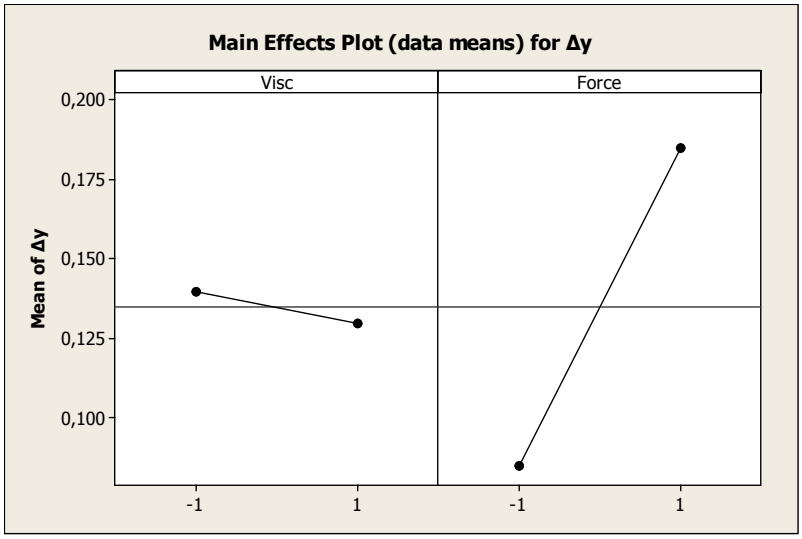

Figure 3.17: Standard factor plot of main effects.

Polymer viscosity, instead, has no statistical influence on the thickness distribution. This is highlighted by the normal probability plot and the Pareto chart (Figure 3.18 and Figure 3.19, respectively) obtained considering a p-value equal to 0.05.

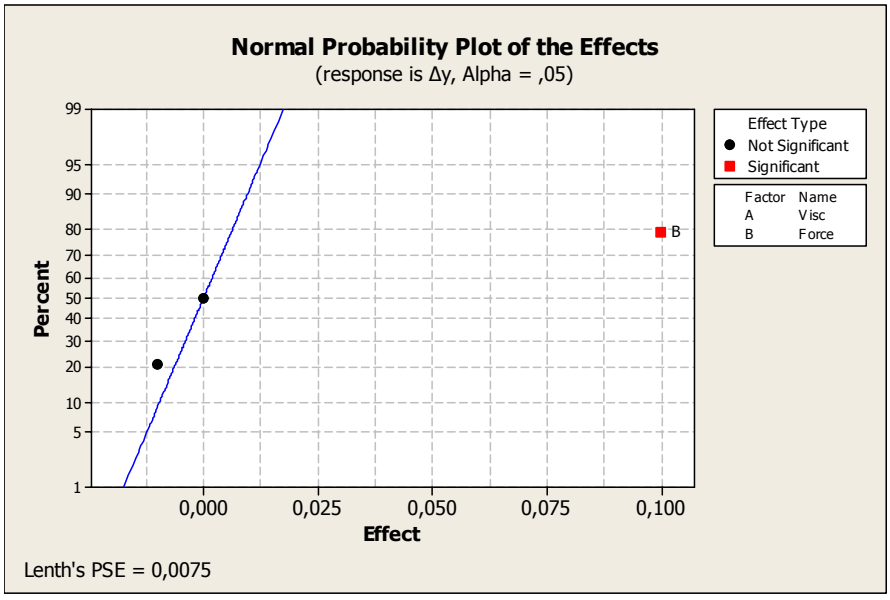

Figure 3.18: Normal probability plot of the effects.

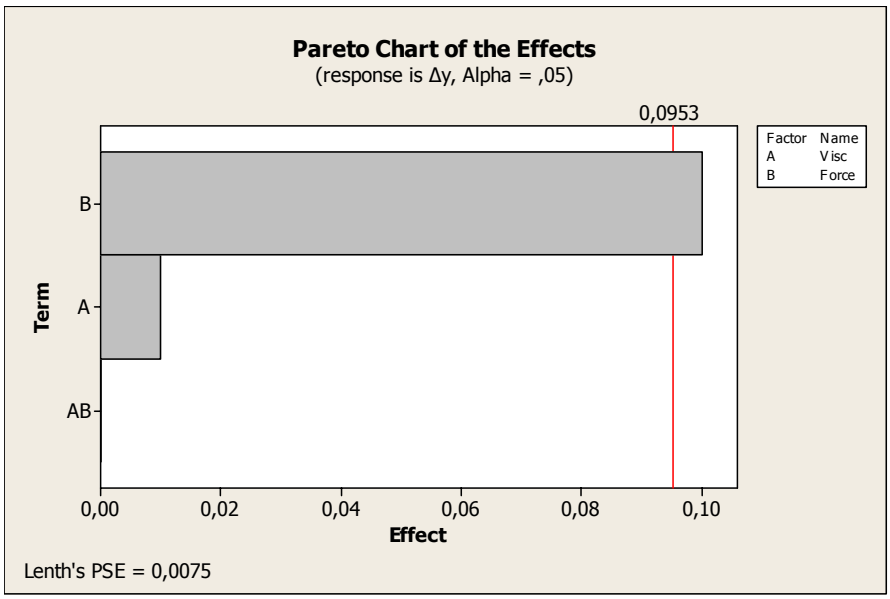

Figure 3.19: Pareto chart.

Figure 3.20 compares the means of the thickness distributions of the sheet metal for the two clamp force levels. The thickness distribution of parts obtained with a low clamp force is more uniform than that obtained with a high force. Also the mean value of the thickness depends on the level of used force. In particular, a higher thickness results using a low clamp force. This is probably due to the different stress state of sheet metal. Using a low clamp force, the deformation process of the sheet blank is more likely a combination of drawing and stretching, resulting in a less demanding stress state.

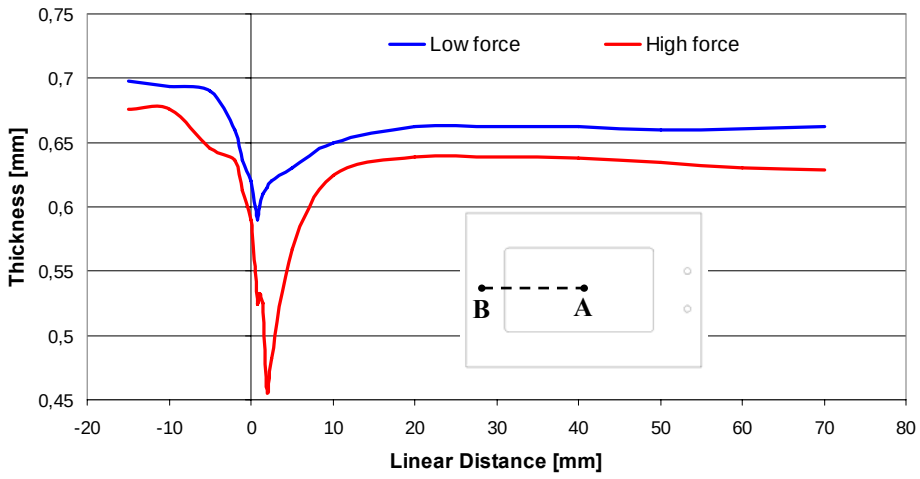

Figure 3.20: Thickness distribution of sheet metal along A-B direction at two levels of clamp force.

In Figure 3.21 the means of thickness distributions of the sheet metal for the two viscosity levels are compared. As the difference between the two levels is comparable to the error measured within each level by replicating the test, it can be conclude that polymer

viscosity has no influence on sheet metal formability. This is probably due to the fact that melt polymers cannot exceed a maximum shear stress of approximately 0.4 MPa, beyond which material degradation starts to occur, while the considered metal sheet has a much higher shear yield stress [23].

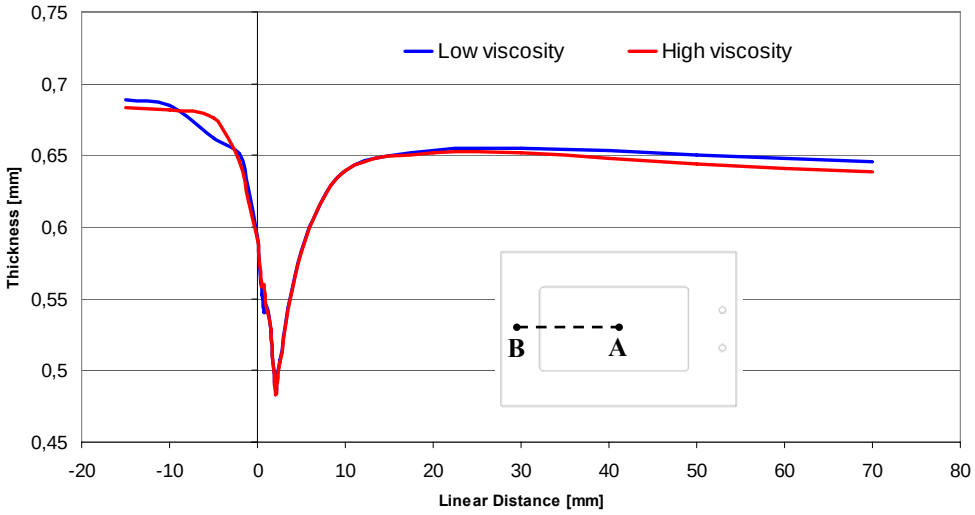

Figure 3.21: Thickness distribution of sheet metal along A-B direction at two levels of viscosity.

In conclusion, obtained results show that the deformation development of the sheet metal in the Polymer Injection Forming process is different from the one in the Viscous Pressure Forming process (described in chapter 2). In VPF, the thickness of the deformed sheet metal depends on process parameters and viscous medium properties. In PIF, thickness distribution depends only on the clamp force, which forces the sheet metal to deform as pure stretching or as a combination of drawing and stretching.

3.2.2.1 Measuring procedure of the sheet metal thickness

The sheet metal thickness was measured by means of the CMM Prismo machine by ZEISS, located at DIMEG lab (Figure 3.22).

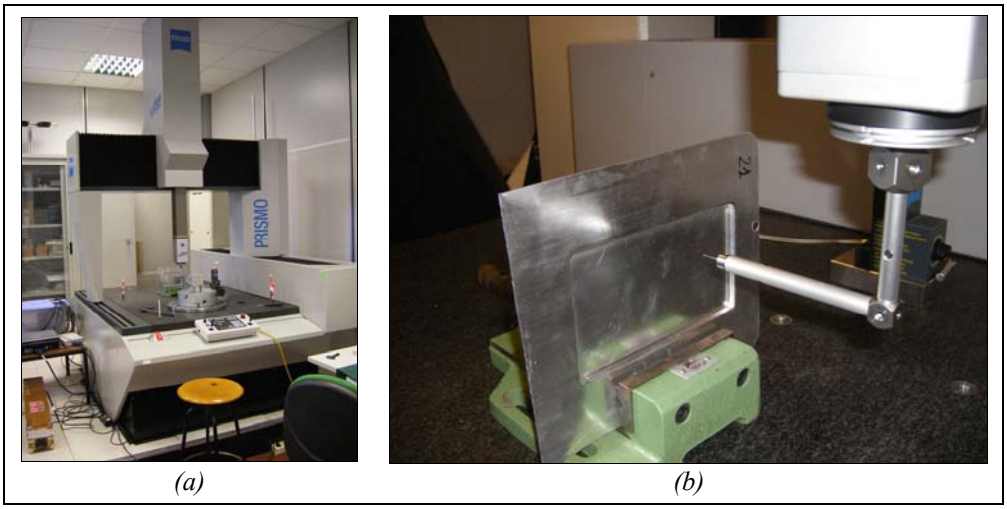

Figure 3.22: (a) CMM Prismo machine at DIMEG Lab; (b) measuring the sheet metal thickness.

A continuous scanning on both sides of the sheet metal was carried out along A-B (Figure 3.23).

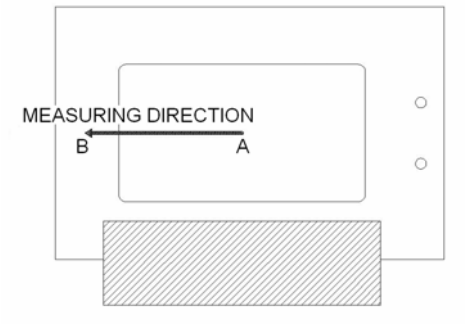

Figure 3.23: Measuring path.

The two measured profiles for each sheet metal part (lines in red and green colour of Figure 3.24 (a)) were processed by a custom made software in LabVIEW™ environment. This software enables to automatically calculate the normal distance between the two curves at several locations (Figure 3.24 (b)). Moreover, this program performs the compensation of the tip radius in order to calculate the real thickness of each sheet metal part.

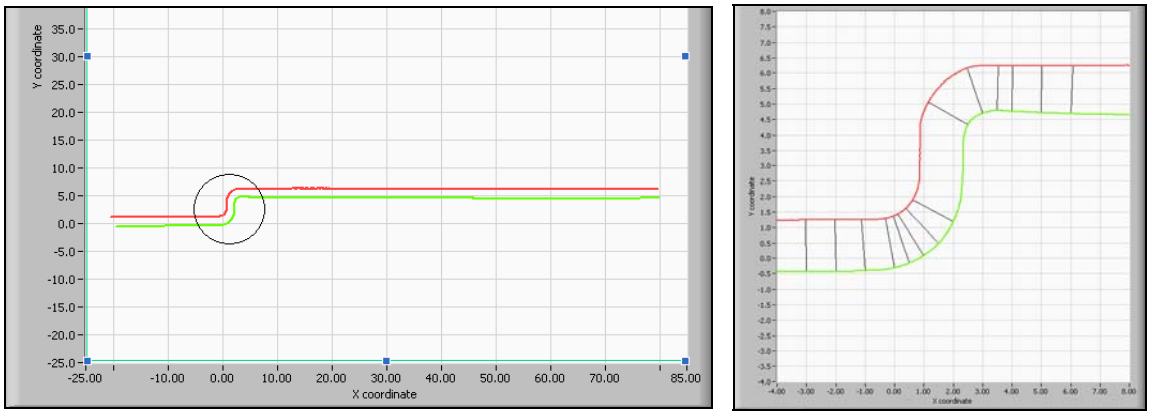

(a) *(b)*

Figure 3.24: (a) Measured profiles processed in LabVIEW™ environment; (b) calculation of normal distances between measured profiles.

3.3 Optimization of process parameters

The results of the screening experiments showed that viscosity, injection speed, melt temperature and mould temperature have no significant effect on metal sheet formability in the PIF process. Therefore, in order to minimize the process cost low viscosity polymers should be preferred. In fact, the machine rate is proportional to the clamping force and in turn to the injection pressure, which is related to viscosity. The injection speed should be set at the maximum limit to decrease viscosity, exploiting the non-Newtonian shear-thinning behaviour of polymer melts. Melt temperature should be set according to suggestions made by polymer producers. As a rule of thumb, it should be considered that increasing melt temperature the polymer viscosity decreases but cooling time increases. Mould temperature should be set to the lowest values possible to decrease the melt cooling time and therefore the overall cycle time.

Clamping force is the only factor that has a significant influence on metal sheet formability. Since the melt pressure acts against the blank holder plate, the clamping force should be large enough to counteract the effect of the internal pressure and continuously provide sealing, in order to avoid flash. However, since the internal pressure is low at the beginning of the process, the clamping force should be kept low at the start and increased as the internal pressure increases so as not to prevent sheet flow into the mould cavity. Unfortunately this is not possible with conventional injection moulding machine, which require the clamping force to be constant during the whole cycle. Therefore, either the sheet metal is formed by pure stretching, strongly limiting the capabilities of the PIF process, or flash is allowed during the forming process and then trimmed in a secondary operation. A third alternative could be to develop a special three-plate mould with a blank holder plate that can be continuously controlled independently from the injection moulding machine.

CHAPTER 4

EXPERIMENTAL INVESTIGATION ON POLYMER-SHEET METAL ADHESION

In order to assure the right functionality of sheet metal-polymer macro composite parts, one of the most important problems is that good bonding strength between plastic part and the sheet metal part should be obtained. For this reason, it is necessary to investigate the adhesion mechanisms between metal, particularly aluminium alloy in this work, and polymer.

In this chapter, a preliminary experimental investigation on adhesion issues between the sheet metal and the plastic part will be presented. At the beginning, a literature review of the knowledge about adhesion mechanisms and theory will be introduced. Then principal destructive tests for estimation of adhesion strength will be described. Finally, experimental tests, as well as obtained results, carried out in order to investigate the influence of the main injection moulding parameters on the adhesion strength between metal and polymer will be discussed.

4.1 Introduction to adhesion

In an adhesively bonded joint the different layers given in Figure 4.1 (a) are the most important for the performance of the joint. Between every layer there is the possibility of an adhesive failure, within every layer there is the possibility of a cohesive failure. Even between the oxide layer and the adherend there is the possibility of an adhesive failure.

This schematic representation of interfaces in an adhesive joint is not very useful to explain the behaviour of these type of joints during joint failure. The joint failure can be explained in better way by using a more detailed model which is presented in Figure 4.1 (b). The model shows the different interphases which are inside an adhesive bond:

- adhesive/primer mixed layer;
- primer/oxide mixed layer;
- barrier layer.

In every phase and between phases different types of bonds are acting. In some cases these interphases turned out to be a weak boundary layer (WBL). The first concept of weak boundary layers was already discussed by Bikerman in his book in 1961 [24]. Diffusion of low molecular weight compounds to the interface can be the origin of WBL. These weak boundary layers can preferably be detected using wedge edge tests and (wet)peel tests as will

be explained in §4.4.2. All these bonds are responsible for the final bond strength and have influence on the durability characteristics of the complete bond.

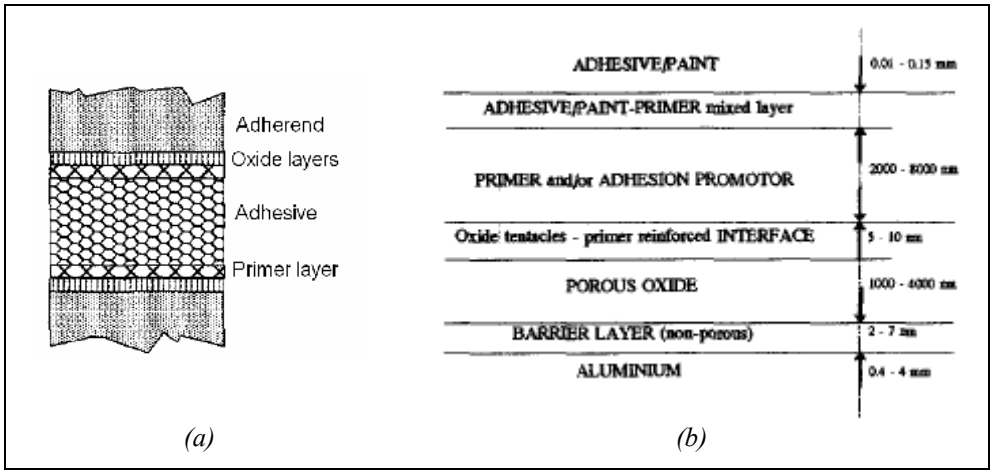

Figure 4.1: (a) Schematic representation of an adhesive joint; (b) schematic representation of adhesive paint oxide interphases.

The different types of bonds given in Figure 4.2 [25], are responsible for the cohesive and adhesive strength of the different layers and phases. These type of bonds are responsible for the interactions between two or more atoms e.g. groups of atoms within molecules and also between different phases. The adhesion forces are due to these different types of physical and chemical bonds. The physical bonds are mainly responsible for the final strength of an adhesive bonded joint.

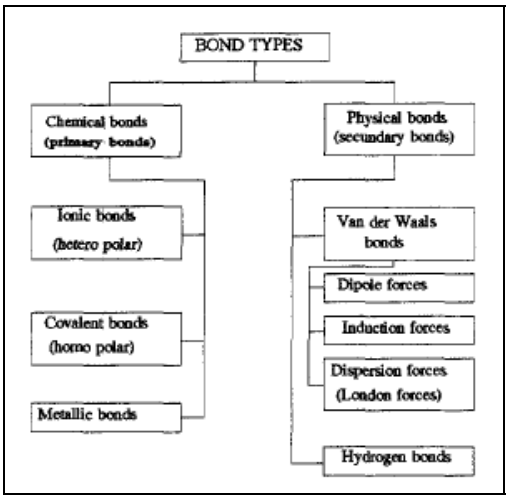

Figure 4.2: Different bond types.

The only evidence that chemical bonds (covalent bonds) play a role in the case of bonding of adhesives to a metal substrate is when phenolic or silane based primers are used. In the case of coupling agents or adhesion promoters being used in primers (like e.g. the silanes) covalent bonds are important for the adhesion between the primer and the oxide. This is termed chemisorption and involves ionic, covalent or metallic interfacial bonds being established.

4.2 Adhesion theory

Adhesion is defined by the state that two bodies are hold together for an extended period by interfacial forces. The forces ranges from valance forces to mechanical interactions. The nature of interfacial adhesion ranges from bioadhesion involving cell adhesion to adhesion of heavy construction materials. The environment of which interfacial adhesion is measured varied from room or body temperature to sub-freezing, and to a few hundreds degree centigrade as in aerospace industry.

Because of the wide range of interfacial adhesion, many theories were developed to describe the phenomena. The theories of adhesion have been classified into four categories. Since the range of adhesion extends from cell adhesion to adhesives tapes used in daily life, and to aerospace industry, each theory does not apply to all phenomena. A particular theory may only apply to a limited range. The appropriate theory must be selected based on chemical/biochemical nature of particular adhesive/adherend combinations.

4.2.1 Mechanical Theory

The Mechanical Theory, also called the Mechanical Interlocking Theory, is the oldest explanation for adhesion. The theory essentially described that mechanical interlocking of the adhesives and the flow into the irregularity of the substrate surface is the source of adhesion (Figure 4.3). The adhesives have to flow into the pores and interstices of the materials to establish mechanical embedding. The embedded adhesives solidify and become inextractable. The adhesive force is determined by the work to break adhesive extension off the adhesive mass. Acid etching may further be used to increase porous area of the tissue for better bonding.

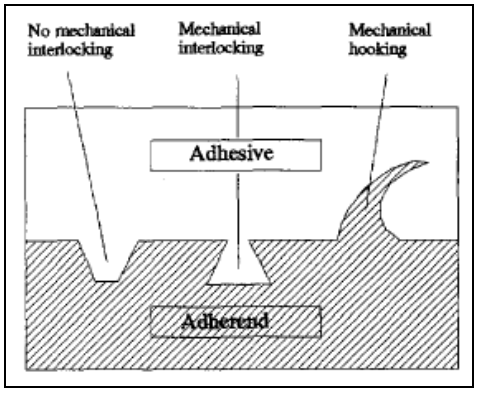

Figure 4.3: Different shapes of surface irregularities [26].

4.2.2 Electrostatic Theory

The Electrostatic Theory describes that an electrical double layer is produced at any interface and the consequence Coulombic attraction largely accounts for adhesion and resistance to separation. The theory can be viewed as treating the adhesives/substrate system as a capacitor that is charged due to contact of the two different materials. The Deryaguin's Theory, as shown in Equation3.1, can be used to represent the Electrostatic Theory,

$$A_c = \frac{h_c \varepsilon_d}{8\pi} \cdot \left(\frac{dV_c}{dh_c} \right)^2 \tag{4.1}$$

where V_c is the discharge potential at the discharge gap, h_c and ε_d is the dielectric constant [25]. A common example often described by the Electrostatic Theory is the adhesion of a plastic film on a layer of paper or another film of plastic.

4.2.3 Diffusion Theory

The Diffusion Theory states that adhesion occurs through inter-diffusion of the adhesive and adherend across the interface. Adhesion is considered a three-dimensional volume process rather than a two-dimensional surface process. The Diffusion Theory applies particularly to polymeric materials where physical entanglement is common. In order for interfacial diffusion to occur, the adhesives and adherend must be thermodynamically compatible to each other.

Industrial techniques to enhance interfacial diffusion include solvent welding, heat welding, and ultrasonic welding. In solvent welding, a solvent common to both adhesive and adherend is applied to allow diffusion of polymers across the interface. In heat welding, materials are melted to allow interfacial diffusion. In ultrasonic welding, ultrasonic wave is directed through a horn that focuses on the interface to melt a thin layer of materials across the interface. Among these techniques, ultrasonic welding is the most often used method.

Interfacial adhesion involving diffusion is also seen in biological environment. The adhesion of polycarbophil (cross-linked polyacrylic acid) to mucus layer of the GI tract is a good example of diffusion of the polyacid chains into mucus layer followed by physical entanglement. Another example occurs in the development of silicones contact lens. The highly flexible polysiloxane chain diffuses toward the cornea and attaches to the cornea epitheliums. The result was a lens difficult to be taken off. This particular example may be more or less related to the Adsorption Theory described below.

4.2.4 Adsorption Theory

The Adsorption Theory is the most widely applied theory on interfacial adhesion. The theory states that surface forces are involved in adhesion, and that polar molecules are oriented in an ordered way so that surface molecules of adhesive and adherend are in contact. Sufficient intimate molecular contact is achieved at the interface that the materials will adhere because of interatomic and intermolecular forces. Typical bond type and bond energy is shown in Table 4.1.

Wetting is the initial physical process occurring in interfacial bonding. Substrates with low surface free energies are less easy to get wet. To facilitate the flow of adhesives, techniques such as etching is applied to increase the surface free energies. Common techniques used are plasma etching or acid etching. While plasma etching is commonly used for the surface of plastics, acid etching is sometimes applied in the case of metal. For example, stainless steel used as coronary stent may be pre-treated with acid before a layer of coating is applied.

Table 4.1: Typical interatomic and intermolecular bond types and energies.

Type	Bond energy (kJ/mol)
Primary bonds	
Ionic	600–1100
Covalent	60–700
Metallic	110–350
Donor–acceptor bonds	
Bronsted acid–base interactions (i.e. up to a primary ionic bond)	Up to 1000
Lewis acid–base interactions	Up to 80
Secondary bonds	
Hydrogen bonds	
Hydrogen bonds involving fluorine	Up to 40
Hydrogen bonds excluding fluorine	10–25
van der Waals bonds	
Permanent dipole–dipole interactions	4–20
Dipole–induced dipole interactions	Less than 2
Dispersion (London) forces	0.08–40

In the biological environment, protein adsorption, cell adhesion, and cell spreading are often described by the Adsorption Theory.

For adhesives used in daily life, epoxies and cyanoacrylates are good examples of the Adsorption Theory. Chains re-alignments were found in studying these systems. Study shown the lowering of the C=O stretching frequency and a shift of anti-symmetric stretching vibration of the C-O-C group when cyanoacrylates was adsorbed onto aluminium. Other commonly used adhesives are polyurethanes, silicones adhesives, polyacrylates, etc. There are also polymers used to enhance adhesion in pharmaceutical formulation such as poly(vinyl pyrrolidone) and a certain celluloses.

4.3 Surface preparation techniques for adhesive bonding

Surface preparation, also known as surface pretreatment, has been utilized since the 1950's when it was first used to improve the performance of adhesive bonds in the airline industry. Since then, preparation of surfaces has been transformed into a very important topic in adhesive bonding. This is due to the process being not only simple and quick, but also significant in its ability to improve bond strength as well as corrosion resistance.

4.3.1 Applications of Surface Pretreatment

There are many methods to treat surfaces prior to bonding. Since there are multiple forms of bonds on which surface preparation techniques are applied, such as metal-to-metal, plastic-to-plastic, rubber to rubber, etc, there are multiple techniques that are utilized to improve bond strength and corrosion resistance. The most common reasons for utilizing surface treatments prior to bonding are [25]:

1) To remove, or prevent the subsequent formation of, any weak layer on the substrate.
2) To maximize the degree of intimate molecular contact that is attained between the adhesive or primer and the substrate during the bonding operation.
3) To ensure that the level of intrinsic adhesion forces which are established across the interfaces are sufficient for obtaining both the initial joint strength and the service life desired.
4) To generate specific topography on the substrate.
5) To protect the surface of the adhesive prior to the bonding operation.

4.3.2 Surface Energy and Surface Pretreatment

The increase in bond strength generated by surface pretreatment is a result of an increase in the surface energy of the system. Processes such as etching, physical abrasion, and chemical modification of surface bonds, are utilized to increase overall surface energy of the system [27]. High surface energy generated by these processes has been shown to physically increase the wettability of the adhesive, hence allowing for a more uniform spread across the surface of the treated materials. Reduction in the formation of weak and irregular layers at substrate allows for an overall stronger joint. Analysis using a goniometer has shown that the contact angle of adhesive on pretreated material is lower, hence more hydrophilic.

The most commonly bonded materials, metals and plastics, can be classified separately into high surface energy and low surface energy materials respectively. Metals, which are generally comprised of numerous grain boundaries and dislocations, inherently have a higher surface energy than plastics, which contain stable chains of non-reactive covalent bonds [28]. As a result, bond strength is always much higher for metals than for plastics.

4.3.3 Surface Preparation of Aluminium and Aluminium Alloys

Aluminium, being a staple material for the airline industry, was the first material to undergo surface pretreatment. Since the 1950's many pretreatments have been developed for metals, however, most have been derived in some part from the initial process developed by Forest Product Laboratories (FPL) for Aluminium Alloys. There are two common surface pretreatments used in industry for the treatment of aluminium and aluminium alloys. They are the FPL Etch Process and the Phosphoric Acid Anodize Etch (PAA).

FPL Process:

The FPL process like most surface pretreatments greatly emphasizes the removal of contamination. The surface is treated according to the following method [29]:

1) Degreasing – Oils and particulates removed using Trichloroethylene solvent.
2) Alkaline Cleaning – Immersed in a non-etch alkaline solution to further remove contamination at 50°F – 80°F.
3) Etching – Immersion of material in a solution of 30 pbw water, 10 pbw sulphuric acid, and 1-4 pbw of sodium dichromate for 9-15 minutes.
4) Final Rinse – Water for 1 – 2 minutes at no greater than 50°C
5) Drying – Air Dry for one hour at no more than 65°C

The sulphuric acid, is used to target the stable oxide layer formed on the surface of the metal. This layer, due to surface energy interactions is etched into craters, which can be seen in Figure 4.4.

Strengthening occurs when adhesive flows amidst the miniature craters. The result in a mechanical interlocking effect between the adhesive and the material bonded.

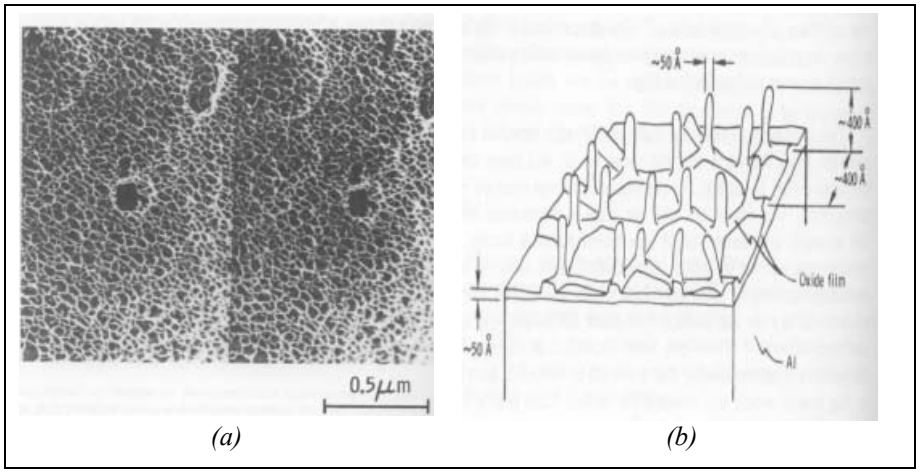

Figure 4.4: (a) STEM Micrograph surface oxide layer using FPL process; (b) Isometric Drawing of Oxide Structure [29].

Phosphoric Acid Anodize Etch (PAA):

The PAA process was designed in replacement of the FPL Process, which was found to fail due to exposure to corrosive elements. The surface treatment, though similar to FPL, included an anodizing process in which a 10V bias is applied across a stainless steel cathode to generate a superficial anodic layer, which resisted corrosion [29]. Figure 4.5 demonstrates the mechanical interlocking effect.

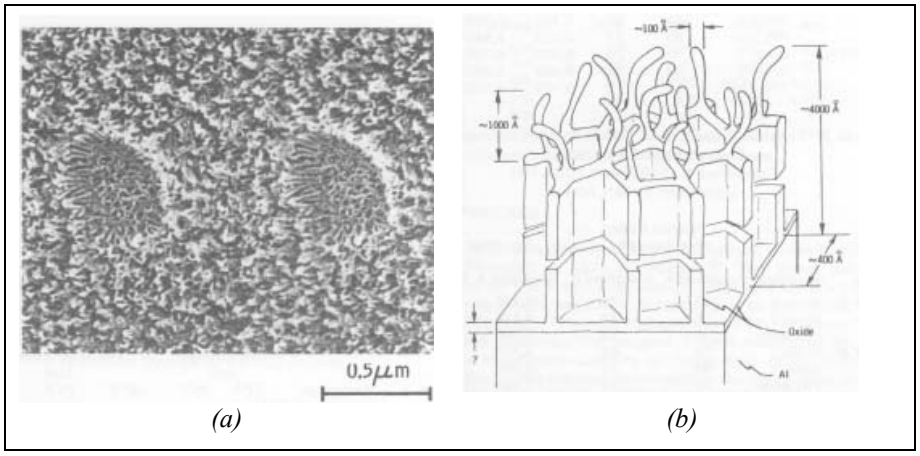

Figure 4.5: (a) STEM Micrograph surface oxide layer using PAA process; (b) Isometric Drawing of Oxide Structure [29].

4.3.4 Surface Pretreatment of Plastics

Due to the low surface energy of plastics, chemical modification of the surface must be performed in order to raise the surface energy and increase bond strength. Since oxide layers do not typically form on plastic surfaces, mechanical interlocking cannot be utilized effectively. Modification of the surface is performed by breaking the covalent bonds on the surface with high-energy particles. These broken bonds will maximize the level of intermolecular contact between the adhesive and the substrate during bonding.

Corona Discharge, Flame and Plasma treatments are generally used for surface preparation of plastics. As shown in Figure 4.6, corona discharge treatment utilizes high voltage electrodes to discharge current through a plastic film to a grounded roller [28].

Similarly, flame treatment uses heat to increase the concentration of reactive hydroxyl groups, ester, ether and oxygen at the surface. Plasma treatment utilizes an RF microwave generator to excite argon or nitrogen to a plasma state. The plasma is then allowed to react with the sample in an evacuatable vacuum chamber [29, 30].

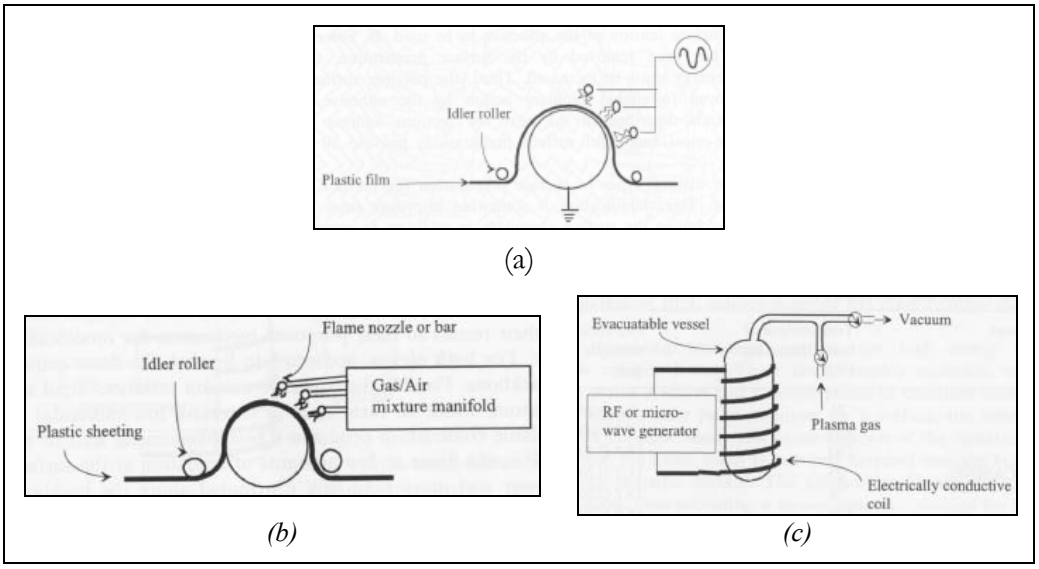

Figure 4.6: (a) Corona Discharge Treatment; (b) Flame Treatment; (c) Plasma Treatment.

4.4 Interfacial adhesion test methods

Numerous test methods exist for characterising adhesives and bonded joints, and may be used to determine fatigue resistance, environmental durability and creep behaviour. Adhesive tests can be divided into those methods that provide mechanical property data for the adhesive, which aids the selection of adhesives, and those methods that can be used to determine the quality of adhesively bonded structures, and thus aid the design process of adhesive joints. Although an extensive range of test methods is available as national and international standards, most of these tests can only be used for qualitative measurements, providing a means of checking the effectiveness of different surface preparations and comparing mechanical properties of different adhesive systems. A limited number of test methods are suitable for generating engineering data, particularly for determining structural integrity of adhesively bonded structures subjected to static, cyclic and environmental effects.

Most of the commonly used test methods are incapable of providing reliable engineering data because the test geometry induces a complex state of stress in the adhesive layer, thus invalidating the results. Two approaches have been adopted in order to overcome this problem.

The first and direct approach is to measure the properties of bulk adhesive specimens. Bulk adhesive specimens are cast and machined to the required shape.

The second approach for determining engineering properties of adhesives is to use specially designed joint geometries with a thin bond line, often referred to as in-situ testing. In order for these test geometries to produce reliable engineering data, the test geometry should provide a pure state of stress, uniformly distributed across the contact surface and through the bond line, free of stress concentrations. The surface treatment should be sufficient to ensure cohesive failure in the adhesive layer. Ideally, the test method should employ simple and easily prepared specimens. Failure force should in principle remain constant with fluctuations in the failure force being attributed to variations in adhesive strength.

The four main loading modes of bonded joints are (see also Figure 4.7):

- Peel loads produced by out-of-plane loads acting on thin adherends.
- Shear stresses produced by tensile, torsional or pure shear loads imposed on adherends.
- Tensile stresses produced by out-of-plane tensile loads.
- Cleavage loads produced by out-of-plane tensile loads acting on stiff and thick adherends at the ends of the joints.

In practice, a bonded joint will simultaneously experiences several of these loading components [31]

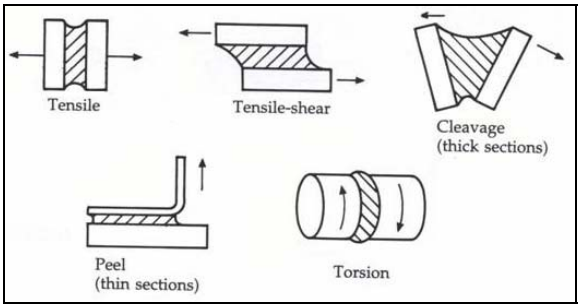

Figure 4.7: Basic loading modes experienced by adhesive joints [31].

To curtail the explanation of the different test methods, only principal adhesion tests will be covered in this report.

4.4.1 Tensile test methods

Transfer of load to an adhesively bonded structure by tension, either directly or indirectly (peel), represents the most severe form of loading, since the strength of the joint relies on the tensile strength of the adhesive, which is low. It is good design practice, therefore, to ensure that the load is transferred by shear or compression and that direct or induced tensile stresses are minimised. Tensile stresses are virtually impossible to avoid, however there is a need for reliable test methods to measure the tensile properties of the adhesive.

4.4.1.1 Butt tension test

The tensile butt joint is the most popular test method used to evaluate the tensile properties of adhesive joints (Figure 4.8) [32-34].

The cylindrical butt joint can be used to test thin bondlines in tension, torsion and compression. The test provides data on the moduli of rigidity and elasticity, and Poisson's ratio. The average strength is taken as the applied load at failure divided by the bond area. The

test is difficult to perform. Significant bending can be induced due to misalignment of the adherends, resulting in premature failure. Care needs to be taken to ensure good alignment during specimen preparation (i.e. bonding of adherends) and testing. A small misalignment can severely reduce strength data.

The tensile stresses in the central region of the adhesive layer for butt tension specimens are uniformly distributed and there are no shear stresses present. In marked contrast, the stress state in the outer edges is highly complex, varying through the thickness of the adhesive layer.

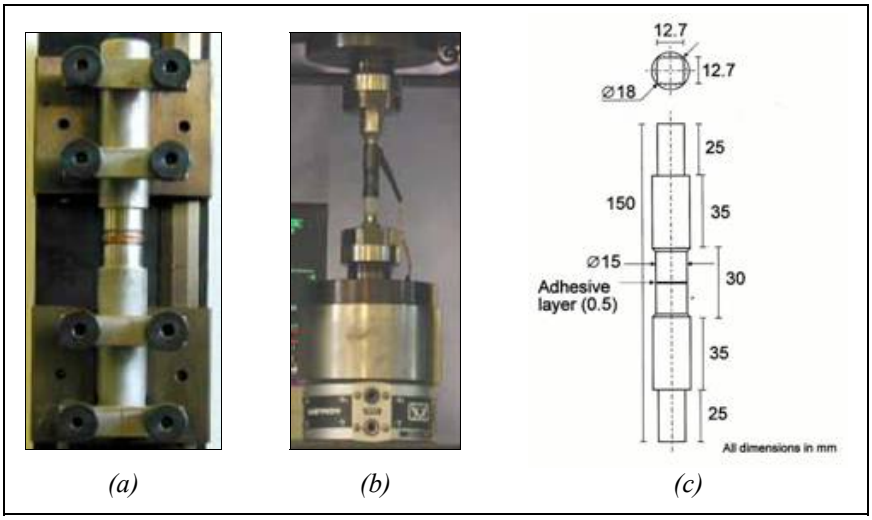

Figure 4.8: (a) Bonding Fixture; (b) alignment fixture; (c) butt joint specimen.

4.4.2 Peel test methods

Since the inception of structural bonding, peel tests have been an integral part of adhesive performance specifications, and have played an important role in the development of adhesives [35, 36]. Peel resistance is defined as the average force per unit test specimen width, measured along the bond line that is required to separate progressively two adherend members of a bonded joint.

Peel stresses arise if one or both adherends are flexible, and hence the test methods are suitable for use in determining peel resistance of thin metallic adherends (e.g. thin aluminium alloy sheet). Adhesion is measured by peeling a thin adhering layer from a rigid substrate or from an identical layer. The peel force is a measure of fracture energy, although the data generated has little use in the stress analysis of a bonded joint [37]. Peel tests are normally used to compare adhesives.

In this section, three popular peel tests will be described. These are listed below:

- T-peel.
- Climbing drum peel.
- Floating roller method.

4.4.2.1 T-peel test

The primary purpose of this test method is to determine the relative peel resistance of adhesive bonds between flexible adherends by means of a T-type specimen (Figure 4.9 (a)).

The term flexible refers to the ability of the adherend to bend through 90° without breaking or cracking. The T-peel test is particularly suited to testing thin aluminium alloys. Specimens are typically 25 mm wide, have a minimum bonded length of 150 mm, and 50 mm long arms [38]. The recommended thickness is 0.5 mm for steel and 0.7 mm for aluminium. Adhesive layer thickness is not specified.

Testing is straightforward and requires no special fixture. The specimen can be readily loaded using standard tension/compression mechanical test equipment. It is important to ensure that the bonded portion of the specimen remains perpendicular to the applied load. The specimen is bent backwards 180° and peeled. Tests are normally conducted at displacement rates of 100 mm/min for metals and 10 mm/min for other adherends. The average peeling load per unit length/width is used to define the peel strength. This is taken from the force-displacement curve after the initial peak reading (Figure 4.9 (b)). At least five to ten specimens should be tested from each batch of material, depending on the standard used.

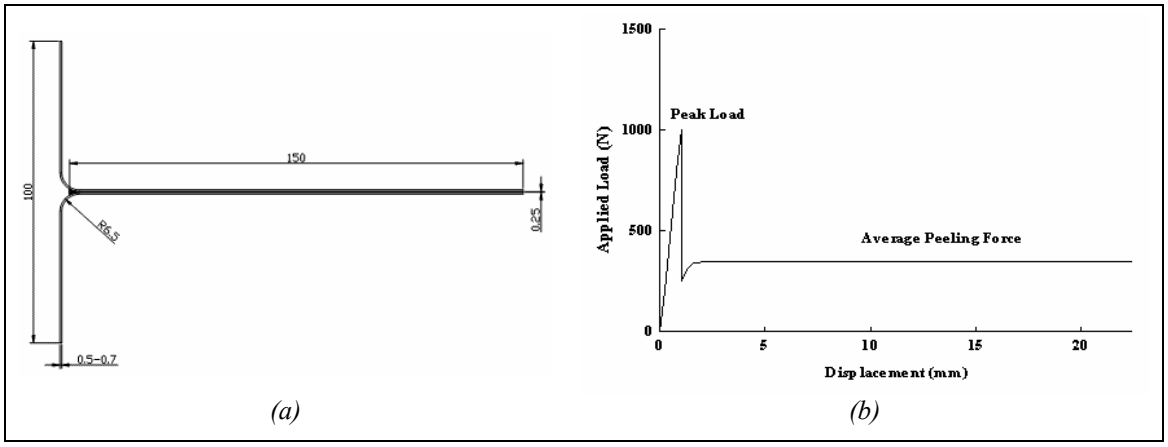

Figure 4.9: (a) Schematic of standard T-peel specimen dimensions (mm); (b) typical force-displacement curve for a T-peel test.

4.4.2.2 Climbing drum peel test

The climbing drum peel test was developed to determine the peel resistance of adhesive bonds between [39, 40]:

- A relatively flexible adherend and a rigid adherend; and
- The relatively flexible facing (or skin) of a sandwich structure and its core.

The test consists of peeling a thin strip of metal from a thick strip by winding the thin strip around a drum. Torque is applied to the drum by pulling down on straps wrapped around the drum. The thin strip of metal is wound on the drum at a smaller radius than the straps. The difference in radius (i.e. moment arm) results in a large torque being applied to the drum compared with that applied on the thin strip. The resultant upward motion causes the thin strip to peel from the thicker strip (Figure 4.10).

The upward motion of the drum causes the thin strip to be peeled from the thicker adherend resulting in bond failure. This test can be used for qualifying skin-to-core bond strength of sandwich structures, and is particularly sensitive to adherend surface preparation. This method provides comparative data of adhesion and is particularly suited to process

control. Direct comparison of different adhesive systems and processes is only applicable for identical specimen configurations and test conditions.

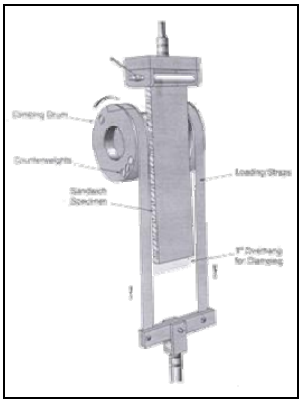

Figure 4.10: Climbing test with sandwich specimen.

4.4.2.3 Floating Roller method

The floating roller peel test [41, 42] has been developed to determine the relative peel strength of adhesive bonds between one rigid adherend and one flexible adherend (Figure 4.11). As with the T-peel test, the average peeling load per unit area is used to define the peel strength. This is taken from the force-displacement curve after the initial peak reading.

The floating roller test is considered the more reliable method of the three peel techniques.

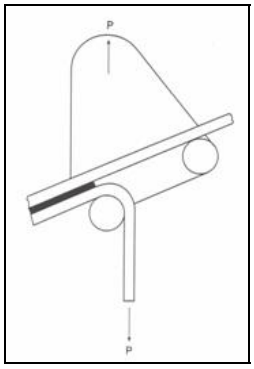

Figure 4.11: Floating roller method.

4.4.3 Shear test methods

ASTM and ISO standards supply a multitude of shear test geometries, each with the objective of producing a state of pure uniform shear in bulk adhesive or within an adhesive layer. In this session only lap joints tests (single, double and modified (Figure 4.12)) will be described.

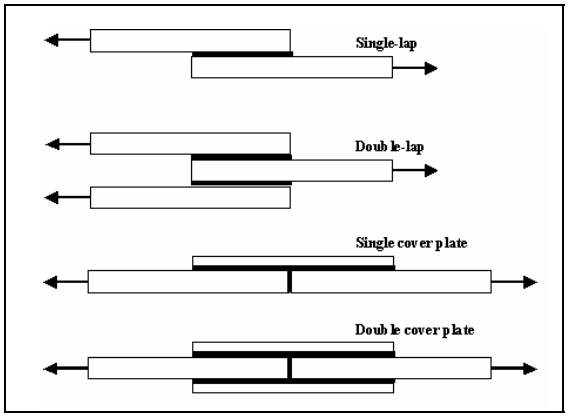

Figure 4.12: Various lap joint configurations (with increasing joint improvement from top to bottom).

4.4.3.1 Single lap joint

Despite all its obvious weaknesses, the lap-shear test is the most widely used method for producing *in-situ* shear strength data of an adhesively bonded joint. The test consists essentially of two rectangular sections, typically 25 mm wide, 100 mm long and 1.6 mm thick, bonded together, with an overlap length of 25 mm [43-45]. Testing can be conducted using standard tension/compression mechanical test equipment.

The lap-shear strength is given by:

$$\tau = \frac{P}{bL} \tag{4.2}$$

where P is the maximum load, b is the joint width and L is the joint length.

The analysis assumes the adherends are rigid, and that the adhesive only deforms in shear. In fact, the resultant stress distribution, across and along the bond length is very complex. The eccentricity of the load path causes out-of-plane bending moments, resulting in high peel stresses and non-uniform shear stresses in the adhesive layer (Figure 4.13). This effectively reduces the structural efficiency of the joint [35].

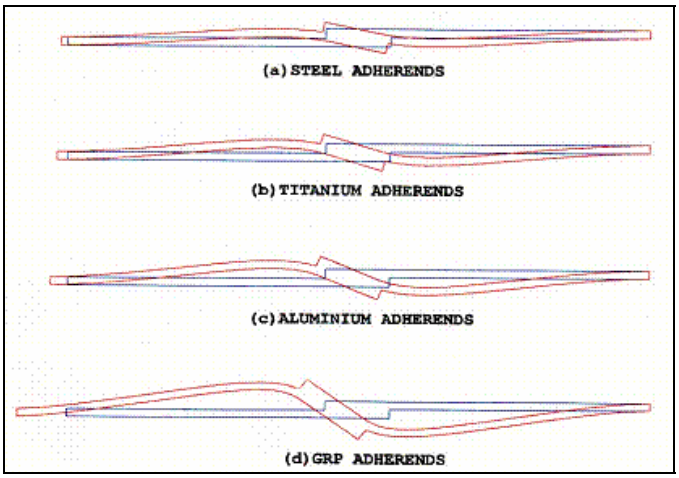

Figure 4.13: Relative deformation of a single-lap joint for different substrate materials.

The main problem with the single-lap shear test is that the average shear strength determined using this method does not correspond to a unique material property of the adhesive and therefore cannot be used as a design parameter (NB. Strength is strongly dependent on the joint geometry).

4.4.3.2 Double lap joint

Attempts to eliminate eccentric loading, responsible for bending of the adherends and rotation of the bonded region, have resulted in the development of a symmetric variant of the single-lap shear test, known as the double-lap joint. However, bending of the outer adherends is unavoidable, since the load is applied to the outer adherends via the adhesive, away from the neutral axis. The bending moment introduces tensile stresses across the adhesive layer at the free end of the overlap and compressive stresses at the other end. The centre adherend is free from the net bending moment. Double-lap joints are twice as strong as their single-lap counterparts. Various constructions of this test configuration are included in both national and international standards [43, 46, 47].

4.4.3.3 Modified lap joint

A number of design modifications have been recommended to reduce/remove peel stresses associated with single-lap and double-lap joints, and thus increase the strength of the bonded joint. An example is the double-butt strap lap joint with and without tapering (internal and external) (Figure 4.14 (a) and (b)). Tapering the adherends, minimises peel stresses, increases bond efficiency (i.e. strength) and alters the failure mode from peel to shear. The peel stresses virtually disappear when using external tapers with 30° fillets [35, 48].

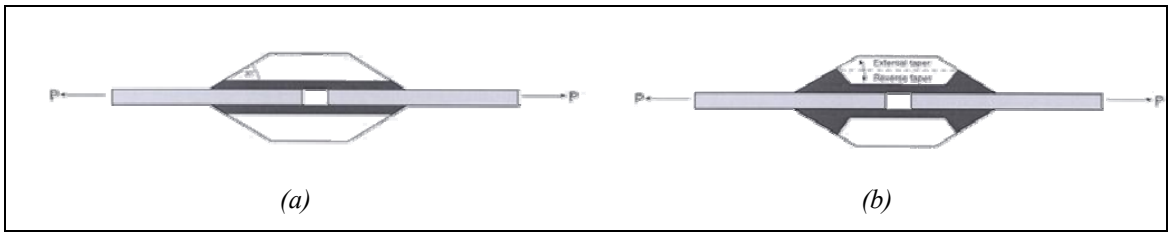

Figure 4.14: (a)Tapered strap joint; (b) bevelled strap joint.

4.4.4 Torsion test methods

4.4.4.1 Torsion loading of a circular rod

Torsion loading of a circular rod is mechanically one of the most accurate methods for characterising the shear properties of bulk resin materials [49, 50]. Specimens may be moulded or machined directly from rods. The ends of the gauge-section are filleted to minimise stress concentrations present at these locations.

The high degree of machining required exposes this specimen geometry to a high risk of machine-induced damage. This is compounded by difficulties in producing castings free of voids and residual stresses place considerable limitations on the materials that can be evaluated using the torsion method.

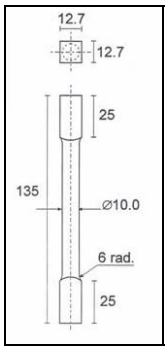

Figure 4.15: Torsion rod specimen.

Surface shear strain is measured using either strain gauges or contact extensometers. Strain gauges are adhesively bonded to the specimen surface at the centre of the gauge-section. The gauges are oriented at ±45° to the longitudinal axis of the specimen. An additional axially aligned strain gauge is recommended to monitor longitudinal strain. Tensile or compressive axial strains must not be present throughout the test duration. The shear modulus is determined from the linear region of the stress-strain curve.

Simple data reduction procedures are available for both linear and non-linear stress-strain response of circular rods in torsion. The analysis procedure developed by Nadai [51] for metals can be used to correct for the non-uniform shear stress distribution through the specimen cross-section, which occurs during non-linear stress-strain behaviour. The accuracy and repeatability of strain measurements, resulting from the large gauge-length, is relatively high compared with other test methods. As with all bulk test specimens, the strength data is dependent on the quality of the specimen. Internal stress concentrations in the form of entrapped air introduced during processing can result in premature failure.

4.4.4.2 Butt torsion test

Butt torsion test is a suitable method for all types of adhesives and is capable of generating reliable shear modulus values and stress-strain curves. Specimen geometry is similar to butt tension specimen (see §4.4.1.1). Contact extensometers are used to measure the angular rotation across the adhesive. A major disadvantage of this method is the difficulty of obtaining high precision strain measurements, due to the very low angular displacements (1–2 degrees) associated with this test configuration [50].

Shear modulus G can be determined from the following equation:

$$G = \frac{2t}{\pi R^4}\left(\frac{T}{\theta}\right) \tag{4.3}$$

where T is applied torque, R is the radius, t is the adhesive layer thickness and q is the angular displacement.

The stiffness of the adherends needs to be considerably higher than the adhesive stiffness, in order to minimise the effect of adherend deformation on the stress-strain response. Strain measurements need to be corrected for the effect of adherend deformation and non-linear stress-strain behaviour (i.e. non-uniform shear stress distribution across the bond area). The shear distribution is high on the external surface and lower in the centre.

4.5 Experimental equipment

In the Polymer Injection Forming process, one of the most important problems is that good bonding strength between the plastic part and the sheet metal part should be obtained. In the traditional manufacturing process of metal/polymer macro-composites, consisting on forming the plastic and metal part separately and then joining the two ones by means of a glue operation, the bonding process is already optimized. However, in the PIF process this phase has not being investigated yet.

In order to produce a metal/polymer part which could be easily used for testing the strength of the bonding between the two materials (Figure 4.16 (b)), the original geometry of the component used in the previous described tests was modified as following. The cavity of the mobile insert of the mould was deleted, resulting in a plane surface. In this manner, during the injection phase of the polymer, the sheet metal blank is not formed and it remains plane. In order to perform this task without modify the mould, a plane plate of 16 mm of thickness was fixed on the mobile cavity, as shown in Figure 4.16 (a).

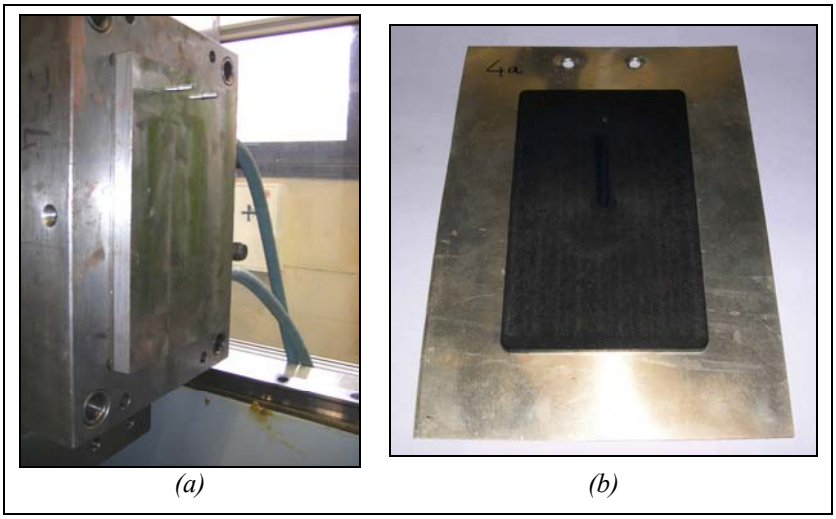

Figure 4.16: (a) Plane plate used for mould cavity geometry modification; (b) metal/polymer macro-composite component obtained with the modified geometry.

In order to test the bonding strength between metal and polymer, a shear test was designed using the composite part as specimen. This task was carried out by means of a MTS universal tensile machine, located at DIMEG Lab, and a special equipment properly designed. This consists of a main plate, to which other component are fixed (Figure 4.17). The slide element is fixed to the main plate at a distance equal to 3.7 mm, in order to let the metal/polymer specimen to pass trough the two elements. Constraints are fixed to the main plate and their function consists on fixing the metal part of the specimen (which is the metal/polymer macro-composite) onto the main plate of the designed device.

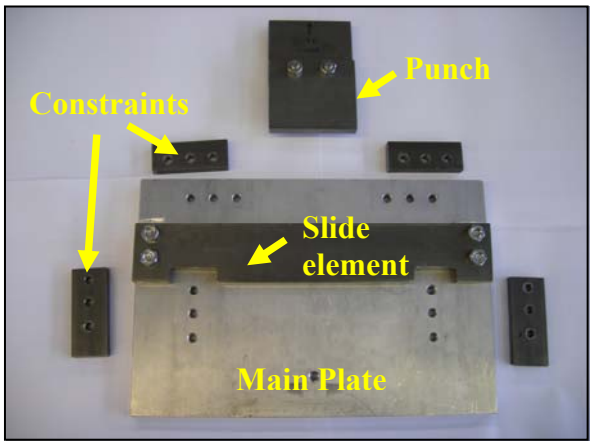

Figure 4.17: Equipment developed for shear testing of metal/polymer macro-composite specimens.

Dimensions of the main plate are reported in the working drawing shown in Figure 4.18.

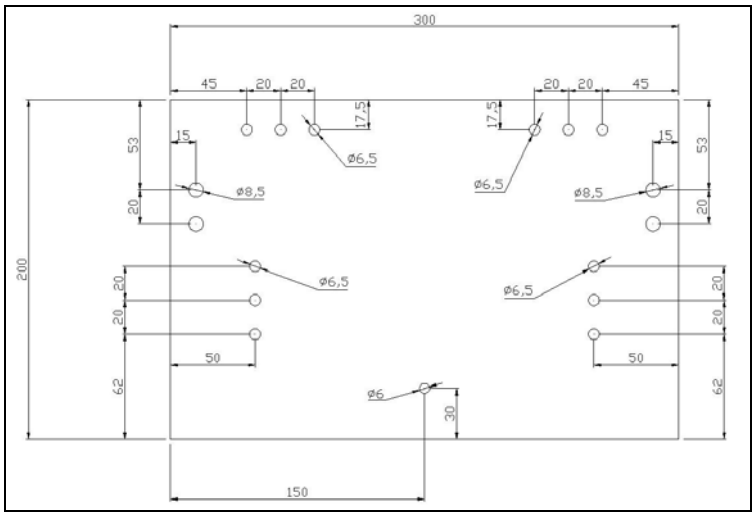

Figure 4.18: Working drawing of the main plate.

The main plate, during the shear test, is fixed onto one of the two vices of the MTS machine. The last component, the punch, is fixed on the other vice, as shown in Figure 4.19.

During the shear test, the metal part is constrained to the main plate, while the plastic part is forced to slide by the punch (Figure 4.20).

Such kind of test was chosen since the metal/polymer macro-composite part produced by means of the PIF process can be used as the test specimen, without any further working. Instead, testing methods described in §4.4 require additional work, in order to prepare testing specimens.

Figure 4.19: Shear test equipment assembled on the MTS machine.

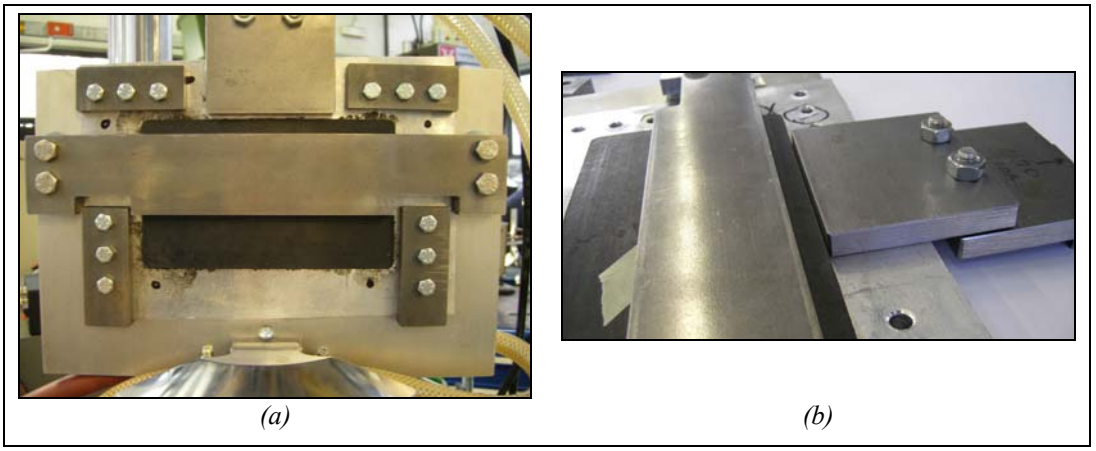

(a) *(b)*

Figure 4.20: Details of the shear test: (a) test specimen assembled on the testing device; (b) punch-specimen interaction.

4.5.1 Materials tested

Metal/polymer macro-composite components for automotive application are nowadays produced mainly by two separate processes, one for manufacturing the metal part, the other for manufacturing the plastic part, as previously discussed. The two parts are joined together by means of an adhesive. In Plastal, the main used adhesive is the 3M Scotch-Grip™ 9348.

The 3M Scotch-Grip™ 9348 is an acrylic based resin. It contains very fine solid adhesive particles immersed in a liquid solvent. The main function of the solvent consists on keeping inert the adhesive particles. Painting a surface, the solvent evaporates and adhesive particles become active.

The main objective of the study on the metal-polymer adhesion carried out in this work consists on investigating the influence of the main injection moulding process parameters on the adhesion quality between the metal and the plastic part. This task was achieved using two different types of adhesives.

The first is the 3M Scotch-Grip™ 9348, the second is the SikaTherm® - 4800 LV.

The SikaTherm® - 4800 LV is a polyurethanic bi-component dispersion used in conjunction with the SikaCure 8011/00 BC which is a polymerizing agent. The two-components SikaTherm adhesive is prepared as a mixture composted by 100 parts of SikaTherm and 7-10 parts of SikaCure.

All the tested specimens were produced with the plastic part made by the PC+ABS+20%GF polymer Bayblend T88-4N from Bayer.

4.5.2 Experimental results

The influence of the main injection moulding process parameters on the adhesion quality between the plastic and the metal part was investigated by means of the shear test equipment described in §4.5.

The injection moulding process parameters considered were the polymer injection temperature and the injection speed. Two types of adhesives were studied: the 3M Scotch-Grip™ 9348 and the SikaTherm® - 4800 LV.

The experimental procedure consisted in manufacturing metal/polymer components by means of the PIF process, changing opportunely the process parameters and the adhesive type. Obtained parts were then used as specimen in the shear test.

Experimental tests were designed according to a three factors 2 levels full factorial design (2^3 DOE) in 8 runs and 3 replications, as listed in Table 4.2. Each setting of high and low was based on the purpose of maximize the influence of the injection moulding parameters on the adhesion quality.

Table 4.2: Factors levels for experimental plan.

	ADHESIVES					
TEMPERATURE.	SikaTherm-4800 LV			3M Scotch-Grip 9348		
240°C	**Injection speed [mm/s]**	40	1) 2) 3)	**Injection speed [mm/s]**	40	7) 8) 9)
		90	4) 5) 6)		90	10) 11) 12)
280°C	**Injection speed [mm/s]**	40	19) 20) 21)	**Injection speed [mm/s]**	40	13) 14) 15)
		90	22) 23) 24)		90	16) 17) 18)

Shear tests were carried out using a deformation speed equal to 0.1 mm/s. Obtained results are summarized in the following figures as force/displacement plots.

Figure 4.21 reports the mean force/displacement response of the 3M Scotch-Grip™ 9348 joint at different polymer injection temperature and injection speed. From these plots it can be concluded that injection speed influence the adhesion quality only at the low polymer injection temperature. When a temperature equal to 240°C is used for the melting polymer, the specimens obtained using a high injection speed decrease the displacement at break. However,

the break force is more or less the same. Instead, when a high temperature (280°C) is used for the injected polymer, the force/displacement response of specimen is independent from the used injection speed.

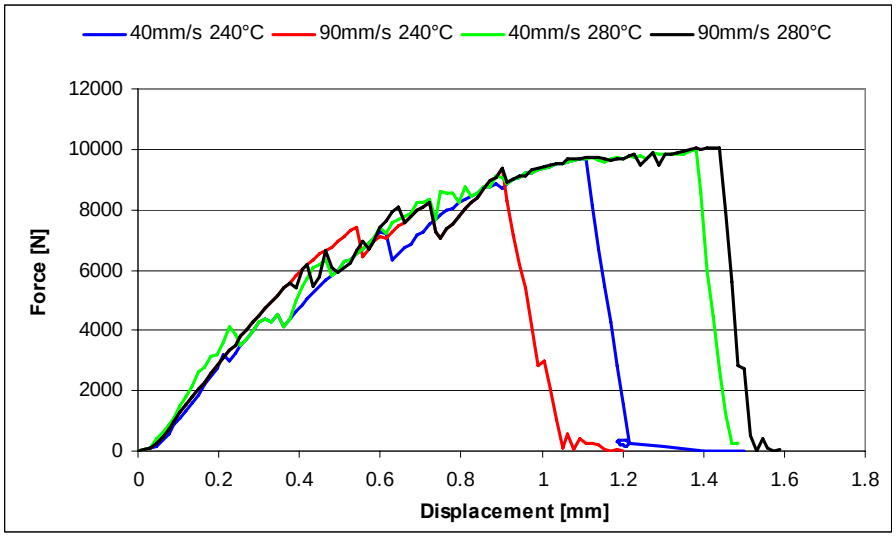

Figure 4.21: Mean force/displacement response of 3M Scotch-Grip™ 9348 joint at different polymer injection temperature and injection speed.

Figure 4.22 reports the mean force/displacement response of the SikaTherm® - 4800 LV joint at different polymer injection temperature and injection speed. From these plots it is clear that both polymer injection temperature and injection speed have no influence on the force/displacement response of the joint.

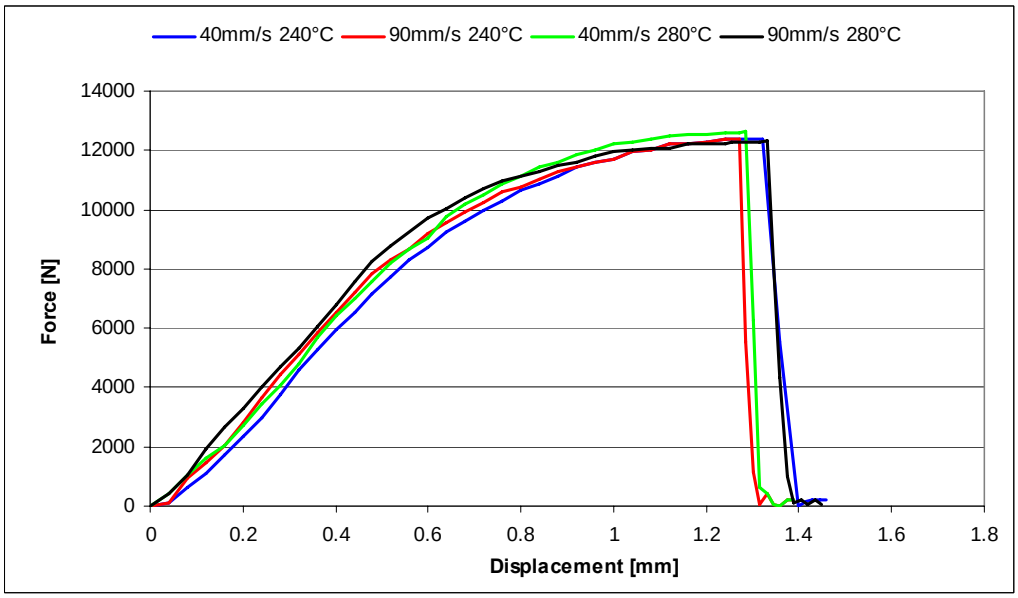

Figure 4.22: Mean force/displacement response of SikaTherm® - 4800 LV joint at different polymer injection temperature and injection speed.

Figure 4.23 compares the mean force/displacement response of the 3M Scotch-Grip™ 9348 joint with the SikaTherm® - 4800 LV one. In this case the specimens are obtained at a polymer injection temperature equal to 240°C. The comparison shows that the Sika joint has a greater force and displacement at break. As a consequence, the Sika joint is stronger than the 3M joint.

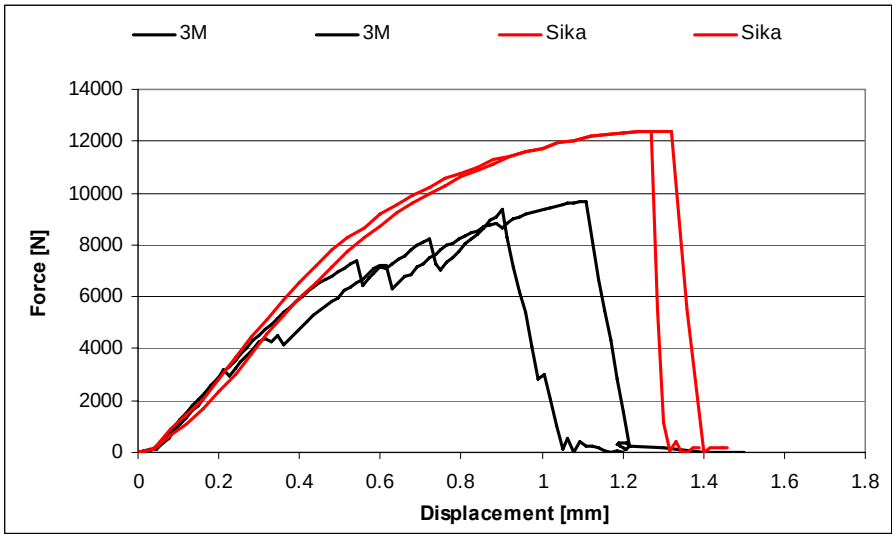

Figure 4.23: Mean force/displacement response of 3M Scotch-Grip™ 9348 joint compared to SikaTherm® - 4800 LV joint obtained with a polymer injection temperature equal to 240°C.

The situation is quite similar also for specimens obtained at a polymer temperature equal to 280°C, as shown in Figure 4.24. In this case, however, the 3M joint shows a higher displacement at break

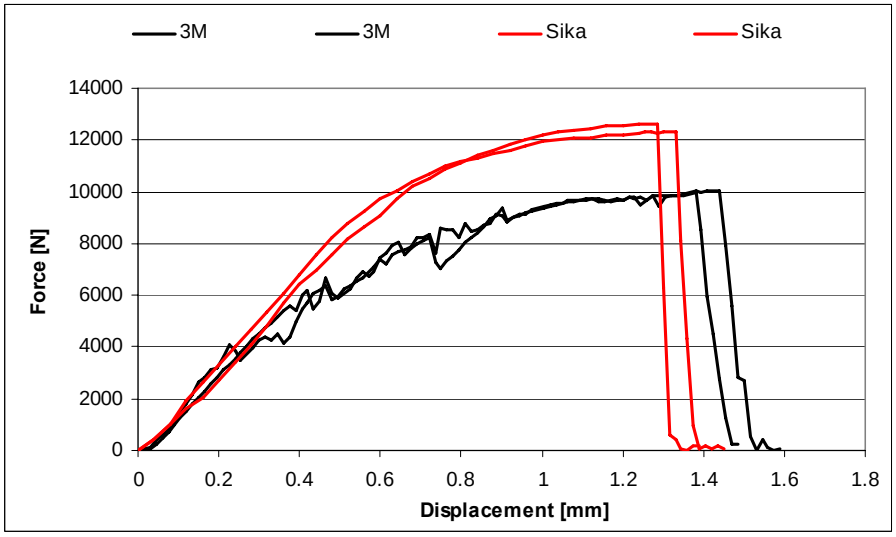

Figure 4.24: Mean force/displacement response of 3M Scotch-Grip™ 9348 joint compared to SikaTherm® - 4800 LV joint obtained with a polymer injection temperature equal to 280°C.

Comparing the force/displacement response of the joints obtained by the two kinds of adhesives, it can be concluded that the behaviour of the Sika joint is smoother. The 3M joint, instead, shows a force/displacement plot as a tooth of a saw profile. This is due to continuous micro-cracks which are originated during the shear test.

CHAPTER 5

MATERIALS CHARACTERIZATION

In order to obtain accurate results from numerical simulations of the Polymer Injection Forming process, as described in the next chapter, it is necessary to describe correctly the mechanical behaviour of the aluminium alloy 1050-O and the rheological behaviour of the Bayblend T-88 4N polymer.

In this chapter the equipment for the mechanical characterization of the sheet metal, as well as the obtained results, will be discussed. Then the rheological characterization of the polymer will be presented.

5.1 Mechanical characterization of the aluminium alloy

The objective of this task consists on obtaining the true stress – true strain curves of the 1050-O aluminium alloy at different temperatures. This allow to know the real material behaviour during the Polymer Injection Forming process.

5.1.1 Test equipment

Material tests were carried out on an hydraulic universal test machine, MTS 322, located at DIMEG lab (Figure 5.1 (a) and (b)).

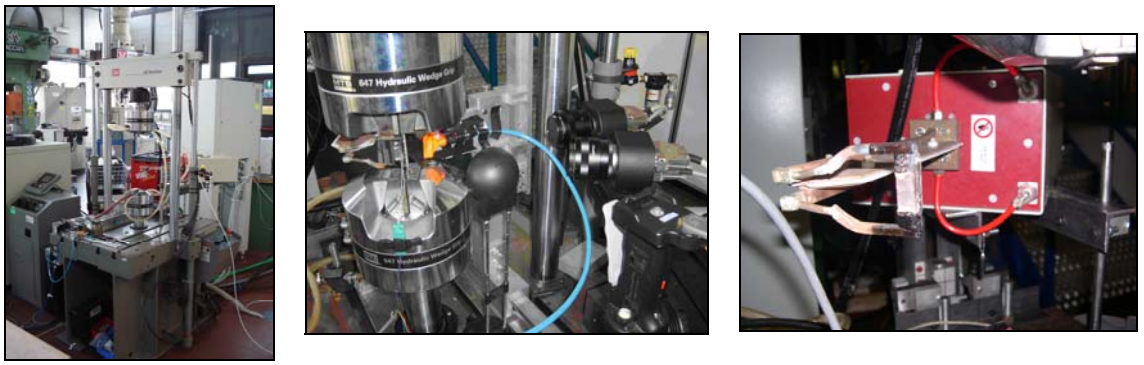

(a) (b) (c)

Figure 5.1: Test equipment employed for the metal mechanical characterization: (a) Universal test machine MTS 322; (b) head of the magnetic induction heater, model Egma 30R.

During the tests at high temperature, a magnetic induction heater, model Egma 30R, was employed (Figure 5.1 (c)). This device is able to heat the sheet metal specimen by electromagnetic induction, where eddy currents are generated within the metal and resistance leads to Joule heating of the metal.

During material tests, specimen deformation was measured by means of the ARAMIS system. This device measures 3D deformation using stereo high-resolution video cameras (Figure 5.2).

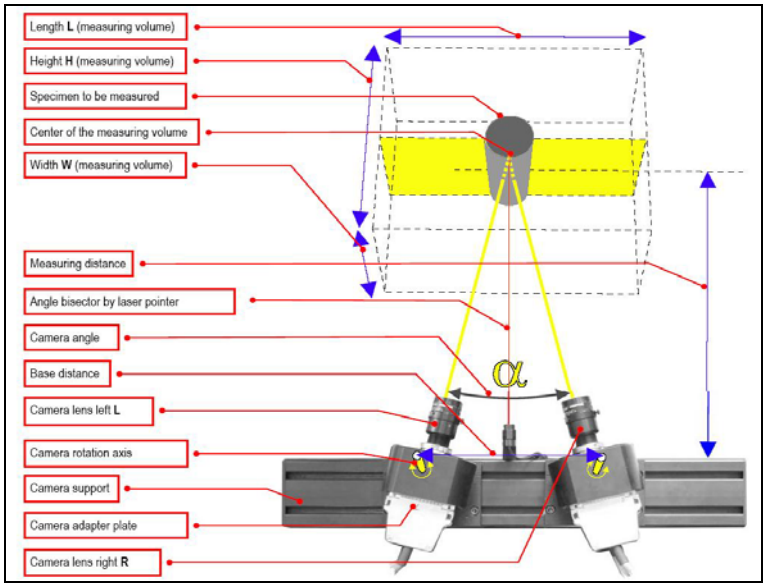

Figure 5.2: Video-cameras arrangement in the ARAMIS measuring system.

The last device employed during the sheet metal material characterization was a thermo-camera made by FLIR SYSTEM. This device was used during the tests carried out at a temperature in the range between 150°C and 300°C and it was employed in order to monitor temperature distribution of the metal specimen.

5.1.2 Tests set-up

Compared to low temperature tests, mechanical characterization of the sheet metal specimens of 1050-O aluminium alloy at high temperature is more difficult. This is mainly due to the very thin thickness of the sheet metal (0.7 mm).

In order to find out the best way to monitor the specimen temperature, several tests were carried out first. At the beginning, tests were performed using a k-thermocouple welded to specimen surface. However the resulting stress-strain curves of the tested material were influenced by the welding. This was highlighted since specimen fracture, at the end of the, mechanical test, was located always in the welding zone. This problem was mainly due to the thin specimen thickness.

Also tests carried out using thermocouples glued to specimen surface were affected by the same problem.

The final solution consists on using a thermo-camera as a system for monitoring specimen temperature.

The geometry of the specimens used in the mechanical tests is reported in Figure 5.3.

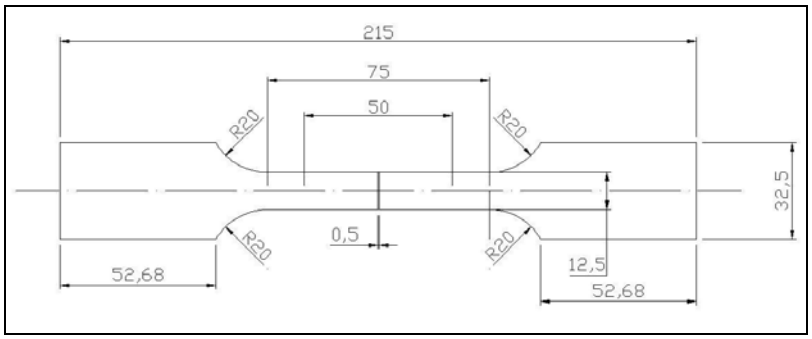

Figure 5.3: Specimen geometry used in mechanical tests.

When preparing the specimens for strain measuring using the ARAMIS system, a stochastic pattern is applied to the surface using a colour spray (Figure 5.4).

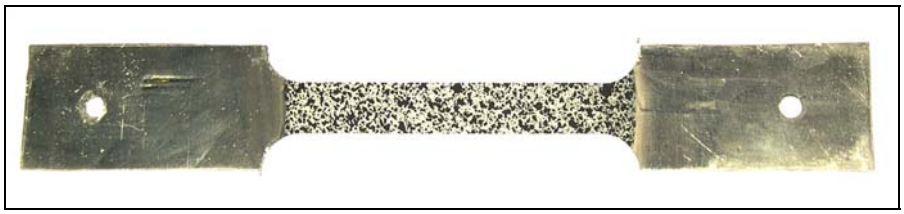

Figure 5.4: Stochastic pattern applied on strain measuring area of specimen.

In order to increase the colour contrast, improving strain measuring accuracy, a white layer of colour was first painted on the area if interest of the specimen. Then a black colour was sprayed over the white layer, creating the stochastic pattern.

5.1.2.1 Thermo-camera calibration

In order to correctly measure the specimen temperature by means of the thermo-camera, its calibration is necessary. In order to perform this task, a comparison between specimen temperature measured by means of a k thermocouple and by the thermo-camera was carried out. Measured values by the thermo-camera were then equalized to the ones obtained by thermocouples changing the parameters relating to surface emissivity of the aluminium surface.

This procedure was repeated at the following temperature: 150°C, 200°C, 250°C, 300°C. For all these temperature, the calibrated emissivity value was equal to 0.9.

The thermo-camera had a double function. First controlling specimen temperature during tests at high temperature. Secondly, determining the working length of specimens, in order to set the test speed on the testing machine. In order to perform this task, at each tested temperature, the length of the area of the specimen at uniform temperature was measured (Figure 5.5). At each temperature, the working length of the specimen was different, as reported in Table 5.1.

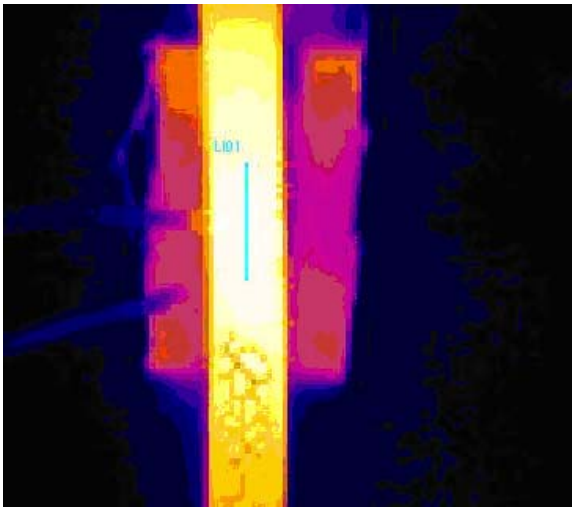

Figure 5.5: Image of the hot specimen from thermo-camera.

5.1.2.2 ARAMIS calibration

In order to measure specimen deformation during the tensile test, the optical measuring system ARAMIS was employed, as mentioned previously. Although this system is able to measure deformations in a 3D spatial domain, during tensile tests of the sheet metal only deformations along two directions are necessary to measure. Therefore, only one camera of the ARAMIS system carried out the deformation measure.

In order to perform accurate measures, the ARAMIS system requires to be calibrated. During tensile tests of the aluminium sheet metal, two different calibration were carried out. The first one was employed for tests at room temperature, the second one for tests at high temperature. This approach was necessary since during the two sets of test the working length of the specimens are different. During tests at room temperature, the working length of specimens is greater, around 50 mm. The cameras of the ARAMIS system were therefore placed at a greater distance from the specimen. Instead, during tests at high temperature, the working length of specimens is around 20 mm, and the cameras of the system need to be placed close to specimens.

The ARAMIS calibration was carried out by means of two comparison blocks. The first one was employed for system calibration, when it measured deformation at room temperature (Figure 5.6 (a)). The second one was employed for system calibration, when it measured deformation at high temperature (Figure 5.6 (b)). The two comparison blocks differ in dimensions of their internal grids. Grid dimensions have to be correlated to dimensions of the stochastic pattern painted on the surface to be measured. During tests at room temperature, ARAMIS cameras were placed at a greater distance from the specimen, as previously explained. So stochastic pattern had to be greater enough, in order to be recognized by the ARAMIS measuring system (Figure 5.7). Therefore, calibration block with a coarse grid was employed for calibration of the ARAMIS system, when it measured specimen deformations at room temperature. Instead, the comparison block with a fine grid was employed in order to calibrate the system when it measured deformation at high temperature. In this case, in fact, ARAMIS camera were placed near the specimen. Therefore the stochastic pattern on the specimen surface needed to be fine, as shown in Figure 5.8.

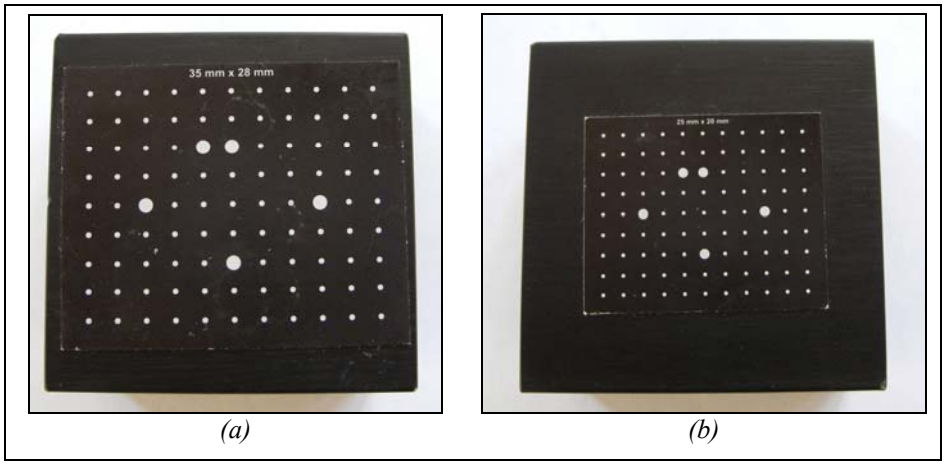

Figure 5.6: Comparison blocks for ARAMIS calibration at: (a) room temperature; (b) high temperature.

Figure 5.7: Stochastic pattern on specimen surface for tensile tests at room temperature.

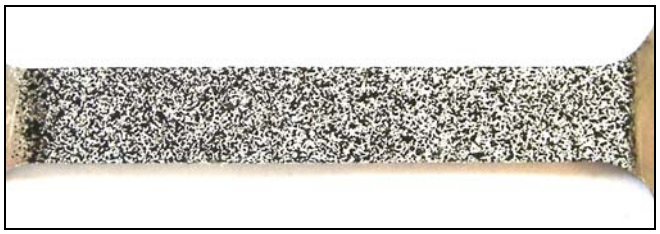

Figure 5.8: Stochastic pattern on specimen surface for tensile tests at high temperature.

5.1.3 Tensile tests

Tensile tests on the 1050-O aluminium alloy sheet were carried out in order to determine both the stress-strain behaviour of the material and its anisotropy characteristics.

During the Polymer Injection Forming process, the sheet metal is in contact with hot polymer. So the forming process of the metal part occurs at a temperature different fro room temperature. For this reason, the material characterization was carried out both at a room temperature and higher temperatures. In particular, 20°C, 150°C, 200°C, 250°C and 300°C were chosen as tests temperatures.

In order to measure the anisotropic behaviour of the 1050-O aluminium alloy, tensile specimens at orientation 0°, 45° and 90° relative to rolling direction were produced.

At each test temperature and specimen orientation, several tensile tests were carried out in order to get reliable material data.

Deformation speed of specimens during tensile tests was set equal to 0.1 [s^{-1}]. This value was obtained from a preliminary numerical investigation on the PIF process.

In order to apply the desired value of deformation speed to the specimen, it is necessary to know the working length of the specimen, according to the following formula:

$$\dot{\varepsilon} = \frac{v}{l} \Rightarrow v = \dot{\varepsilon} l \tag{5.1}$$

where l is the working length of the specimen, $\dot{\varepsilon}$ is the strain rate in [s^{-1}] and v is the speed of the vice of the tensile machine.

During the tests at high temperature, the working length of specimens was obtained by means of the thermo-camera, as explained in §5.1.2.1. It was assume equal to the part height of the specimen at uniform temperature.

Table 5.1 summarizes specimen working length and corresponding vice speed in order to get a deformation speed of the specimen equal to 0.1.

Table 5.1: Working length and vice speed at different test temperature.

	20°C	**150°C**	**200°C**	**250°C**	**300°C**
L [mm]	50	24.2	22.7	21.6	16.6
V [mm/s]	5	2.022	2.271	2.159	1.662

5.1.3.1 Data analysis

As previously described, in order to calculate the stress-strain behaviour of the 1050-O aluminium alloy, the tensile force from the testing machine and corresponding specimen displacements measured by the ARAMIS system were used.

Figure 5.9 shows principal strains in a typical tensile test specimen.

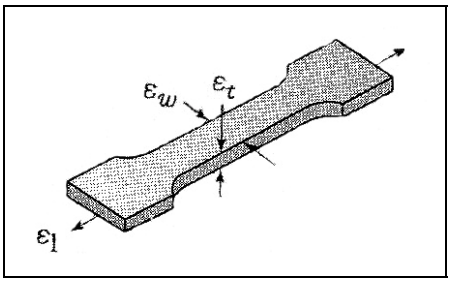

Figure 5.9: Principal strains in a tensile-test specimen.

Since the ARAMIS system plots the principal strains, a mathematical elaboration was necessary in order to calculate the corresponding specimen stress, as explained in the following.

$$\sigma = \frac{F}{A} \qquad A = s \cdot t \tag{5.2}$$

where σ is the stress, F is the force as measured by the tensile machine, A is the section area of the specimen, s is the width of the specimen and t is the thickness.

The true strain is derived from:

$$\varepsilon = \int_{l_0}^{l} \frac{dl}{l} = \ln\left(\frac{l}{l_0}\right) \qquad l = l_0 \cdot e^{\varepsilon_l} \tag{5.3}$$

where l is the true length of the specimen and l_0 is the initial length.

Deformation along the width and the thickness of the specimen can be calculated from the following equations:

$$s = s_0 \cdot e^{\varepsilon_w} \qquad t = t_0 \cdot e^{\varepsilon_t} \tag{5.4}$$

The volume of the metal specimen in the plastic region of the test remains constant, hence:

$$0 = \varepsilon = \varepsilon_l + \varepsilon_w + \varepsilon_t \Rightarrow \varepsilon_t = -\varepsilon_l - \varepsilon_w \tag{5.5}$$

So, the stress of the tested specimen can be calculated as a function of major strain only, as expressed in the following formula:

$$\sigma = \frac{F}{s_0 \cdot t_0 \cdot e^{-\varepsilon_l}} \tag{5.6}$$

5.1.3.2 Tests results

Obtained results are summarized in the following figures, which plots the stress-strain behaviour of the 1050-O aluminium alloy sheet at different test temperatures (20°C, 150°C, 200°C, 250°C and 300°C) and specimen orientation relative to rolling direction (0°, 45°, 90°).

Figure 5.10 to Figure 5.14 plot the stress-strain curves at different specimen orientations at each tested temperature.

Figure 5.15 to Figure 5.17 plot the stress-strain curves at different tested temperatures at each specimen orientation.

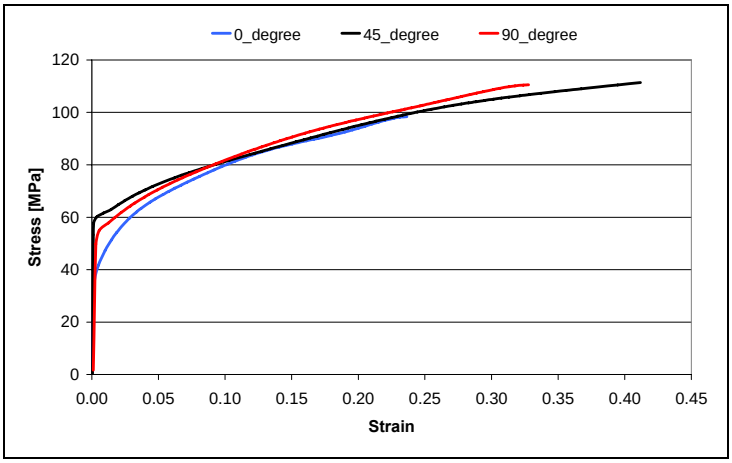

Figure 5.10: Stress-strain behaviour of the 1050-O aluminium alloy sheet at 20°C and at orientation 0°, 45° and 90° relative to rolling direction.

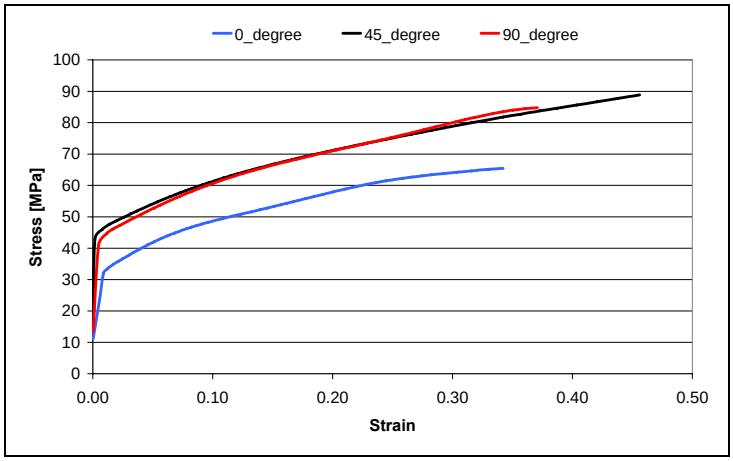

Figure 5.11: Stress-strain behaviour of the 1050-O aluminium alloy sheet at 150°C and at orientation 0°, 45° and 90° relative to rolling direction.

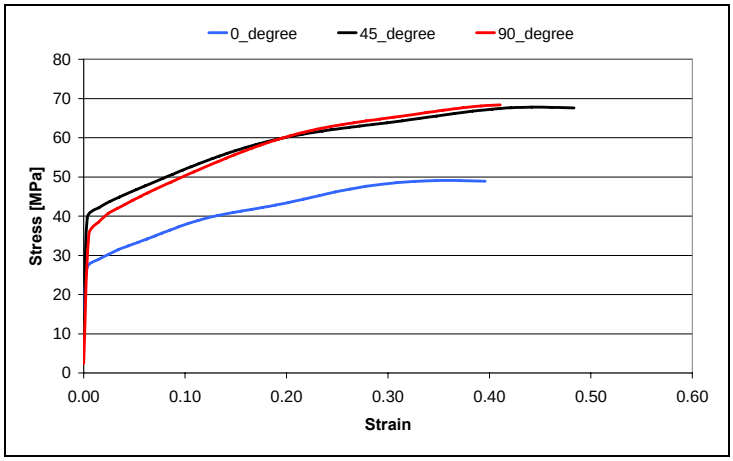

Figure 5.12: Stress-strain behaviour of the 1050-O aluminium alloy sheet at 200°C and at orientation 0°, 45° and 90° relative to rolling direction.

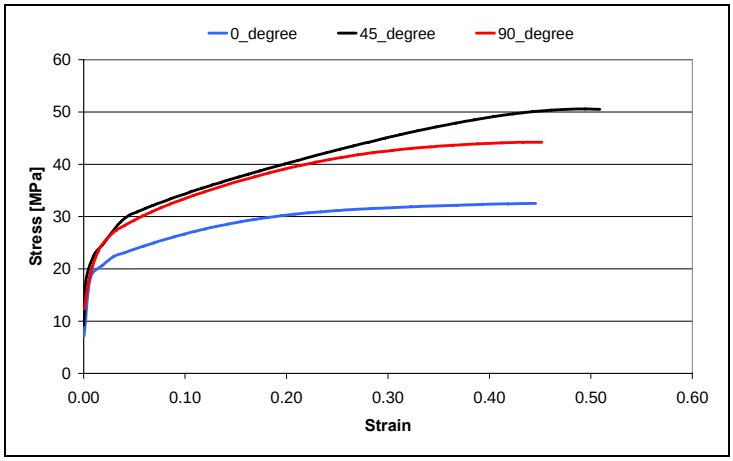

Figure 5.13: Stress-strain behaviour of the 1050-O aluminium alloy sheet at 250°C and at orientation 0°, 45° and 90° relative to rolling direction.

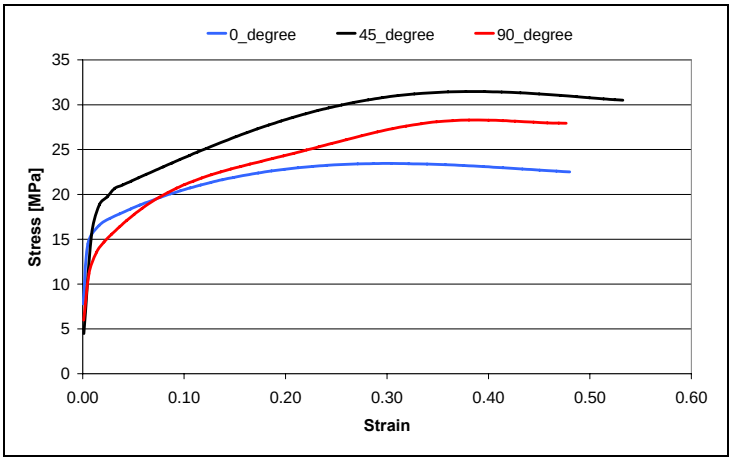

Figure 5.14: Stress-strain behaviour of the 1050-O aluminium alloy sheet at 300°C and at orientation 0°, 45° and 90° relative to rolling direction.

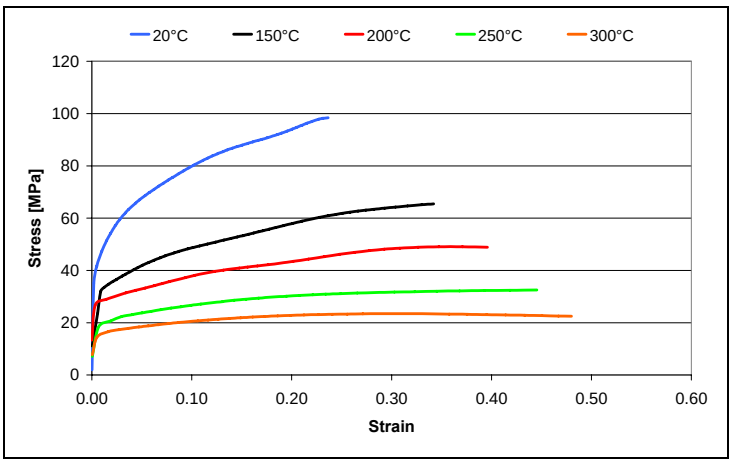

Figure 5.15: Stress-strain behaviour of the 1050-O aluminium alloy sheet at 20°C, 150°C, 200°C, 250°C, 300°C and at orientation 0° relative to rolling direction.

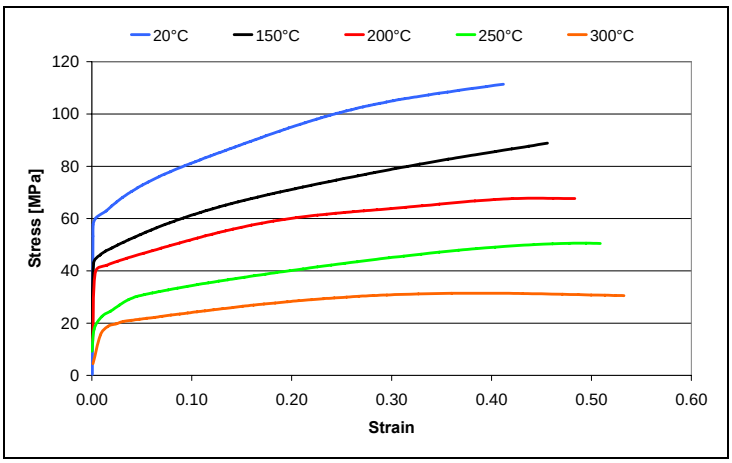

Figure 5.16: Stress-strain behaviour of the 1050-O aluminium alloy sheet at 20°C, 150°C, 200°C, 250°C, 300°C and at orientation 45° relative to rolling direction.

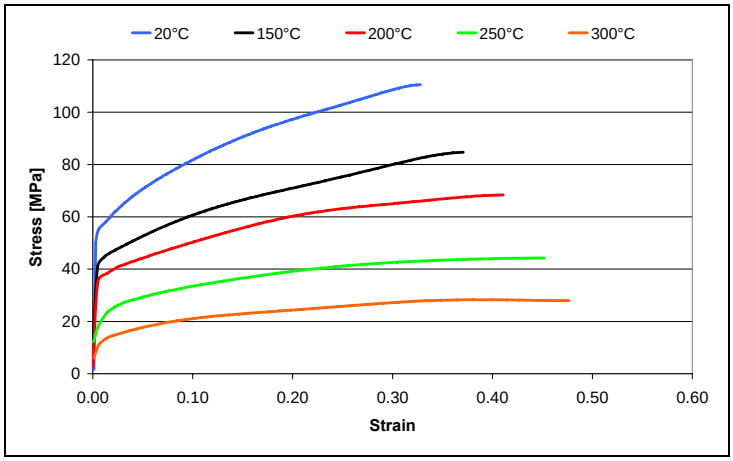

Figure 5.17: Stress-strain behaviour of the 1050-O aluminium alloy sheet at 20°C, 150°C, 200°C, 250°C, 300°C and at orientation 90° relative to rolling direction.

From the above reported plots, it can be concluded that the material tested is anisotropic since the stress-strain behaviour depends on the specimen orientation. In particular, specimens oriented at 45° relative to rolling directions have the major stress and strain at break.

Specimens oriented at 0° are characterized by the minus stress and strain at break. Specimens oriented at 90° show stress-strain curves close to the ones obtained by specimen at 45°, but stress and strain at break are lower.

The anisotropic characteristics of the aluminium sheet are more evident at high temperature. For tests at room temperature, instead, the stress-strain behaviour of the material is quite similar.

Figure 5.15 to Figure 5.17 show that increasing test temperature the material becomes more and more ductile, with lower stress and much higher strain at break. The temperature effects on material ductility are greater for specimens at 0° of orientation.

5.1.3.3 Anisotropy

In order to calculate material anisotropy of the 1050-O aluminium alloy specimen, at least five tensile tests at each testing temperature and specimen orientation were carried out. Replications of tests were necessary to assure results consistency. For each test, the normal anisotropy was calculated by means of the following formula using strain values obtained by the ARAMIS system:

$$R = \frac{\varepsilon_w}{\varepsilon_t} = \frac{\ln\left(\frac{w_0}{w_f}\right)}{\ln\left(\frac{t_0}{t_f}\right)} = \frac{\ln\left(\frac{w_0}{w_f}\right)}{\ln\left(\frac{w_f l_f}{w_0 l_0}\right)} \tag{5.7}$$

The subscripts *o* and *f* refer to the original and final dimensions, respectively. An *R* value of unity indicates that the width and thickness strains are equal to each other; that is, the material is isotropic.

Table 5.2 summarizes the mean values of normal anisotropy obtained for tensile tests in the same conditions.

Table 5.2: Obtained mean values of normal anisotropy.

	SPECIMEN ORIENTATION		
TEMPERATURE	**0°**	**45°**	**90°**
20°C	0.65	0.95	0.95
150°C	0.71	0.87	0.84
200°C	0.74	0.88	0.81
250°C	0.78	0.89	0.75
300°C	0.79	0.89	0.70

Since the 1050-O specimen is obtained by a rolled sheets, it will present also a planar anisotropy. Thus, the *R* value of this specimen will depend on the specimen's orientation with respect to the rolling direction of the sheet. In this case, an average *R* value, $\overline{R}$, is calculated as following:

$$\overline{R} = \frac{R_0 + 2R_{45} + R_{90}}{4} \tag{5.8}$$

where the subscripts 0, 45 and 90 refer to angular orientation (in degree) of the test specimen with respect to the rolling direction of the sheet. An isotropic material has an $\overline{R}$ value of unity.

The planar anisotropy of a sheet, ΔR, can also be defined in terms of directional *R* values as:

$$\Delta R = \frac{R_0 - 2R_{45} + R_{90}}{2} \tag{5.9}$$

which is the difference between the average of the *R* values in the 0° and 90° directions to rolling and the *R* value at 45°. An isotropic material has an ΔR value equal to zero [52].

Obtained values are reported in Table 5.3.

Table 5.3: Calculated values of the average anisotropy and planar anisotropy as a function of testing temperature.

TEMPERATURE	AVERAGE ANISTROPY	PLANAR ANISTROPY
20°C	0.88	- 0.15
150°C	0.83	- 0.10
200°C	0.83	- 0.11
250°C	0.83	- 0.13
300°C	0.82	- 0.14

From the obtained results it can be concluded that average anisotropy is nearly constant at high temperature. At room temperature, instead, the high value of the average anisotropy is a consequence of the most isotropic behaviour of the 1050-O aluminium alloy.

5.1.4 Modelling of the mechanical behaviour of the 1050-O alloy

Results accuracy obtained by numerical simulations of a manufacturing process strongly depends upon goodness of input parameters. In numerical simulations of the PIF process, which will be described in the chapter six, the mechanical behaviour of the 1050-O alloy, as obtained by tensile tests above described, was implemented.

As it will be widely explained in the following chapter, the deformation process of the sheet metal during the PIF process was analyzed by means of the numerical code ANSYS Multiphysics. This code has several models for describing the stress-strain behaviour of a material. Among this models, the Voce model and the Hill model were used in order to model the stress-strain behaviour of the 1050-O aluminium alloy.

The Voce model is a non-linear isotropic hardening model. Hill's criterion is an extension to the Von Mises yield criterion to account for the anisotropic yield of the material.

5.1.4.1 The Voce model

The Voce hardening law for nonlinear isotropic hardening behaviour is specified by the following equation [53]:

$$\sigma = K + R_0 \cdot \varepsilon_{pl} + R_\infty \cdot (1 - \exp(-b \cdot \varepsilon_{pl})) \tag{5.10}$$

where:

K = elastic limit

R_0, R_∞ e b = material parameters characterizing the isotropic hardening behaviour of materials

ε_{pl} = equivalent plastic strain

The Voce model is plot in Figure 5.18.

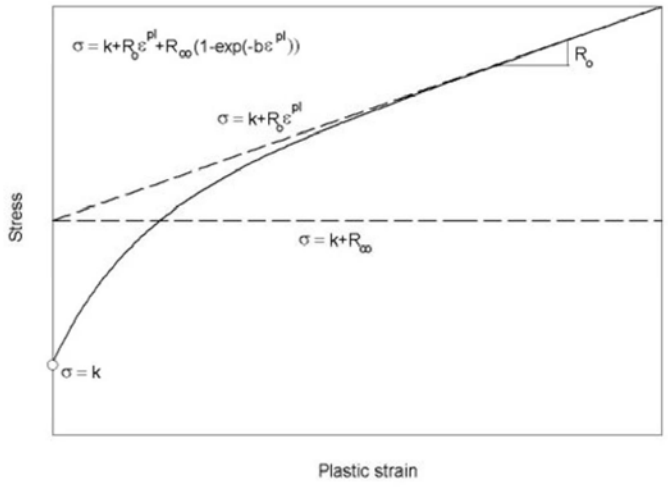

Figure 5.18: Nonlinear isotropic hardening stress-strain curve.

The advantage of this model is that the material behaviour is defined as a specified function which has only four material constants.

The material constants for the 1050-O aluminium alloy were obtained by fitting material tension stress-strain curves obtained by the carried out tests. Obtained results for each testing temperature and specimen orientation are summarized in Table 5.4.

Table 5.4: Obtained material constants of the Voce model.

Specimen oriented at 0° with respect to the rolling direction of the sheet					
	20°C	**150°C**	**200°C**	**250°C**	**300°C**
k	38,404	30,334	26,294	19,199	14,237
R_0	126,844	53,522	43,710	27,049	15,784
R_∞	30,513	18,129	9,175	6,411	5,529
b	28,727	12,723	14,382	13,735	21,424
Specimen oriented at 45° with respect to the rolling direction of the sheet					
	20°C	**150°C**	**200°C**	**250°C**	**300°C**
k	59,602	44,364	39,251	26,468	17,028
R_0	32,646	61,686	7,458	10,734	14,356
R_∞	43,379	16,647	25,363	26,177	9,828
b	5,544	10,312	7,232	2,953	10,679
Specimen oriented at 90° with respect to the rolling direction of the sheet					
	20°C	**150°C**	**200°C**	**250°C**	**300°C**
k	53,059	41,384	35,517	22,844	11,135
R_0	93,307	78,873	42,242	24,235	24,786
R_∞	28,009	14,961	22,687	13,348	8,515
b	12,074	13,886	5,57	9,658	20,135

5.1.4.2 Hill's model

Hill's criterion is an extension to the Von Mises yield criterion to account for the anisotropic yield of the material. When this criterion is used with the isotropic hardening option, the yield function is given by [53]:

$$f(\sigma) = \sqrt{\{\sigma\}^T [M] \{\sigma\}} - \sigma_0(\overline{\varepsilon}^p) \tag{5.11}$$

where:

σ_0 = reference yield stress

$\overline{\varepsilon}^p$ = equivalent plastic strain

The material is assumed to have three orthogonal planes of symmetry. Assuming the material coordinate system is perpendicular to these planes of symmetry, the plastic compliance matrix [M] can be written as:

$$[M]=\begin{bmatrix} G+H & -H & -G & 0 & 0 & 0 \\ -H & F+H & -F & 0 & 0 & 0 \\ -G & -F & F+G & 0 & 0 & 0 \\ 0 & 0 & 0 & 2N & 0 & 0 \\ 0 & 0 & 0 & 0 & 2L & 0 \\ 0 & 0 & 0 & 0 & 0 & 2M \end{bmatrix} \tag{5.12}$$

F, G, H, L, M and N are material constants that can be determined experimentally. They are defined as:

$$F=\frac{1}{2}\left(\frac{1}{R_{yy}^2}+\frac{1}{R_{zz}^2}+\frac{1}{R_{xx}^2}\right) \tag{5.13}$$

$$G=\frac{1}{2}\left(\frac{1}{R_{zz}^2}+\frac{1}{R_{xx}^2}+\frac{1}{R_{yy}^2}\right) \tag{5.14}$$

$$H=\frac{1}{2}\left(\frac{1}{R_{xx}^2}+\frac{1}{R_{yy}^2}+\frac{1}{R_{zz}^2}\right) \tag{5.15}$$

$$L=\frac{3}{2}\left(\frac{1}{R_{yz}^2}\right) \tag{5.16}$$

$$M=\frac{3}{2}\left(\frac{1}{R_{xz}^2}\right) \tag{5.17}$$

$$N=\frac{3}{2}\left(\frac{1}{R_{xy}^2}\right) \tag{5.18}$$

The yield stress ratios R_{xx}, R_{yy}, R_{zz}, R_{xy}, R_{yz} and R_{xz} are specified by the user and can be calculated as:

$$R_{xx}=\frac{\sigma_{xx}^{y}}{\sigma_0} \tag{5.19}$$

$$R_{xx}=\frac{\sigma_{yy}^{y}}{\sigma_0} \tag{5.20}$$

$$R_{xx}=\frac{\sigma_{zz}^{y}}{\sigma_0} \tag{5.21}$$

$$R_{xy} = \sqrt{3}\frac{\sigma_{xy}^{y}}{\sigma_0} \tag{5.22}$$

$$R_{yz} = \sqrt{3}\frac{\sigma_{yz}^{y}}{\sigma_0} \tag{5.23}$$

$$R_{xz} = \sqrt{3}\frac{\sigma_{xz}^{y}}{\sigma_0} \tag{5.24}$$

where: σ_{ij}^{y} = yield stress values.

Since the sheet metal specimen is very thin, a bi-dimensional stress state is considered. So the [M] matrix is reduced to a 3x3 matrix. The software automatically calculate matrix coefficients starting from yield stress at each temperature, which are summarized in Table 5.5.

Table 5.5: Yielding stress of the 1050-O aluminium alloy at different testing temperatures.

	Testing Temperature				
	20°C	**150°C**	**200°C**	**250°C**	**300°C**
σ_0 [MPa]	38.4	30.3	26.3	19.2	14.3
σ_{xx} [MPa]	38.4	30.3	26.3	19.2	14.3
σ_{yy} [MPa]	53.1	41.4	36.5	22.8	11.1
σ_{zz} [MPa]	0	0	0	0	0
σ_{xy} [MPa]	59.6	44.4	39.2	26.5	17
σ_{xz} [MPa]	0	0	0	0	0
σ_{yz} [MPa]	0	0	0	0	0

It was assumed as the reference direction the *x* axes, i.e. the orientation at 0° relative to rolling direction. The *y* direction refers to specimens at 90° of orientation and direction *xy* refers to specimens at orientation 45°.

Since stress state is considered bi-dimensional, σ_{zz}, σ_{xz} and σ_{yz} are equal to zero.

5.2 Rheological characterization of the polymer

One of the most influencing factor on the correctness of numerical simulations of the injection moulding process is the accuracy of the material input data. In particular, in the filling phase, the most important material characteristic is the rheological behaviour. The filling phase has been considered because of its large influence on the final components characteristics.

The complete characterization of polymer rheology requires two different devices:

1. Drag flows rheometer in which the shear is generated between a moving and a fixed surface, as for example cone and plate rheometers. This family of devices is suited to characterize the viscosity behaviour at very low shear rate (i.e. from 0.01 up to 10 [1/s]),
2. Pressure driven rheometer in which shear is generated by a pressure difference over a closed channel, as for example capillary and slit-die rheometers. This family of instruments is suited to characterize the viscosity behaviour at high shear rate (i.e. from 10^2 up to 10^5 [1/s]).

Normally the complete rheological characterization of a polymer is not necessary because during the filling phase high shear rates are developed (i.e. $10^3 \div 10^5$ [1/s]). For this reason the device used to obtain the values of the rheological models constants, implemented in the numerical codes, is the capillary or slit-die rheometers.

During the plastication phase in the injection moulding machine, the polymer is melted by the heat generated by electric heaters and overall by the action of a rotating screw. Because of these combined actions the rheological properties of the material, as measured at the nozzle, could be different from the properties of the unprocessed polymer.

In order to overcome this problem, at DIMEG lab a rheometer for the characterization of polymer under the same conditions of the injection moulding process was developed. The device is able to characterize in a easy and accurate way the material at high shear rate and melting the polymer in the same manner of the industrial process (equal mechanical-thermal history.). In this way accurate rheological data for the numerical simulations of the injection moulding process can be provided.

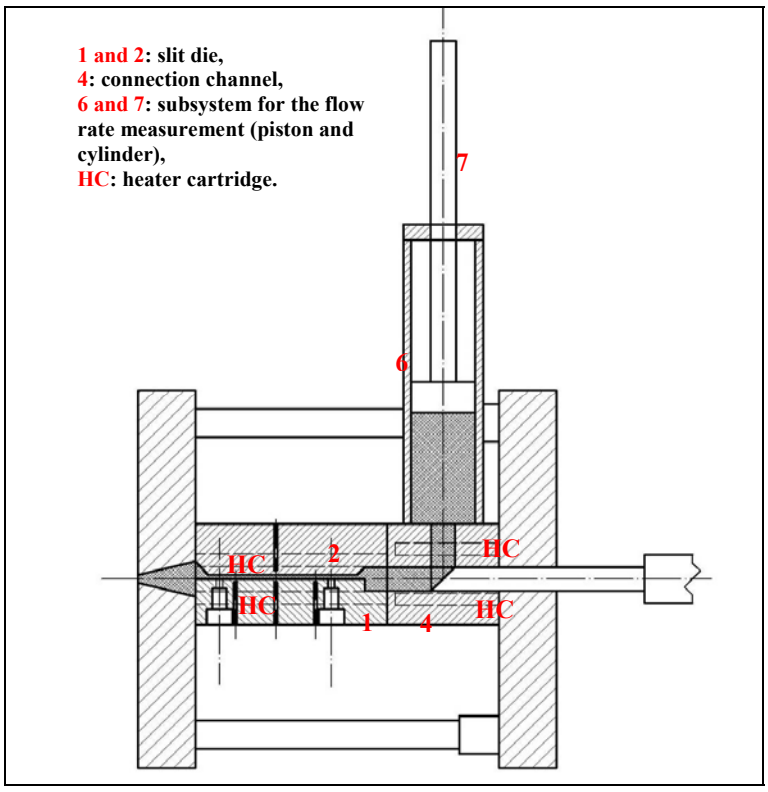

Figure 5.19: Scheme of the device developed at DIMEG lab for accurate measurement of polymer rheological behaviour.

The above mentioned device was employed in order to characterize the rheological behaviour of the polymer Bayblend T 88-4N. The material characterization was carried out at four different temperatures in order to model temperature dependency of the polymer viscosity.

Obtained data were fitted with the Cross-WLF model, in order to model the rheological behaviour of the polymer in the numerical simulation codes, as explained in the following chapter.

The mathematical formulation of the Cross-WLF model is reported in the following equations [23]:

$$\eta = \frac{\eta_0}{1 + \left(\frac{\eta_0 \dot{\gamma}}{\tau^*} \right)^{(1-n)}} \tag{5.25}$$

$$\eta_0 = D1 \cdot \exp\left[\frac{-A1\left(T - T^*\right)}{A2 + \left(T - T^*\right)} \right] \tag{5.26}$$

where:

η is the viscosity in [$Pa \cdot s$];

$\dot{\gamma}$ is the shear rate in [s^{-1}];

T is the absolute temperature;

$T^* = D2 + D3 \cdot P$;

$A2 = \tilde{A2} + D3 \cdot P$;

n, ,D1, D2, D3, A1, are model coefficients.

Parameters values of the Cross-WLF model obtained for the analyzed polymer are reported in Table 5.6.

Table 5.6: Parameters values of Cross-WLF model for Bayblend T 88-4N.

n	Tau* [Pa]	D1 [Pa·s]	D2	D3	A1	A2˜ [K]
0,3649	78900	$4{,}57 \cdot 10^{11}$	417.15	0	26,663	51,6

Viscosity of the Bayblend T 88-4N, obtained according to the Cross-WLF model, is plot in Figure 5.20.

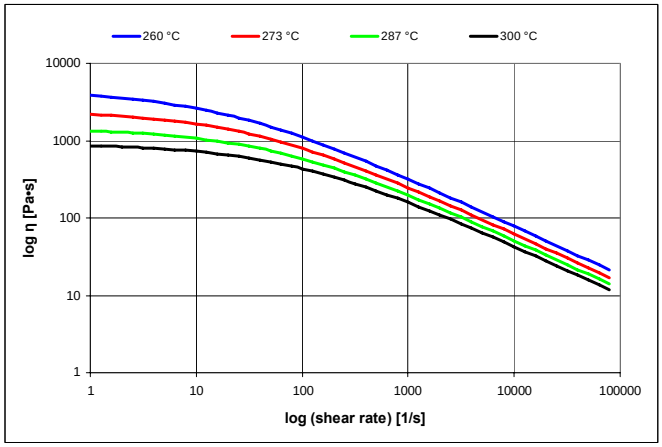

Figure 5.20: Measured viscosity of the Bayblend T 88-4N, plot according to the Cross-WLF model.

CHAPTER 6

NUMERICAL INVESTIGATION ON PIF PROCESS

Compared to the two separate processes of polymer injection moulding and sheet metal forming, the main distinctive characteristic of the PIF process is the mutual interaction between the molten polymer (fluid) and the sheet metal blank (solid). The pressure of the melted flow acting on the contact area with the sheet metal blank is responsible for the sheet deformation which in turn causes a perturbation of the initial flow. Therefore, in order to numerically model the PIF process, it is necessary to couple the phenomena occurring in the polymeric and metallic regions and consider their mutual interactions.

In this chapter a numerical investigation of the fluid (i.e. the melted polymer) structural (i.e. the sheet metal) interaction during the PIF process is presented. The evolution of the injection phase, the fluid-solid interaction, the development of plastic strains of the sheet metal during the forming process and the distribution of the thickness of the formed sheet have been analyzed by the finite volume (ANSYS CFX) and finite element methods (ANSYS Multiphysics).

6.1 Multi-physics simulation

Multi-physics (MP) may be defined as closely coupled interactions amongst the separate component of continuum physics phenomena. However most CAE analysis software tools have been developed in the context of a single of related discipline group such as:

- Computational Fluid Dynamics (CFD), i.e. fluid flow, heat transfer and combustion.
- Computational Structural Mechanics (CSM), i.e. structures, dynamics, contact and heat transfer.
- Computational Electro Magnetics (CEM).
- Computational Aero Acoustics (CAA), i.e. acoustics coupled with fluid flow.

Until recently, unless their interactions were natural, as in the case of thermo-mechanics or thermo-fluid, the interaction between any other phenomenon has largely been ignored or greatly simplified.

One of the reasons that such interactions have been ignored is due to the distinctive approaches used in solver strategies by the various phenomena specific software, for example:

- CFD typically uses Finite Volume (FV) techniques with segregated iterative solvers.

- CSM uses Finite Element (FE) techniques with direct solvers or at least the structure to employ direct solvers.
- CAA & CEM uses either FE/FV techniques.

The distinctive features of the above solvers, combined with their consequent heritage software structure, have made all but the loosest coupling between phenomena very difficult.

When physical phenomena are coupled this means that information from one has to be transformed and included in the simulation of another, predominantly either through changing boundary conditions or through the provision of a source term (e.g. a body force). Hence, in all types of MP analysis, it is essential that data for volume source and boundary conditions from one phenomenon to another is mapped or filtered in such a way that there is no loss in accuracy. In addition, if mesh movement is required then the mesh and geometries must deform compatibly.

6.1.1 Classifying multi-physics

Most CAE software vendors claim multi-physics capabilities, but in reality, what most of them offer at the present time, is multi-disciplinary, i.e. data generated by one code is used as input into another, either as boundary data or as a volume source, where the data transfer is one way. This is distinguishable from full multi-physics analysis, which involves the two way exchange of information, which could involve implicit convergence within a time-step (e.g. thermo-mechanical). There is also an additional level of sophistication with regard to multi-physics, i.e. closely coupled multi-physics. This type of analysis adds a further level of complexity since both time and space accurate exchange of data is required. Hence, the type of problem under consideration will influence the level of coupling that is required for MP analysis, as detailed below.

6.1.1.1 Levels of physical coupling

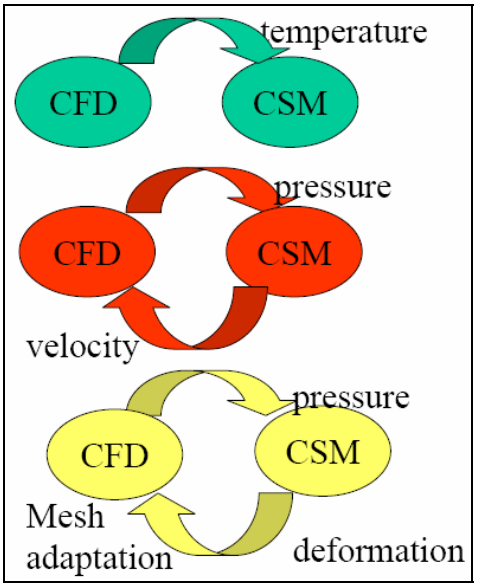

Figure 6.1: Levels of Coupling in multi-physics analysis [54].

As shown in Figure 6.1, for Multi-Physics analysis it is convenient to consider three possible levels of coupling between phenomena specific software:

• Low level of coupling

One way, where phenomenon A imposes boundary conditions or a volume source on phenomenon B, but the effect of phenomenon B on A is ignored. This is usually achieved by simple file between codes. Low-level coupling is essentially multidisciplinary, e.g. an electric field loading a thermal calculation.

• Medium level of coupling

Two-way coupling both to and from phenomenon A to phenomenon B, which is more complex, requires mesh compatibility and imposes time step constraints.

• High level of coupling

Again, this involves two way coupling , but in such a way as to be both time and space accurate; this is very challenging in every respect, e.g. dynamic fluid structure interaction.

6.1.1.2 Multi-physics solver approach

There are two main solution strategies for Multi-Physics analysis:

- Directly Coupled Solution, i.e. a monolithic scheme, where all the variables are solved for in one integrated scheme. The direct method usually involves just one analysis that uses a coupled-field element type containing all necessary degrees of freedom. Coupling is handled by calculating element matrices or element load vectors that contain all necessary terms.
- Staggered Solution or Load Transfer Methods, which may be either explicit or implicit, where groups of variables, usually associated with a specific phenomenon, are solved for in a suite of schemes [55, 56]. The stagger method involves two or more analyses, each belonging to a different field. The coupling of the two fields is carried out by applying results from one analysis as loads in another analysis.

6.2 Multi-physics approach for numerical simulation of PIF process

The numerical model proposed for the PIF process is based on a multi-physics architecture which allows combining the effects of two different, yet interrelated physical phenomena, within one, unified simulation environment.

This kind of numerical simulation involves the definition of two different domains. The first one is the fluid region and it represents the volume to be filled by the melted polymer. The second one is the structural domain and it is defined in order to model the sheet metal deformation. The fluid-solid interaction is modelled by means of an interface acting on the polymer-metal contact surface. This is used to enforce the coupling constraints between the two different domains.

The different physics of the problem are analyzed separately over the spatial domain by means of different numerical codes (Figure 6.2). The flow evolution of the melted polymer is solved in ANSYS CFX using the Finite Volume Method. The sheet metal deformation is solved in ANSYS Mechanical using Finite Element Method. The two analyses are coupled using the bidirectional Fluid Structure Interaction (FSI) solver [57].

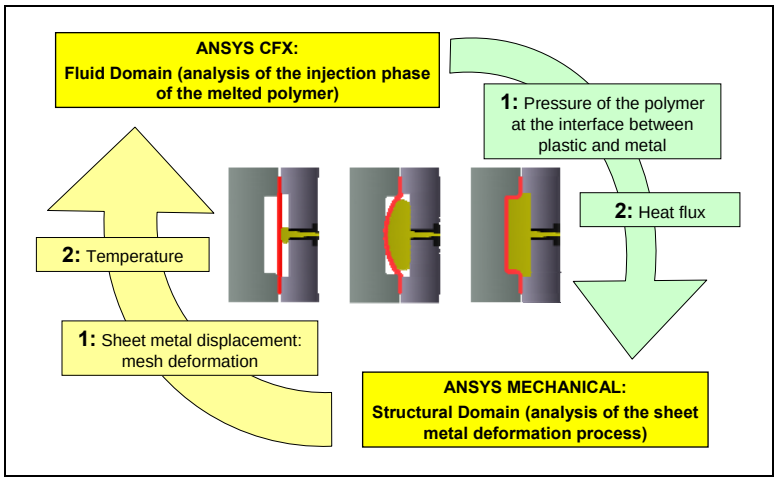

Figure 6.2: Multi-Physics analysis (Two-Way Coupling) approach of PIF process.

FSI is a method used in coupled field analyses between fluids and solids structures. This method is used when the fluid causes the geometry to deform and the deformed geometry in return causes the flow to change. There are two different types of FSI that are mainly based on how the loads are transferred between the fields. The first one is when loads are transferred in one direction, from one field to the other. This method is called unidirectional FSI and is typically employed when fluid pressure causes the deformation of the solid in such a way that it does not affect the flow of the fluid (see *Low level of coupling* in §6.1.1.1). The second type is the bidirectional FSI in which loads are transferred in both directions (see *High level of coupling* in §6.1.1.1) [53].

The numerical simulation of the PIF process requires that the FSI interface transmits the loads generated by the polymer, in terms of heat fluxes and pressure, to the metal sheet and it passes the deformed shape and temperature distribution of the metal sheet back to the fluid domain. For this reason, the bidirectional FSI solver was employed in this work (Figure 6.2).

6.2.1 The solution process

The ANSYS Multi-field solver is an automated tool for solving coupled field problems in the ANSYS® environment by means of the Load Transfer Method. Each physics is created as a field with an independent solid model and mesh. Surfaces or volumes are identified for coupled load transfer. A multi-field solver command set configures the problem and defines the solution sequencing. Coupled loads are automatically transferred across dissimilar meshes by the solver. The solver is applicable to static, harmonic, and transient analysis, depending on the physics requirements. Any number of fields may be solved in a sequential (or mixed sequential-simultaneous) manner.

Two versions of the ANSYS Multi-field solver, designed for different applications, offer their own benefits and different procedures:

- MFS - Single code: The basic ANSYS Multi-field solver used if the simulation involves small models with all physics field contained within a single product executable (e.g., ANSYS Multiphysics). The MFS - Single code solver uses iterative coupling where each physics is solved sequentially, and each matrix equation is solved separately. The solver iterates between each physics field until loads transferred across the physics interfaces converge.

- MFX - Multiple code: The enhanced ANSYS Multi-field solver used for simulations with physics fields distributed between more than one product executable (e.g., between ANSYS Multiphysics and ANSYS CFX). The MFX solver can accommodate much larger models than the MFS version. The MFX - Multiple code solver uses iterative coupling where each physics is solved either simultaneously or sequentially, and each matrix equation is solved separately. The solver iterates between each physics field until loads transferred across the physics interfaces converge.

The solution algorithm for the ANSYS Multi-field solver (MFX) is shown in Figure 6.3. The solution loop consists of two loops: the multi-field time loop and the multi-field stagger loop.

The time loop corresponds to the time step loop of the multi-field analysis. Within each time step is the stagger loop. The stagger loop allows for implicit coupling of the fields in the Multi-field solution. The number of stagger iterations applies to each time step in the multi-field analysis. Within each step in the time step loop, the field solutions are repeated in the stagger loop until convergence. The number of iterations executed within the stagger loop is determined by the convergence of the loads transfer between solid and fluid fields or the maximum number of stagger iterations specified. For a transient analysis performed in CFX, like the one of the PIF process, the stagger iteration contains many CFX coefficients iterations, which loop until convergence or until the maximum number of coefficient iterations is reached. Load transfers between the two fields occur at each stagger loop. Global convergence is checked after the load transfer. If global convergence of the load transfer is not achieved, another stagger loop is performed.

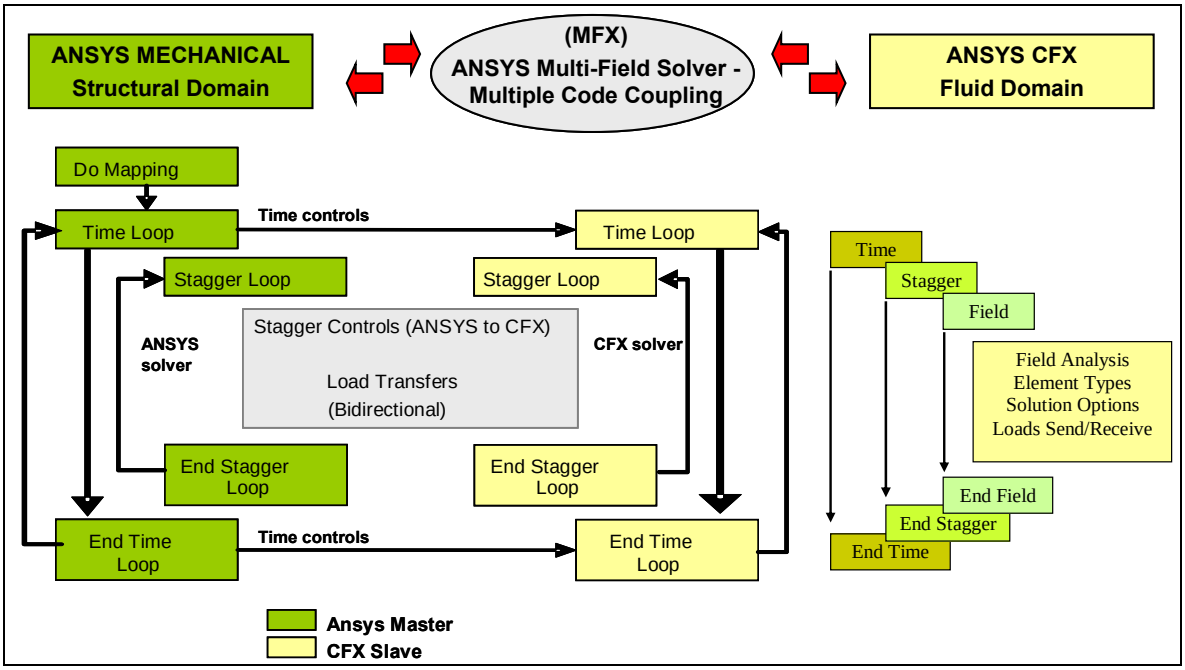

Figure 6.3: ANSYS Multi-field solver process [53].

The solution order of the two solvers has to be specified. Two ways are possible:

- Simultaneous solution. In this case the ANSYS and CFX field solvers yield the following behaviour. ANSYS requests its loads from CFX, CFX requests its loads from ANSYS, then both solvers execute simultaneously (Figure 6.4 (a)).
- Sequential solution. In this case the ANSYS and CFX field solvers work sequentially, according to user-specified order, and results/loads from one field solver are applied to the other (Figure 6.4 (b)).

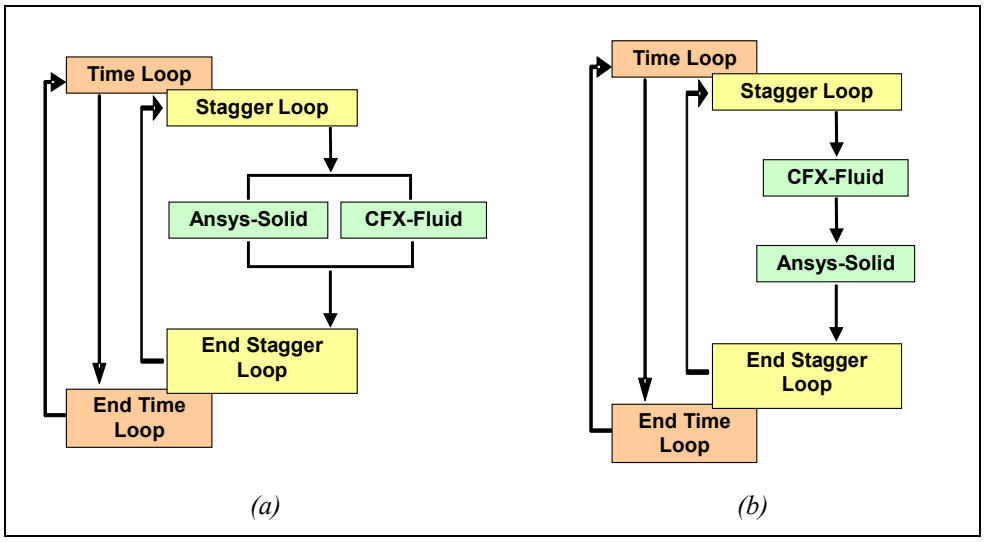

Figure 6.4: Solution technique of multi-physics problem: (a) ANSYS and CFX fields solved simultaneously; (b) ANSYS and CFX fields solved sequentially, CFX first.

Weakly coupled fields (see *Low level of coupling* in §6.1.1.1) can often be solved simultaneously. In this case, the overall simulation time may decrease because no field solver must wait for results/loads from another field solver. If the fields are too strongly coupled (see *High level of coupling* in §6.1.1.1), however, this approach may also destabilize the solution process because less recent results/loads are applied in each field solver. Strongly coupled fields should be solved sequentially, which ensures that the most recent results/loads from one field solver are applied to the other. Multiple stagger iterations are often required to obtain a fully implicit solution by the end of each multi-field time step. Moreover, in most simulations, the physical processes in one field solver drive those in another field solver. In such cases, it is better that the "driver" field solver be solved first.

Since the numerical simulation of the PIF process presents a high level of coupling between the fluid domain and solid domain, the sequential solving technique was employed. Besides, considering that forces generated by the fluid fields lead to strains in the solid field, it is right to consider the fluid domain as the "driver" field. So, in the solution process, it was specified to solve the CFX field first [53, 57].

6.2.2 Load transfer

Load transfer is the process by which one field transmits mesh-based quantities to another field. The transfers occur from a surface to a surface or from a volume to a volume. The ANSYS Multi-field solver automatically transfers coupled loads across dissimilar meshes.

For the bidirectional FSI the interpolation is done in ANSYS Mechanical and two different interpolation methods are available.

- In a profile preserving interpolation (Figure 6.5), each node on the receiver side maps onto an element on the sender side (α_i). The transfer variable is then interpolated at α_i. The transfer value is $T_i = \varphi(\alpha_i)$. Thus, all nodes on the receiver side query the sender side.

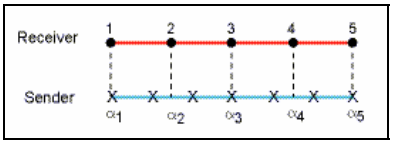

Figure 6.5: Profile Preserving Interpolation.

- In a globally conservative interpolation (Figure 6.6), each node X on the sender maps onto an element on the receiver side. Thus, the transfer variable on the sender is split into two quantities that are added to the receiver nodes. As shown in Figure 6.6, the force at node 4 splits into forces at nodes 3' and 4'.

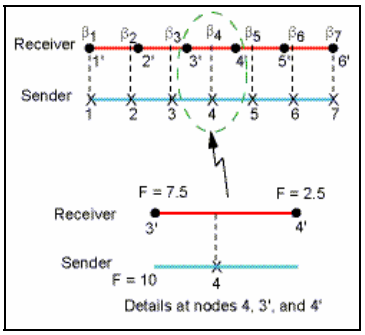

Figure 6.6: Globally Conservative Interpolation.

Some important points to remember about the interpolation methods are:

- For a profile preserving interpolation, the forces and heat rate will not balance on this interface. For a globally conservative interpolation, total force and total heat rate will balance on this interface. However, locally the distributions might not agree.

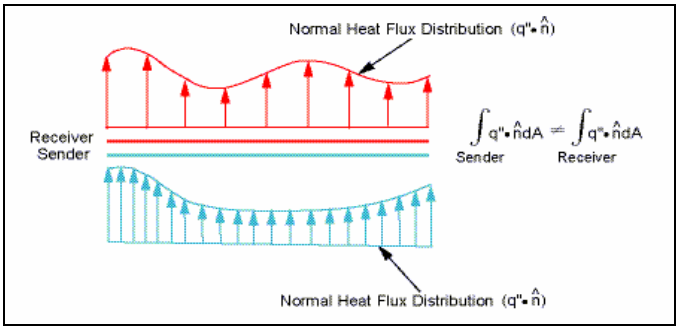

Figure 6.7: Profile Preserving Interpolation – Load Imbalances.

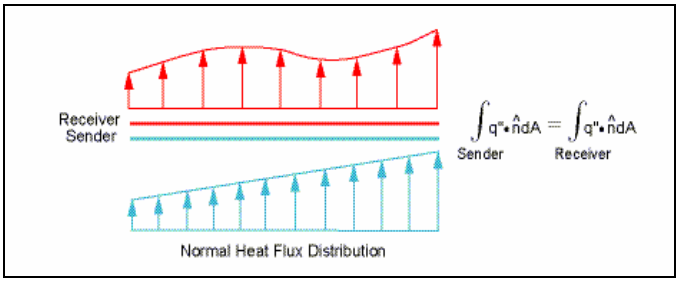

Figure 6.8: Globally Conservative Interpolation – Load Balance.

- It makes physical sense to conserve quantities like heat flux and force at the surface interfaces. Similarly, heat generation should be conserved at volumetric interfaces. However, it does not make physical sense to conserve displacements or temperatures on a integral basis. However, displacement and temperature profiles should be adequately captured across interfaces.
- As shown in Figure 6.9, for a profile preserving interpolation, you should have a coarse mesh on the sending side and a fine mesh on the receiver side, rather than the converse. When the coarse mesh is on the sending side, the receiver adequately captures the normal heat flux profile. On the receiver side, a fine mesh ensures a sufficient number of nodes. When the coarse mesh is on the receiver side, the receiver does not adequately capture the normal heat flux profile due to an insufficient number of nodes on the receiver side.

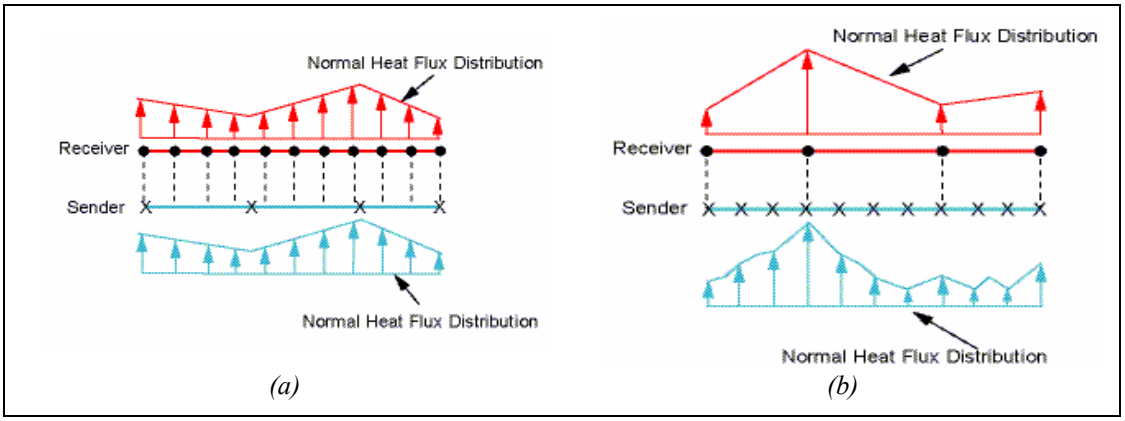

Figure 6.9: Profile Preserving Interpolation: (a) coarse mesh on the sending side; (b) coarse mesh on the receiver side.

- As shown in Figure 6.10, for a globally conservative interpolation it is better to have a fine mesh on the sending side and a coarse mesh on the receiver side than the converse. When the fine mesh is on the sending side, the receiver adequately captures the forces. When the fine mesh is on the receiver side, the load distribution on the receiver might not be captured, even though the total force on the receiver is equal to the total force on the sender.

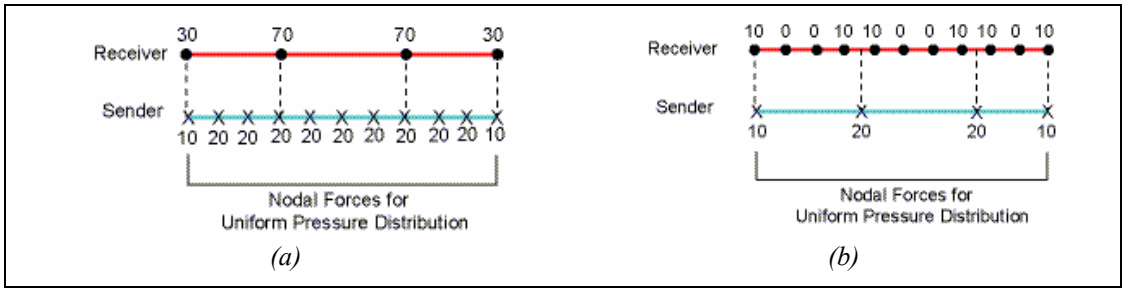

Figure 6.10: Globally Conservative Interpolation: (a) fine mesh on the sending side; (b) fine mesh on the receiver side.

Due to previous reasons and considering that:

- Profile Preserving Interpolation is better for transfer of heat flux and force density;
- Globally Conservative Interpolation is better for transfer of heat flow and forces;
- both Profile Preserving Interpolation and Globally Conservative Interpolation are good for transfer of mesh displacement and temperature;
- more accurate results are obtained using force density instead of forces;

a Profile Preserving Interpolation transfer method with a coarse mesh on the sending side (fluid domain side) was used in numerical simulations of the PIF process [53, 57].

6.2.3 Mapping

In order to transfer loads across a dissimilar mesh interface, the nodes of one mesh must be mapped to the local coordinates of an element in the other mesh. The Multi-physics solution algorithm must perform two mappings for every surface to surface and volume to volume interface. For example, in a fluid-solid interaction problem, fluid nodes must be mapped to the solid elements to transfer displacements. Likewise, solid nodes must be mapped to the fluid elements to transfer stresses (Figure 6.11).

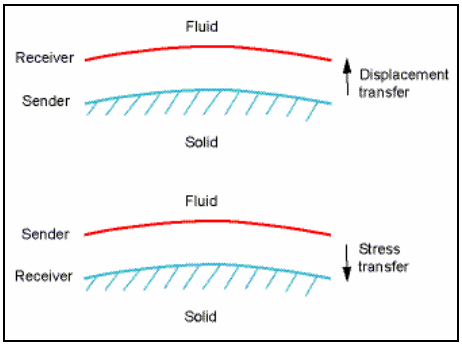

Figure 6.11: Fluid-Solid Interaction Load Transfer.

There are two mapping algorithms available: global and bucket search.

6.2.3.1 Global Method

As the name implies, the node in question loops over all the existing elements of the other mesh and tries to locate an element that it can be mapped to. Most nodes find a unique

element and are mapped easily. However, occasionally a node is mapped to two or more elements. This occurs when a finite nonzero gap/penetration exists between the two meshes. The element that minimizes the distance is then selected. In Figure 6.12 (a), node N_1 is found in elements e_1 and e_2, so it is mapped to the element which minimizes the gap distance (e_1 because $d_1 < d_2$).

Sometimes a node does not map to any element. This occurs when the interface edges are not aligned. In Figure 6.12 (b), node N1 does not map to any element, so it is mapped to the closest node (N1').

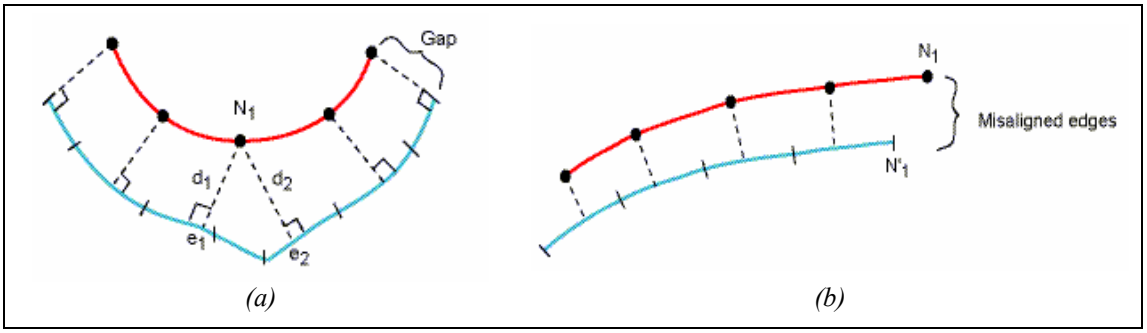

Figure 6.12: Global mapping method: (a) node mapped to minimize gap; (b) node mapped to closest node.

The global method has a complexity of θ(n x m) where *n* is the number of nodes mapped onto *m* elements. If *n* and *m* are of the same order, the time required to compute the mapping grows quadratically and leads to computational inefficiency, especially for large models.

6.2.3.2 Bucket Search Method

The bucket search method is designed to alleviate the inefficiency problem that the global method has when the number of nodes increases. For a given node, the bucket search method restricts the elements over which it loops. This is accomplished as follows:

1. All elements are distributed in Cartesian boxes (also referred to as buckets).
2. The node in question is then located in a box.
3. The global method is used for the node in question, but the elements are restricted to that box only.

For example, in Figure 6.13 (a), elements e_1, e_2, and e_3 are in box 1, elements e_3 and e_4 are in box 2, and e_4, e_5, and e_6 are in box 3. Node N_1 searches only over the elements in box 3.

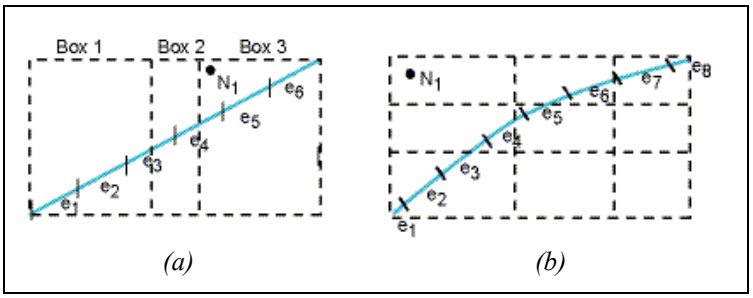

Figure 6.13: Bucket Search Method: (a) node in Box 3 with three elements; (b) nine boxes and node in empty Box.

When the node in question is in a box with elements, the mapping is identical to global mapping. While this procedure appears straightforward, it is more complex when the node in question is in an empty box as shown in Figure 6.13 (b). This can occur when there are gap/penetration issues or the interface edges are misaligned.

The mapping is then different than global mapping. The mapping procedure requires locating the nearest boxes that have elements and choosing only one box for element looping.

The bucket search method has a complexity of θ(n) where *n* is the number of nodes to be mapped onto *m* elements. However, to achieve this increased efficiency, buckets must be created and the m elements must be placed in them, at an additional computational expense

Due to simplicity of the model geometry, the Global Mapping Method was used in numerical simulations of the PIF process [53, 57].

6.3 Validation of the fluid field

As described previously, the fluid domain of the multi-physics problem, which models the filling phase of the mould by melted polymer, was solved by means of the CFX solver. This is a general computational fluid dynamics (CFD) software that contains several different equation solvers. In order to successfully simulate the mould filling phase of the PIF process, a right setting of the CFD environment was necessary. This task was carried out considering the traditional injection moulding process since, in this process, only the fluid field exists. A validation of CFX simulations was performed comparing obtained results with ones from Moldflow Plastics Insight®, which is a commercial software for numerical simulations of the injection moulding process.

The model geometry used for the CFX validation was the one obtained from the two mould inserts described in §3.1, without the sheet metal blank (Figure 6.14).

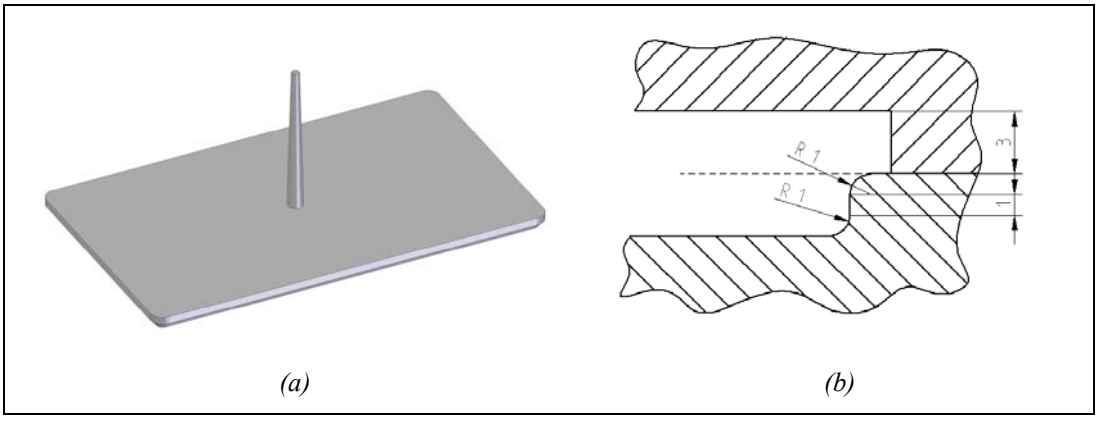

Figure 6.14: 3D model used in CFX validation: (a) 3D model; (b) cross sectional view.

6.3.1 CFX model

In order to reduce computational times, the symmetry of the model geometry with respect to ZX and ZY planes was considered (Figure 6.15).

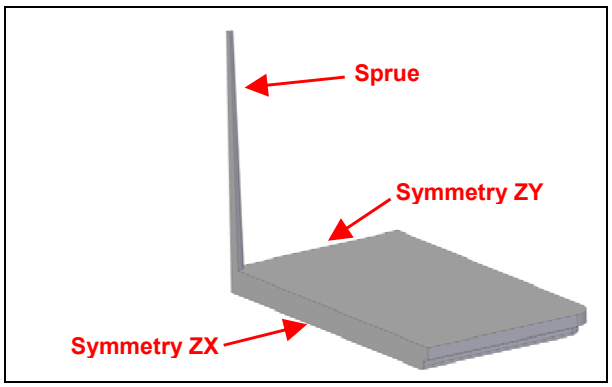

Figure 6.15: 3D model used in the CFX simulation.

The problem definition requires a transient simulation since at the beginning the mould cavity is empty (or filled by air) while at the end it is full filled by melted polymer. In order to model this behaviour, a multiphase approach with the surrounding air and the melted polymer as the two phases was used [58]. Since in this flow there is no inter-phase mass transfer and the fluids are distinct in their composition, it was considered a Free-Surface flow. This approach is suitable to numerically compute flows that involve immiscible fluids separated by a well-defined interface, like the injection moulding process in which melted polymer push air forward [59]. In order to simplify the multifield model, the homogeneous multiphase approach was employed. In this approach, a common flow field, as well as other relevant field variables as temperature and turbulence, is shared by both fluids (air and polymer) [60].

Thermo-dynamic properties of the air were obtained by the CFX database. The used polymer was Bayblend T88-4N by Bayer (PC+ABS+20%GF) which rheological properties were experimentally obtained, as described in chapter 5. The rheological behaviour was modelled by means of the Cross-WLF equation which parameters are reported in chapter 5.

Thermal properties of the polymer were derived from the Moldflow Plastics Insight® material database.

The PVT behaviour of the polymer was modelled in CFX by means of the modified 2-domain Tait model. This model is the model that Moldflow uses to account for material compressibility during a flow simulation. The compressibility of a material affects the volume of plastic required. The 2-domain Tait PVT model is given by the following equations:

$$v(T,P) = v_0(T) \cdot \left[1 - C\ln\left(1 + \frac{P}{B(T)}\right)\right] + v_t(T,P) \tag{6.1}$$

where:

V(T,P) is the specific volume at temperature T and pressure P.

V_0(T) is the specific volume at zero gauge pressure.

T is the temperature, in K.

P is the pressure, in Pa.

C is a constant, 0.0894.

B accounts for the pressure sensitivity of the material and is defined below

The upper temperature region (T > Ttrans) can be described by the equations:

$$T > T_{trans} \begin{cases} v_0 = b_{1m} + b_{2m} \cdot (T - b_5) \\ B(T) = b_{3m} \cdot \exp\left[-b_{4m} \cdot (T - b_5)\right] \end{cases} \quad (6.2)$$

where:

b_{1m}, b_{2m}, b_{3m}, b_{4m} and b_5 (which represents the transition temperature, T_{trans}, at zero gauge pressure) are data-fitted coefficients

The lower temperature region (T < Ttrans) can be described by the equations:

$$T < T_{trans} \begin{cases} v_0 = b_{1s} + b_{2s} \cdot (T - b_5) \\ B(T) = b_{3s} \cdot \exp\left[-b_{4s} \cdot (T - b_5)\right] \end{cases} \quad (6.3)$$

where:

b_{1s}, b_{2s}, b_{3s}, and b_{4s} are data-fitted coefficients.

The dependence of T_{trans} on pressure can be described by the equation:

$$T_{trans}(P) = b_5 + b_6 \cdot P \quad (6.4)$$

where:

b_5 and b_6 are data-fitted coefficients.

For non-amorphous (crystalline) materials, the following additional transition function is required:

$$v_t(T, P) = b_7 \exp\left(\left(b_8 \cdot (T - b_5)\right) - \left(b_9 P\right)\right) \quad (6.5)$$

where:

b_5, b_7, b_8, b_9 are data-fitted coefficients.

Coefficients values of the modified 2-domain Tait PVT model of the polymer Bayblend T 88-4N were get from Moldflow material database and they are summarized in Table 6.1.

Table 6.1:Coefficient values of the modified 2-domain Tait PVT model of the polymer Bayblend T 88-4N.

2-domain Tait PVT model coefficients

b5	399.15	K	b2s	1.754e-007	m^3/kg-K
b6	2.5e-007	K/Pa	b3s	3.49659e+008	Pa
b1m	0.0008037	m^3/kg	b4s	0.003622	1/K
b2m	3.984e-007	m^3/kg-K	b7	0	m^3/kg
b3m	2.78502e+008	Pa	b8	0	1/K
b4m	0.004849	1/K	b9	0	1/Pa
b1s	0.0008033	m^3/kg			

The PVT behaviour of the Bayblend T 88-4N is plot in Figure 6.16.

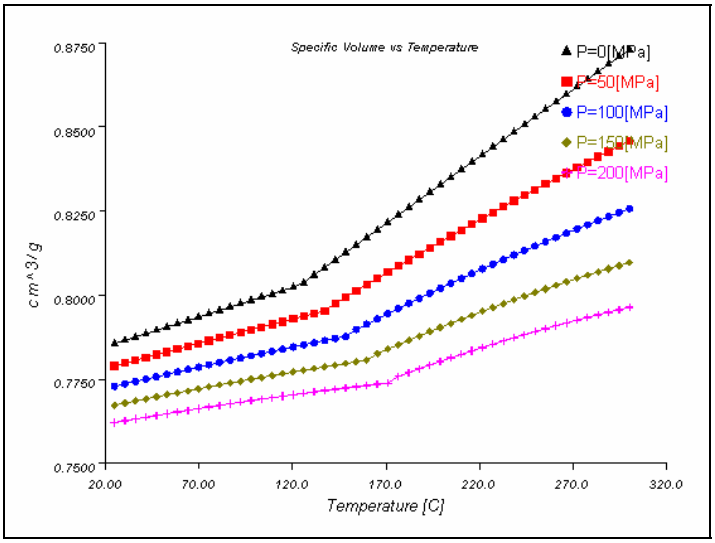

Figure 6.16: PVT behaviour of the Bayblend T 88-4N as obtained by Moldflow material database.

The simulation was set up as follows:

- polymer temperature at injection: T_m= 280°C;
- mould temperature: T_{mould}= 70°C;
- polymer mass flow rate at injection: Q = 0.0355311 kg/s;
- injection time: t_{inj} = 1.2 s;

In order to consider thermal phenomena within the fluid field, a thermal energy model was implemented. The thermal energy approach allows to model the transport of enthalpy through the fluid domain without including the effects of mean flow kinetic energy. It is consequently adequate for low speed flows where kinetic effects are negligible, as in the injection moulding process. Since melted polymers are high viscosity fluids, thermal contribution due to viscous dissipation are not negligible. So, also viscous dissipation term was included in the thermal energy model.

Due to high viscosity of melted polymers, the turbulence model in the simulation was set to laminar.

Figure 6.17 (a) shows the applied boundary conditions. As previously mentioned, at the end of the injection moulding process the mould cavity is filled only by the melted polymer. So, air which filled the mould cavity at the beginning of the process has to flow outside. This phenomenon was implemented in the numerical simulations by means of air vents added to the original 3D CAD model (Figure 6.17 (b)). The air vents were modelled as small gaps (0.1 mm of height) all around the geometry of the cavity. In the CFX environment, an opening boundary condition was assigned to gap surfaces and a relative pressure of 0 Pa was set at inlet. By means of the same boundary condition, it was specified that only air was allowed to flow outside the domain.

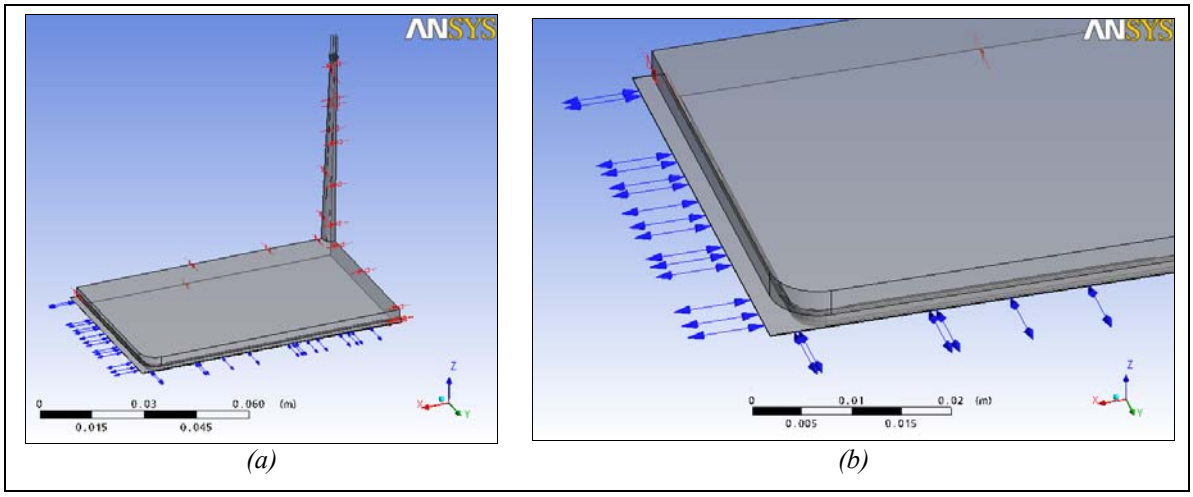

Figure 6.17: (a) Boundary conditions of the CFX model; (b) detail of "opening" boundary condition.

The CFX FEM model used in the simulation was made by 124004 tetrahedra (Figure 6.18).

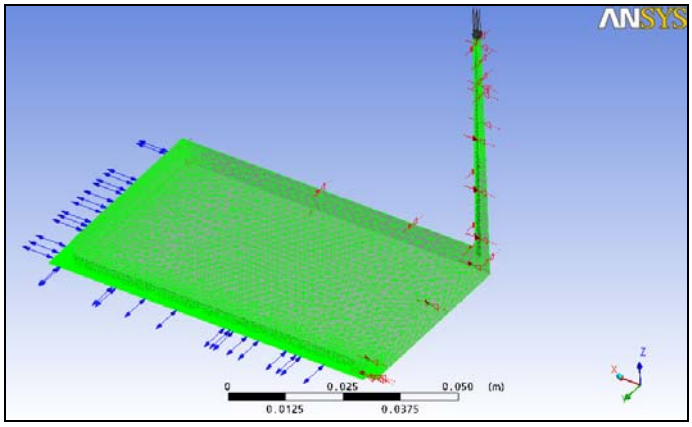

Figure 6.18: FEM model used in CFX simulation.

6.3.2 Moldflow model

Moldflow Plastics Insight® is one of the most popular commercial software for numerical simulations of the injection moulding process. Since reliability of this solver is very good, results obtained by Modflow were used in order to calibrate the CFX simulation and validate its results.

Since in Moldflow is not allowed to use symmetry boundary conditions, the entire 3D model of the mould cavity (see Figure 6.14 (a)) was employed [61].

The FEM model consists of 23385 tetrahedra (Figure 6.19).

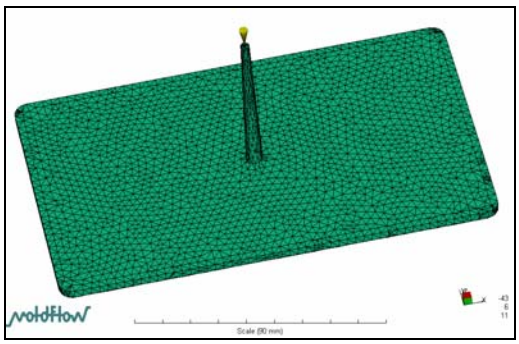

Figure 6.19: FEM model used in Moldflow simulation.

Process parameters of the simulation were set as follows:

- Injection time: T_{inj}= 0.6 s;
- Packing time: T_{pack}= 0.6 s;
- Packing pressure was set as shown in Figure 6.20;

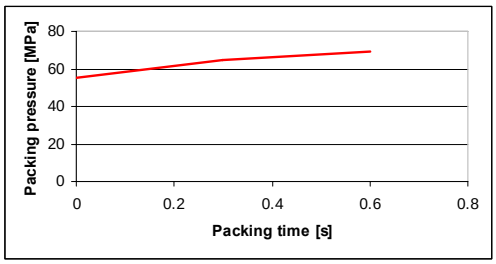

Figure 6.20: Packing pressure profile set in Moldflow analysis.

The other process parameters of the simulation were set as in the CFX analysis.

6.3.3 CFX vs. Moldflow results

Polymer pressure at injection location of both CFX and Moldflow simulations are compared in Figure 6.21. It can be seen that CFX pressure prediction is very close to the one obtained by Moldflow analysis. This means that CFX environment was successfully set in order to right model the injection moulding process.

In Figure 6.22 (a) and (b) it is compared the mould filling pattern obtained respectively by CFX and Moldflow analyses. The two filling phase evolutions result to be in good agreement, as a confirmation of the reliability of results obtained by the CFX simulation.

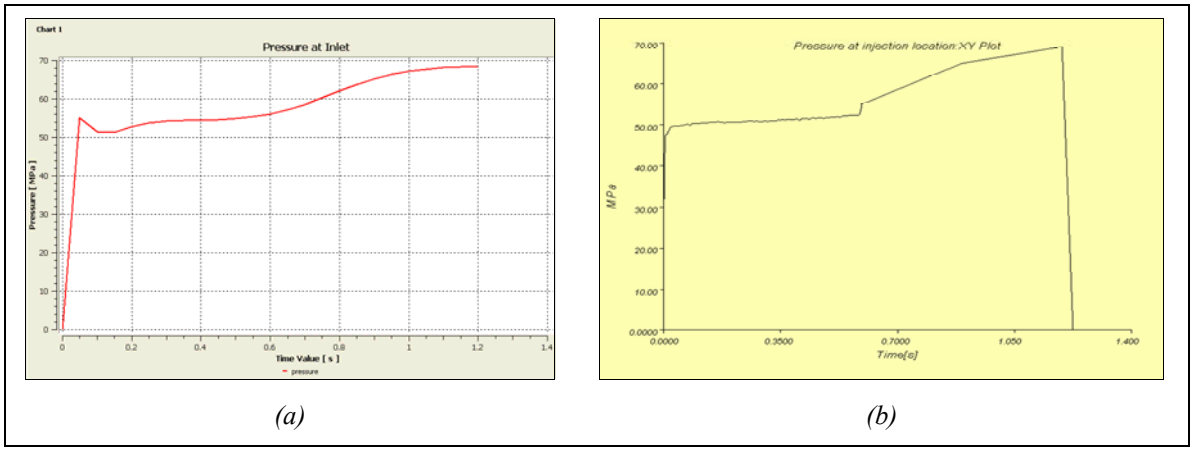

Figure 6.21: Polymer pressure at injection location.

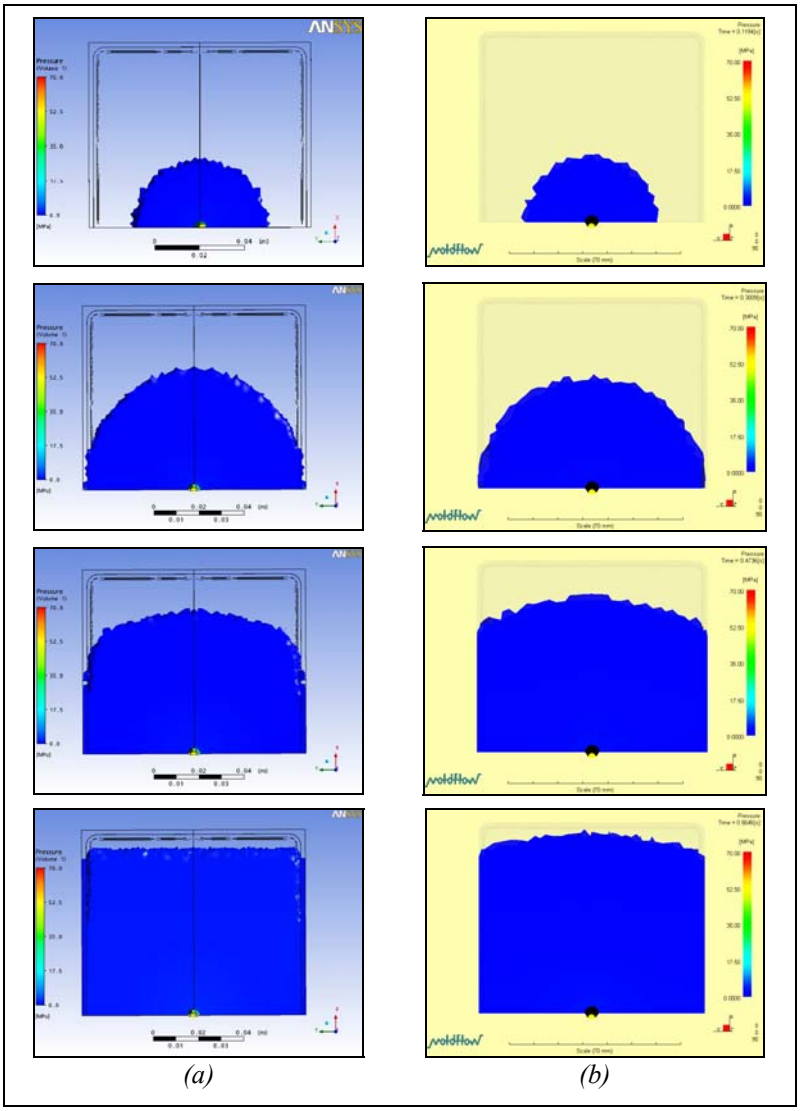

Figure 6.22: Mould filling pattern obtained by: (a) CFX simulation; (b) Moldflow simulation.

6.4 Multi-physics numerical model of PIF process

Numerical simulations of the PIF process were carried out on the composite part described in §3.1. The 3D model used in simulations includes: (i) the polymer injection system, (ii) the mould cavity, (iii) the sheet metal and (iv) the mould (Figure 6.23 (a)). As previous explained, such component well summarizes the main features of the metal-polymer macro-composites which nowadays are produced by means of the traditional manufacturing technologies.

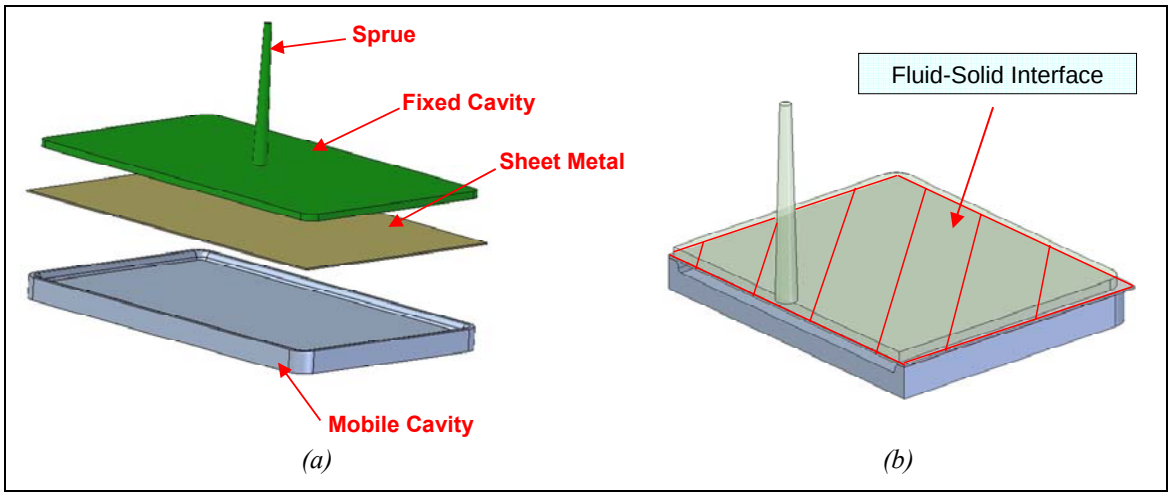

Figure 6.23: (a) 3D model used for numerical simulations of the PIF process; (b) indication of the surface designed as the fluid-solid interface.

As previously described, the melted polymer is injected from the nozzle of the injection machine and flows along the sprue gate of the mould. When it reaches the mould cavity, it forces the sheet metal blank, which is clamped between the two halves of the mould, to deform according to the contour of the mould cavity.

3D models of the sprue and the fixed cavity represent the domain of the thermo-fluid-dynamics analysis performed in ANSYS CFX. 3D models of the sheet metal blank and the mobile cavity are used in the ANSYS Multiphysics environment in order to analyse the deformation process of the metal blank and its contact-state evolution with the mobile cavity.

As previously described, the two solvers exchange forces and displacements information about the interaction between the melted polymer and the sheet metal by means of a fluid-solid interface. The model surface designed as the interface is shown in Figure 6.23 (b). It falls on the top surface (polymer-side) of the sheet metal blank.

6.4.1 The fluid field

The CFX environment for the analysis of the fluid field was defined as described in §6.3.1 (Figure 6.24 (a) and (b)). In order to reduce computational times, the symmetry of the model geometry with respect to ZX and ZY planes was considered again. The fluid-solid interface was set in order to transmit to the ANSYS Multiphysics solver the force density and receive displacements from the same solver. Mesh density on the fluid-solid interface surface was well defined in order to satisfy the requirements described in §6.2.2. The total number of tetrahedra of the FEM model is 122326 (Figure 6.24 (c)).

Thermal flows trough the polymer-sheet metal interface were ignored due to a limitation of mesh-element formulation in the ANSYS Multiphysics solver (as described in §6.4.2). However, temperature effects of the polymer melt on the sheet metal blank can be neglected because of the very short contact time between them before the end of the deformation process of the metal sheet. In order to assign a temperature boundary condition to the fluid-solid interface, the following considerations are taken into account: (a) the short time gap between the placement of the sheet metal on the injection mould and the starting time of the PIF cycle (typically 2 s), (b) the short duration of the filling phase, (c) the air gap between the metal blank and the mould during most of the filling time. For these reasons, the deformation process of the sheet metal blank may reasonably be assumed to be adiabatic and the heat exchanged with the mould can be neglected. So, an ambient temperature equal to 20°C was assigned to the fluid-solid interface as thermal boundary condition.

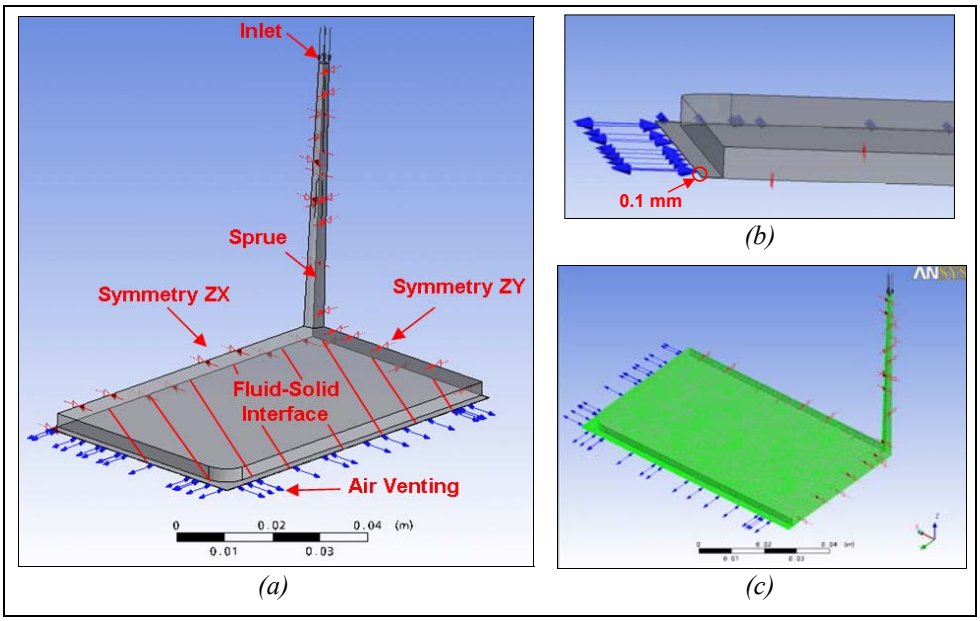

Figure 6.24: (a) Boundary conditions of the CFX model; (b) detail of "opening" boundary condition; (c) FEM model of the fluid domain.

6.4.2 The solid field

As did in the fluid field, also in the solid field the symmetry of the model geometry with respect to ZX and ZY planes was considered in order to reduce computational times. The 3D model used in simulations is shown in Figure 6.25 (a) while the FEM model is reported in Figure 6.25 (b).

Defined boundary conditions are:

- fixed constraints along the boundaries of the sheet metal;
- symmetry boundary conditions with respect to ZX and ZY planes;
- fixed constraints applied to the mobile insert model;
- fluid-solid interface on the top surface (polymer-side) of the sheet metal;
- a friction coefficient equal to 0.2 between the sheet metal and the mould;

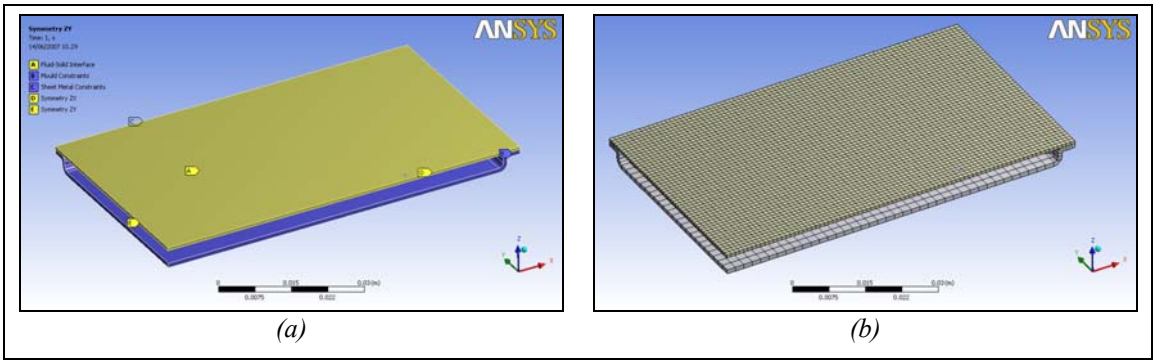

(a) *(b)*

Figure 6.25: (a) Boundary conditions of the ANSYS Multiphysics model; (b) ANSYS Multiphysics FEM model.

The mould was meshed with the ANSYS element type "Shell 181". The contact surface of the sheet metal was meshed with element type "Conta174". The target surface of the mould was meshed with element type "Target 170". The contact problem was defined as a rigid-to-flexible contact problem.

In order to model stress-strain properties of the AA1050-O aluminium alloy, the Voce model was employed in ANSYS Multiphysics. The experimental stress-strain curves were therefore fitted with the Voce model (as described in chapter 5).

In order to well model the deformation evolution of the sheet metal during the PIF process, the metal blank was meshed with ANSYS element type "SHELL 181" which supports the Voce model. SHELL181 is suitable for analyzing thin to moderately-thick shell structures. It is a 4-node element with six degrees of freedom at each node: translations in the x, y, and z directions, and rotations about the x, y, and z-axes. SHELL181 is well-suited for linear, large rotation, and/or large strain nonlinear applications. The drawback of using this type of element is that SHELL 181 does not have thermal degrees of freedom. Due to this limitation, it was not possible to carry out a thermo-structural simulation in the ANSYS Multiphysics environment. So only force density information and mesh displacements were exchanged between ANSYS CFX and ANSYS Multiphysics through the defined fluid-solid interface.

In chapter 5 the Voce model constants were derived at different temperatures. However, due to the reasons described above, in numerical simulations of the PIF process the stress-strain behaviour of the AA1050-O aluminium alloy was modelled only at a one reference temperature, which was assumed to be equal to 20°C.

The anisotropic stress-strain behaviour of the AA1050-O aluminium alloy was modelled by means of the Hill model (see chapter 5).

6.5 Numerical results

Figure 6.26 and Figure 6.27 show the evolution of the filling phase of melted polymer. At time 0.1 s, the polymer contacts the sheet metal blank; at time 0.4 s the sheet metal contacts the mould surface and at time 1.2 the mould cavity is completed filled by the polymer.

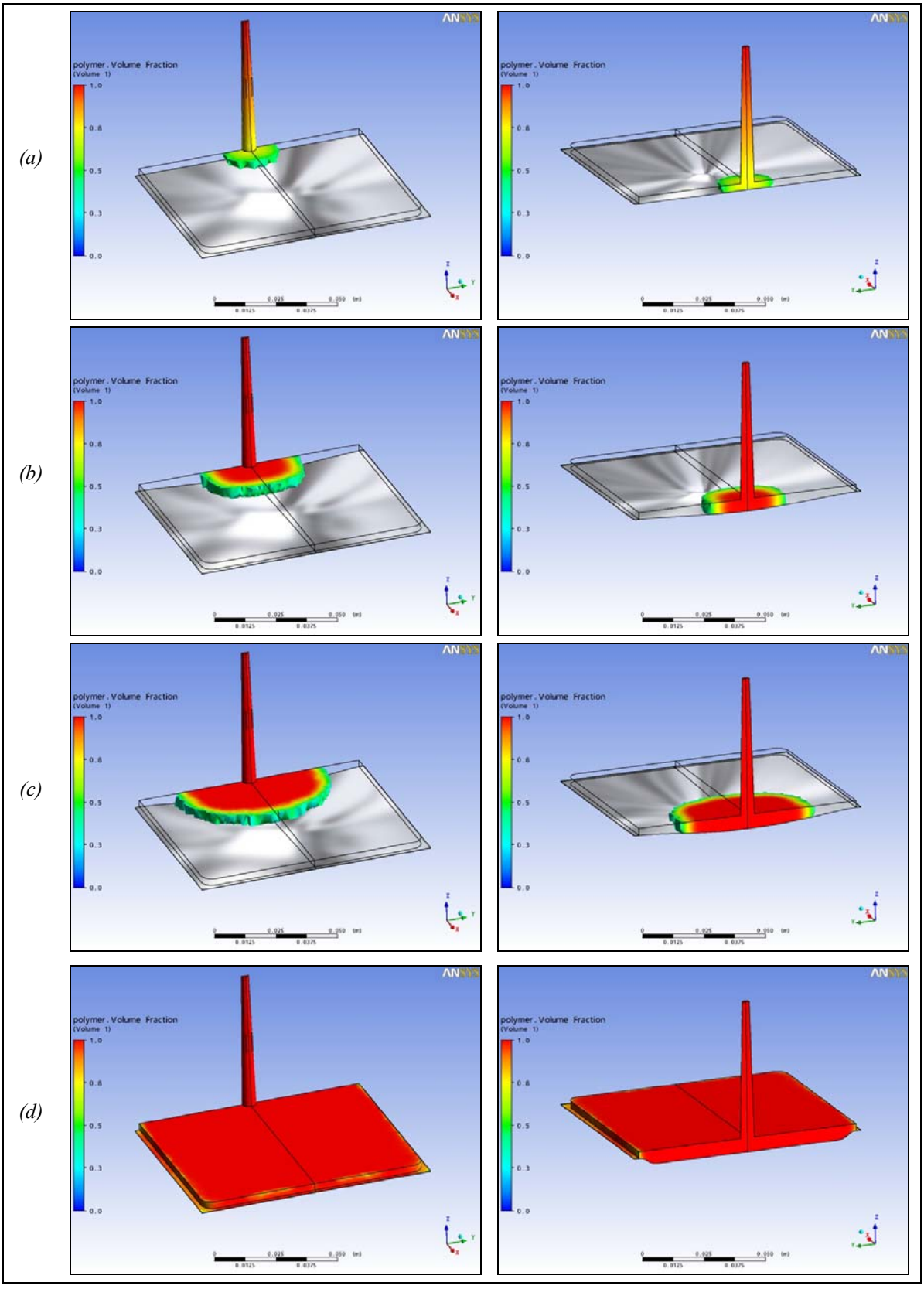

Figure 6.26: Evolution of the filling phase at time: (a) 0.1 s; (b) 0.2 s; (c) 0.4 s; (d) 1.2 s.

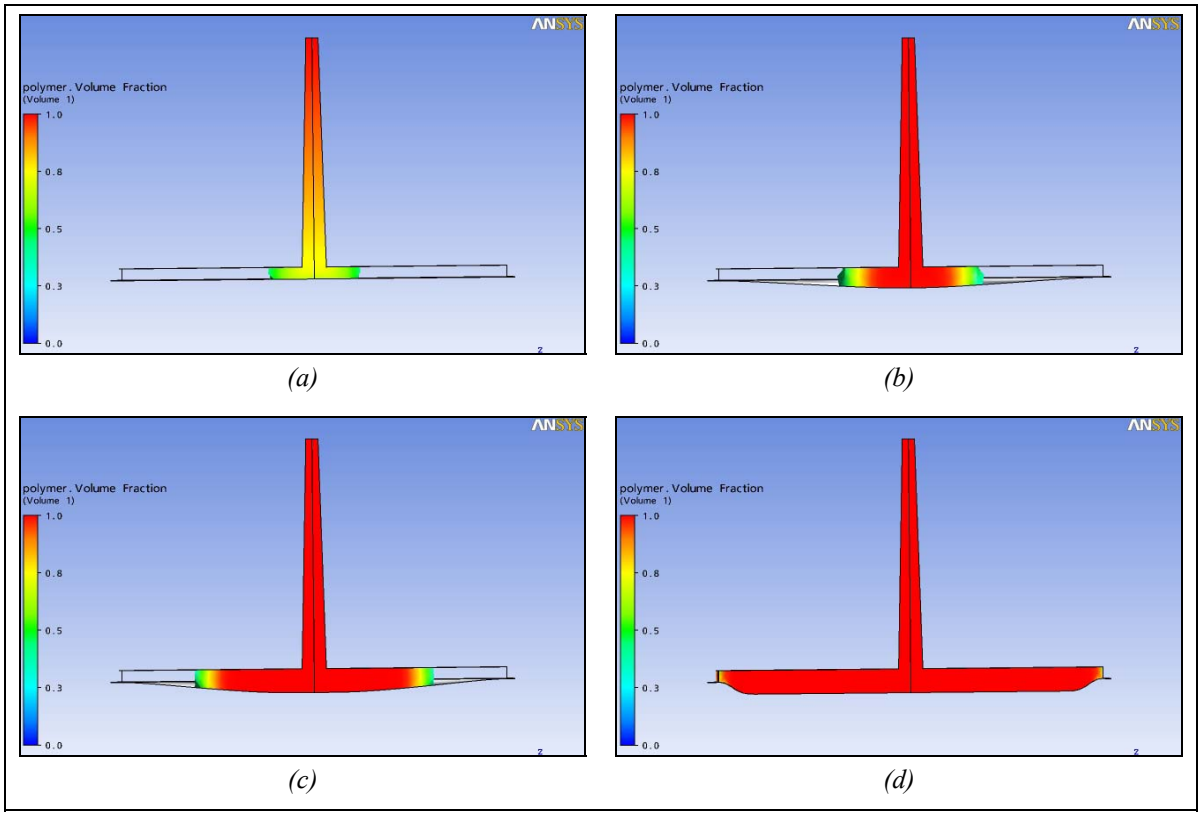

Figure 6.27: Evolution of the filling phase (bottom view) at time: (a) 0.1 s; (b) 0.2 s; (c) 0.4 s; (d) 1.2 s.

During the filling phase, as plastic flows into the cavity, the melted polymer in contact with the mould wall quickly freezes. This creates a frozen layer of plastic between the mould and the molten plastic. Due to the frozen layer, the flow front expands as material from behind is pushed forward. This outward flow is known as fountain flow.

Figure 6.28 shows the temperature distribution of the melted polymer during the filling phase. It can be seen that temperature of the polymer in contact with the mould wall is very low, compared to the injection temperature, and it is close to the mould temperature. These layers of cold plastics are the frozen layers. The frozen layer gains heat as more molten plastic flows through the cavity, and loses heat to the mould. When the frozen layer reaches a certain thickness, equilibrium is reached. This phenomenon can be easily seen in Figure 6.28: between the two frozen layers, melted polymer flows with a temperature close to the injection temperature.

Figure 6.29 graphs polymer viscosity during the filling phase of the mould. Since the polymer viscosity was modelled with the Cross-WLF model, its value depends on both temperature and shear rates. From Figure 6.29 it can be seen that viscosity of the polymer in contact with mould walls is very high. This is a direct consequence of the frozen layer, in which both temperature and shear rates are very low.

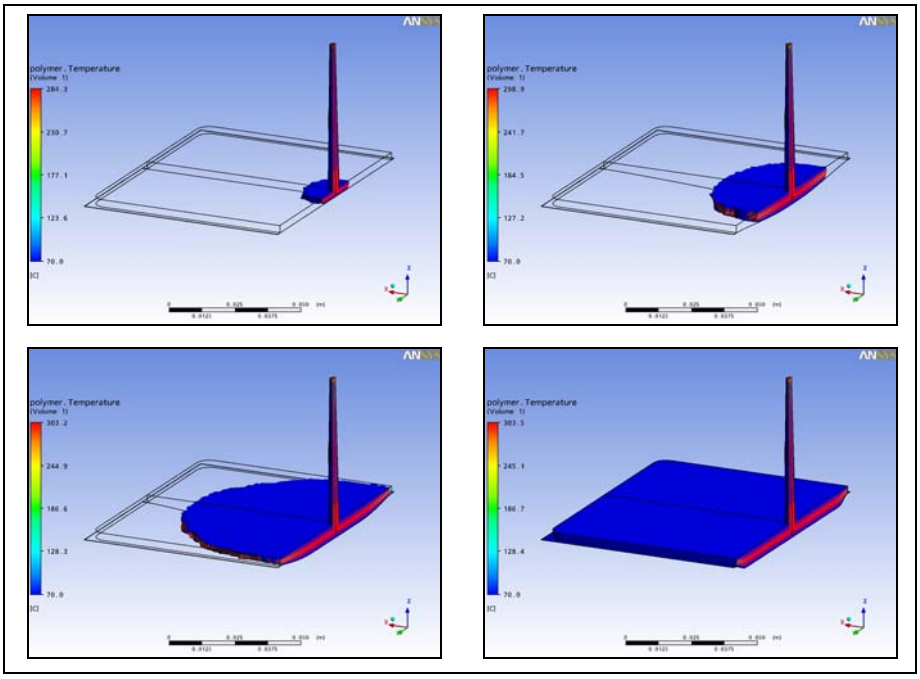

Figure 6.28:Polymer temperature distribution during the filling phase of the PIF process.

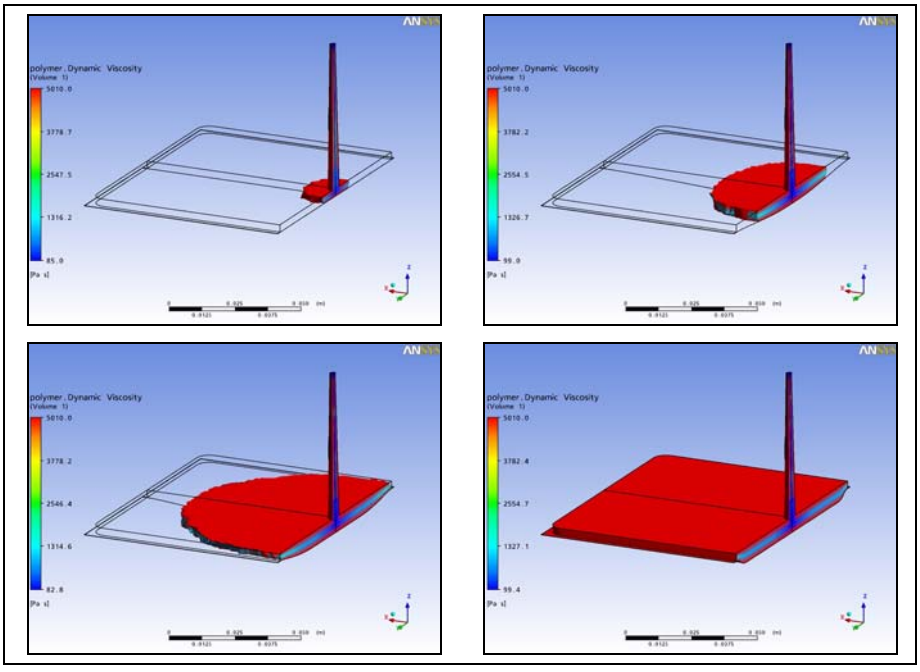

Figure 6.29:Polymer viscosity during the filling phase of the PIF process.

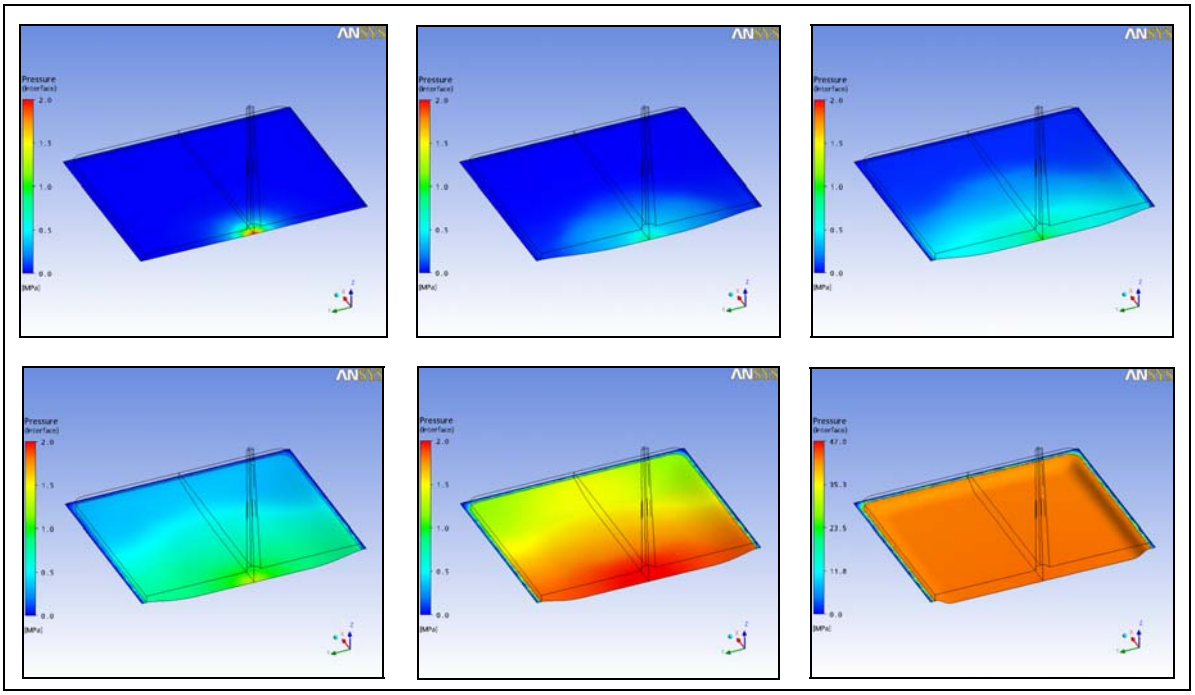

Figure 6.30:Polymer pressure distribution at the fluid-solid interface during the filling phase of the PIF process.

Figure 6.30 shows the polymer pressure distribution at the fluid-solid interface. Due to polymer viscosity, the pressure is higher in the central area, around the gate, and it decreases going away. During the filling phase of the mould cavity, the polymer pressure along the flow front is equal to 0 Mpa. During the packing phase it increases as a consequence of a smaller polymer flow rate. The force generated by the polymer pressure at the fluid-solid interface is responsible of the sheet metal deformation.

Figure 6.31 shows the progress of deformation of the meshes of the sheet blank. The sheet blank begins to deform as the polymer melt is injected to contact with it. When the pressure of the polymer melt reaches almost 1.5 MPa, the sheet blank is deformed to touch the bottom of the mould. As the polymer melt is injected continually, it forces forming of the sheet blank to proceed. This results in an increase of the contact area between the sheet blank and the mould cavity. The greater the contact areas, the higher the pressure of the polymer melt needed for deformation of the sheet blank to proceed, and the higher the pressure that can be built up in the deformed sheet blank.

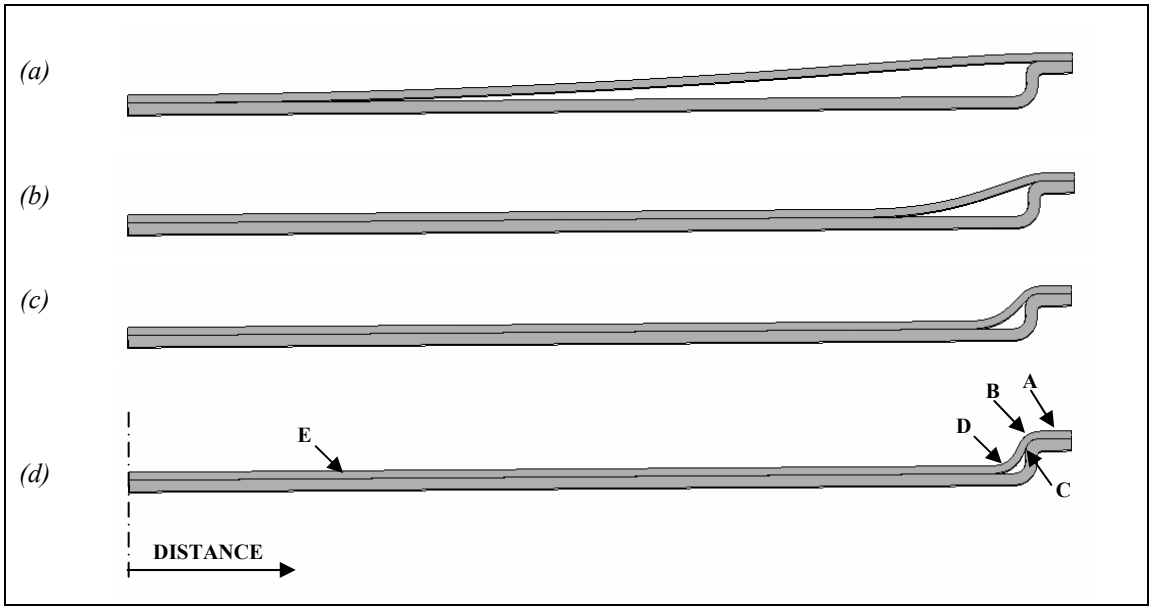

Figure 6.31: The deformed meshes of the sheet metal blank at different times: (a) 0.4 s; (b) 0.9 s; (c) 1.1 s; (d) 1.2 s.

Figure 6.32 and Figure 6.33 show development of the maximum and minimum principal plastic strains on the mid-plane of the sheet blank. In the inner region, in contact with the bottom of the mould, both the maximum and the minimum principal plastic strains show very small changes. In particular, after time 0.4 s, the strain in this part increases slowly. It is because the central part of the sheet blank has already been deformed to be in contact with the bottom of the mould cavity. In region (D) these strains show obvious change. This is because the deformed blank in this region is still not in contact with the corner region of the mould.

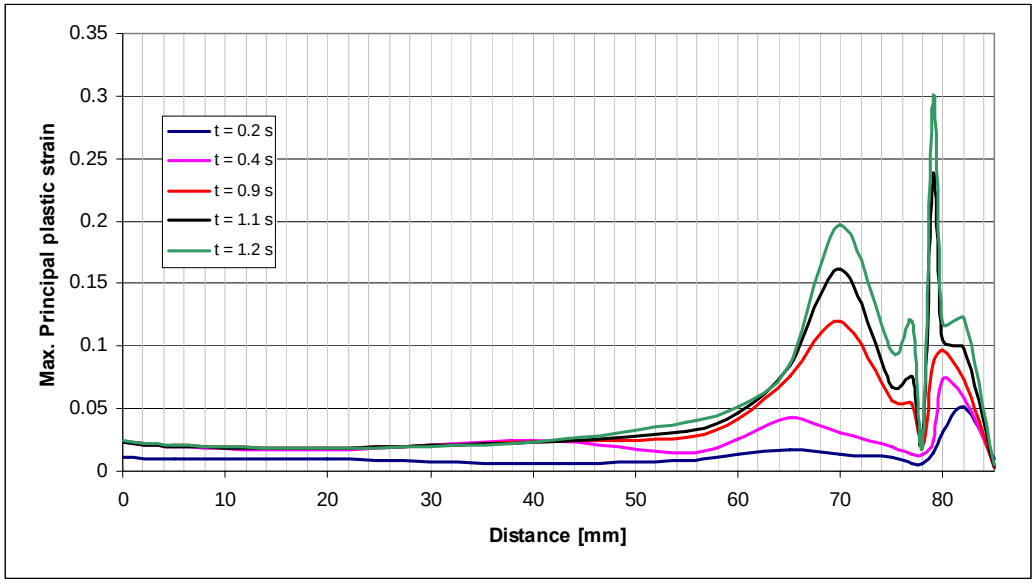

Figure 6.32: Development of the maximum plastic strain on the mid-plane of the sheet metal blank.

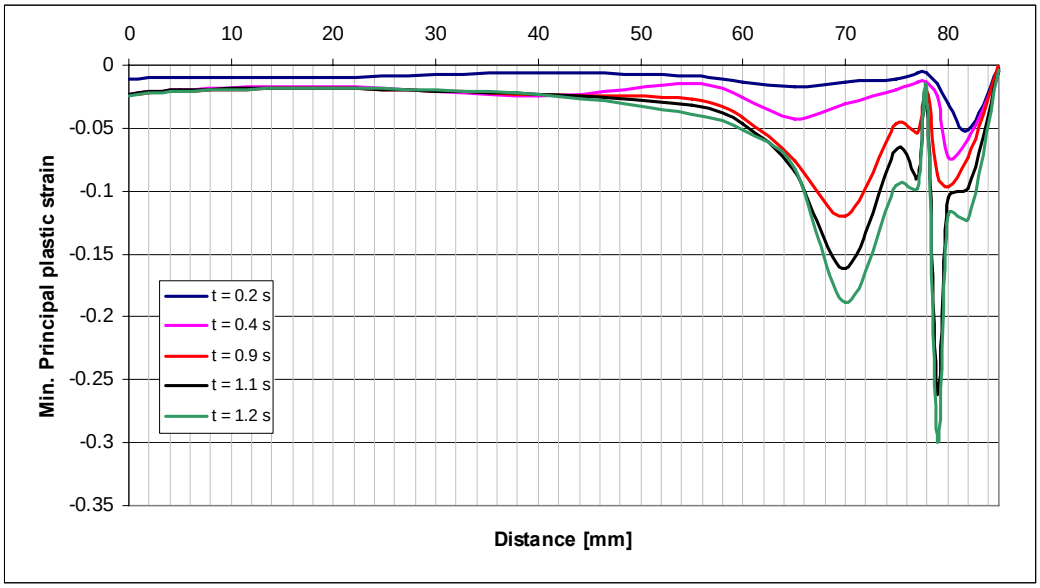

Figure 6.33: Development of the minimum plastic strain on the mid-plane of the sheet metal blank.

According to the contact situation between the deformed sheet blank and the mould shown in Figure 6.31, the sheet blank being deformed can be divided into five different regions. These are the outside region (A), the mould entry contact region (B), the side-wall contact region (C), the free region (D) and the bottom contact region (E).

From above analysis it can be concluded that region (A) and region (E) are in the deformation mode of stretch forming.

From Figure 6.31 and Figure 6.32 it can be seen that further deformation of the sheet blank is mainly concentrated on regions (B), (C) and (D). The deformation in these regions is complex because of the effects of the mould entry radius and support of the bottom and side-wall of the mould around the root corner of the mould cavity. So deformation in these regions should be examined in detail.

Figure 6.34 shows the distribution of the equivalent plastic strain in these regions. The greatest deformation occurs at the inner surface of region (B) and the outer surface of region (D).

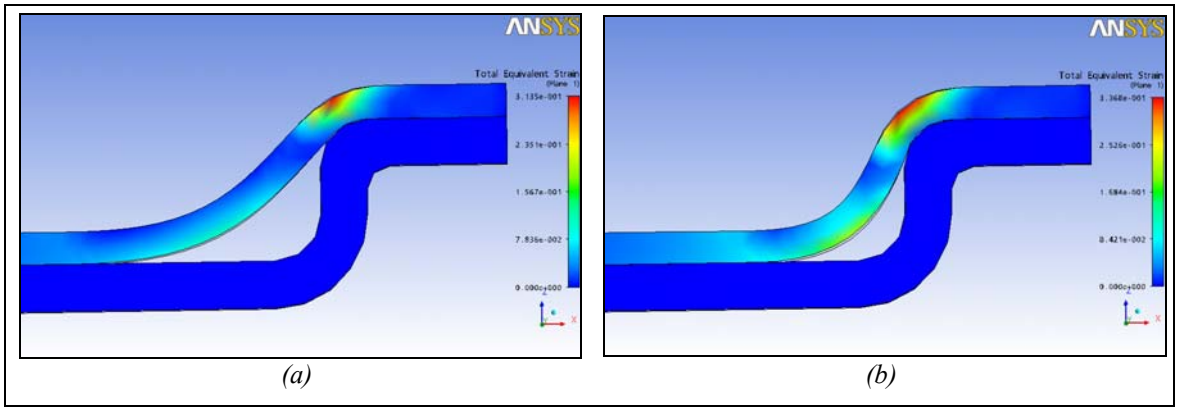

(a) *(b)*

Figure 6.34: Distribution of the equivalent plastic strain in the deformed sheet metal blank around the root corner of the mould at different times: (a) 1.1 s; (b) 1.2 s.

Figure 6.35 and Figure 6.36 show distribution of the maximum and minimum principal plastic strains in these regions, respectively.

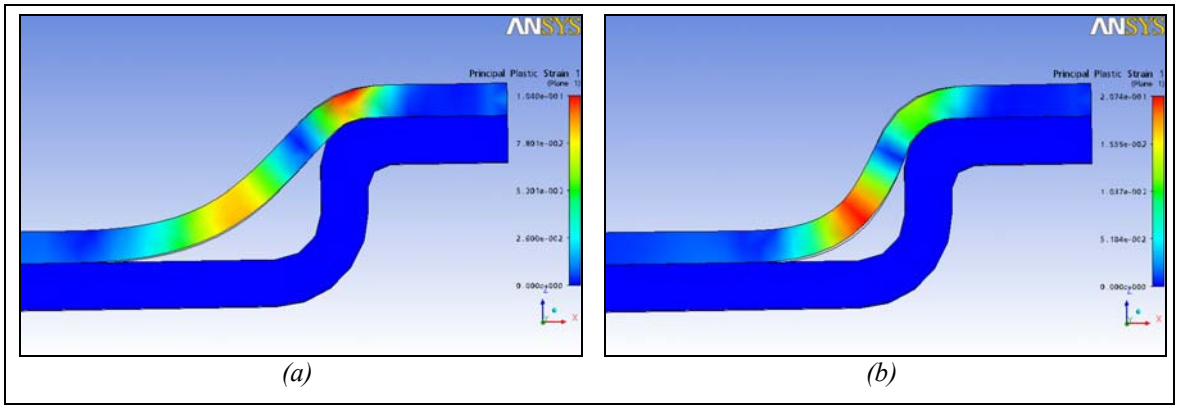

(a) *(b)*

Figure 6.35: Distribution of the maximum plastic strain in the deformed sheet metal blank around the root corner of the mould at different times: (a) 1.1 s; (b) 1.2 s.

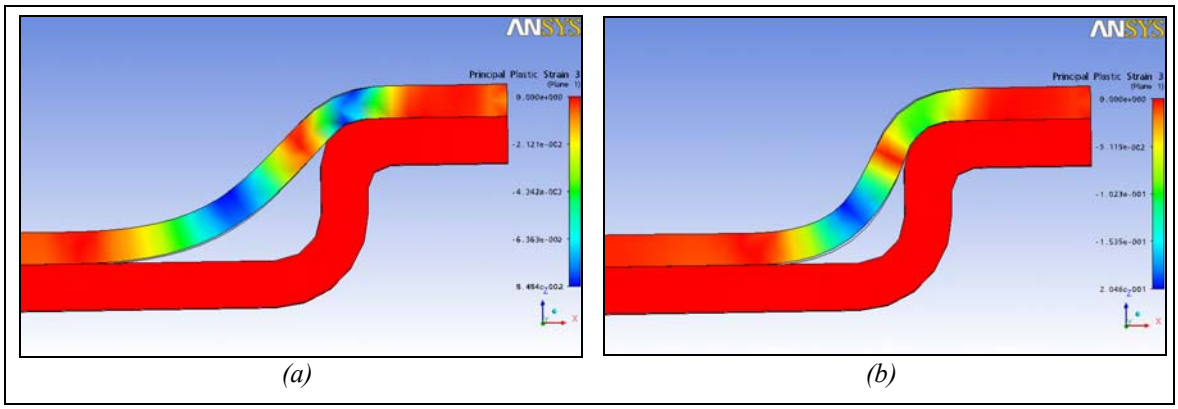

(a) *(b)*

Figure 6.36: Distribution of the minimum plastic strain in the deformed sheet metal blank around the root corner of the mould at different times: (a) 1.1 s; (b) 1.2 s.

Figure 6.37 shows distribution of the equivalent plastic strains on the deformed sheet metal blank at different times.

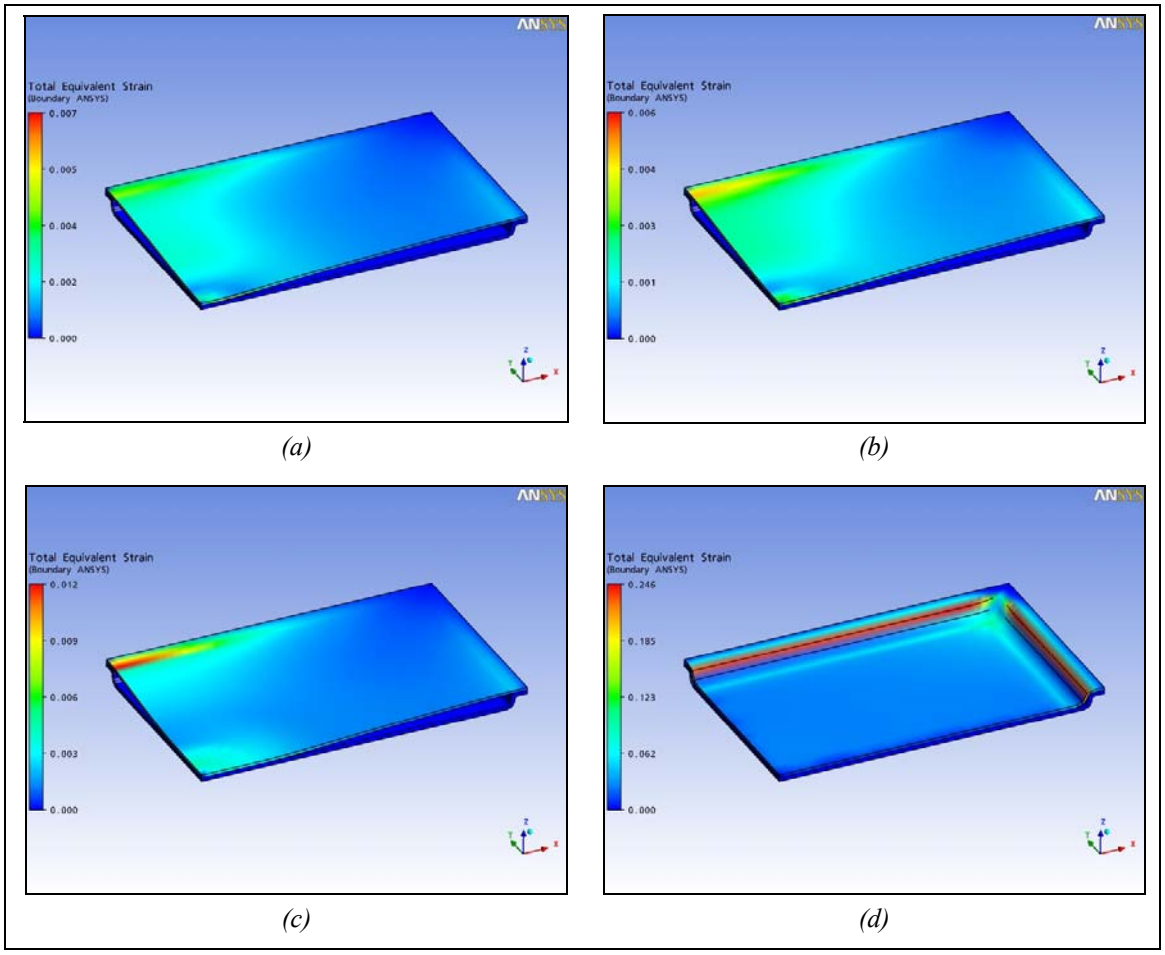

Figure 6.37: Evolution of the distribution of the equivalent plastic strain on the deformed sheet metal blank at different times: (a) 0.1 s; (b) 0.2 s; (c) 0.4 s; (d) 1.2 s.

CHAPTER 7

PROCESS MONITORING AND SWITCHOVER CONTROL SYSTEM

For many years, injection moulding has been considered almost a black art, requiring considerable experience to cope with the complexities of the process. Unquestionably, some of these difficulties are based on a poor understanding of the complex interaction between the thermoplastic material, process parameters and the tooling during the injection moulding process. In principle, injection moulding should be a fairly simple process; plastic is placed into a hopper, melted in a barrel, and injected into a mould under high pressure. The parts emerging from the process should duplicate the features in the cavity. In reality, however, achieving a part with the required dimensional characteristics and physical properties is very difficult.

In order to overcome this problem, the equipment industry has conducted extensive research in order to monitor both the process and the material behaviour directly.

At the beginning of this chapter, a literature review of the state-of –the-art research and developments in injection moulding process monitoring and control will be presented. In particular, control strategies will be focused on the switchover control from the filling to the packing phase.

In the second part of the chapter it will be presented the developed software for monitoring of the Polymer Injection Forming process and optimization of its switchover point from the filling to the packing phase.

7.1 Literature review

7.1.1 Injection moulding process monitoring

Injection moulding is characterized by having many variables, internal and external, affecting the end result. Thermoplastic materials are also unpredictable since they behave as non-Newtonian fluids when molten. Furthermore, it has been demonstrated statistically that the properties of the finished part are affected only indirectly by the machine settings (as explained below). Sensing equipment installed in most machines is also inadequate for giving a true picture of the state of the process since most of the measured parameters have only an indirect effect in the quality of the part. Interdependencies between different machine factors are also very difficult to predict, particularly between settings and plastic variables.

In order to overcome this problem, the equipment industry has conducted extensive research in order to monitor both the process and the material behaviour directly. In order to achieve effective control of part quality, it is necessary to take into account both of these aspects and to understand their interrelations. Pressure measurements are best used to describe the injection moulding process and factors affecting it, particularly when measured inside the cavity. The rheology of the molten polymeric material is best described by temperature measurements. The main difficulties lie in determining where to take these readings and how to interpret the results.

In the case of pressure measurements, there are three basic sensor locations: in the cavity, in the nozzle and indirect measurement of hydraulic pressure. The indirect method has long been the standard for conventional injection moulding. While it is inexpensive and relatively simple to install and maintain, the actual measurement is so far removed from the process that it is capable of providing only general process information.

Cavity sensors are more desirable since they are able to describe the behaviour of the plastic while it is flowing and cooling. Continuously recorded graph of the cavity pressure allows detailed recording of the processes in the injection, compression and holding pressure phases. It alone correlates with all significant moulding features such as weight, morphology, degree of forming, burr formation, shrink marks and cavities as well as shrinkage and deformation. Cavity pressure is the parameter which clearly characterizes the injection moulding process. Typical and constantly recurring characteristic points along the cavity pressure curve are shown in Figure 7.1. The cavity pressure curve reflects the condition of the moulding during the entire injection moulding process [62]. On the other hand, cavity sensors must travel with the mould; otherwise they must be reinstalled when the moulds are changed. If a different sensor is used in each mould, the cost rises quickly, particularly in the case of multi-cavity moulds. If the sensors are interchanged between moulds, the risk of damage becomes a problem, together with the increased time for mould set-up.

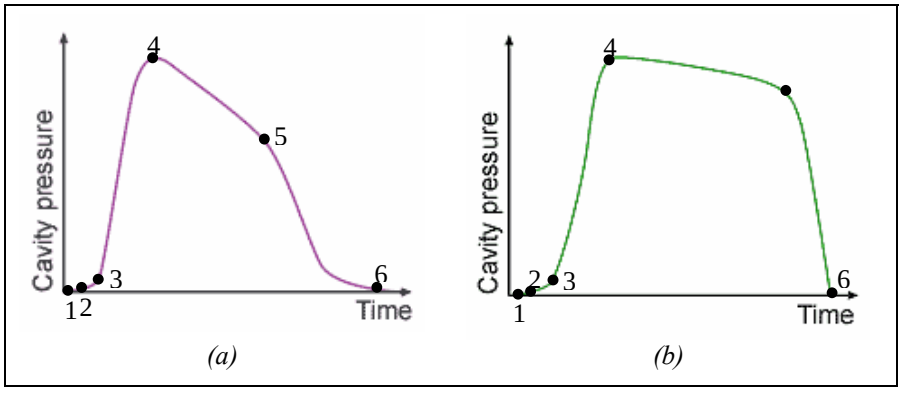

Figure 7.1: Cavity pressure characteristics for: (a) amorphous thermoplastics; (b) semi-crystalline thermoplastics [67].

In view of these problems, pressure sensors have been developed to be used directly at the injection moulding nozzle. These sensors are more suitable for general industrial applications since they remain with the machine, rather than with the mould. Pressure sensors mounted at the nozzle lack the same capacity to describe the behaviour of the plastic inside the mould as a cavity sensor; but they are able to provide a wealth of information regarding the overall process. Nozzle pressure sensors are preferred over hydraulic sensors because they

bypass the errors caused by changes in the viscosity of the hydraulic oil, friction in the ram, plastic composition, etc. They are also viewed as an effective way to achieve uniformity in the shot weight, which is considered by many as a good predictor of part dimensions and quality.

Temperature sensors may also be installed at the nozzle along with the pressure transducer. Such sensors are effective in monitoring the uniformity and the state of the melt. For instance, a sharp temperature drop at the end of the injection phase may indicate the presence of partially melted material in the barrel. This type of information would be difficult to read from sensors installed in the cavity.

One of the most attractive aspects of using sensors in injection moulding machines is to allow closed loop control. Work has been done in this area to allow unattended operation of machines and automatic compensation for external variables such as the introduction of regrind material. Closed loop control can also be used to optimize characteristics of the process such as the holding time or the peak pressure.

Considerable work has been done trying to determine the best way to monitor and control the injection moulding process so as to allow prediction of the part quality before the mould opens [63].

7.1.1.1 Nozzle pressure and temperature sensors

By use of a nozzle sensor, it is possible to extract the profiles for both the pressure and the temperature of the melt during the injection cycle (Figure 7.2). The basic stages of injection moulding may be seen in this profile (i.e. injection, holding, screw return and cooling).

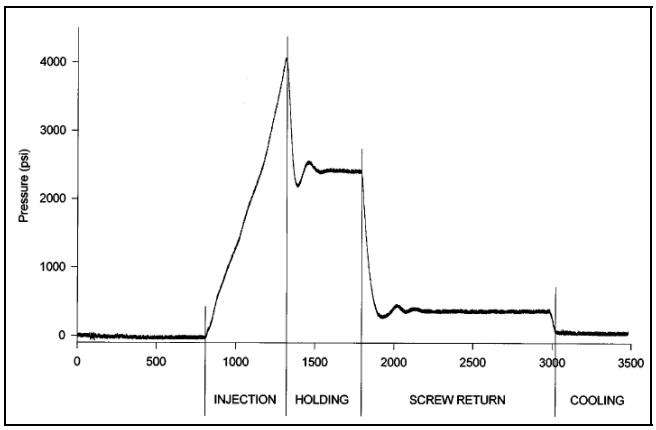

Figure 7.2: Typical pressure profile for the injection cycle.

The key to achieving benefits from these readings is to understand the meaning of the different features in the curve, and to interpret changes as imbalances in the process. Once changes are interpreted, the cause of a given problem may be more readily determined. Figure 7.3 shows the basic components of the injection stage and how they may be read in the pressure profile. The arrival of the melt to different areas, such as the sprue or runner, may be identified in the pressure profile as inflection points (points where the general trend of the pressure suddenly changes because of changes in resistance to the flow). It is important to remember that this interpretation is based purely on the pressure of the melt measured directly at the nozzle of the machine. The pressure read at this point is mostly dependent on the

hydraulic pressure, and is insensitive to material freezing. The advantage of reading the pressure directly at the nozzle is that any factors that may have an effect on this reading (such as hydraulic oil temperature, friction, or plastic composition) are taken into account without their having to be measured directly.

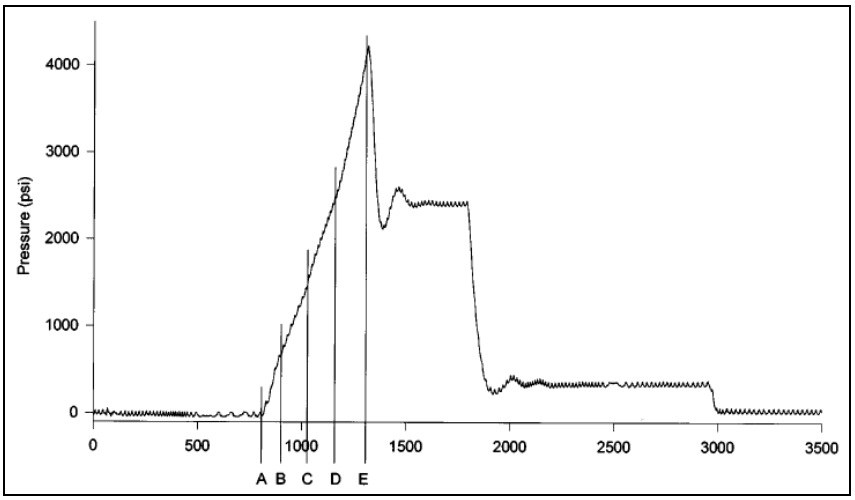

Figure 7.3: Basic components of the injection phase. A) Passage of melt through the nozzle, B) Melt front reaching sprue, C) Melt front reaching the runners, D) Mould fill-up, E) End of packing stage.

Five inflection points (Figure 7.3) have been identified by Churchward, et al. [64] during the injection phase: A) initial movement of the melt past the sensor, B) melt front entering the runner, C) melt front entering the cavity, D) cavity fill-up and E) switchover to holding pressure. The locations of these points in the curve, as well as the area underneath, serve as the basic tools to interpret the state of the injection stage. The features present in the pressure curve have been categorized into three types: point values, average values, and smoothness of a segment. The point values and averages give information that may be used for fault detection, interferencing, and SPC . The smoothness of a segment provides information about the stability of the process [65].

As illustrated in Figure 7.3, the area between A) and B) corresponds to the resistance encountered at the nozzle. This is equivalent to the pressure obtained during an air shot, i.e., when material is extruded through the nozzle while the injection unit is not in contact with the mould. Between B) and C) the melt encounters the resistance of the sprue and runners, followed by the resistance at the cavity between C) and D). At D), the cavity is full and the packing stage begins. This point also corresponds to the boost point, where the machine switches from velocity control to pressure control. After point E), the pressure drops quickly as the ram switches to the holding stage. A fluctuation is seen at the beginning of the holding stage corresponding to vibrations in the machine caused by the large drop in pressure. At the end of the holding stage the pressure drops, again causing pulsation in the hydraulic system. The stage following is the screw return, or back pressure. The final pressure drop signifies the change into the freezing or cooling stage where the pressure drops almost to zero. The analogy just described may be drawn for the other stages of the injection cycle. However, the injection phase provides the most information as it has the most features. Closed loop control could be achieved by analyzing all the critical points, slopes, and areas of the pressure curve and comparing them to patterns that are known as acceptable. In short, the goal is to

standardize the variation into a logical sequence that may be analyzed by a computer. Any deviations of the process from what is known as the norm would cause the computer to react by giving the appropriate corrective actions to the controller of the machine.

The temperature of the melt, as detected at the nozzle, may also give valuable information. The temperature of the melt will increase sharply during injection as the shear and compression in the melt cause it to heat up. The material characteristics, initial temperature, flow velocity and pressure will dictate the increase. Controlling the change in temperature during injection may be important in preventing material degradation [63].

Orzechowski et al. tested a monitoring software while an injection moulding process was running full production for six days. The mould was a sixteen cavity cold runner tool producing electrical connectors. The nozzle of the injection machine was equipped with a sensor for measuring both pressure and temperature. Three parameters were selected in order to track the behaviour of the moulding process over extended periods of time. These parameters included the peak pressure, mean temperature and the integral of the pressure curve. Peak pressure was selected as the key feature that could sense any changes in the injection phase. The mean temperature was monitored to gather information about changes in the properties of the melt over extended periods of time. Finally, the integral of the pressure (i.e. the area under the pressure curve) detected any major changes in the overall pressure pattern.

The main objective during the testing phase was to prove the efficacy of the monitoring system in an industrial environment. The data gathered was interpreted and correlated to intentional and unintentional changes that had an effect on part quality. Certain aspects of the process were also optimized by interpreting the features in the pressure curve. Some of the external factors studied included the time required to reach steady state, changes in ambient temperature, changes in injection speed, throat starvation, regrind introduction and material lot changes.

One of the most striking observations made early in the study was the time that it took the machine to reach true steady state. When starting cold, short shots were observed for up to 60 to 75 shots. However, it was noted that the mean temperature of the melt did not reach a steady state for 110 to 120 shots (Figure 7.4 (a)). Although the actual time required to reach steady state is mould and machine specific, a discrepancy between the time required to produce full shots and the time to reach true steady state was observed. The peak pressure required about the same amount of time to achieve steady state (Figure 7.4 (b)), although the initial trend was downward in contrast to the upper moving trend of the temperature.

The importance of this finding must be clearly understood. Operators may waste time and material changing machine parameters without first allowing it to stabilize, thus never seeing the true effects of their changes. In other instances, the operator may leave a machine believing that it is properly set, only to come back an hour later to a machine that is producing bad parts. This may occur if the machine drifts out of control as it reaches its true steady state. The operator, of course, has no means to predict or observe these changes.

Factors affecting the time to achieve steady state include barrel and mould temperatures, environmental temperature and hydraulic oil temperature [63].

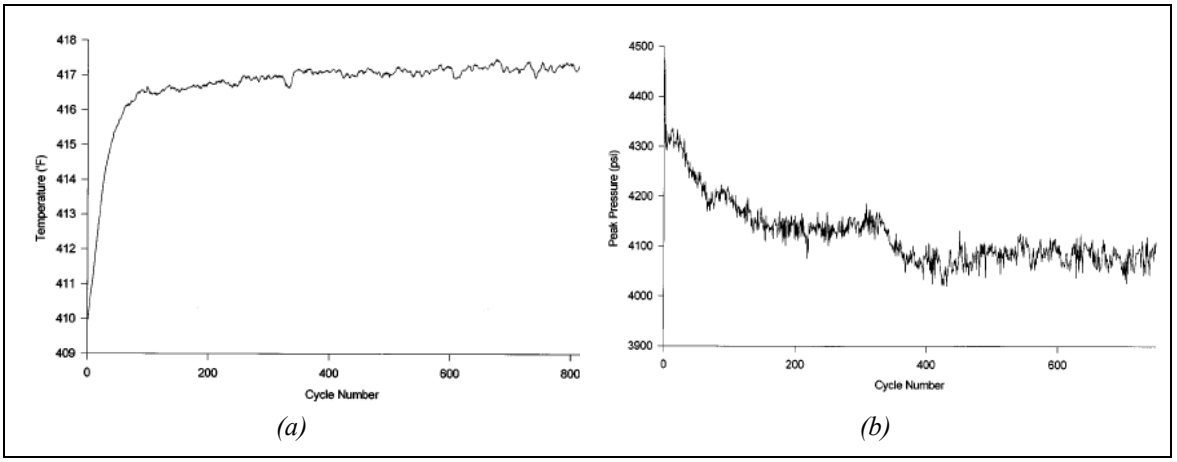

Figure 7.4: (a) Mean temperature profile during a 24 hour period of operation; (b) Peak pressure profile during a 24 hour period of operation.

Speight in [66] used a data acquisition system from an injection moulding process in order to optimize the velocity to pressure phase transfer. The injection machine was set up to produce instrument housings from a two impression mould.

Since the packing/compression phase during the injection moulding process has a strong influence on the peak cavity pressure, which influences part weight and specific dimensions; it is desirable to minimize quality criteria variation and promote consistent product quality. An efficient velocity to pressure phase transfer significantly reduces process variation, while a poorly set transfer adversely effects process stability.

Figure 7.5 shows mean nozzle melt pressure and coefficient of variation for 10 moulding cycles, processing HDPE, in the research environment, obtained by Speight [66]. It can be seen that during the velocity to pressure phase that the coefficient of variation is high, indicating a poor transfer setup. Figure 7.6 shows mean nozzle melt pressure and coefficient of variation for 25 moulding cycles, processing ABS, in the same manufacturing environment. The coefficient of variation at transfer only occurs for a short period of time, indicating a more efficient transfer setup. Process monitoring of the statistical variation at transfer indicates the performance of the velocity to pressure transfer, but involved computation, therefore by focusing on the screw displacement during the transfer phase, provides an alternative source of information.

Figure 7.7 shows mean nozzle melt pressure, ranging from 10 to 30 bar set hydraulic pressure, processing HDPE in the research environment. The velocity to pressure phase transfer time period is shown to be influenced by the actual set packing/holding pressure level. Figure 7.8 shows that the screw displacement curves correspond to the respective pressure levels. This time period is most important in determining the ideal packing/compression phase, and should be minimized at all times. Figure 7.8 also shows that the screw displacement curve, during the velocity to pressure phase time period, may be characterized as kick-backward; kick-forward; or a smooth transition screw movement. The screw displacement curve for 25 bar hydraulic pressure shows the nearest profile to a smooth curve, inferring an efficient packing/compression phase. Figure 7.9 shows the cavity melt pressure curves for the varying hydraulic packing/holding pressure levels. The curve corresponding to 25 bar hydraulic pressure shows the most desirable ideal cavity pressure

curve. Considering Figure 7.7-Figure 7.9, the relationship between screw displacement and cavity melt pressure during the packing/compression phase is observed, for changes in hydraulic packing/holding pressure levels. This relationship has been verified throughout a full experimental investigation and is shown to be a robust approach. Figure 7.10 shows the nozzle melt pressure coefficient of variation for the varying hydraulic packing/holding pressure levels. It can be clearly observed that the process variation is highest for velocity to pressure phase transfer, when screw kick-backward movement occurs. Figure 7.11 shows that cavity melt pressure coefficient of variation is directly related to the coefficient of variation for nozzle melt pressure, during screw kick-backwards movement. The most noticeable effect is that the coefficient of variation is highest for the packing/ holding phases where screw kick-backward movement occurs, and therefore should be avoided during machine setup.

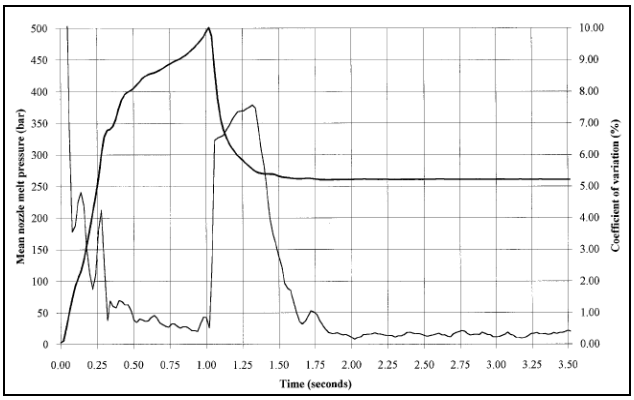

Figure 7.5: Mean nozzle melt pressure and coefficient of variation during the velocity to pressure phase transfer, packing/compression phase; research environment; processing HDPE.

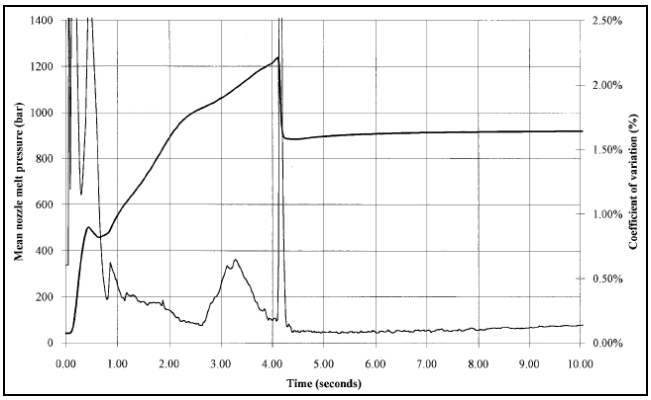

Figure 7.6: Mean nozzle melt pressure and coefficient of variation during the velocity to pressure phase transfer, packing/compression phase; manufacturing environment; processing ABS.

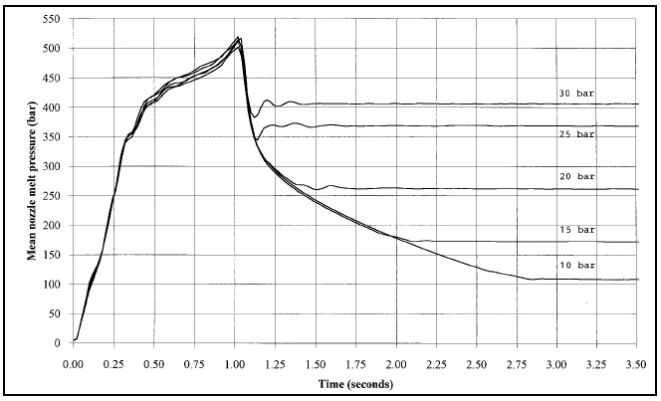

Figure 7.7: Mean nozzle melt pressure during the velocity to pressure phase transfer, packing/compression phase for a range of packing/holding pressures 10 to 30 bar; research environment; processing HDPE.

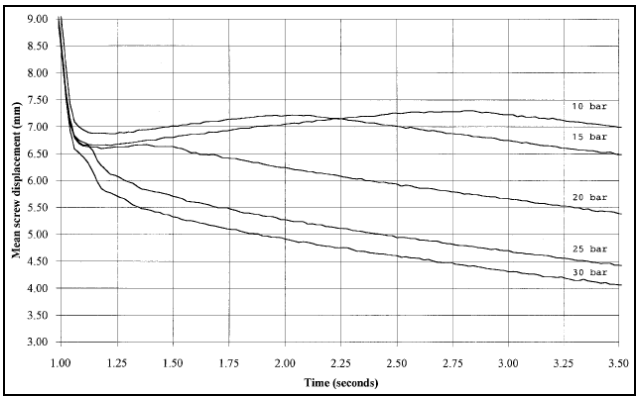

Figure 7.8: Mean screw displacement during the velocity to pressure phase transfer, packing/compression phase for a range of packing/holding pressures 10 to 30 bar; research environment; processing HDPE.

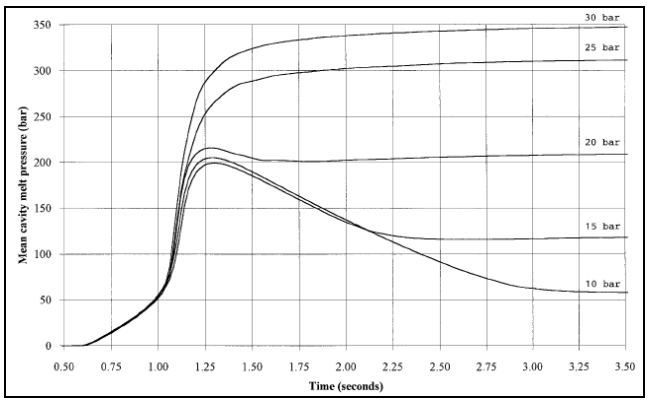

Figure 7.9: Mean cavity melt pressure during the velocity to pressure phase transfer, packing/compression phase for a range of packing/holding pressures 10 to 30 bar; research environment; processing HDPE.

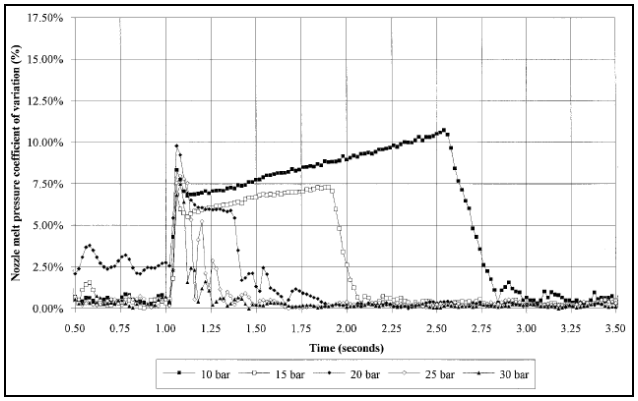

Figure 7.10: Mean nozzle melt pressure coefficient of variation during the velocity to pressure phase transfer, packing/compression phase, for a range of packing/holding pressures 10 to 30 bar; research environment; processing HDPE.

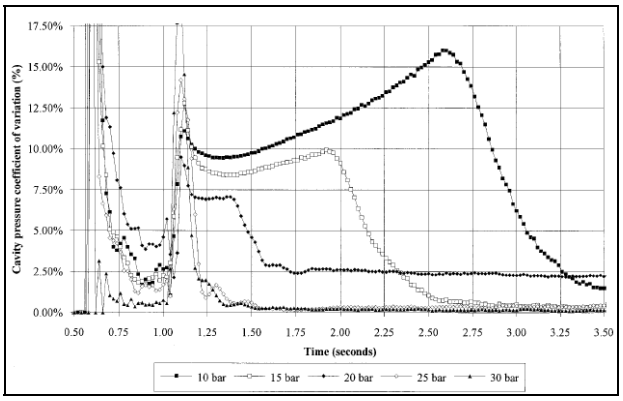

Figure 7.11: Mean cavity melt pressure coefficient of variation during the velocity to pressure phase transfer, packing/compression phase for a range of packing/holding pressures 10 to 30 bar; research environment; processing HDPE.

Figure 7.12 shows the effect of various screw injection velocities on mean nozzle melt pressure, ranging from 20 to 60 mm/s. The packing/holding pressure level remained constant throughout the experiment. The velocity to pressure phase transfer time period is shown to decrease for the decreasing injection velocities, implying that a more efficient packing/compression phase occurs at the lower injection velocities; for this case study, i.e. a critical packing/compression phase pressure balance was achieved. Referring to Figure 7.13 shows that in fact the smoothest velocity to pressure transfer phase screw displacement curve occurs for 30 mm/s, which corresponds accurately with the mean cavity melt pressure curves shown in Figure 7.14.

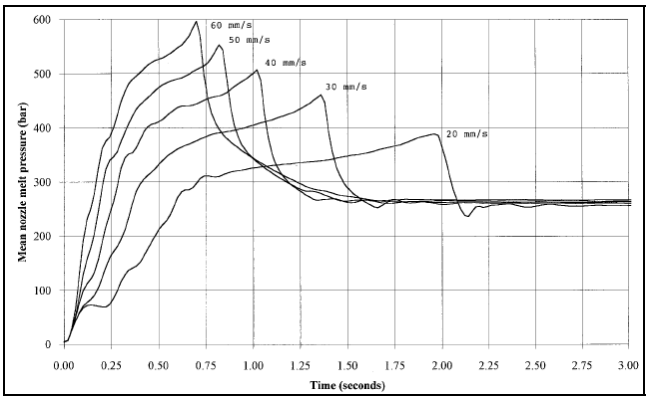

Figure 7.12: Mean nozzle melt pressure during the velocity to pressure phase transfer, packing/compression phase; for a range of injection velocities 20 to 60 mm/s, research environment; processing HDPE.

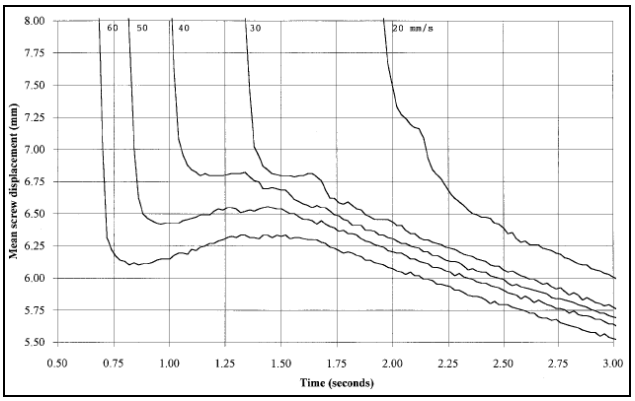

Figure 7.13: Mean screw displacement during the velocity to pressure phase transfer, packing/compression phase; for a range of injection velocities 20 to 60 mm/s, research environment; processing HDPE.

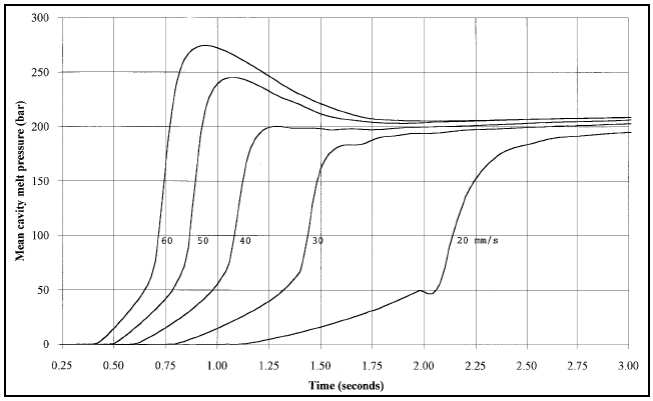

Figure 7.14: Mean cavity melt pressure during the velocity to pressure phase transfer, packing/compression phase; for a range of injection velocities 20 to 60 mm/s, research environment; processing HDPE.

The emphasis of the paper by Speight [66] has been to show how an efficient packing/compression phase can be achieved by visually inspecting the screw displacement during the velocity to pressure phase transfer.

7.1.2 Injection moulding process/quality control

Control of injection moulding is significantly challenged by the nonlinear behaviour of the polymeric materials, dynamic and coupled process physics, and convoluted interactions between the mould geometry and final product quality attributes. A system's view of a conventional injection moulding process is presented in Figure 7.15. The machine parameters are indicated on the left side of the figure, and some common moulded part measures of quality are listed on the right. In this figure, the process is decomposed into five distinct but coupled stages. The output of each stage not only directly determines the initial conditions of the next stage, but also influences some of the final qualities of the moulded part.

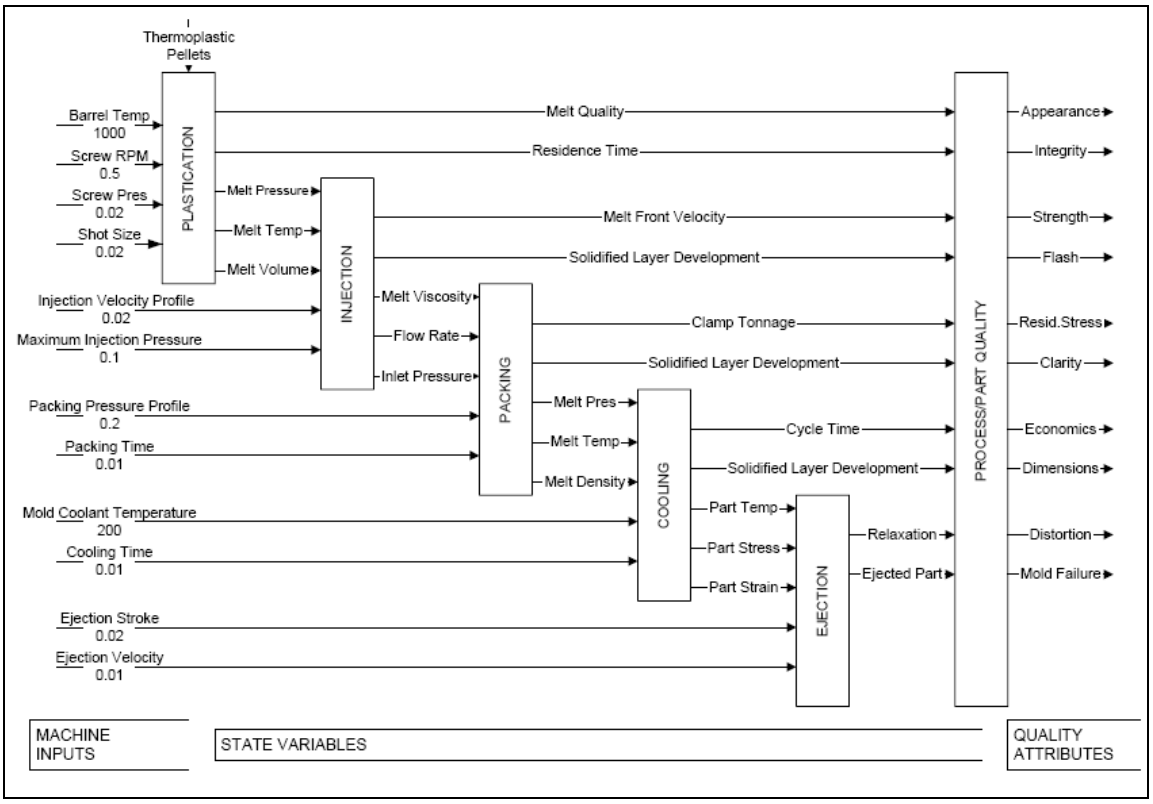

Figure 7.15: System's view of the injection moulding process.

Process variability in injection moulding further complicates process control. The sources of variability are attributed to the thermoplastic resin, the injection moulding machine, and environmental factors.

Product inconsistencies among a batch of moulded parts are most frequently blamed on lot-to-lot variations in material properties. Small changes in viscosity, density, or composition may occur when regrind is mixed with virgin material, a material is used after it has been stored over an extended period of time, or a switch is made between different batches of the same material grade. Small changes in material properties can lead to inconsistencies in part weight, part dimensions, aesthetic, strength, etc.

The second source of variability is process machinery. Moulding machines of different injection cylinder and clamp design will have very different machine dynamics, and provide different levels of moulded part quality for the same process set points. Even identical

machines from the same manufacturer can induce significant quality variation as a result of differences in their controller and varying amounts of wear in the melt and hydraulic delivery systems. Finally, parts moulded from the same press may vary due to internal controller variation relating to the shot size, injection velocity, switchover point, pack pressure, etc.

The third source of variability is human and environmental interaction with the process. For instance, process engineers have different definitions of 'optimal' and can induce product inconsistency through the modification of standard process set points such as injection velocity, pack pressure, back pressure, cooling time, and ejection set-up. Press operators directly determine cycle time and part handling, and may influence some process settings. The physical environment will also introduce variation. For instance, outdoor temperature may affect the effectiveness of evaporative coolers that determine the temperature of the plant water. Indoor temperature can likewise have significant effect on the mould wall temperature as well as the post-moulding behaviour of the melded parts. Humidity can effect the dryness of the polymeric material entering the barrel, thus, introducing further quality inconsistencies [67].

Process control should primarily be used to select a group of controllable parameters that will gain control over the process variables, to improve the parameter repeatability and to improve the parameter set ability. There are three primary process control strategies that can be used with any process variable: open-loop control, closed-loop control and adaptive-control (see Figure 7.16). The primary difference among these three control strategies is the way process variable set points are maintained. In an open-loop controlled system there is no feed back via a transducer to the comparator. Essentially this means that the output from the process is unknown. In a closed-loop controlled system the set point of the variable is maintained at a certain value with different strategies. In an adaptive control system, however, changes in the process are determined by mathematical model and set points of the variable are changed to get the same output [68].

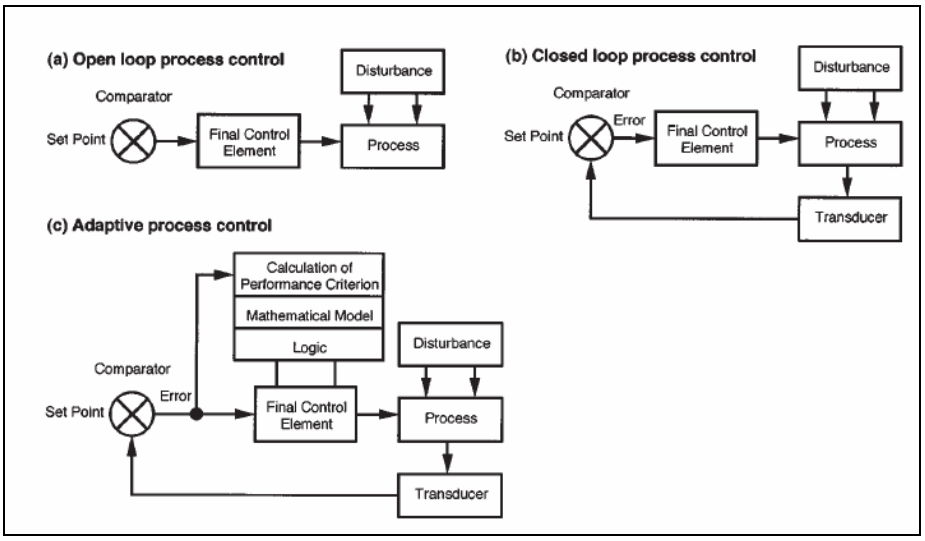

Figure 7.16: Block diagrams of various control strategies for injection moulding [68].

Numerous researches have been conducted in the past two decades in searching for suitable process control systems and technologies either on-line or off-line to achieve part

quality. However, there are a host of variables involved in the complex injection moulding process. It has been found that all the prior studies can be organized into a multiple-level structure system, which consists of one feed forward loop (process setup) and three feedback loops (i.e., Level 1: machine control, Level 2: process control, and Level 3: quality control). The three feedback loops are cascaded so that the output from the previous controller becomes the command to the next controller.

An overview of injection moulding control is shown in Figure 7.17. At the innermost level, only the machine actuators are regulated. This level of control will ensure proper execution of the programmed machine inputs (see Figure 7.15). At the second level, state variables such as melt temperature and melt pressure are controlled to track pre-specified profiles. This will provide more precise control of the state of the melt. At the outermost level, the machine inputs are adjusted so as to improve the quality of the part through better set points given feedback of part quality.

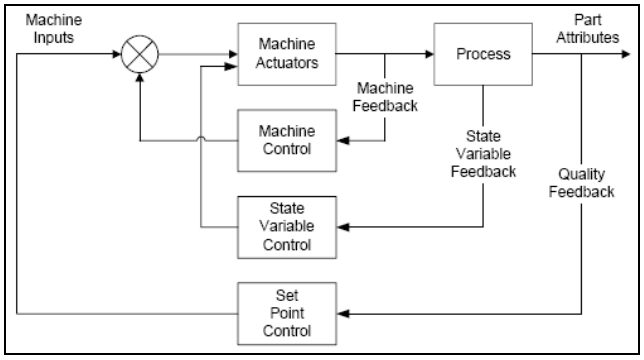

Figure 7.17: System diagram of injection moulding control.

The logic behind the control strategy in Figure 7.17 can be explained by an example. Consider specification of packing pressure profile as a machine input for control of a moulded part width. In this case, the machine actuator will be the hydraulic servo valve to the injection cylinder, and 'machine control' will ensure a specified packing pressure at the melt inlet. However, the packing pressure will be non-uniformly distributed in the mould, due to polymer viscosity. This motivates 'state variable control' to regulate the cavity pressure more precisely based on feedback of measured pressure inside the mould. In this case, the input to the hydraulic servo-valve will be augmented to provide the additional level of precision. While this additional level of control ensures realization of the specified cavity pressure, it may still not lead to a satisfactory moulded part because of a poorly-specified cavity pressure. Set point control is incorporated to adjust the specified cavity pressure. Each of these control levels will be discussed next [67, 69].

7.1.2.1 Determination of processing conditions

The process conditions are the setting values of Level-1 parameters for specific combination of machine, mould, and material. Typically, they can be set at the machine console. As already acknowledged in many researches, the final quality of moulded parts is a function of process conditions, which can be expressed as a mapping,

$$q(n,t) = f(p_s(t), n, t) + v(n,t) \tag{7.1}$$

where q is the collection of Level-3 parameters including quantitative and qualitative variables; n is the cycle number, and t is the time from the starting of that cycle; $p_s(t)$ is the collection of processing variables, and v is the disturbances; f is the mapping from process conditions to quality without considering the disturbances. Unfortunately, f is so complicated that a little is known about it, thus making process setting a difficult job.

Nevertheless, Eq. (7.1) is often simplified in order to attain the solution to produce the acceptable quality in practice. For example, it is considered reasonable to ignore the machine and processing dynamics to determine the so-called optimal process conditions for a static optimum problem. By doing so, the methods of determining the optimal process conditions can be categorized into two groups based upon how Eq. (7.1) is represented: first principle model or empirical model.

In the first approach, it includes use of sophisticated CAE tools and mathematical models to assist the process setup. Most of the commercial CAE software packages for injection moulding are based on rigorous, first-principle models, which provide reasonably accurate description of the injection moulding process. Reliable CAE simulation tools could help to setup injection-moulding machine in a more scientific manner and replace the traditional ad-hoc, trial-and-error approach. The information provided to the CAE software includes machine specification, mould geometry and material properties, and the output is the suggested processing conditions to achieve acceptable quality parts. It is noted that the quality requirements may vary based on the different part functions. Therefore, there is always a quality criterion that needs to be optimized subject to the constraint of Eq. (7.1), even though it may not be expressed explicitly. Hence, different optimization algorithms are usually combined with the model presentation to obtain the optimal process conditions. For example, Turng et al. has integrated a CAE software with an optimization tool to help the users find the optimal process to achieve a variety of optimization objectives while satisfying certain constrains [70].

On the other hand, the empirical models consist of more diverse methods, such as numerical regression analysis, design of experiment (DOE), artificial neural networks (ANN), and expert systems. Among them, ANN is the most popular method, in which some indices of part quality such as weight, thickness, warpage, shrinkage, flash, strength, etc. are established as the output of neural networks while the input are either machine variables or process variables. It is not surprising that the results indicate that process variables based networks can predict the part quality more accurately than machine variables. It is because the process variables are more directly related with the polymer being processed and the limitation exists in machine control system. One drawback of ANN is that it needs to be trained with a set of well-prepared data capable of describing the process accurately. Otherwise, the model has little usage for process setting. Often, DOE is employed to generate experimental data covering the feasible parameter space [67, 69].

7.1.2.2 Machine control

The injection moulding machine (IMM) level control is relatively well established compared to process and quality control. Nowadays, there are many commercial control systems available in the market to deal with IMM control. For instance, programmable logic controllers (PLC) are well suited for IMM control and are being widely used in these systems. Since the load disturbances of the injection-moulding machine are very difficult to model and predict, the traditional PID control cannot always guarantee high standard machine

performance. Therefore, there is continuous effort in pursuing advanced control technologies to improve machine control.

Since barrel temperature, injection speed, ram position, and hydraulic pressure are closely related to the injection stage, there are some advanced control strategies developed to control these parameters.

Regarding to injection velocity, there are many adaptive control schemes ranging from self-tuning regulator (STR), sliding mode control (SMC), generalized predictive control (GPC), fuzzy logic control (FLC) to iterative learning control (ILC).

Since nonlinear and time-varying characteristics are inherent in injection-moulding machine, the advanced adaptive process control technologies are capable of reaching higher standard performance than conventional PID if the machine dynamics are well understood. However, it seems the industries are still reluctant to utilize advanced control technologies in their machine controllers, which are still presently dominated by PID. The reasons lie in the fact that advanced control schemes highly rely on the underlying machine dynamic models. Both the structure and coefficient parameters of the advanced control schemes need to be carefully validated before they are incorporated in the closed-loop with confidence. The modelling work has to be carried out by control engineering experts for different machines, which is very costive and time-consuming. In comparison, traditional PID has the advantages of simple structure, easy tuning, and no special assumptions on the machine dynamics even though its performance is moderate.

7.1.2.3 Process control

As mentioned earlier, the process (Level-2) variables are more closely related to part quality than the machine (Level-1) variables. Hence, it is more desirable to control the process variables to achieve constant part quality. As early as in the late 1980's, Agrawal et al. already suggested using process variables (then called the plastic variables) as the control parameters [71]. Many recent studies have since confirmed the soundness of this suggestion with results showing that polymer melt temperature and pressure have strong influence on the quality of the moulded part. Especially, the cavity pressure throughout all phases of injection moulding plays a dominant role concerning about part quality defined by part weight, thickness, or other dimensional features like shrinkage and warpage.

Besides cavity pressure, there are other process variables that are widely employed in injection moulding process control, such as melt pressure in nozzle, melt temperature in nozzle or cavity, melt viscosity, mould separation, etc. These variables cannot be independently controlled without manipulating a set of Level-1 machine parameters. Sometimes, one of the machine parameters, such as hydraulic pressure or valve opening, is selected as the manipulating variable to compensate for the variations of other parameters and the environment.

There is no doubt that proper selection and control of process variable are important to improving the process capability, increasing the part quality, and reducing the production cost. There are two conditions that have to be satisfied for the variables to qualify for on-line control. First, the signal should be measurable on-line via commercially available transducers. Second, the measured variable should closely reflect the process and the properties of moulded parts. That is the reason why the cavity pressure and temperature are preferred for process control over other variables. However, each variable has its pros and cons. For example, directly flash mounted pressure transducers inside the cavity may not be feasible if

surface finish is critical. In this case, upstream information in the nozzle or mould separation could be the options.

7.1.2.4 Quality control

Quality is the final goal of injection moulding control that starts with process setup. Comparing to the statistic setup procedures in which the process conditions are sought through static optimization, quality control is based on dynamic quality models that relate the desired quality to process variables and/or machine variables. The process conditions or process variables have to change from cycle to cycle to compensate for the possible disturbances from material, machine dynamics, and process dynamics.

As pointed out before, on-line quality measurement is difficult to implement in practice, which means there is no direct on-line feedback for quality control. Thus, there has been no real closed-loop quality control for injection moulding. All the current strategies of quality control fall into an observer-based control system structure as shown in Figure 7.18. How well the system can regulate the pre-selected quality variable largely depends on the capability of adaptation and accuracy of the quality observer based on process and/or machine variables.

Numerous researches have investigated the possible methods to construct a generic, accurate, and economical quality observer. Similar to the approaches used to determine the process settings, they vary from empirical models, first-principle based models, or a combination of both. As to the specific quality indices, part weight and part dimensions are the two most popularly selected quality variables because they can be quantitatively measured with high resolution.

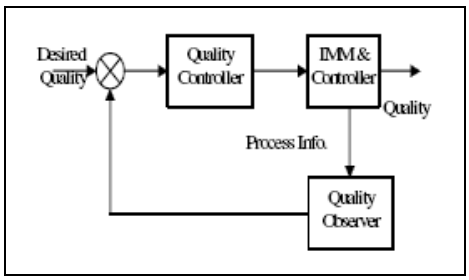

Figure 7.18: Observer-based quality control system structure.

It seems that the on-line quality sensor cannot be circumvented towards automatic quality control. Fortunately, there are a number of on-going studies that report progress along this line. For example, by using ultrasonic transducers, both melt-front velocity and the gap between the solidifying melt and mould wall surface during cooling can be detected. Hopefully, the innovative quality sensor will eventually enable on-line quality control. Otherwise, one has to refine the generic first principles model and construct the "virtual sensor" for quality response, which is not a trivial.

7.1.3 Switchover control in the injection moulding process

Plastic processors have noted for years that the quality and uniformity of injection moulded part is significantly affected by the ability to identify the proper moment to switch from high velocity injection phase of the moulding cycle to low velocity pressure controlled packing phase. Most operators agree that the switch/over should occur when the mould is

roughly 90% filled. This allows for rapid filling of the mould and allows the ram to decelerate before the plastic completely fills the mould. If the mould fills completely before the ram slows, a pressure spike will occur which will slightly over pack the mould (see pressure profile (1) in Figure 7.19). The amount of over packing will depend on just how fast the ram was travelling and thus, a significant level of variability is introduced if end of fill occurs as the ram is decelerating.

If the ram slows too early, the plastic has time to cool significantly as the final portions of the mould are filled. The rapidly solidifying polymer provides extra resistance to the pressure forcing the plastic into the mould and causes a variable amount of under packing that depends on just how early the switch/over event occurred (see pressure profile (2) in Figure 7.19).

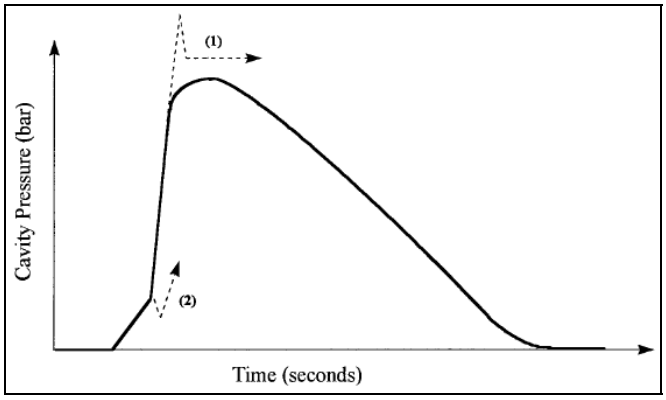

Figure 7.19: State of packing/compression phase using cavity pressure measurements [66].

A number of techniques have been developed to trigger the switchover. These include time, screw (ram) position, hydraulic pressure, nozzle pressure, cavity pressure, and tie bar load or deflection.

Time is the oldest and easiest control mode for transfer in injection moulding. The control device is merely an electrical timer. Thus, for timed transfer from fill to pack, the pressure and injection speed are maintained for a specified length of time. However, since the timer does not control the pressure/injection speed interaction during filling nor the viscosity of the resin, timed transfer is considered the least reproducible method for the transfer from fill to pack. Although not considered ideal, timed transfer still typically determines the pack/hold, hold/cooling and cooling/mould open transitions. Moreover, timers are still present as "safety" measures on the transfer from fill to pack so if the machine does not reach the set position for the preferred transfer, the fill stage will eventually time out.

Ram position is commonly used for transfer from fill to pack in injection moulding. For this, the machine can monitor the position of the ram using one or more transducers, such as a potentiometer, optical encoder, or linear variable differential transformer (LVDT). When the set position is reached, the machine switches control. While such controls are typically used with injection velocity-controlled machines, position transfer can be attained when the shot size indicator (on the injection unit) trips an electrical micro switch. Unlike timed transfer, position transfer delivers a constant volume (shot) of melt to the mould. In conjunction with controlled ram velocity, such transfer permits uniform delivery of polymer melt to the mould cavities. Ram position has been suggested as a control for packing, but is not generally available on commercial machines.

Hydraulic pressure is available on most injection moulding machines, but is not as commonly used as position for the transfer from fill to pack. In hydraulic pressure transfer, the machine switches from fill to pack when the pressure in the hydraulic lines behind the injection cylinders reaches the set position. With well-maintained machines and properly-set controls, hydraulic pressure transfer is more consistent than ram position transfer. While position transfer delivers a constant volume of material, polymers expand upon heating and the constant volume of melt does not always produce consistent part weights. Hydraulic pressure can compensate somewhat for changes in viscosity and for expansion of the melt. However, hydraulic pressure transfer is not easily set up as position transfer.

Cavity pressure is not commonly used for transfer although it can be used for the fill/pack, pack/hold and hold/cooling transitions. Moreover, cavity pressure transfer is considered the most accurate method for transfer because it measures both material changes (such as viscosity) and machine behaviour. Cavity pressure increases linearly as the mould is filled and then spikes as packing begins. As shown in Figure 7.20, correct switchover occurs immediately before the rapid increase in cavity pressure. Since premature switchover does not permit complete filling of the mould, the cavity pressure decreases as the part is filled during packing phase. Delayed switchover over-packs the mould (and often produces flash); this correspond to a rapid rise in cavity pressure during fill and a subsequent reduction in pressure at transfer to packing. While both cavity and hydraulic line pressure enable fairly accurate transfer from fill to pack, only cavity pressure permits an accurate switchover from pack to hold. For either method, the transfer from hold to cooling occurs at the time when a consistent part weight is reached.

Since cavity pressure must be monitored in the mould, the expense and positioning of the pressure transducers is a major problem. Cavity pressure measurement is highly dependent on the position of the pressure transducer. Ideally, a pressure sensor can be placed about one-third of the way into the cavity. However, multi-cavity moulds, particularly family moulds or those with artificially-balanced runner systems require multiple transducers. Additionally, the transducers can be mounted flush with a cavity wall or behind ejector pins. The former is more accurate; whereas, the latter allows the transducers to be used in other moulds without disassembling the mould.

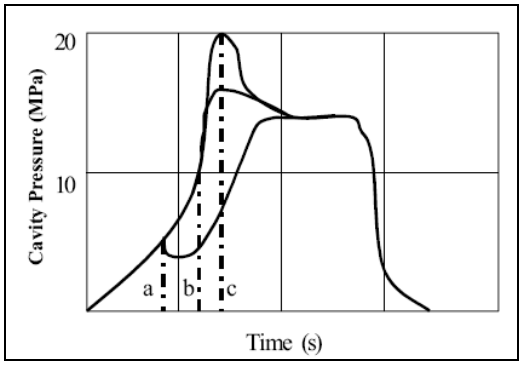

Figure 7.20: Cavity pressure for different switching points: a) premature switchover, b) correct switchover, and c) delayed switchover.

Nozzle pressure transfer is a method for reducing the cost, but maintaining some of the advantages of cavity pressure transfer. Consequently, it is also not commonly used. For this, a

pressure transducer is installed in the nozzle of the injection moulding machine. Since this transducer is farther from the mould cavity, it is not as accurate as cavity pressure measurements. Nozzle pressure is also not always useful for family moulds or those with artificially-balanced runner systems.

As a transfer mode, tie bar deflection is relatively uncommon. Typically a transducer or other device measures the strain in a tie bar. Since this strain changes with the cavity pressure, measuring tie bar deflection is a simpler (and less expensive) way to monitor the cavity pressure. This method has been shown to correlate with cavity pressure. However, the relatively small changes in strain have produced practical problems in amplifying the signals from the transducers [72].

7.1.3.1 Switchover control based on cavity pressure

At least two different strategies have been employed in using cavity pressure for switchover: 1) one step injection or 2) two step injection.

Under the "one step injection" strategy (see Figure 7.21 (a)), the plastic is injected at high velocity throughout the injection phase. The end of injection is identified when the cavity pressure exceeds a threshold value. This value is set somewhat less than the desired packing pressure value so that switchover will occur before the mould is completely full. This allows the injection ram time to slow down without causing a pressure spike when the polymer fills the mould cavity.

Under the "two step injection" strategy (see Figure 7.21 (b)), the plastic is injected at high velocity until the mould is roughly 90% full. Then the velocity is reduced to a low value and the last 10% of the mould fills slowly as the pressure ramps up to the desired packing pressure. Here the switchover pressure is set equal to the desired packing pressure since the slowly moving ram can respond to the switchover signal without causing a spike in the cavity pressure.

Using the "one step" strategy the operator would begin with a pressure threshold setting that caused a pressure spike (as seen in Figure 7.21 (a)) then reduce the setting until the spike disappeared. This method uses the pressure threshold value to identify how "full" the mould is. The shape of the cavity pressure curve responds to the physics occurring in the mould during filling and packing. The pressure is zero until the polymer flow front passes the transducer location (typically near the gate). The pressure increases approximately linearly as the cavity fills. This linear increase is due to the force required to push a viscous material through a confined channel. The slope of the increase is a function of the length of flow past the sensor, the injection velocity, and the polymer viscosity. If the intent is to switchover when the mould is a specified percent filled, the pressure sensor will produce error if the injection velocity changes, if the melt temperature changes, or if the material changes viscosity. The "two step" method does not have this problem since the switchover event is occurring after the mould is full [73].

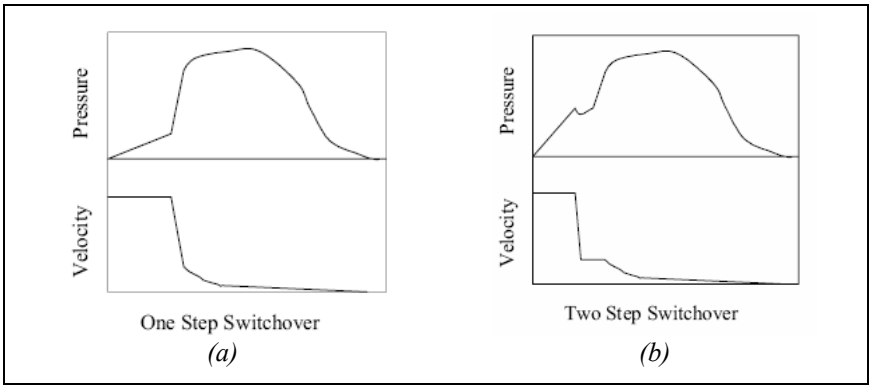

Figure 7.21: Typical ram velocity and cavity pressure curves produced during: a) one step injection; b) two step injection [73].

7.1.3.2 Influence of cavity pressure transducer position

During the cycle of an injection-moulded part, the most consistent method transferring from the injection phase to pack phase is by using cavity pressure. Locating a transducer near the gate should be the optimum location to monitor and transfer pressure; this area of the part experiences all plastic pressure throughout the filling phase.

In [74] Piemme et al. compared data produced by transferring at several different locations along the flow length of the part. Four ejector pin cavity pressure transducers were placed inside the cavity in the following locations: one near the gate, two locations half way to end of fill, one just prior to end of flow, and the last at end of fill.

Fifty parts from each cavity pressure transducer location were moulded using the same moulding conditions. Process data was collected to monitor cycle-to-cycle consistency for each process. The parts were then weighed and their weights compared to see which location was most consistent, and if injection speed had any affect.

The results of this experiment showed that location of the transducer along the flow length, from near gate to end of fill, did not effect the consistency of the process. The moulding process also seemed to did not have any effect on the consistency of process.

7.2 The developed software for process monitoring

In-line monitoring of the injection moulding operations requires continuous measurements of different parameters while the machine is running. These measurements can be performed by direct contact with the molten material, such as in the case of pressure and temperature, or by monitoring the material through an optical window as with the infrared sensors, optical and fluoroscopy techniques, or by indirect contact with the plastics, such as with ultrasonics.

The body of literature related to the monitoring of plastic injection moulding operations is quite extensive. The process monitoring problem has been approached in many different ways since there are many processing parameters and there are no specific techniques that measure all parameters. Material monitoring has not been addressed to the extent of the process, in part because of the incapability of the current sensors to measure and interpret material physical properties. The existing literature on sensors for in-line monitoring of the process of injection moulding operations, to a limited extent monitoring of the material physical

properties, is predominately related to pressure and temperature measurements, infrared sensors, optical analyzers, fluorescence detectors, and, to a lesser extent, ultrasonics. In-line monitoring of injection moulding has been applied to most parts of the equipment. Figure 7.22 shows the major functioning units of the process and identifies the different areas which can be subjected to monitoring operations.

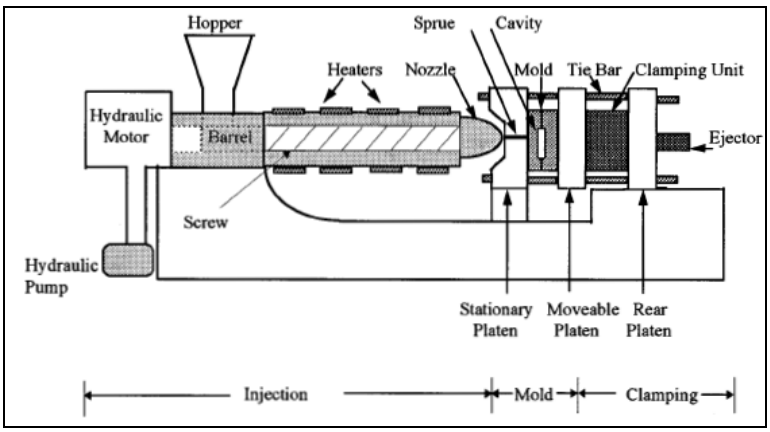

Figure 7.22: injection moulding machine showing the three major functions units.

The developed monitoring software can manage information from both the injection, the clamping and the mould unit. It is programmed as a modular system which can manage both analogue and digital input/output signals. Due to its general-purpose structure, the software can be use for monitoring of both the traditional injection moulding process and the Polymer Injection Forming process, as well as other particular processes such as gas-assisted injection moulding, co-injection, and others.

Signals to be acquired are read by means of a National Instruments 6036 E data acquisition card that also provides A/D conversion and multiplexing (8 differential input channels, 2 analogue output channels, 16 bit resolution with a maximum sampling rate of 200 kS/s (input/output)). A National Instruments SCB-68 shielded board is also employed to isolate the transducer signal from the data acquisition system. An Intel Pentium 2.4 GHz based personal computer running LabVIEW for Windows (National Instruments) is used.

As previously mentioned, the monitoring software can manage different types of sensors, such as pressure sensors and thermocouples. In order to acquire signals from the injection machine located at DIMEG lab (for example machine pressure, ram displacement, ram speed, digital signals relating to start filling and start packing) an electrical connection between the SCB-68 shielded board and the I/O signal board of the ENGEL machine was made.

The "start filling" digital signal from the injection machine is used as a switch in order to provide the computer with a signal corresponding to the start of a new injection cycle.

Figure 7.23 shows the components of the developed data acquisition system for process monitoring.

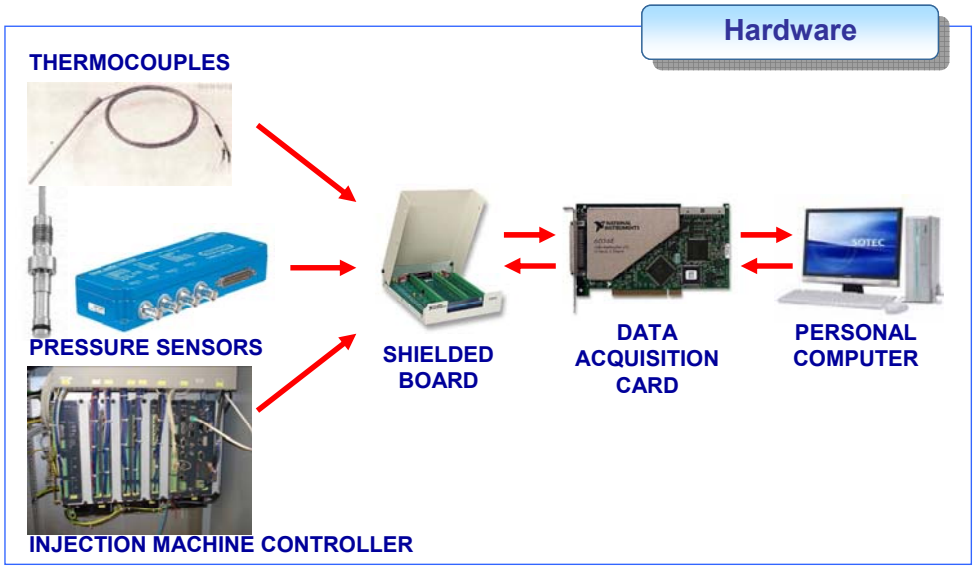

Figure 7.23: Components of data acquisition system for process monitoring.

The monitoring program was crated using a combination of LabVIEW (National Instruments) and .NET (Microsoft) programming software. All required settings, such as number of channels to read, acquisition rate, signal input ranges, channels names, are configurable using the main window of the program, as illustrated in Figure 7.24.

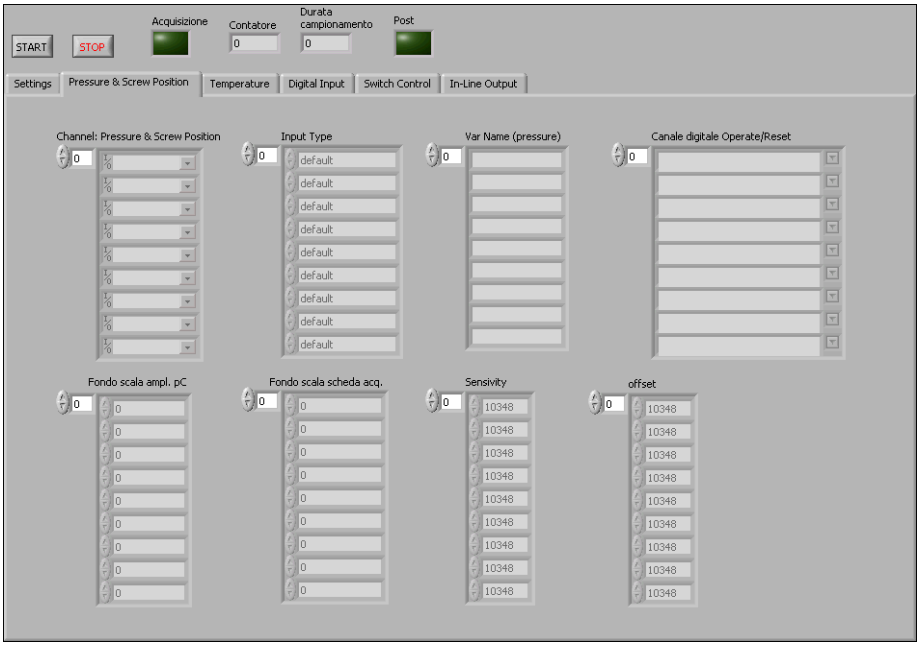

Figure 7.24: Main window of the monitoring software.

Although acquisition rate of analogue signals is adjustable, all the experiments were carried out with a sampling rate of 1 kHz per channel. The monitoring software can display acquired data both in-line, during the process, and off-line, from data saved to PC disk. The

in-line visualization is carried out by means of the in-line viewer (Figure 7.25) while the off-line viewer is used to display data saved to disk (Figure 7.26).

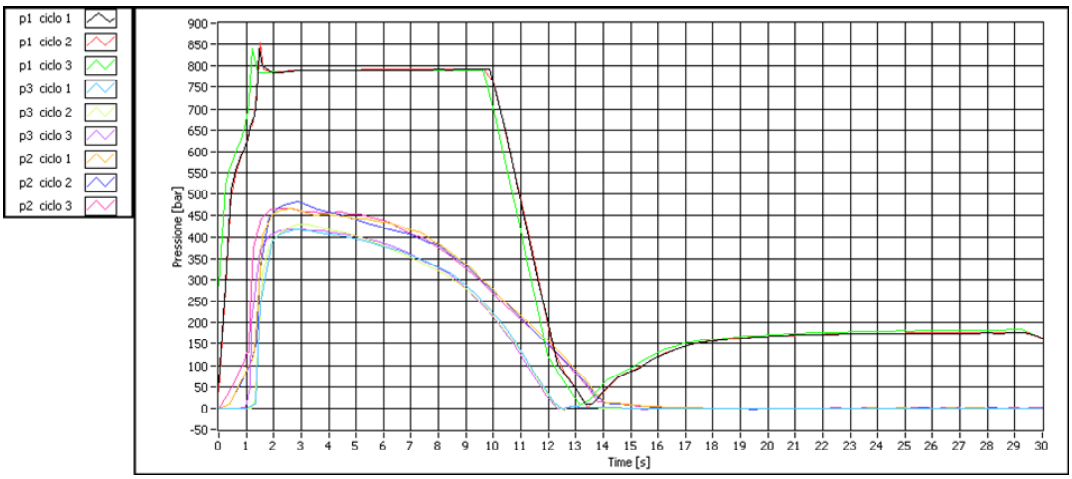

Figure 7.25: In-line data viewer: example of nozzle pressure and cavity pressure.

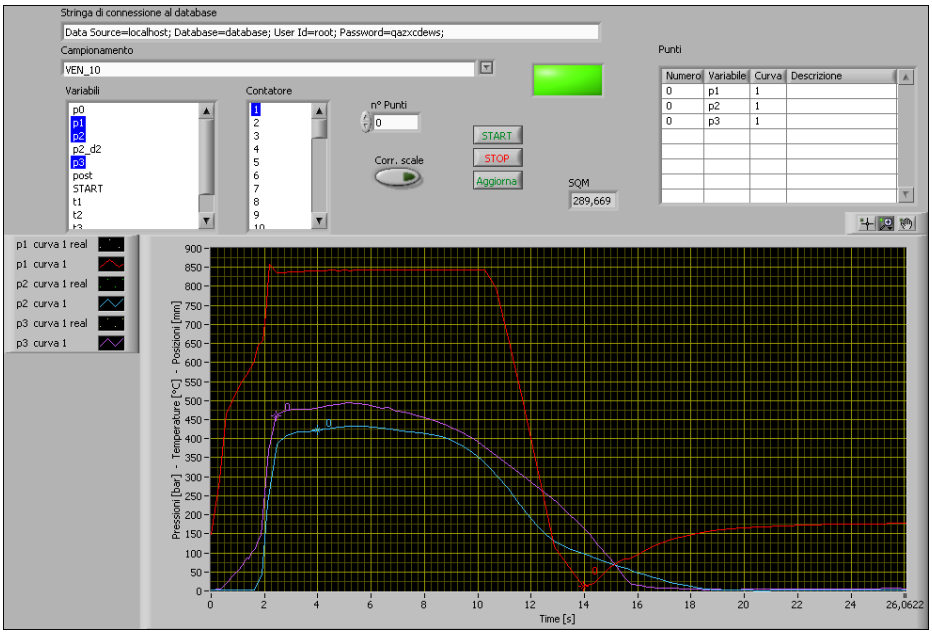

Figure 7.26: Off-line data viewer: example of nozzle pressure and cavity pressure.

At the end of each cycle, acquired data are processed, eventually displayed and saved to disk for future analysis. In addition, the software can compute the mean value, the peak value, the integral and up to the third derivative of the acquired curves. This tools are useful when data analysis is carried out.

In order to carry out automatic process monitoring it is necessary to analyze all the critical points, slopes and areas of the acquired signals and comparing them to patterns that are known as acceptable. In short, the goal is to standardize the variation into a logical sequence that may be analyzed by a computer. Any deviations of the process from what is know as the

norm would cause the computer to highlight the deviation. This task was achieved by means of the sub-program named *Active Monitoring*. Once a robust set of processing conditions have been established, *Active Monitoring* records user-defined quality control limits. During the production, the program detects any tendency of the process to drift away from the centre of the window. It can then produce a warning for corrective actions to be taken.

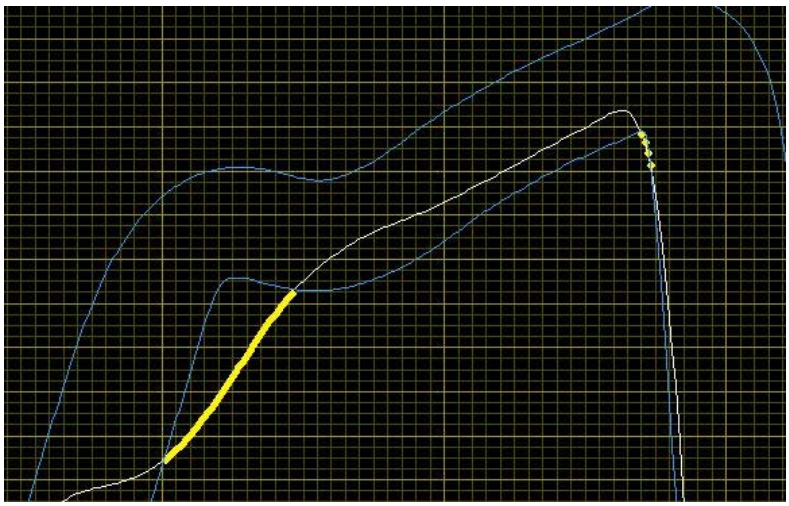

Figure 7.27: Example of user-defined quality control limits of an in-cavity pressure profile: detection of points outside the control range.

By use of sensors and direct readings of the I/O signals board of the injection machine it is possible to extract the profiles for many variables, such as temperature and pressure of the melt during the injection cycle. The key to achieve benefits from these readings is to understand the meaning of different features in the curves, and to interpret them. In order to perform this task, it is important to identify the inflection points of the acquired curves. Within the monitoring software, an algorithm for the automatic detection of the inflection points of acquired curves has been implemented. As viewed in Figure 7.28, which graphs the ram displacement during an injection cycle, the algorithm can identify the meaningful points between the acquired ones.

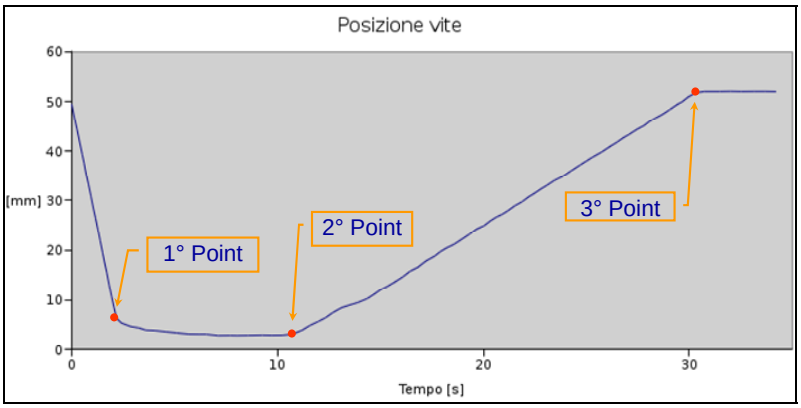

Figure 7.28: Results of the algorithm for detection of inflection points when applied to a typical ram displacement profile during an injection cycle.

The last issue of the developed monitoring software concerns data storage. Acquired data are store to the hard disk of the PC for future visualization or analysis. Two different solutions are possible. The first one concerns data storage using specific binary file format; the second one consists on saving data by means of a Database (MySQL). The latter solution is preferred since data management are more flexible. The true challenge of data storage concerns the amount of data to be saved. Considering, for example, the monitoring of five different analogue signals from an injection moulding machine, which is manufacturing a part with a cycle time equal to 45 seconds. If the scan rate of acquired signals is 1 kHz, data volume to be stored would be equal to 1 Gbyte per day. In order to solve the problem, a compression algorithm has been developed. The algorithm works separately on each acquired channel and reduces the number of curve-profile points minimizing data volume. It is possible since among acquired data there are a lot of redundant data which can be deleted without loss of information. The issue concerns the determination of meaningful and meaningless points, by means of analysis of derivatives of acquired profiles. A compression ratio up to 1:100 can be achieved by a such kind of algorithm (depending on original scan rate and type of acquired signal). Figure 7.29 reports an example of the application of the compression algorithm to a in-cavity pressure profile acquired by means of the developed monitoring software (number of initial acquired points: 3000; number of points after the application of the compression algorithm: 22; compression ratio: 1:136).

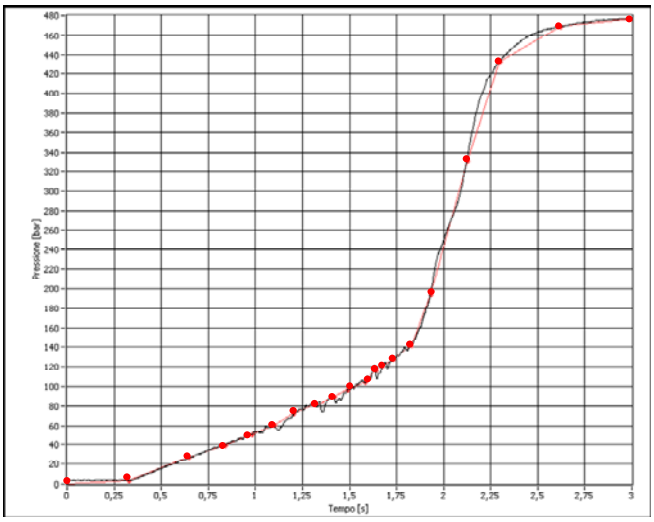

Figure 7.29: Application of the compression algorithm to an acquired in-cavity pressure profile.

7.3 Automatic detection of the volumetric filling of the mould

The process sequence of the Polymer Injection Forming process, as described in chapter 2, is the following:

(i) A sheet metal blank is hung on one of the open halves of the mould.

(ii) During the closing of the mould, the blank metal can be subjected to cutting process in order to get the desired sheet size. During the same operation, the blank can be shaped by deep drawing or by bending the sheet metal into the basic product shape.

(iii) When the mould is completely closed, the polymer is injected into the remaining cavity and a second, nearly hydrostatic, deformation step is applied to shape the metal sheet into its

definite form. In this phase of the PIF process, the physical adhesion between the metal sheet and the injected polymer is obtained.

(iv) Finalizing the production cycle, the composite part is ejected from the mould.

During the third phase of the process, the clamping force is kept low enough to allow sheet flow into the mould cavity. In this case the decreasing pressure from the injection phase to the holding phase is particularly important in order to avoid flash. Therefore, the main requirement for optimum moulding quality is correct switching from the filling phase to the holding pressure phase. If switching takes place prematurely, the mould is filled under holding pressure (internal stress), and with late switching it is overloaded. All traditional switching methods determine the volumetric filling of the cavity over a filling series without holding pressure based on: (i) time; (ii) hydraulic pressure; (iii) screw position; and (iv) cavity pressure.

For the screw position method, the injection screw will travel at a set velocity until a predetermined distance is achieved, then a set holding pressure is used to pack out the part. When using the hydraulic pressure method, the screw will travel forward until oil pressure in the injection cylinder reaches a set value, then the machine switches to holding pressure. Finally, the cavity pressure method looks for pressure in the mould, instead of hydraulic pressure in the injection cylinder.

The value thus optimized is used in production to switch to holding pressure at a fixed level. This approach includes several problems: it is a time-consuming method of optimizing the volumetric filling; each change in the process (e.g. new injection speed) requires the switching value to be re-defined; the fixed switching value cannot react to changes in the process; fluctuations in viscosity produce different pressure curves and thus also different moulding quality; constant set parameters means fluctuating quality.

Compared to the traditional injection moulding process, the switching from the filling phase to the holding pressure phase in the PIF process is more critical. The lower clamping force used in the latter process can cause flash if a pressure spike occurs. Also, process variability in PIF is greater due to the extra-process of sheet metal forming.

In order to overcome problems relating to fixed switching values in both traditional injection moulding and PIF processes, a PC-based software for automatic switching point detection has been developed. The software algorithm is set to the fastest reaction times in order to detect in real time the kink in the cavity pressure curve occurring during volumetric filling (after filling the cavity and before compression of the melt). During the filling phase of the mould, the melt pressure increases nearly constant due to increasing of the flow length. The melt pressure raises up more quickly when the mould is filled and the compression phase begins, since the phenomenon is nearly hydrostatic. By means of the continuous monitoring of the slop of the melt pressure curve acquired by a in-cavity sensor pressure (Figure 7.30 (a)) it is possible to detect if the filling phase is still in progress (Figure 7.30 (b)) or the compression phase is begun (Figure 7.30 (c)). When the compression phase is detected, the control algorithm drives the injection moulding machine to switch to pressure-driven control by means of a digital signal.

The compression phase of the *n_th* injection cycle is detected by means of the analysis of the instantaneous derivative of the pressure curve, which is compared to the slope of the pressure curve during the compression phase of the *n-1* injection cycle, as shown in .

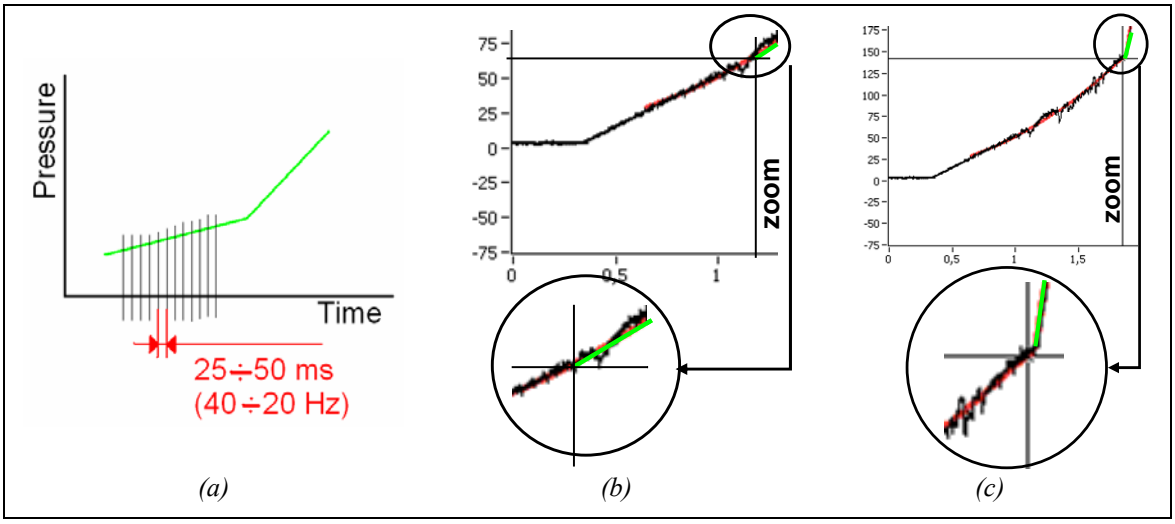

Figure 7.30: Automatic detection of the volumetric filling of the mould: (a) working of the control algorithm; (b) premature switching; (c) late switching.

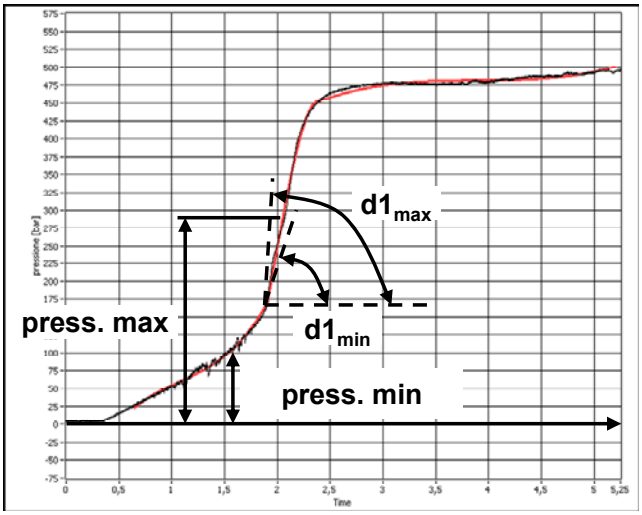

Figure 7.31: Automatic detection of the volumetric filling of the mould: implementation of the control algorithm.

With automatic detection of the volumetric filling, switching takes place when the cavity is full. Process influences such as viscosity fluctuations are compensated. The result is much more consistent mouldings: manual optimization no longer necessary; compensation for viscosity fluctuations; more constant moulding quality; machine-independent system; holding pressure fillings excluded; premature switching is no longer possible; and flashing problems are removed.

7.3.1 Investigation of performances achieved by different switchover control strategies

The objective of the present work was to study the influence of different switchover methods on both part quality (part weight) and process variability (melt pressure). Obtained

results for both the traditional injection moulding process and the PIF process were compared.

The work was divided into four phases. Phase one involved running typical injection moulding processing conditions, collecting shots and changing the switchover method. Part quality and process variability consistency were evaluated by analyzing the variance of part weight and melt pressure at nozzle, respectively. Phase two involved same steps of phase one, which were applied to the PIF process. Phase three involved taking the standard process of traditional injection moulding and removing the hold pressure in order to freeze the part at time of switchover. So, the entire weight of the part was solely dependent upon the switchover method. Again, the shot to shot consistency of both part quality and process variability were compared by means of the variance of part weight and melt pressure at nozzle. Phase four consists on the same steps of phase three, when applied to the PIF process.

7.3.1.1 Experimental

The test composite part is the same rectangular cover-plate described in chapter 3, which is made of an aluminium blank joint to a polymeric substrate of polypropylene Sabic P48M10. The machine used was the same all-electric 1000 kN ENGEL E-Motion injection moulding machine, which was described in chapter 3. The nozzle of the moulding machine was fitted with a 4083A Kistler piezo-resistive transducer, which is capable of measuring the pressure directly from the melt stream. During the process, the sheet metal blank was first hanged on the core plate; the mould was then closed and clamped so that the injected polymer deformed the blank during the filling phase. The mould was equipped with a Kistler 6157BB piezo-electric transducer for measuring cavity pressure, located at 10 mm from the gate.

A gram scale was used to weight the part to the nearest thousandths of a gram. The signals produced by sensors were read using a National Instruments PCI E-6036 data acquisition card that also provided A/D conversion and multiplexing. A National Instruments SCB-68 shielded board was also employed to isolated the transducer signal from the data acquisition system. An Intel Pentium 4 2.4 GHz based personal computer running the monitoring and control program developed in LabVIEW® for Windows (National Instruments) was used.

All the experimental tests were carried out with a nozzle temperature set to 240°C and a clamp force equal to 600 kN. The mould temperature was stabilized with all cooling circuits at 40 °C.

Phase 1

In this phase a traditional injection moulding process with an holding-pressure and holding-time of 300 bar and 30 sec respectively was carried out. An extra-cooling time of 20 s was set in order to let the part to cooling down to the ejection temperature.

Test A:

The machine was set for the standard injection moulding process using the position switchover method. Switching ram position was experimentally determined in order to obtain parts which were approximately 99% full at time of switchover. After the stabilization of the process, 25 consecutive shots were collected.

Test B:

The machine settings were changed in order to switchover by machine pressure (which is equivalent to the hydraulic pressure for an hydraulic machine). The switching pressure level was adjusted in order to keep switchover position constant. 25 consecutive shots were collected.

Test C:

Process conditions were changed in order to switchover by cavity pressure. The switching pressure level was adjusted in order to switch near the kink in the cavity pressure. The switchover position resulted to be close to the ones of Test A and Test B. Again, 25 consecutive shots were collected.

Test D:

Process conditions were changed in order to switchover by the automatic switching point detection algorithm. As in previous tests, 25 consecutive shots were collected.

Phase 2

In this phase the Polymer Injection Forming process with an holding-pressure and holding-time of 300 bar and 30 sec respectively was carried out. Extra cooling-time was set as in Phase 1.

Tests A, B, C and D were carried out as described in Phase 1. However, in Test B and C switchover pressure levels were adjusted in order to take into account the extra pressure for sheet metal deformation.

Phase 3

In this phase the holding pressure specified in Phase 1 was removed, but the holding time was kept. All other process conditions were equal to the ones of Phase 1.

Tests A, B, C and were carried out as described in Phase 1.

Phase 4

In this phase the holding pressure specified in Phase 2 was removed, but the holding time was kept. All other process conditions were equal to the ones of Phase 2.

Tests A, B, C and were carried out as described in Phase 2.

7.3.1.2 Results analysis and discussion

Obtained data were graphed in order to make results interpretation more easy.

Figure 7.32 shows the variances of part weights between runs for each switchover method for both traditional injection moulding process and PIF process. For both processes, the tests with the lowest standard deviation fall in the tests carried out with the automatic switching point detection algorithm. Comparing part weight variances obtained by the two processes, it can be concluded that parts manufactured by PIF present a great variability with all the analyzed switchover methods.

The more variability of parts quality manufactured by PIF can be caused by the extra process variability induced by the sheet metal deformation process.

In confirmation of the above, it is interesting to analyze the Figure 7.34 which plots the variances of peak nozzle pressure between runs for each switchover method for both traditional injection moulding process and PIF process. The standard deviation of peak pressure for PIF results to be the largest, for each of the analyzed switch over method. This result is a confirmation of the more intrinsic process variability of the PIF process, when compared to the injection moulding process. Figure 7.34 shows that for both PIF and injection moulding a higher consistency of process variability can be obtained when the automatic switching point detection algorithm is employed.

Phase 3 and Phase 4 data are analyzed in order to determine the actual amount of material variation in the part at time of switchover (holding pressure was removed in order to "freeze" part conditions at time of switchover). Figure 7.33 plots the variances of part weights between runs for each switchover method for both traditional injection moulding process and PIF process, when holding pressure was removed. The situation is very similar to the one presented in Figure 7.32: switchover by the automatic switching point detection algorithm produces parts with the most consistent weights. Variance of parts weight manufactured by PIF process results to be larger than the one obtained by injection moulding process.

Figure 7.32 and Figure 7.33 reveal additional interesting information when analyzed together. Figure 7.32, when compared to Figure 7.33, shows that for both PIF and injection moulding processes, the variability from shot to shot part weight is reduced as the part is filled out. This happens for each of the analyzed switchover methods.

A similar conclusion can be obtained comparing Figure 7.34 with Figure 7.35, which plot the variances of peak nozzle pressure between runs for each switchover method for both traditional injection moulding process and PIF process, when holding pressure was removed. Process variability results to be less when the holding pressure is used in both the PIF and the injection moulding processes.

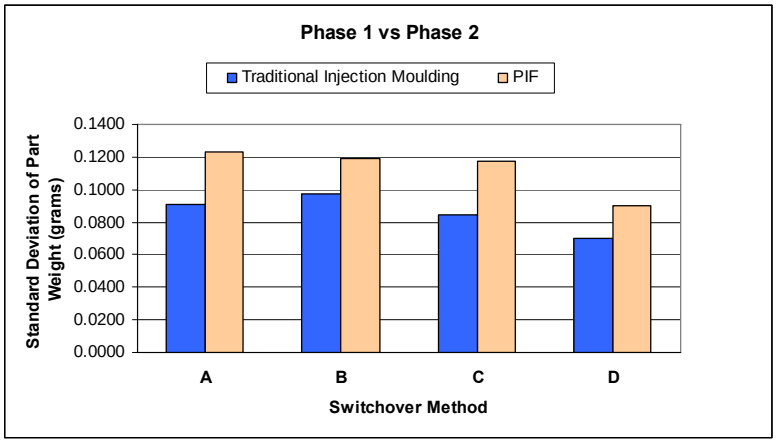

Figure 7.32: Variations of part weight for different switchover methods in traditional injection moulding process and PIF.

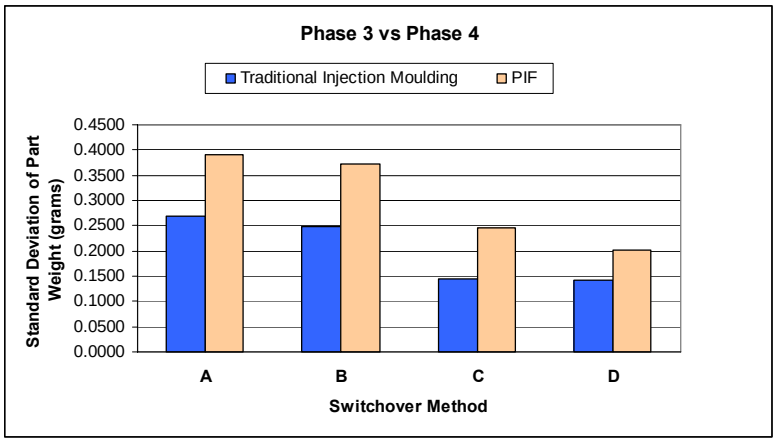

Figure 7.33: Variations of part weight for different switchover methods in traditional injection moulding process and PIF (without packing pressure).

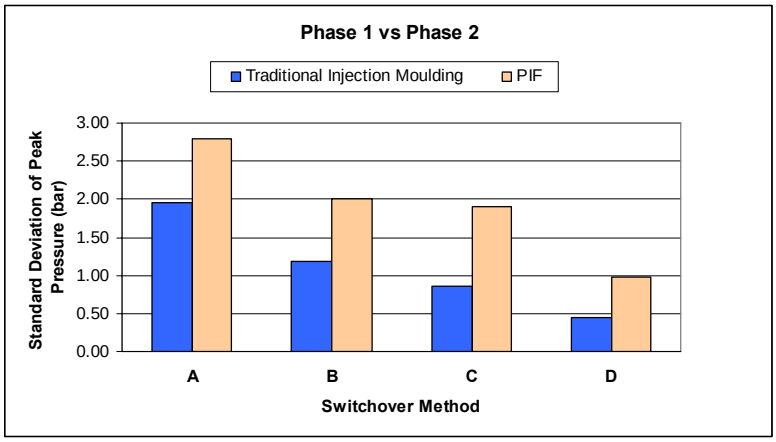

Figure 7.34: Variations of peak nozzle pressure for different switchover methods in traditional injection moulding process and PIF.

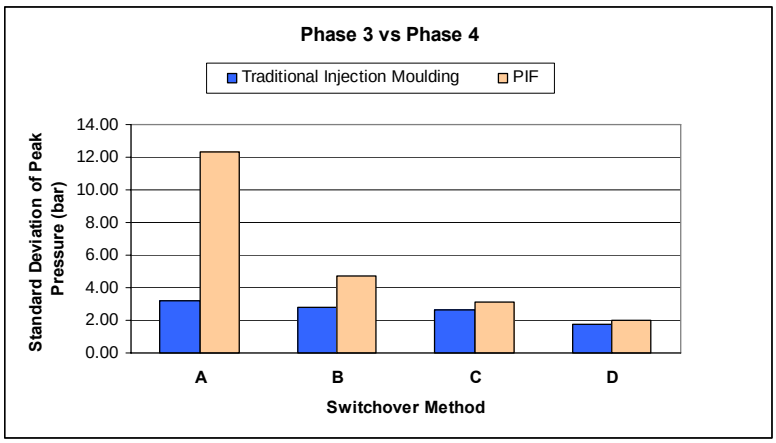

Figure 7.35: Variations of peak nozzle pressure for different switchover methods in traditional injection moulding process and PIF (without packing pressure).

7.3.1.3 Conclusions

This study shows that for both traditional injection moulding and Polymer Injection Forming processes, a filling to packing transfer based on the developed automatic switching point detection algorithm leads to a more process robustness. Obtained results show that both part quality (evaluated by means of part weight variances) and process variability (evaluated by means of variance of melt pressure at nozzle) are better when this algorithm is used.

Another considerations which comes from results analysis is that as the part fills out more and more, the amount of plastic at time of switchover has less and less influence on the part. Therefore, holding pressure can partially masks over the inconsistencies of switchover variance. However, this conclusion comes from the analysis of a thick walled part, where holding pressure has a great impact on the final part weight.

Considering a thin walled part, where the holding pressure has a less effect on the final weight of the part, differences in part quality resulting from different switchover methods can be more evident [75].

CHAPTER 8
CONCLUSIONS

Composite parts made of a sheet metal blank bonded to a plastic substrate are increasingly used in manufacturing aesthetic and functional parts for many industrial sectors such as automobiles, aircrafts, electronics and electrical appliances.

The manufacturing of this kind of components is usually time-consuming and labour intensive resulting in a very expensive production. In most cases, the polymer and the metal parts are first manufactured separately by injection moulding and sheet metal forming processes respectively. Then they are joined together mainly by the adhesion bonding method.

Due to these drawbacks, companies in the automotive field, and not only, are looking for other innovative manufacturing processes in order to increase productivity and, at the same time, minimize production costs and improve the quality of the final metal/polymer macro-composite products.

Polymer Injection Forming (PIF) is a new technology to manufacture sheet metal/polymer macro-composite components in a one-operation production process. During the process, a metal blank is shaped inside an injection mould by using the injection pressure of the molten polymer. In the same step the polymer is permanently bonded to the metal sheet creating a fully finished product in only one production step. Thus, the PIF technology is a combination of the injection moulding and sheet metal forming processes.

In spite of its industrial relevance, the scientific knowledge of the above process is still very poor. Experimental investigations, both in the laboratory and in the field, continue to be more common than numerical ones. Models and simulations suffer from many heavy assumptions, mainly those related to the description of the polymer-metal interactions [1], and prove to be inadequate to evaluate the effects of process parameters on process performance and product quality. The causes of this are both the complexity of the phenomena to model as well as the recentness of these technologies (PIF process was patented in 2003 [16]).

The aim of this Ph.D. thesis consists on increasing the scientific knowledge about the Polymer Injection Forming process by means of both a numerical and an experimental approach. Several aspects of this new manufacturing process have been studied:

(i) The influence of the main injection moulding process parameters on the sheet metal formability has been experimentally investigated according to the Design of Experiments (DOE) method. The metal blank formability was mainly evaluated measuring the thickness

distribution curves of the deformed sheet metal parts. Obtained results show that the deformation development of the sheet metal in the Polymer Injection Forming process is different from the one in the Viscous Pressure Forming (VPF) process. In VPF, the thickness of the deformed sheet metal depends on process parameters and viscous medium properties. In PIF, thickness distribution depends only on the clamp force, which forces the sheet metal to deform as pure stretching or as a combination of drawing and stretching. Polymer viscosity, injection speed, mould temperature and melt temperature result to have little influence on the formability of the sheet metal blank.

(ii) A new approach has been proposed to model the forming processes of sheet metal-polymer composites such as PIF and PICF. It is based on a multi-physics numerical model of the process that was calibrated through physical-simulation experiments and validated on a lab pilot plant. Both the mechanical behaviour of the aluminium alloy 1050-O and the rheological behaviour of the Bayblend T-88 4N polymer were experimentally determined in order to obtain accurate results from the numerical simulations. Thanks to its features, the approach proves to be suitable for investigating the mutual metal-polymer interactions and, therefore, provides a reliable tool in designing the process as well as its control. That approach is based on a combination of the finite element method (FEM) and Finite Volume Method (FVM) and it allows to analyse the deformation features, thickness distribution and evolution of plastic strains during the forming process of the sheet metal blank.

(iii) The influence of the main injection moulding process parameters on the adhesion quality between the plastic and the metal part was investigated by means of a custom shear test. The experimental procedure consisted in manufacturing metal/polymer components by means of the PIF process, changing opportunely the process parameters and the adhesive type. Obtained parts were then used as specimen in the shear test. Experimental tests were designed according to a three factor 2-level full factorial design (2^3 DOE). Obtained results show that melt temperature and injection speed have different influence on metal/polymer adhesion strength, depending on the type of adhesive used for the joint.

(iv) Polymer Injection Forming process is characterized by having many variables, internal and external, affecting the end result. Thermoplastic materials are also unpredictable since they behave as non-Newtonian fluids when molten. Furthermore, like in traditional injection moulding process, the properties of the finished part are affected only indirectly by the machine settings. Sensing equipment installed in most machines is also inadequate for giving a true picture of the state of the process since most of the measured parameters have only an indirect effect in the quality of the part. Interdependencies between different machine factors are also very difficult to predict, particularly between settings and plastic variables. To overcome these problems, an approach consisting on monitoring both the process and the material behaviour directly by means of in-mould process variables measurements was proposed. These approach was implemented in a PC-based software for the monitoring and control, in particular the switch-over point, of the PIF process. Obtained results showed the efficiency of this method in optimizing the process and maximizing its repeatability.

The work presented in this thesis was carried out at the DIMEG Labs, University of Padua, Italy, from January 2005 to December 2007, under the supervision of ing. Giovanni Lucchetta.

REFERENCES

[1] Z. J. Wang, J. G. Liu, X. Y. Wang, Z. Y. Hu and B. Guo, *Viscous pressure forming (VPF): state-of-the-art and future trends*, Journal of Material Processing and Technology, 2004. 151: p. 80-87.

[2] M. L. Roades and L. J. Roades, *Method and apparatus for die forming sheet materials*, US Patent 5 085 068, 1992.

[3] H. Gilmore, R. Resnick and R. Ross, *ARPA Flexible Fabrication Program, Viscous pressure forming*, First interim technical report, EH-VPF-95-0001, 1995.

[4] H. Gilmore, R. Resnick and R. Ross, *ARPA Flexible Fabrication Program, Viscous pressure forming*, Second interim technical report, EH-VPF-95-0002, 1995.

[5] J. Liu, B. Westhoff, M. Ahmetogla and T. Altan, *Application of viscous pressure forming (VPF) to low volume stamping of difficult-to-form alloys -results of preliminary FEM simulations*, Journal of Material Processing and Technology, 1996. 59(1): p. 49-58.

[6] J. Liu, A. Tuz, M. A. Ahmetoglu and T. Altan, *Viscous pressure forming (VPF) technology of plasticity*, in: Proceedings of the Fifth International Conference on Technology of Plasticity, Columbus, OH, USA, 1996: p. 671-674.

[7] W. Xinyun, *Numerical simulation and experimental research on viscous pressure forming process of thin-walled sheet metal parts*, PhD Dissertation, Harbin Institute of Technology, 2002.

[8] X. Y. Wang, J. C. Xia, G. A. Hu, Z. J. Wang and Z. R. Wang, *Sheet bulging experiment with a viscous pressure-carrying medium*, Journal of Material Processing and Technology, 2004. 151: p. 340-344.

[9] Z.J. Wang, X.Y. Wang and Z.R. Wang, *Viscous pressure forming (VPF) of corrugated thin-walled sheet part with small radius*, Journal of Material Processing and Technology, 2004. 145: p. 345-351.

[10] L. Jianguang, W. Zhongjin and W. Zhongren, *Numerical simulation of the influence of viscous adhesive stress on the viscous pressure bulging process of hemispherical sphere*, Trans. Nonferrous Met. Soc. Chin., 2003. 13(6): p. 1354-1359.

[11] Z.R. Wang, B.G. Teng, S.J. Yuan, L.H. Lang and Z.J. Wang, *Simulation of some cases of hydroforming and viscous pressure forming*, Journal of Material Processing and Technology, 2004. 150: p. 25-29.

[12] J. Liu, M. Ahmetoglu and T. Altan, *Evaluation of sheet metal formability, viscous pressure forming (VPF) dome test*, Journal of Material Processing and Technology, 2000. 98: p. 1-6.

[13] M. Ahmetoglu, J. Hua, S. Kulukuru and T. Altan, *Hydroforming of sheet metal using a viscous pressure medium*, Journal of Material Processing and Technology, 2004. 146: p. 97-107.

[14] T. Altan, S. Jirathearanat, M. Strano and A. Shr, *Adaptive FEM process simulation for hydroforming tubes*, in: Proceedings of the International Conference on Hydroforming, Fellbach/Stuttgart, Germany, 2001.

[15] W. Xinyun, W. Zhongjin and W. Zhongren, *Numerical simulation of aluminum alloy ladder parts with viscous pressure forming*, Trans. Nonferrous Met. Soc. Chin., 2003. 13(2): p. 391-397.

[16] H. C. E. Van Der Aa, A. S. Verdier and H. G. J. De Wolf, *WO Patent No. 03057446*, 17 July 2003.

[17] Corus, www.corusgroup.com/en/design_and_innovation.

[18] M. Chen, X. Zhang, Q. Lei and J. Fu, *Finite element analysis of forming of sheet metal blank in manufacturing metal/polymer macro-composite components via injection moulding*, International Journal of Machine Tools & Manufacture, 2002. 42: p. 375-383.

[19] D. C. Montgomery, *Design and Analysis of Experiments*, John Wiley and Sons, New York, 2004.

[20] R. Neugebauer, T. Altan, M. Geiger, M. Kleiner and A. Sterzing, *Annals of the CIRP*, 2006. 55/2: p. 793-816.

[21] G. Lucchetta and R. Baesso, *Polymer Injection Forming (PIF) Of Thin-Walled Sheet Metal Parts - Preliminary Experimental Results*, in Proceedings of 10th ESAFORM International Conference on Material Forming, Zaragoza, Spain, 2007: p. 1046-1051.

[22] Moldflow Plastics Insight® Release 6.1 Material Database.

[23] C. W. Macosko, *Rheology: principles, measurements and applications*, VCH Publishers, New York, 1994.

[24] J. J. Bikerman, *The Science of Adhesive Joints*, Academic Press, New York, 1961.

[25] A. J. Kinloch, *Adhesion and Adhesives: Science and Technology*, Chapman and Hall, London, 1990.

[26] R. Oosting, *Toward a New Durable and Environmmentally Compliant Adhesive Bonding Process for Aluminium Alloys*, Master degree thesis, Delft University Press, The Netherlands, 1995.

[27] W. C. Wake, *Adhesion and the Formulation of Adhesives*, Applied Science Publishers Limited, London, 1976.

[28] A. V. Pocius, *Adhesion and Adhesives Technology - An Introduction 2nd edition*, Hanser, 2002.

[29] W. F. Ray, *Surface Preparation Techniques for Adhesive Bonding*, William Andrew Publishing, 1989.

[30] D. Dunlap, J. Parekhji and A. J. Your, *Interfacial Adhesion*, In Partial Fulfillment of the Course Requirements for MatE 210, Experimental Methods in Materials Engineering, 2002.

[31] AdhesivesToolkit, www.adhesivetoolkit.com.

[32] BS EN 26922: *Adhesives—Determination of Bond Strength in Direct Tension*, 1993.

[33] ASTM D 897-01: *Standard Test Method for Tensile Properties of Adhesive Bonds*, ASTM Standards Volume 15.06.

[34] ASTM D 2095–96 (2002): *Standard Test Method for Tensile Strength of Adhesives by Means of Bar and Rod Specimens,* ASTM Standards Volume 15.06.

[35] *Adhesives and Sealants*, Engineered Materials Handbook, ASM International, 1990. Volume 3.

[36] D. E. J. Saunders, *A Critical Review of Test Methods for Adhesively Bonded Joints*, unofficial NPL Report, January 1992.

[37] A. J. Harris and R. D. Adams, *An Assessment of the Impact Performance of Bonded Joints in Use in High Energy Absorbing Structures*, Proceedings of the Institute of Mechanical Engineering, 1985. 199 (C2): p. 121-131.

[38] ISO 11339: *Adhesives—T-Peel for Flexible-to-Flexible Bonded Assemblies,* 2003.

[39] BS 5350 Part C13: *Methods of Test for Adhesives. Adhesively Bonded Joints: Mechanical Tests. Climbing Drum Peel Test*, 1990.

[40] ASTM D 1781–98: *Standard Test Method for Climbing Drum Peel for Adhesives*, ASTM Standards Volume 15.06.

[41] ISO 4578: *Adhesives—Determination of Peel Resistance of High-Strength Adhesive Bonds—Floating Roller Method*, 1997.

[42] ASTM D 3167–97: *Standard Test Method for Floating Roller Peel Resistance of Adhesives*, ASTM Standards Volume 15.06.

[43] BS 5350—Part C5: *Adhesives—Determination of Bond Strength in Longitudinal Shear*, 1990.

[44] BS EN 1465: *Adhesives—Determination of Tensile Lap-Shear Strength of Rigid-to-Rigid Bonded Assemblies*, 1995.

[45] ASTM D 1002–01: *Standard Test Method for Apparent Shear Strength of Single-Lap Joint Adhesively Bonded Metal Specimens by Tension Loading (Metal-to-Metal)*, ASTM Standards Volume 15.06.

[46] ISO 9664: *Adhesives—Test Methods for Fatigue Properties of Structural Adhesives in Tensile Shear,* 1995.

[47] ASTM D 3528–96 (2002): *Standard Test Method for Strength Properties of Double-Lap Shear Adhesive Joints by Tension Loading*, ASTM Standards Volume 15.06.

[48] *Adhesive Bonding Handbook for Advanced Structural Materials*, European Space Research and Technology Centre, European Space Agency, Noordwjik, The Netherlands, 1990.

[49] G. D. Dean, B. C. Duncan, R. Adams, R. Thomas and L. Vaughn, *Comparison of Bulk and Joint Specimen Tests for Determining the Shear Properties of Adhesives*,

MTS Adhesive Programme, Project 1: Basic Mechanical Properties for Design, NPL Report CMMT(B)51, April 1996.

[50] R. Thomas and R. Adams, *Test Methods for Determining Shear Property Data for Adhesives Suitable for Design Part 2: The Torsion Method for Bulk and Joint Specimens*, NPL Report CMMT(B)56, 1996.

[51] A. Nadai, *Plasticity. A Mechanics of the Plastic State of Matter*, McGraw-Hill, New York, 1931: p. 128-130.

[52] S. Kalpakjian and S. R. Schmid, *Manufacturing Processes for Engineering Materials*, Prentice Hall, 2003.

[53] D. E. Steward and Z. Leyk, *ANSYS 10.0 Documentation*, Meschach Library Copiright, 1993.

[54] M. Cross and A. Slone, *A review of Commercial MPA Capability - 2005 update*, FENET Thematic Network Competitive and Sustainable Growth, Budapest, Hungary, 2005.

[55] FENET, www.fe-net.org.

[56] M. Cross and A. Slone, *FENET - Multi-Physics Analysis (MPA) Theme: A review of Commercial MPA Capability in 2005*, Summary of Projects Findings, MALTA, 17th -20th May, 2005.

[57] R. Baesso and G. Lucchetta, *Fluid Structure Interaction Analysis in Manufacturing Metal/Polymer Macro-Composites*, in Proceedings of the 9th International Conference on Numerical Methods in Industrial Forming Processes, Porto, Portugal, 2007: p. 729-734.

[58] C. F. Vahlund, *Using a Finite Volume Approach to Simulate the Mould Filling in Compression Moulding*, Journal of Reinforced Plastics and Composites, SAGE Publications, 2003. 22: p. 499-515.

[59] M. Darwish, *Development and Testing of a Robust Free-Surface Finite Volume Method*, LNCSR internal project report, 2003.

[60] D. E. Steward and Z. Leyk, *ANSYS CFX 10.0 Documentation*, Meschach Library Copiright, 1993.

[61] Moldflow Plastics Insight® Release 6.1, *Online help*, 2006.

[62] C. Collins, *Monitoring cavity pressure perfects injection molding*, Assembly Automation, MCB University Press, 1999. 19(3): p. 197-202.

[63] S. Orzechowski, A. Paris and C. J. B. Dobbin, *A Process Monitoring and Control System for Injection Molding Using Nozzle-Based Pressure and Temperature Sensors*, Journal of Injection Molding Technology, 1998. 2(3): p. 141-148.

[64] G. Churchward, E. Kosior and S. N. Bhattacharya, *Method for determining molding characteristic and injection molding machine*, in Proceedings of the Annual Technical Conference, SPE ANTEC 2004, 1993. 98.

[65] Z. Chen, L. S. Turng and K. K. Wang, *Adaptive online quality control for injection-molding by monitoring and controlling mold separation*, In Proceedings of the Annual Technical Conference, SPE ANTEC 2004, 1991. 444.

[66] R. G. Speight, *Optimization of Velocity to Pressure Phase Transfer for the Polymer Injection Molding Process*, Journal of Injection Molding Technology, 1997. 1(1): p. 25-35.

[67] D.O. Kazmer and K. Danai, *Control of Polymer Processing*, The Control Handbook, CRC & IEEE Press, 2001.

[68] H. R. Sheth and R. E. Nunn, *An Adaptive Control Methodology for the Injection Molding Process. Part 1: Material Data Generation*, Journal of Injection Molding Technology, 1998. 2(2): p. 86-94.

[69] Z. Chen and L. Turng, *Advances in Injection Molding Process/Quality Control*, in Proceedings of the Annual Technical Conference, SPE ANTEC 2004, 2004: p. 697-701.

[70] L. S. Turng, M. Peic and D. K. Bradley, *Process Simulation and Optimization for Injection Molding - Experimental Verifications and Field Applications*, Journal of Injection Molding Technology, 2002. 6(2): p. 143-155.

[71] A. R. AGRAWAL, I. O. PANDELIDIS and M. PECHT, *Injection-molding process control: a review*, Polymer Engineering and Science, 1987. 27(18): p. 1345-1357.

[72] B. Sheth, C. M. F. Barry and N. R. Schott, *Improved part quality using cavity pressure switchover*, Dynisco Instruments Literature.

[73] R. Edwards, C. L. Thomas and R. Peterson, *Controlling Injection Phase/Packing Phase Switchover Using an Ultrasonic Sensor*, Journal of Injection Molding Technology, 2001. 8(12).

[74] J. C. Piemme and M. P. Downey, *An Investigation of Cavity Pressure Transducer Position when Used for Velocity to Pressure Transfer with Various Injection Molding Process Strategies*, in Proceedings of the Annual Technical Conference, SPE ANTEC 2001.

[75] R. Baesso and G. Lucchetta, *Switchover Control in the Polymer Injection Forming Process*, in proceedings of the Annual Technical Conference, SPE ANTEC 2008 (Accepted).